



HAL
open science

Achievements and Prospects of Global Broadband Seismographic Networks After 30 Years of Continuous Geophysical Observations

A. T. Ringler, R. E. Anthony, R. C. Aster, C. J. Ammon, S. Arrowsmith, H. Benz, C. Ebeling, A. Frassetto, W. -Y. Kim, P. Koelemeijer, et al.

► **To cite this version:**

A. T. Ringler, R. E. Anthony, R. C. Aster, C. J. Ammon, S. Arrowsmith, et al.. Achievements and Prospects of Global Broadband Seismographic Networks After 30 Years of Continuous Geophysical Observations. *Reviews of Geophysics*, 2022, 60, 10.1029/2021RG000749 . insu-03824251

HAL Id: insu-03824251

<https://insu.hal.science/insu-03824251>

Submitted on 21 Oct 2022

HAL is a multi-disciplinary open access archive for the deposit and dissemination of scientific research documents, whether they are published or not. The documents may come from teaching and research institutions in France or abroad, or from public or private research centers.

L'archive ouverte pluridisciplinaire **HAL**, est destinée au dépôt et à la diffusion de documents scientifiques de niveau recherche, publiés ou non, émanant des établissements d'enseignement et de recherche français ou étrangers, des laboratoires publics ou privés.



Distributed under a Creative Commons Attribution - NonCommercial 4.0 International License

Reviews of Geophysics®



REVIEW ARTICLE

10.1029/2021RG000749

Key Points:

- Long running globally distributed seismographic networks are fundamental to understanding Earth's interior structure and processes
- Networks have expanded beyond initial mid-twentieth century design which were focused on recording signals from earthquakes and explosions
- Global seismic data combined with data from nearby geophysical instrumentation continue to facilitate new discoveries in Earth science

Correspondence to:

A. T. Ringler,
aringle@usgs.gov

Citation:

Ringler, A. T., Anthony, R. E., Aster, R. C., Ammon, C. J., Arrowsmith, S., Benz, H., et al. (2022). Achievements and prospects of global broadband seismographic networks after 30 years of continuous geophysical observations. *Reviews of Geophysics*, 60, e2021RG000749. <https://doi.org/10.1029/2021RG000749>

Received 24 SEP 2021
Accepted 5 JUL 2022

Author Contributions:

Conceptualization: A. T. Ringler, R. E. Anthony, R. C. Aster
Investigation: P. Koelemeijer
Methodology: A. T. Ringler, R. E. Anthony, R. C. Aster, C. J. Ammon, S. Arrowsmith, H. Benz, W.-Y. Kim, H. C. P. Lau, V. Lekić, J. P. Montagner, P. G. Richards, D. P. Schaff, M. Vallée, W. Yeck
Project Administration: A. T. Ringler, R. E. Anthony, R. C. Aster, C. J. Ammon, S. Arrowsmith, H. Benz, W.-Y. Kim, H. C. P. Lau, V. Lekić, P. G. Richards, D. P. Schaff, M. Vallée, W. Yeck

© 2022 The Authors. This article has been contributed to by U.S. Government employees and their work is in the public domain in the USA.

This is an open access article under the terms of the [Creative Commons Attribution License](https://creativecommons.org/licenses/by/4.0/), which permits use, distribution and reproduction in any medium, provided the original work is properly cited.

Achievements and Prospects of Global Broadband Seismographic Networks After 30 Years of Continuous Geophysical Observations

A. T. Ringler¹ , R. E. Anthony¹ , R. C. Aster² , C. J. Ammon³ , S. Arrowsmith⁴ , H. Benz⁵ , C. Ebeling⁶, A. Frassetto⁷, W.-Y. Kim⁸ , P. Koelemeijer^{9,10} , H. C. P. Lau¹¹ , V. Lekić¹² , J. P. Montagner¹³ , P. G. Richards⁸, D. P. Schaff⁸ , M. Vallée¹³, and W. Yeck⁵ 

¹Albuquerque Seismological Laboratory, U.S. Geological Survey, Albuquerque, NM, USA, ²Department of Geosciences, Warner College of Natural Resources, Colorado State University, Fort Collins, CO, USA, ³Department of Geosciences, The Pennsylvania State University, University Park, PA, USA, ⁴Roy M. Huffington Department of Earth Sciences, Southern Methodist University, Dallas, TX, USA, ⁵National Earthquake Information Center, U.S. Geological Survey, Denver, CO, USA, ⁶Scripps Institution of Oceanography, University of California, San Diego, La Jolla, CA, USA, ⁷Incorporated Research Institutions for Seismology Consortium, Washington, DC, USA, ⁸Lamont Doherty Earth Observatory, Columbia University, Palisades, NY, USA, ⁹Department of Earth Sciences, Royal Holloway University of London, Egham, UK, ¹⁰Department of Earth Sciences, University of Oxford, Oxford, UK, ¹¹Department of Earth and Planetary Science, University of California, Berkeley, Berkeley, CA, USA, ¹²Department of Geology, University of Maryland, College Park, College Park, MD, USA, ¹³Institut de Physique du Globe de Paris, Université Paris Cité, CNRS, Paris, France

Abstract Global seismographic networks (GSNs) emerged during the late nineteenth and early twentieth centuries, facilitated by seminal international developments in theory, technology, instrumentation, and data exchange. The mid- to late-twentieth century saw the creation of the World-Wide Standardized Seismographic Network (1961) and International Deployment of Accelerometers (1976), which advanced global geographic coverage as seismometer bandwidth increased greatly allowing for the recording of the Earth's principal seismic spectrum. The modern era of global observations and rapid data access began during the 1980s, and notably included the inception of the GEOSCOPE initiative (1982) and GSN (1988). Through continual improvements, GEOSCOPE and the GSN have realized near-real time recording of ground motion with state-of-art data quality, dynamic range, and timing precision to encompass 180 seismic stations, many in very remote locations. Data from GSNs are increasingly integrated with other geophysical data (e.g., space geodesy, infrasound and Interferometric Synthetic Aperture Radar). Globally distributed seismic data are critical to resolving crust, mantle, and core structure; illuminating features of the plate tectonic and mantle convection system; rapid characterization of earthquakes; identification of potential tsunamis; global nuclear test verification; and provide sensitive proxies for environmental changes. As the global geosciences community continues to advance our understanding of Earth structure and processes controlling elastic wave propagation, GSN infrastructure offers a springboard to realize increasingly multi-instrument geophysical observatories. Here, we review the historical, scientific, and monitoring heritage of GSNs, summarize key discoveries, and discuss future associated opportunities for Earth Science.

Plain Language Summary Global seismographic networks (GSNs) record information-rich ground motion signals that allow scientists and nations to identify and quantify global earthquakes and other seismic sources, and to rapidly assess their significance and impacts on society. In addition to providing a global standard for the monitoring and assessment of such events, these networks provide unique high-quality data that are fundamental to revealing Earth's structure and dynamic behavior. Scientific applications of GSNs, supplemented by regional data, include imaging the deep interior of the Earth and its plate tectonic system, modeling the structure and dynamics of the inner core, imaging and understanding the rupture of earthquake faults, detecting, discriminating, and characterizing nuclear and other explosions, and improving our general understanding of Earth's ubiquitous seismic wavefield and the unique information that it conveys from the deep interior to the surface and atmosphere of the planet. Leveraging the extensive and hardened infrastructure at these global observatories facilitates the recording of other signals of geophysical interest, such as the magnetic field, low frequency sound waves, and meteorological observations. We review the heritage of GSNs, including their history and resulting scientific achievements, and summarize future opportunities for these networks to contribute further to improved advancements in Earth science.

Supervision: A. T. Ringler, R. E.

Anthony, R. C. Aster

Visualization: A. Frassetto

Writing – original draft: A. T. Ringler,

R. E. Anthony, R. C. Aster, C. J. Ammon,

S. Arrowsmith, H. Benz, W.-Y. Kim, H.

C. P. Lau, V. Lekić, P. G. Richards, D. P.

Schaff, M. Vallée, W. Yeck

Writing – review & editing: A. T.

Ringler, R. E. Anthony, R. C. Aster, C.

J. Ammon, S. Arrowsmith, H. Benz, C.

Ebeling, W.-Y. Kim, P. Koelemeijer, H.

C. P. Lau, V. Lekić, J. P. Montagner,

P. G. Richards, D. P. Schaff, M. Vallée,

W. Yeck

1. Introduction

Global seismographic networks (GSNs) have a centennial-scale history of acquiring ground motion data to monitor and study seismic sources, including earthquakes and nuclear tests, and to utilize seismic waves to image Earth's internal structure. In addition, the extensive global coverage of these networks, while being supplemented by regional networks, increasingly allows them to serve as multi-use platforms for a large number of geophysical applications spanning the solid Earth, oceans, cryosphere, and atmosphere.

During the last four decades, technological advances (e.g., sensor design, low-noise and low-power electronics, and the modern Internet) have fundamentally changed the methods by and scale at which seismic data are acquired and distributed. Early global networks relied on analog instruments that were capable of recording ground motions across relatively narrow frequency bands, often on photographic paper. GSNs today deliver highly calibrated digital recordings of ground motion in the frequency range of approximately 50 Hz to periods of a day in near-real time with global data curation and internet access (Steim, 2015). The transmission of seismic data in near-real time has become critical for the rapid characterization of global earthquakes (e.g., Yeck et al., 2020) and tsunami warnings (e.g., Kanamori & Rivera, 2008). Broadband seismic data have also led to fundamental advances in understanding fault rupture processes (e.g., Hayes et al., 2018; Nettles et al., 2011) and to the imaging of Earth's interior at increasingly improved resolution. This progress reflects the rich variety of information encoded in global elastic waves, which range from higher frequency (~0.5 to 10 s) body waves (e.g., Kennett et al., 1995) to long-period surface waves, and very long-period normal mode oscillations at frequencies below 10 mHz (e.g., Deuss et al., 2013).

GSNs are also critical to global nuclear monitoring and discrimination, which provided major additional motivation for their creation. Multi-decadal continuity of global seismic observations has additionally revealed temporal evolution of climate signals such as glacial earthquakes (Ekström, Nettles, & Tsai, 2006), storm activity (Aster et al., 2010), and ocean temperature (Wu et al., 2020). Although the seminal focus for creating GSNs was to provide the highest quality of seismic data possible (Lay et al., 2002), many stations have evolved to record additional types of data as well that include infrasound, magnetic field, and meteorological data (pressure and temperature).

Late twentieth century design goals of most currently operating GSNs have now been met (Butler et al., 2004), and most operational efforts now focus on improving the performance of established stations and maintaining overall network robustness and data quality (Leith, 2008). However, as we describe here, the continual improvement of seismic data quality often involves making non-seismic measurements to assess increasingly subtle influences while furthering interdisciplinary Earth system science, and opportunities continue to exist for integrating additional types of geophysical instrumentation into these networks.

This paper reviews the instrumentation, scientific accomplishments, and mission-driven operations of digital GSNs. We do not focus on one particular network as these data are widely exchanged and integrated, both with each other and with many thousands of other temporarily collected and long-term seismic data sets, and the details of various networks are documented elsewhere (B. A. Romanowicz et al., 1984; Butler et al., 2004; D. Anderson et al., 2015; Engdahl et al., 1982; Hanka & Kind, 1994; Lay et al., 2002; Park et al., 2005; Peterson & Hutt, 2014; Suarez et al., 2008; Roullet et al., 2010). We focus on reviewing the historical context and development of these networks as well as some of the historic scientific discoveries that they have enabled, particularly since the advent of the digital era. Finally, we discuss their continuing roles in catalyzing future interdisciplinary opportunities.

2. A Brief History of Modern Global Seismographic Networks

Following the late nineteenth century discovery that seismic waves generated by earthquakes traversing the deep Earth could be globally detected (Dewey & Byerly, 1969; Von Rebeur-Paschwitz, 1889), interest expanded in establishing an international community of seismologists and seismic stations. Pioneering efforts to establish a global network can be traced back to the Milne network, which was deployed from the late 1890s to the early 1900s and grew to approximately 30 identically engineered seismographs that were mostly sited near coastal cities and at mid-latitudes (Milne, 1900). Predominantly using surface wave observations (often the highest amplitude signals in earthquake seismograms) recorded by this network, Milne produced one of the first (for the

year 1899) global catalogs of seismicity. During this time, the international Jesuit network of seismometers also began operating. This network was predominantly located in the Americas and Britain and was composed of a heterogeneous mixture of seismic instrumentation (Udias & Stauder, 1996). These earliest global networks were critical for establishing a basic understanding of seismic wave propagation and for revealing the one-dimensional (1D) large-scale structure of the Earth, including the definitive discovery of the core (Oldham, 1906), its liquid outer core in 1914 by B. Gutenberg (Knopoff, 1999), indications of a solid inner core in 1936 by I. Lehmann (Brush, 1980), and the compilation and analysis of increasingly detailed global seismogram and seismic phase travel time observations (e.g., Jeffreys, 1931b).

During the 1950s the political leadership of the United Kingdom (UK), the United States of America (USA), and the Union of the Soviet Social Republics (USSR) desired to negotiating a Comprehensive Test Ban Treaty (CTBT), intended to impede the development of new nuclear weapons by countries that already possessed nuclear capabilities. Progress slowed because it was not clear that nuclear test explosions conducted underground could be characterized well enough to permit verification of compliance. In 1959 U.S. seismologist Carl Romney, who was involved in the trilateral CTBT negotiations, stated in congressional testimony that on the basis of what was then demonstrably known about explosion monitoring using seismological methods “the number of earthquakes indistinguishable from 5 kt explosions would probably be 700 to 3,000 per year, of which 100 to 500 would be in the USSR and China” (Richards & Zavales, 1996). Such testimony turned out in retrospect to be inaccurate in its assessment of realizable seismic monitoring capabilities. As became apparent even by the early 1970s, the number of earthquakes indistinguishable from 5 kt explosions in the USSR and China were very few in number (in fact, nearly zero per year rather than “100 to 500”). Romney's testimony was based upon cautious estimates that drew upon answers to multiple fundamental technical questions, including:

1. How many earthquakes occur each year, and where, at different magnitude levels?
2. What would be the magnitude levels down to which a hypothesized global network of seismic stations could achieve reliable detection and identification?
3. What was the relationship between the yield of an underground nuclear explosion, and its seismic magnitude?

In each of these areas, the congressional testimony offered in 1959 was based upon understanding and numerical estimates that were quite different from what was discovered and accepted in later years.

Seismology was a small-scale science in the 1950s. President Eisenhower's Science Advisor James Killian developed a Panel on Seismic Improvement, chaired by Lloyd Berkner, that made detailed recommendations including that 100–200 of the existing stations in the world be equipped with modern instruments as soon as possible. Annual budgets of about \$18 million were outlined for such improvements. Since seismology in the United States prior to 1960 had received national support at the level of only about \$0.7 million annually, and since funding at the level recommended by the Berkner Panel was actually appropriated and spent, this surge in verification research had an enormous impact on seismology by funding the conception and rapid deployment of the World-Wide Standardized Seismograph Network (WWSSN). As described below, monitoring capability has steadily improved in the more than 60 years since the WWSSN was proposed, and underwent a major evolution when it became possible to utilize the capabilities of regional seismic monitoring rather than relying solely on teleseismic methods.

Deployment of the WWSSN in the early 1960s (Figure 1) substantially improved global seismic station coverage and enhanced monitoring capabilities for both nuclear explosions and earthquakes (Oliver & Murphy, 1971; Peterson & Hutt, 2014). The WWSSN incorporated uniform sensors and recording systems. Each station hosted three short-period seismometers and three long-period seismometers along with a galvanometer system to record seismograms on photosensitive paper. The exceptional improvements in seismic observations enabled by the WWSSN are worth noting. For example, in the late 1970s, Keiiti Aki (Aki & Richards, 1980, p. 563), wrote the WWSSN “is by far the finest general-purpose global system of seismograph stations ever operated ... The easy availability of well-calibrated seismograms on a global scale ... is making seismology truly a global science.” He further pointed out that the WWSSN enabled a wave-theoretical approach to the study of ground motions, involving waveform and spectral analysis, as opposed to the more primitive ray-theoretical approach in which only seismic phase arrival times and amplitudes were used. These successes with WWSSN data were a prime rationale for further progress in the quality of seismic data acquisition and methods for distribution and analysis.



Figure 1. World-Wide Standardized Seismographic Network in July 1978. Reproduced from Peterson and Hutt (2014), public domain.

By the 1960s it was realized that hand-digitized records could provide improvements in what information could be recovered from analog systems (Steim, 2015). This idea was taken one step further at Caltech by directly digitizing the output of a seismometer locally (Miller, 1963). With digital advances along with a number of other improvements (National Research Council, 1977), the WWSSN evolved during the 1970s into the Global Digital Seismograph Network (GDSN; Figure 2; Engdahl et al., 1982). The GDSN included the Seismic Research Observatory and the Abbreviated Seismic Research Observatory systems that facilitated observations of seismic signals (e.g., as generated from great earthquakes) in excess of 300 s period (Woodward & Masters, 1989). This network was further augmented by the Global Telemetered Seismograph Network, which supplemented the above networks for research and monitoring (Survey et al., 1982), especially in the southern hemisphere.

Although the GDSN produced data that was used for both estimating source parameters (Dziewonski et al., 1981) and deriving reference seismic velocity models for the Earth (Dziewonski & Anderson, 1981), a limitation of the network was that it was often unable to resolve very long period (>60 s) ground motions (Engdahl et al., 1982). In the 1970s global ground motion observations were extended to substantially longer periods than what the GDSN was capable of recording through the start of the International Deployment of Accelerometers (IDAs) network (Agnew et al., 1976, 1986). However, gravimeters record only the vertical component of ground motion. The GEOSCOPE initiative to install high dynamic-range, 3-component, broadband seismometers across the world helped to demonstrate some of the possible directions that could be utilized to improve long-period seismology (B. A. Romanowicz et al., 1984). This development in part provided momentum for current, modern digital broadband 3-component global networks (Roult et al., 2010). However, it was the culmination of electronics and communications advances in the late 1980s that enabled digital, low-noise records of ground motion from around the globe to be acquired in near-real time.

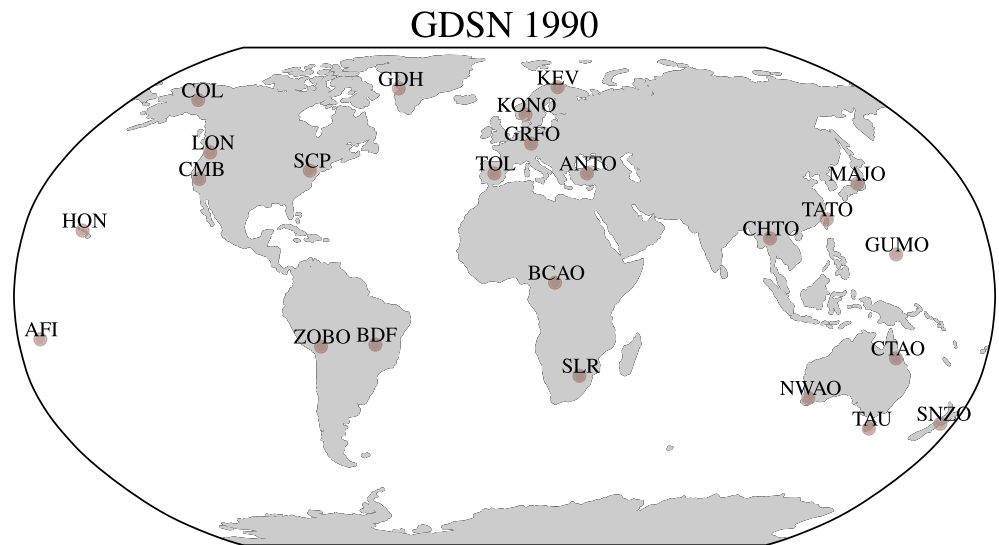


Figure 2. The Global Digital Seismograph Network (GDSN) as operating in 1990. This network included the Digital World-Wide Standardized Seismograph Network (network code DW), the Modified High Gain Long Period Network (network code AS), and the Seismic Research Observatory Network (network code SR).

2.1. The Development of Low-Frequency and Broadband Global Sensor Networks

Beginning in the early 1960s, the WWSSN provided unprecedented global coverage and high-quality short-period data suitable for nuclear explosion monitoring and for locating and characterizing earthquakes. However, instrument noise increased substantially below 0.05 Hz for the Sprengnether Press-Ewing sensor-galvanometer system that was employed in this network (Peterson & Hutt, 2014). Consequently, only very large or deep earthquakes produced strong enough long-period surface waves and free oscillations of the Earth (called “normal modes”) to be recorded at a good signal-to-noise ratio (SNR) with these instruments. The theory underpinning normal mode seismology was becoming well developed at this time (e.g., Dahlen, 1968) and it was recognized that normal mode records could be used to infer both deep Earth structure as well as source parameters of large earthquakes (Gilbert, 1971). Interest in consistently recording >100 s period normal modes following large earthquakes led to the development of the IDA network (Agnew et al., 1976). This pioneering network of 24 LaCoste and Romberg gravimeters (Figure 3) provided the first high-quality global recordings of very long period seismic signals (Buland et al., 1979; LaCoste, 1983).

However, the IDA network of gravimeters was unable to sample the horizontal wavefield and had relatively limited dynamic range that caused distortion of the ground motion records when large amplitude surface waves were present. While instrumental dynamic range was improved in the GDSN (Figure 2), long-period observations of ground motion were becoming obscured by noise introduced by local pressure and temperature variations. To improve upon the shortcomings of these networks the French GEOSCOPE program was initiated to deploy a global network of 3-component Streckeisen STS-1 seismometers (B. A. Romanowicz et al., 1984). The Streckeisen STS-1 seismometer (Figure 4) was initially designed with a flat velocity response to 20 s and made use of a novel leaf-spring design and feedback system (Wielandt & Streckeisen, 1982). In 1984, a new low-noise operational amplifier was developed that enabled the lower corner frequency of the instrument response to be electronically extended to 360 s (Wielandt & Steim, 1986). By utilizing advances in force feedback electronics, first applied to a seismometer in 1972 by Axel Plešinger (Kolář, 2020), this very broadband (VBB) version of the Streckeisen STS-1 was able to record a much larger portion of the seismic spectrum than any prior seismographic system.

The GEOSCOPE network reached about 20 stations at the end of the 1980s (Figure 5) and evolved with technological improvements moving to stations with additional environmental recordings such as pressure (Montagner et al., 1998) that became progressively available (Roult et al., 2010). By January 2021, the network had expanded to 33 stations, most of which were operating Streckeisen STS-1 seismometers. Secondary broadband and/or strong motion sensors, together with environmental sensors, have been added to most of the GEOSCOPE stations. At the beginning of operation of the GEOSCOPE network, the full output of the STS-1 VBB could not be used, as

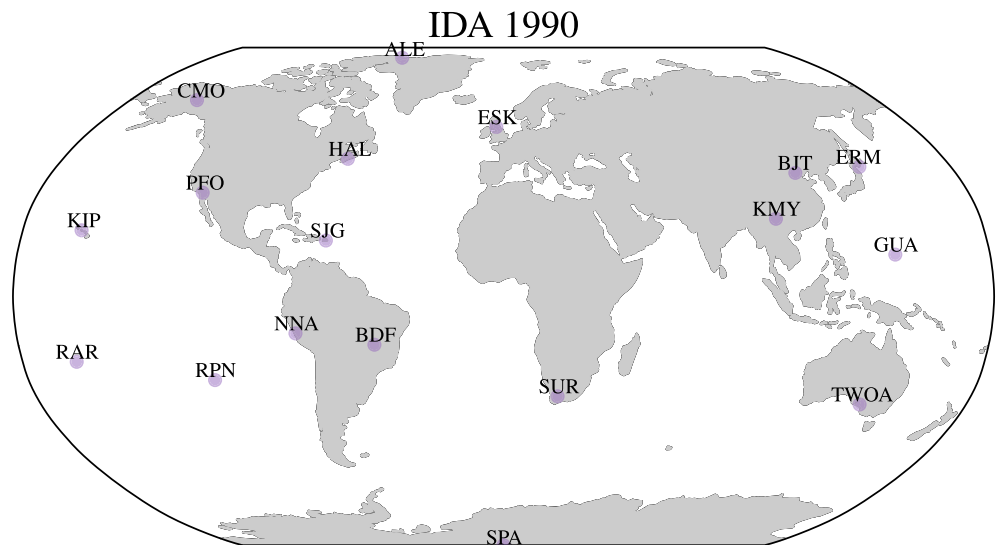


Figure 3. International Deployment of Accelerometers (IDAs) network of LaCoste and Romberg gravimeters (network code ID) in 1990.

current recording systems were unable to digitize the entire seismic signal. Storage capacity was also an issue and two separate recordings were used for continuous long period signals (sampled at 0.1 Hz) and for time windows following large earthquakes (sampled at 5 Hz). These limitations motivated the development of a true 24-bit digitizer combined with adequate storage, to record the entire dynamic range of these new sensors. These advances would provide a path for seismologists to utilize a single data stream to record most of the seismic wavefield of interest from frequencies as high as 5 Hz down to about once per day, for example, Earth tides (Figure 6). Between these two extremes it also becomes possible to record normal modes (100–3,000 s period, orange) which entail the excitation of the entire Earth after large earthquakes. Similar, but constantly excited Earth hum, by way of ocean processes, can be observed in the 50–300 s band (green) and is the excitation of seismic energy through atmospheric processes. Primary oceanic microseisms (6–25 s, pink), secondary oceanic microseisms (3–12.5 s period, brown), and earthquakes at various distances (gray) are also shown.

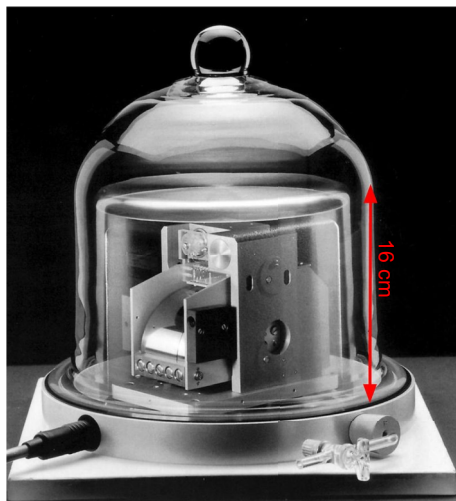


Figure 4. Vertical component Streckeisen STS-1 seismometer inside an evacuated bell jar. The sensor is shielded from magnetic field changes using a ferromagnetic cover made out of μ -metal. Figure modified from Streckeisen GmbH: https://streckeisen.swiss/assets/downloads/sts-1_brochure.pdf.

2.2. The Global Seismographic Network

The early success of GEOSCOPE highlighted the limitations of the concurrently operating global networks in the early 1980s. The 150 station GSN network was proposed with near-real time telemetry in the 1984 Incorporated Research Institutions for Seismology (IRIS) “Rainbow” proposal (IRIS, 1984; Smith, 1986). The proposal articulated a community facility, an instrument pool to allow scientists access to portable instruments (Aster et al., 2005), a data center and system for archiving and distributing seismic data, and plans for the GSN. Although specific GSN instrumentation had not been decided on at the time, a proof-of-concept station with a 24-bit digitizer and VBB Streckeisen STS-1 installed at the Harvard University, was showing great promise in being able to provide very wide band seismic data. Around this same time the ability to send data over the internet using the “Dial-A-broadband-Seismogram” approach was also being developed to transmit near real-time data (Steim, 1987). This prototype station ultimately became the design inspiration for the GSN with the prototype 24-bit digitizer evolving into the Quanterra Q680. The Q680 employed a compression algorithm, which utilized taking the differences between consecutive discrete samples, now known as STEIM-1 compression (Ahern et al., 2012). This reduced the throughput of telemetered seismic data, as well as its subsequent

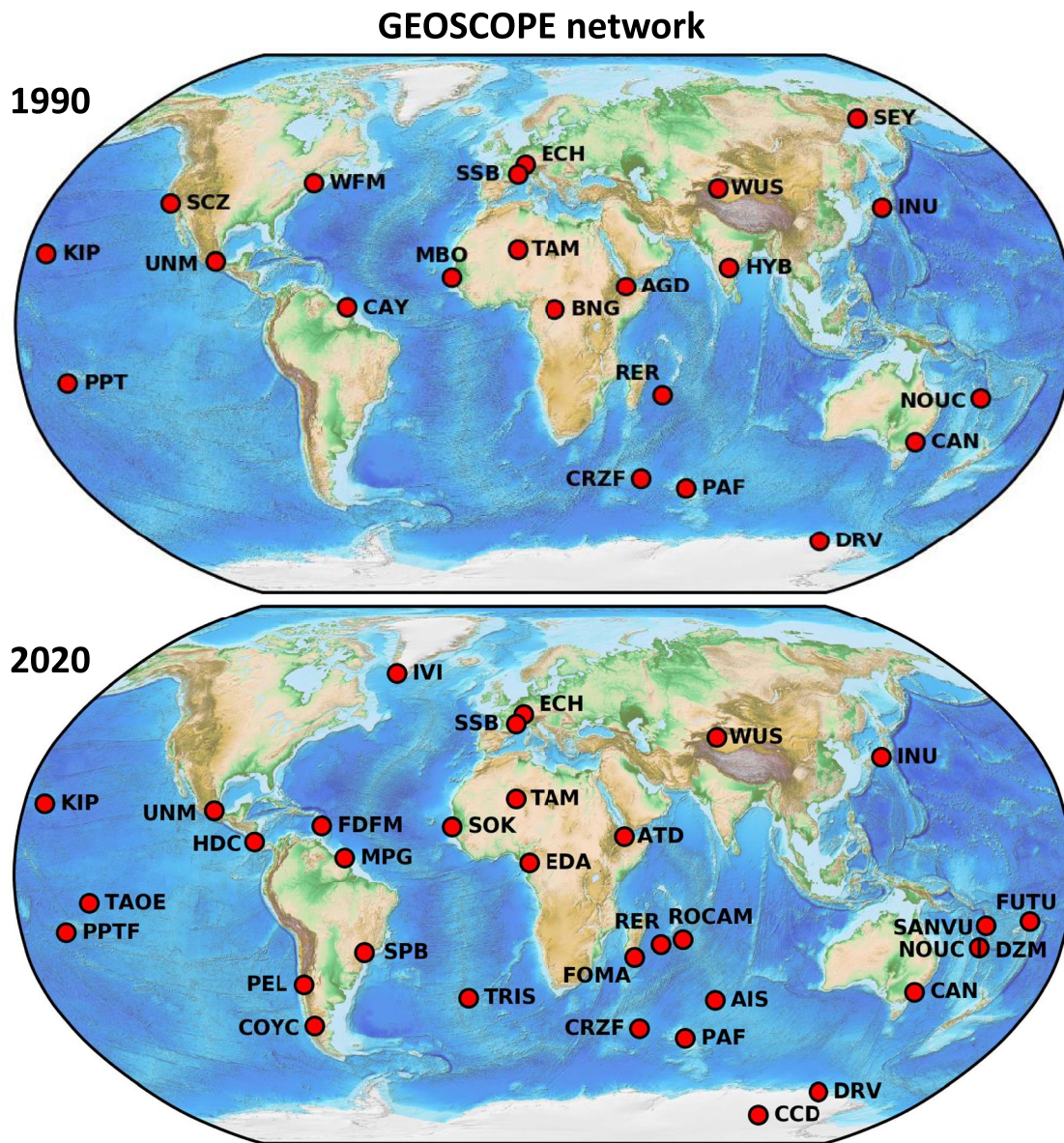


Figure 5. GEOSCOPE network (network code G) in 1990 and 2020.

archival, and allowed IRIS to substantially modify a plan of uniform satellite telemetry by widely realizing GSN data communications over the early Internet. Largely using the existing station locations from the IDA and GDSN networks, GSN stations began being deployed in the late 1980s (Peterson & Hutt, 1989), with many becoming operational by the mid-1990s with the large-scale footprint of the network approaching that of 2021 (Figure 7).

The modular design of the GSN often allows for easy incorporation of new technologies as they become available (Figure 8). For example, when the 26-bit Quanterra Q330HR digitizer was introduced, it was possible to upgrade the network and take advantage of the increased dynamic range of the new recording system without disturbing the seismometer and other systems. By the mid-2000s, GSN stations began incorporating additional instrumentation including a secondary broadband seismometer, a strong-motion accelerometer (Figures 6 and 8), and environmental sensors (Figure 8). The secondary broadband sensors have many applications including providing lower-noise high-frequency (>20 Hz) data, which is used by the CTBTO (Bell, 2018), enabling quality control of the station by comparing seismograms with the primary sensor (Ringler, Hagerty, et al., 2015), and providing a redundant recording in the event of primary sensor failure. As will be discussed in detail in Section 10, simultaneous recordings of local environmental conditions such as pressure and magnetic field variations can

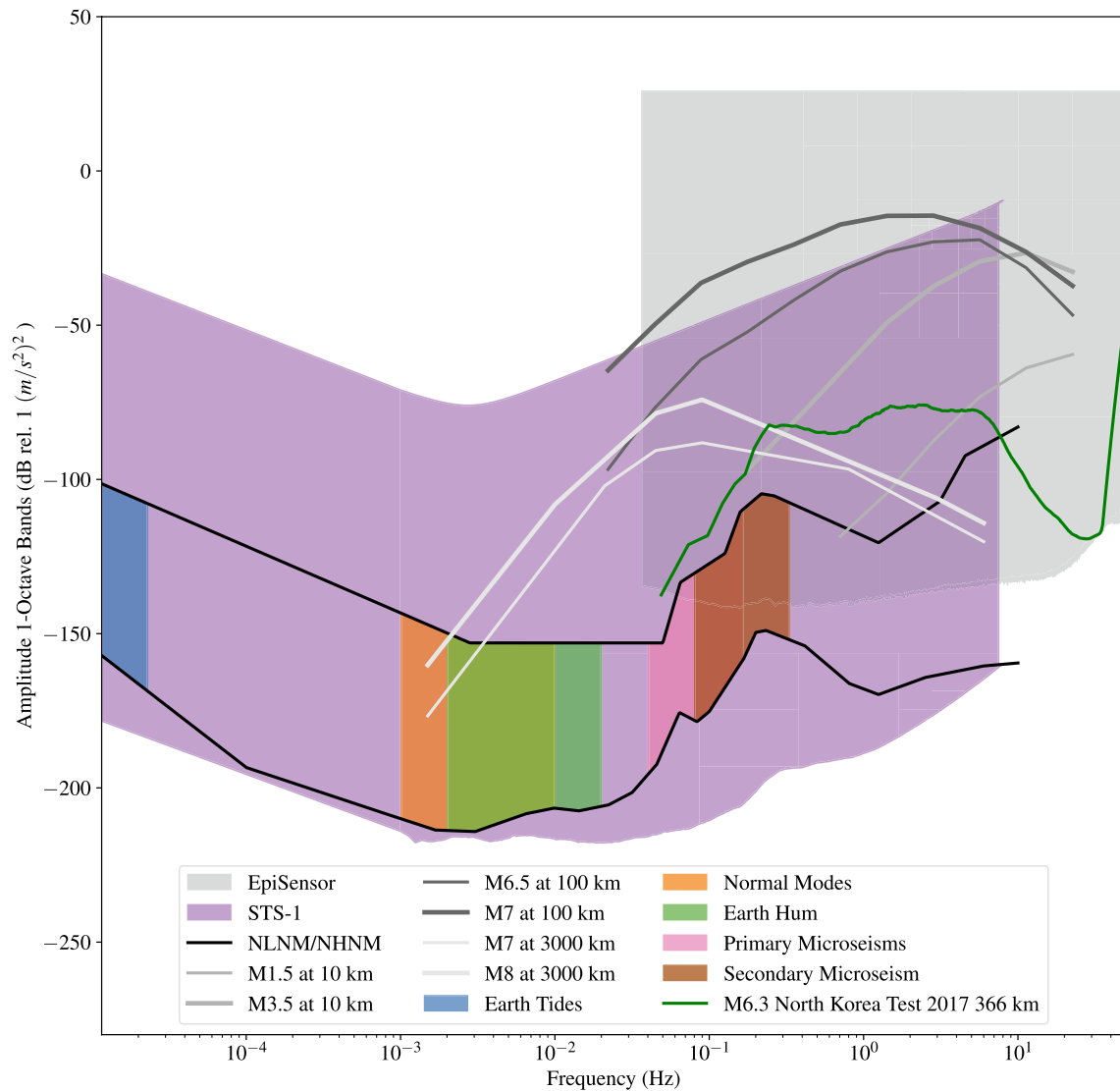


Figure 6. Fundamentals of Earth's seismic acceleration power spectral density and corresponding broadband instrumentation dynamic ranges. The effective dynamic range of the very broadband (VBB) Streckeisen STS-1 seismometer (Ringler & Hutt, 2010) is shown in purple. The effective dynamic range of the Kinematics Episensor strong motion accelerometer (Ringler, Evans, & Hutt, 2015) is shown in gray. The Peterson (1993) New Low- and High-Noise Models (NLNM/NHNM), based on global broadband seismic background observations, are shown in black. We have also included the secondary oceanic microseism region (brown), the primary oceanic microseism region (pink), the Earth hum band (green), the normal mode band (orange), and the Earth tide region (blue). Fourier amplitude spectra produced from teleseismic earthquakes observed at a range of $\sim 3,000$ km are shown in light gray, from the near-field (~ 10 km) earthquakes are shown in gray, and from intermediate distance (~ 100 km) earthquakes are shown in dark gray (Clinton & Heaton, 2002). Finally, the event Fourier amplitude spectrum from GSN station MDJ (Mudanjiang, Heilongjiang Province, China), located 366 km from the 2017 North Korea M_w 6.3 underground nuclear explosion, is shown in green.

be used to both reduce unwanted signals recorded on seismic instruments (e.g., Beauduin et al., 1996; Ringler et al., 2020) and to provide information about the elastic properties of the material in which the seismometer is emplaced (Tanimoto & Wang, 2020). The most recent equipment update to the GSN has been the incorporation of Streckeisen STS-6 and Nanometrics T-360 seismometers (Figure 7). These sensors have noise performance similar to a Streckeisen STS-1 but can be installed in both boreholes and (shallower) postholes. Borehole and posthole seismometer installation reduces both high-frequency and long-period seismic noise compared to surface vaults (Hutt et al., 2017; Ringler et al., 2019; Withers et al., 1996; Young et al., 1996) and mitigates sensor susceptibility to pressure (Alejandro et al., 2020; Sorrells, 1971) and ambient temperature (Doody et al., 2017) variations. While network operators attempt to mitigate noise by various installation methods and shielding, many stations are located in remote regions where facilities and access to infrastructure are limited (Figure 9).

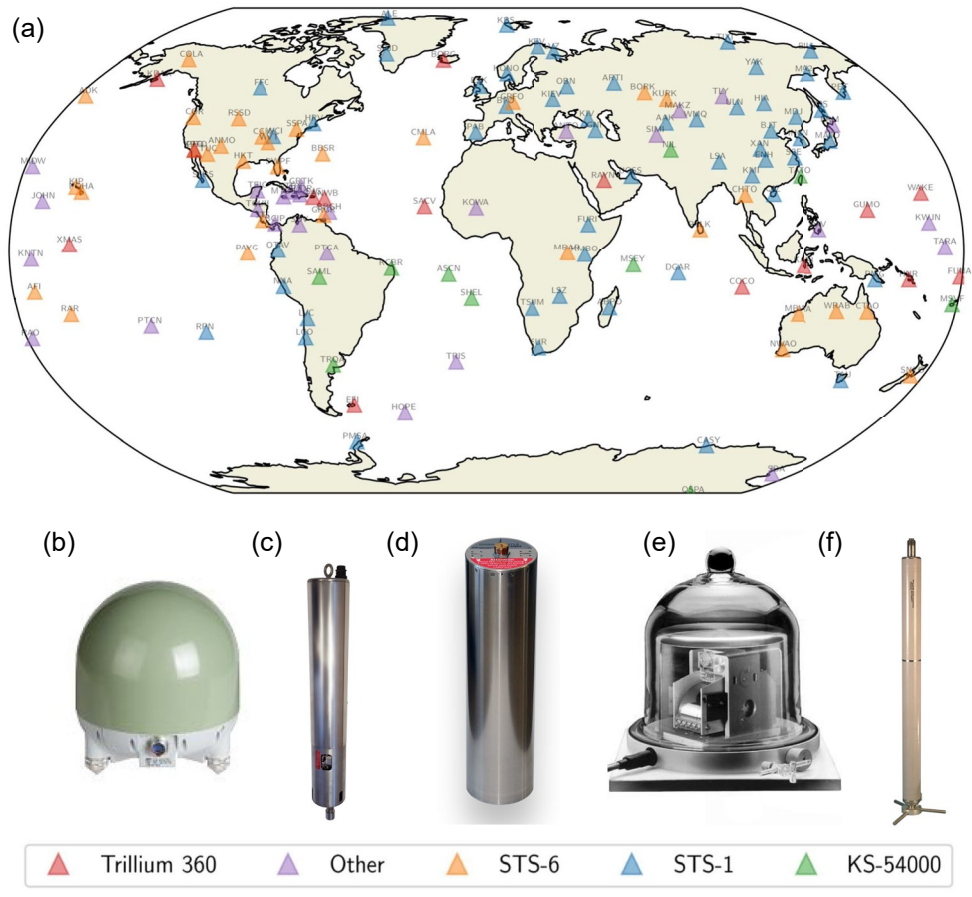


Figure 7. (a) The Global Seismographic Network as of 2021 with stations colored by primary (location code 00) sensor type. The network includes the Incorporated Institutions for Seismology (IRIS)/International Deployment of Accelerometers (network code II), the IRIS/USGS network (network code IU), the USGS Caribbean network (network code CU), and the New China Digital Seismograph Network (network code IC). (b) Nanometrics T-360 GSN sensor (red); (c) Nanometrics T-120 borehole sensor (purple); (d) Streckeisen STS-6 sensor (orange); (e) Streckeisen STS-1 sensor (blue); and (f) GeoTech KS-54000 sensor (green). These instruments range from a height of approximately 16 cm (e) to 2 m (f) and are not shown to scale. Figure modified from Ringler, Anthony, Davis, et al. (2022).

2.3. Additional Very Broadband Seismographic Network Programs

Although much of our discussion focuses on the evolution of GSNs with a view towards the seminal GEOSCOPE and the GSN, additional notable initiatives contributing to global coverage using broadband instrumentation and data exchange between various networks are now ubiquitous. These additional important contributing networks include the German GEOFON broadband network created in the 1990s with the goal to provide multi-use data and supplementing global coverage (Hanka & Kind, 1994; Hanka & Saul, 2008). Other long standing efforts include the NARS network (<https://seismologie.sites.uu.nl/research-projects/nars/>), a mobile seismographic network operated by Utrecht University, which has been operational since 1983 (Nolet & Vlaar, 1981). While instruments and deployments in the NARS network have varied through time, Streckeisen STS-2 instruments were installed as part of deployments in Baja California, Spain and Botswana. While not global in scale, the MedNet network operates approximately 36 VBB stations around the Mediterranean region utilizing Streckeisen STS-1 seismometers (Boschi et al., 1991; Mazza et al., 2008). Continental-scale efforts have also taken place, notably the efforts of AfricaArray (<https://africaarray.net/>), which now runs 30 broadband stations in 14 countries (Dirks, 2006; Nyblade et al., 2008). More recently, central Europe has been covered in seismic instrumentation during the AlpArray (<http://www.alparray.ethz.ch/>) project, with the majority (>70%) of the 628 stations that were deployed during the 2 years having corner periods at 120 s or beyond (Hetényi et al., 2018). A full description of the increasingly large number of local- to continental-scale networks and stations that are routinely accessed through

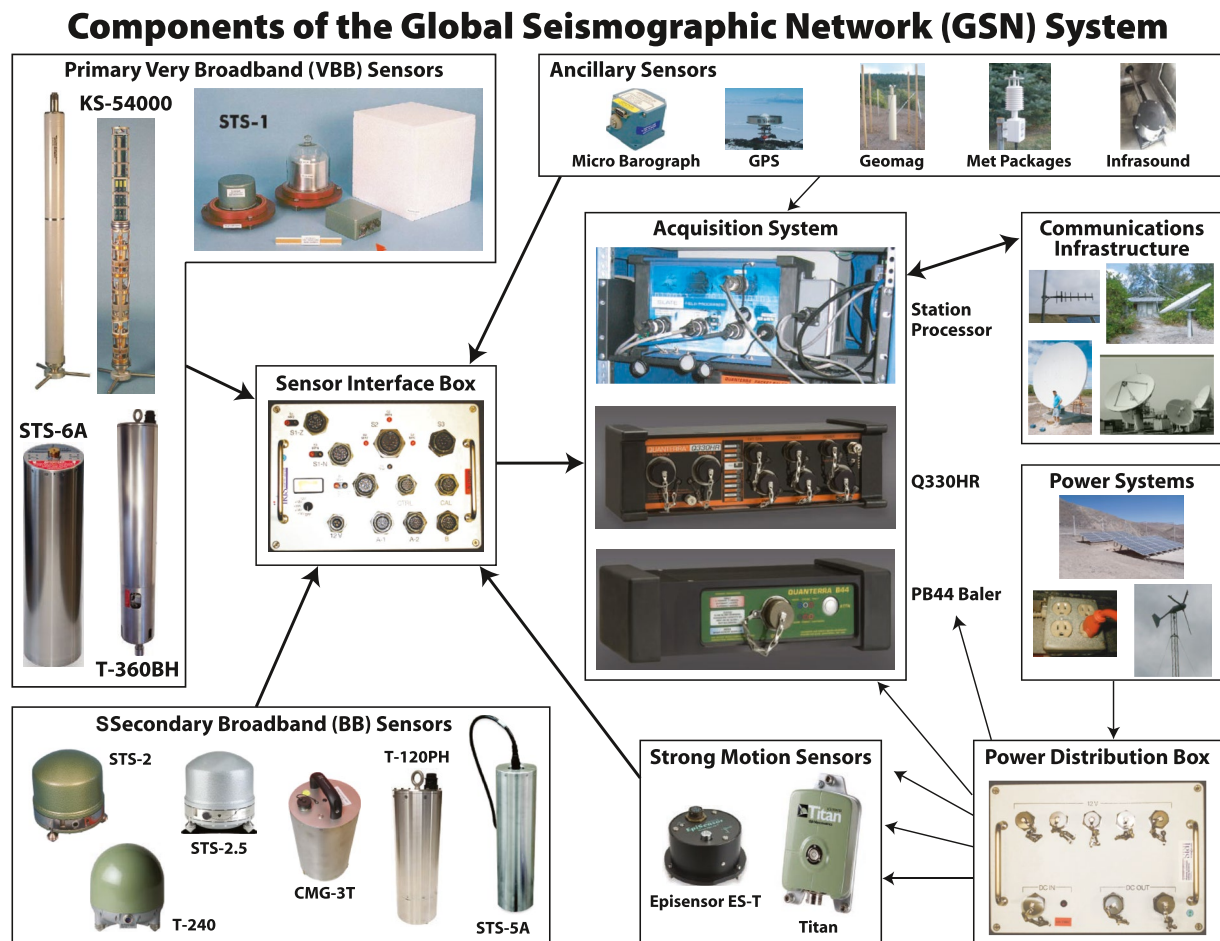


Figure 8. Current instrumentation used in the global seismographic network (GSN). The instruments in the top left are the primary sensors, while secondary sensors are shown at bottom left. In addition, all GSN stations are equipped with a strong motion accelerometer that will remain on-scale in the event of local seismic accelerations larger than ~ 0.05 g (Figure 6). All of these units are recorded on Quanterra Q330HR digitizers as shown in the middle. Many stations also have additional sensors to monitor environmental conditions as shown in the top right. Figure from Kent Anderson and Katrin Hafner; IRIS Consortium.

federated data centers and contribute to global seismic coverage and science goes beyond the scope of this work, but global seismological studies indeed utilize large amounts of openly available data acquired by both permanent and temporary broadband networks (e.g., Aster et al., 2005). In fact, international data as well as GSN data are some of the most highly requested data from the IRIS Data Management System (DMS) as shown in Figure 10.

2.4. International Community Structures

The International Federation of Digital Seismograph Networks (FDSNs; <http://www.fdsn.org/>) has played an essential role in organizing both regional and global networks and stations to advance global seismology (Figure 11), including establishing data standards, coordinating international documentation and assignment of network names, and facilitating the free and open exchange of seismic data (Suarez et al., 2008). Part of the success of the FDSN has arisen from its dedicated community leadership, its structure of voluntary and free membership, and the sustained participation of founding organizations that include the GSN, GEOSCOPE, GEOFON, and the Pacific-21.

Another contribution of the FDSN has been the adoption of the Standard for the Exchange of Earthquake Data (SEED) format (Ahern et al., 2012). The adoption of a universal format across all contributing networks has greatly improved international capabilities and allows for uniform processing and streamlined methods that avoid the need to convert to various other formats. Despite the proposal of several other data formats (e.g., Krischer et al., 2016), the SEED format has remained the standard for data archival since its inception in the 1980s. The

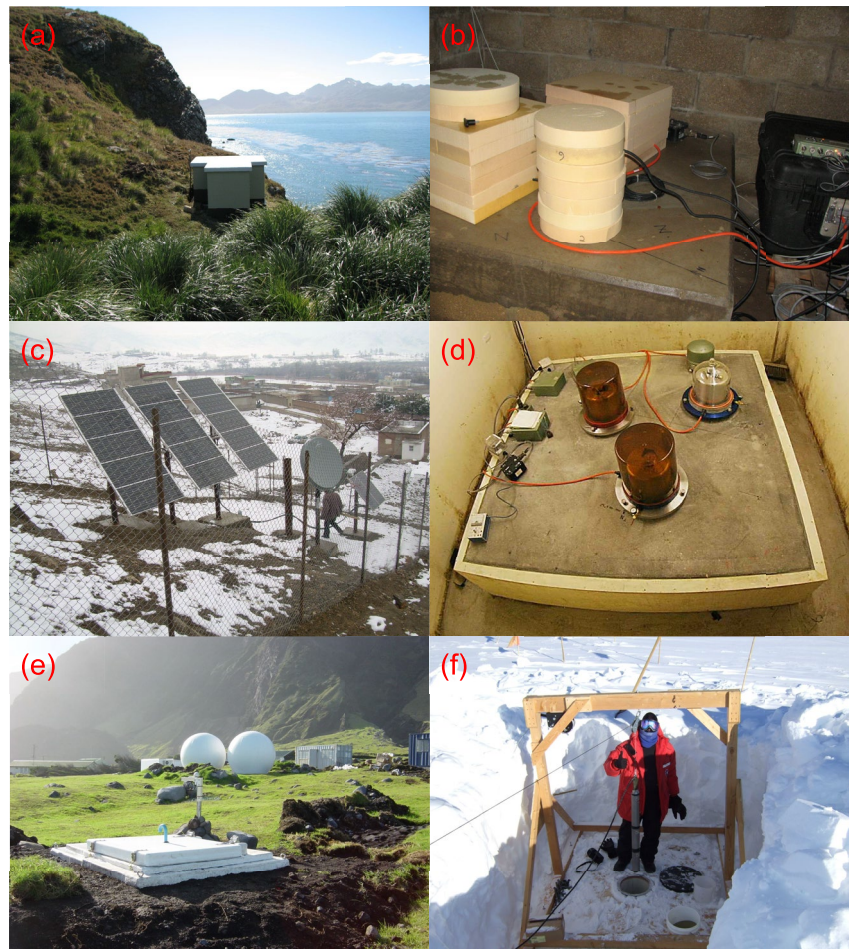


Figure 9. (a) The vault of global seismographic network (GSN) station HOPE (Hope Point, South Georgia Island). (b) The inside of the HOPE vault from panel (a). (c) The vault and solar panels for GSN station KBL (Kabul, Afghanistan). (d) The inside of the vault at GSN station CASY (Casey, Antarctica). (e) The underground vault and nearby weather station at GSN station TRIS (Tristan da Cunha). (f) Kent Anderson installing a Guralp CMG-3TB at GSN station QSPA (Quiet Zone South Pole Remote Earth Science Observatory). Panels (a and b) of this figure are courtesy of Robert Mellors IDA all other parts are public domain.

FDSN recently provided guidance via a working group for an ongoing update of the SEED format as well as a new scheme, called StationXML (<https://www.fdsn.org/xml/station/>), that will eventually expand and replace the metadata content of the longstanding SEED format.

Along with making data accessible and free to different scientific organizations, the FDSN has also provided standards for instrumentation (B. A. Romanowicz & Dziewonski, 1987; Suarez et al., 2008) as well as documentation of stations through the FDSN Station Book. This success has continued with the recent adaptation of FDSN web services for international data query and acquisition. By introducing standard protocols, international users can acquire globally distributed data and other data and metadata from 19 federated international data centers (e.g., Van Fossen et al., 2015). Along with the IRIS DMS, a few of the other federated data centers are Istituto Nazionale di Geofisica e Vulcanologia (INGV), Institut de Physique du Globe de Paris (IPGP), Eidgenössische Technische Hochschule (ETH), and Geological hazard information for New Zealand (GeoNet). Access to seismic data from Japanese stations is handled by the National Research Institute for Earth Science and Disaster Resilience (NIED) DMC, while Observatories and Research Facilities for European Seismology ORFEUS and the European Integrated Data Archive provide access to data and archived data, respectively, from seismic stations across Europe. These institutions nowadays develop the standards for data access and distribution jointly with the GSN.

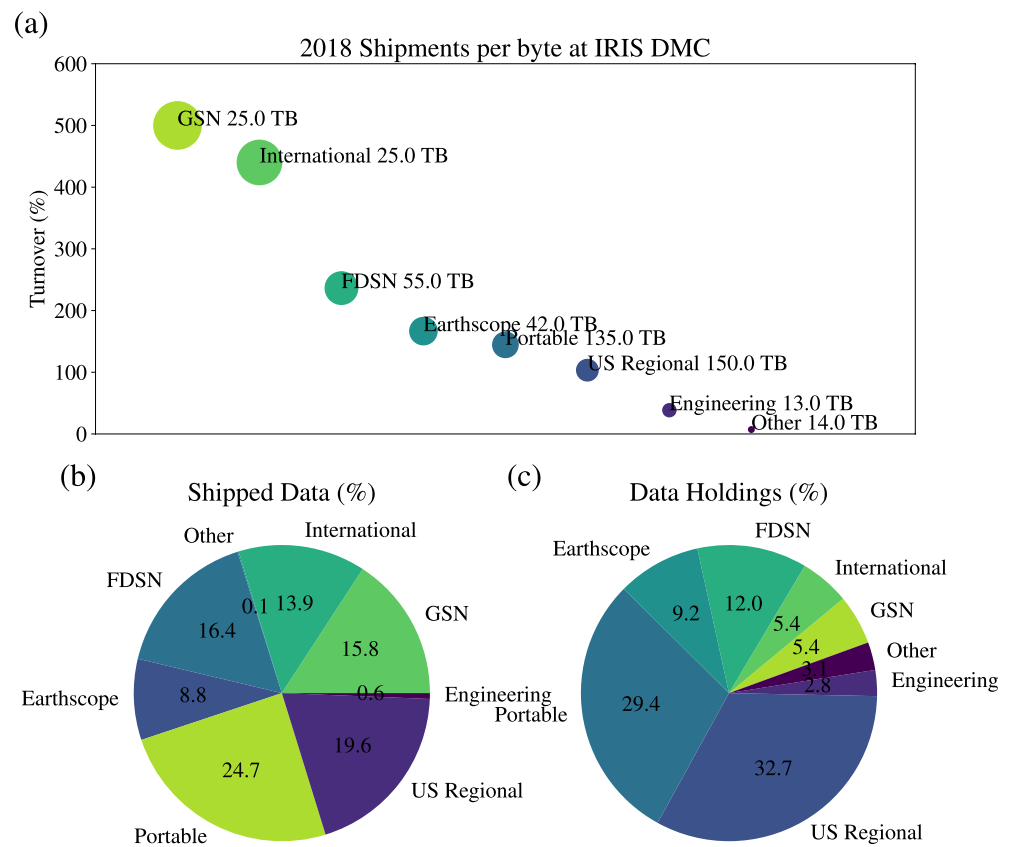


Figure 10. Shipments of data as compared to total holdings at the Incorporated Research Institutions for Seismology (IRIS) Data Management System (DMS) for 2018. (a) Turnover percentage by different data types, which data are shipped relative to total data holdings. Larger circles denote a higher percentage of requested data. (b) Total shipped data by data type. (c) Total data holdings at the DMS. This figure was adapted from Ringler et al. (2020).

2.5. Quality Control

Supporting high-quality seismic stations in remote locations requires involved operational and logistical scheduling. Budgetary constraints also require prioritizing which stations get serviced at what time. This makes remote quality control attractive to identify and troubleshoot problematic stations that require on-site maintenance. Because many stations have a long history, it can also be difficult to identify subtle issues that appear over time. This has motivated network operators to continuously refine their quality control methods as science motivates ever-increasing demands on the data.

The most basic form of quality control is identifying stations that are not providing data. Although data availability of the GSN has consistently improved over the years (Figure 12), data completeness at some locations remains relatively low compared to many short-term deployments. For example, the EarthScope USArray Transportable Array (TA) of broadband seismic stations in the United States and Canada realized greater than 98% availability (Busby et al., 2018). Attaining similar data return rates from all stations, for example, within GEOSCOPE and the GSN, is hindered by the extreme remoteness and multinational locations of many of stations, which limit the ability to rapidly perform maintenance and repairs.

Timing quality and background noise levels at a station provide two fundamental metrics for data quality. Most modern data loggers are capable of providing timing quality information that is packaged and archived with the data (Ringler, Anthony, Wilson, et al., 2021). This makes it possible to identify stations, retrospectively and in near real time, where the timing is untrustworthy and researchers can exclude these time periods from their analyses. While the magnitude of timing errors during these periods may not be known, it can often be deduced by using observations from co-located stations with independent timing systems (Ringler, Anthony, Wilson, et al., 2021) or from travel time changes associated with repeating events (Y. Yang & Song, 2020, 2021).

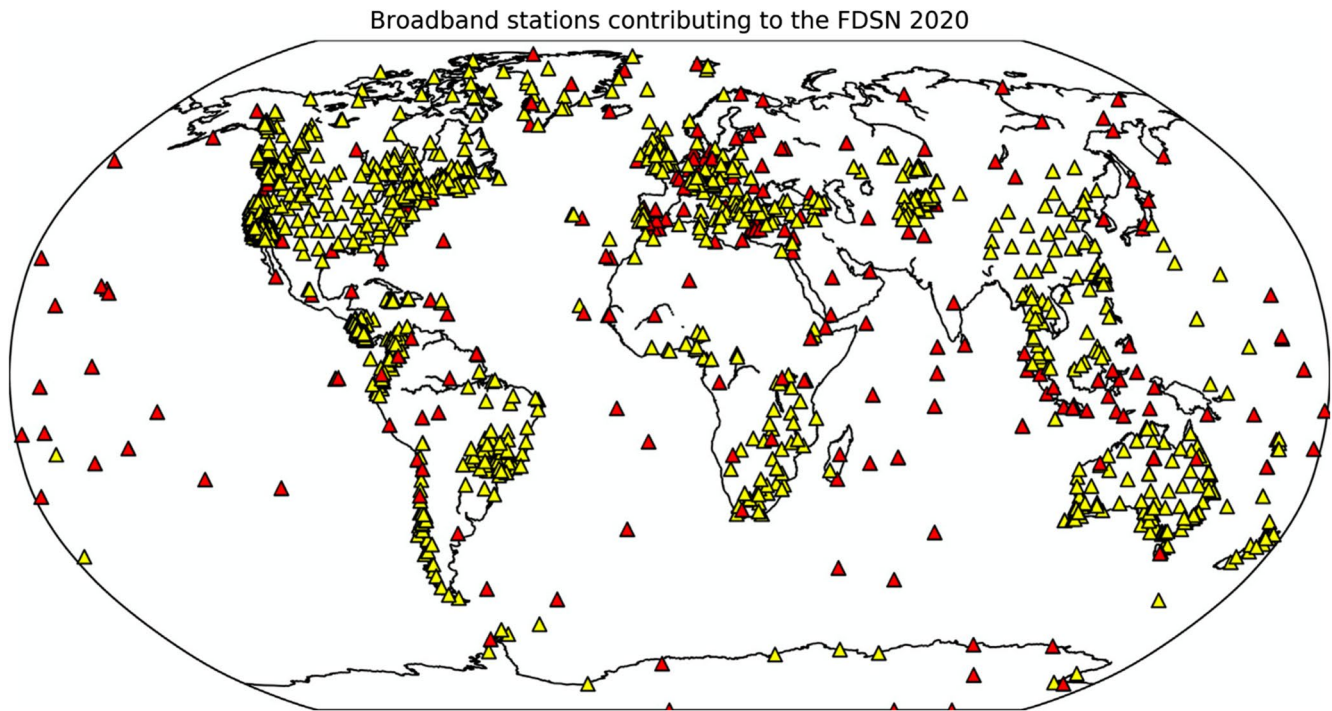


Figure 11. The Federation of Digital Seismograph Networks (FDSN) stations as of 2020. Contributions from global networks are shown in red and other regional networks are shown in yellow. From B. A. Romanowicz (2021).

Station noise levels ultimately determine the fidelity a signal of interest can be recorded at. A systematic investigation of noise levels was performed on seismic records from 1995 across GEOSCOPE (Stutzmann et al., 2000). Although many GSN stations, such as ones located on islands, have relatively high noise levels, some GSN stations consistently record some of the lowest noise levels in the world in different period bands. For example, stations like BFO (Black Forest Observatory, Schiltach, Germany) and ANMO (Albuquerque, New Mexico) provide some of the lowest noise data at periods greater than 10 s (e.g., Forbriger et al., 2021; Ringler et al., 2019). Similarly, QSPA (South Pole, Antarctica) has observed the quietest noise levels in the world at short-periods (<1 s, Anthony et al., 2021).

Berger et al. (2004) showed that the lower bound of GSN noise levels has systematically improved at periods greater than 10 s for the vertical components compared to levels attained in 1993 (Figure 13). Although station noise level improvements would be expected with improved instrumentation, the detailed characterization of noise level improvements could be dependent on the processing methods used (Anthony, Ringler, Wilson, Bahavar, & Koper, 2020). With the planned wide-scale deployment of Streckeisen STS-6 seismometers in deep boreholes, updating global seismic noise models will be an important future task as these provide fundamental quantitative benchmarks for station quality.

Timing quality and noise levels give basic information about the quality of data coming from a station, but only provide a preliminary assessment, and some modes of instrument failure or degradation will still pass these metrics. For example, Ekström, Dalton, and Nettles (2006) identified progressive changes in the long-period gain of several stations operating Streckeisen STS-1 seismometers by comparing synthetic and recorded earthquake seismograms (Figures 14a and 14b). This was surprising because it had been previously argued that the Streckeisen STS-1 seismometer only needed to be calibrated at the time of manufacturing as the electronic feedback system should be stable (Wielandt & Streckeisen, 1982).

Identifying and addressing such response changes requires more refined quality control methods than simple noise and timing quality checks. Around the same time Ekström, Dalton, and Nettles (2006) identified gain changes, Davis et al. (2005) examined GSN network calibration using the 20.5 min-period “breathing” mode, ${}_0S_0$, which has a nearly uniform global amplitude, following the M_w 9.1–9.3 Sumatra-Andaman earthquake. Although several stations were identified as likely having calibration problems, Geotech KS-54000 responses were reported

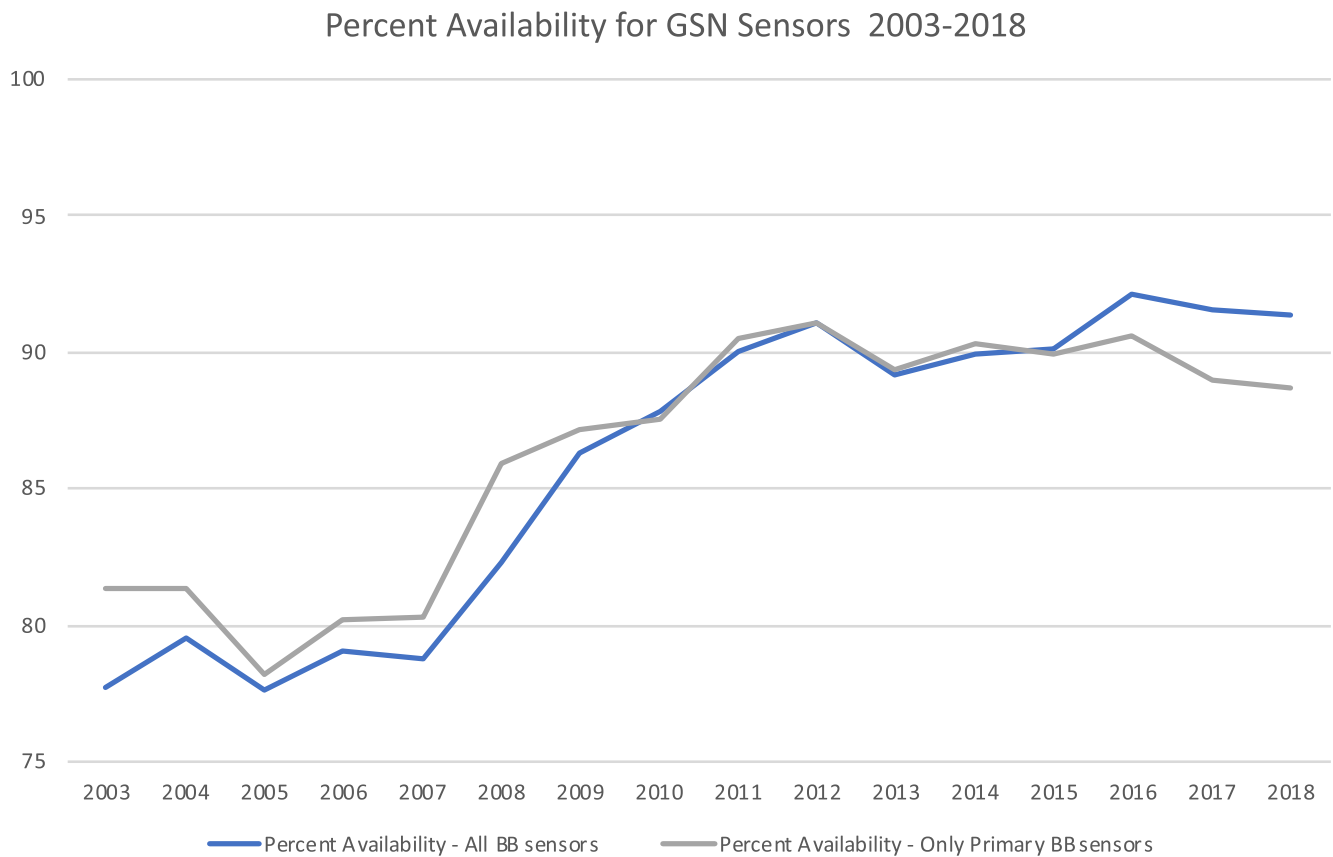


Figure 12. Data availability of the global seismographic network (GSN) from 2003 to 2018 for the primary broadband sensor (gray) and the all broadband sensors (blue). Figure produced by Katrin Hafner; IRIS Consortium.

as being stable over time and stations identified as problematic were isolated to Streckeisen STS-1 sensors. It was also not possible to identify these STS-1 gain changes using solid Earth tides (Davis & Berger, 2007). Finally, using ratios between co-located sensors at GSN sites, it was shown that the gain changes were period dependent and were consistent with an overdamped corner of the amplitude response of the Streckeisen STS-1 (Ringler et al., 2010, Figure 14b). Through engineering experiments it was shown that the cause of the Streckeisen STS-1

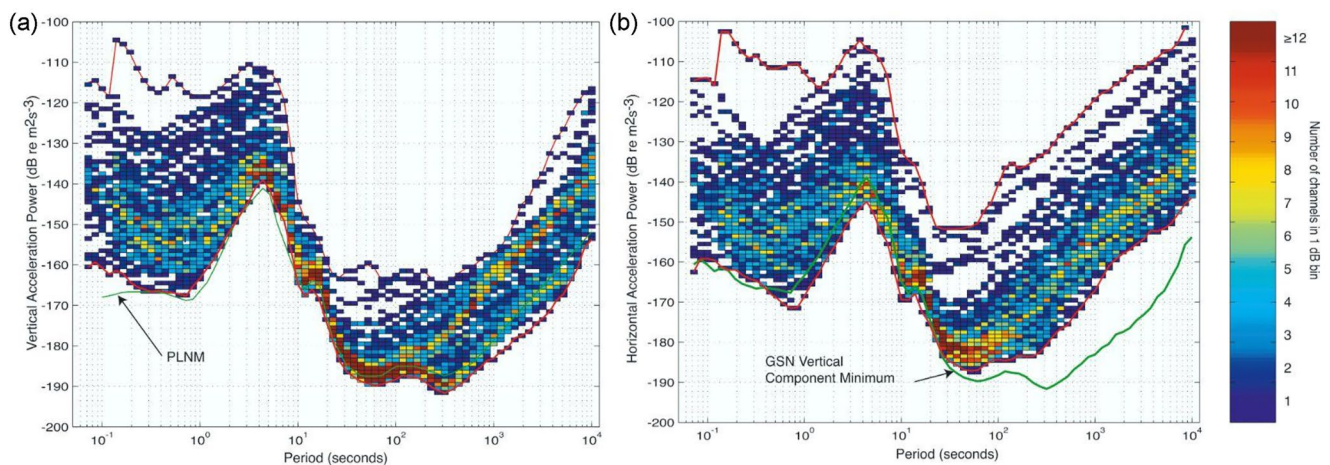


Figure 13. (a) Probability density functions (PDFs) of noise levels as a function of frequency across the global seismographic network (GSN) for 118 stations. The colors indicate how many stations' spectral estimates lie in each 1 dB by 1/14th decade rectangle. For reference the Peterson New Low-Noise Model (PNLNM; Peterson, 1993) is shown in green. Panel (b) same as panel (a), but for the horizontal components. From Berger et al. (2004).

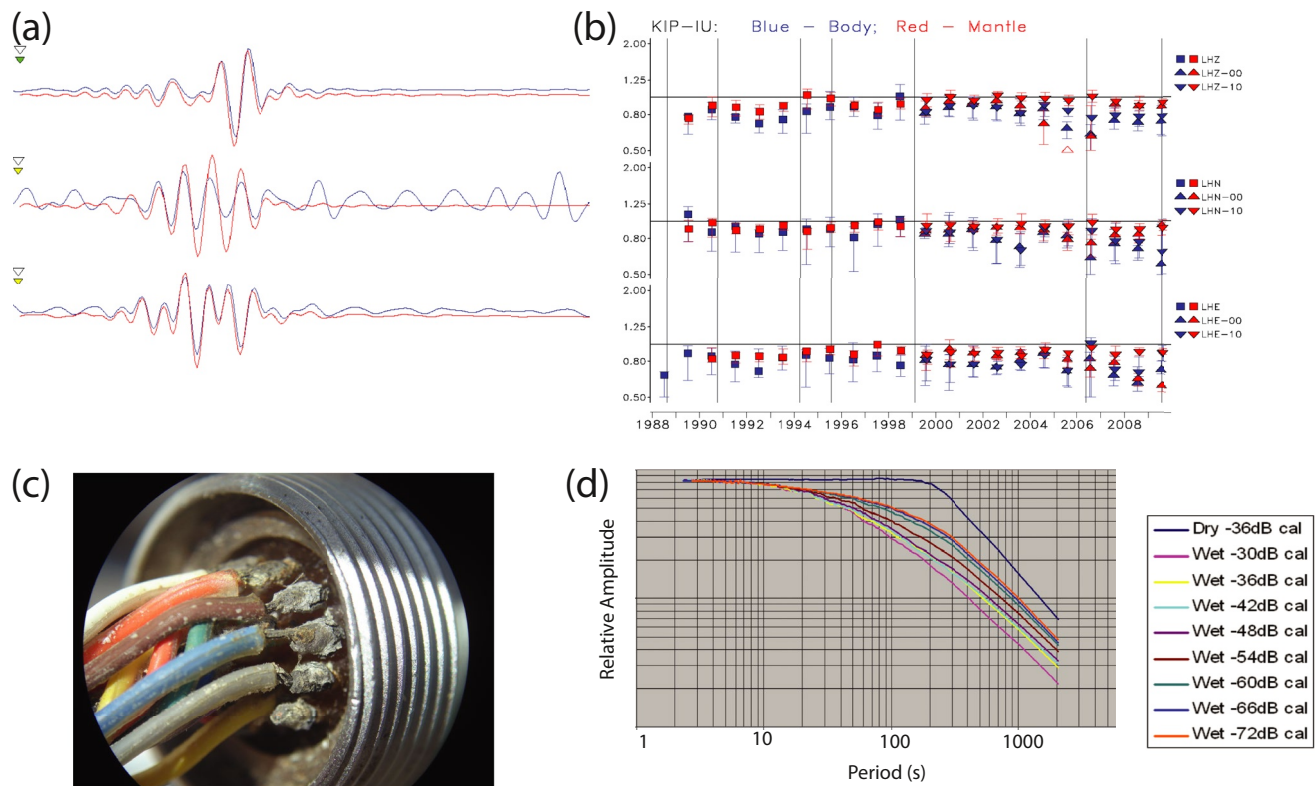


Figure 14. (a) Example comparison of a synthetic waveform (red) and data (blue) for the joint IU/G station KIP (Kipapa, Hawaii) for an earthquake on 7 April 2009. The East-West trace (second) shows a lower amplitude relative to the synthetic. (b) Synthetic amplitude comparison summary as a function of year for KIP. (c) Corrosion on the STS-1 connector at IU station KMBO (Kilima Mbogo, Kenya). (d) Amplitude response curves from the feedback electronics box at KIP using different amplitude calibration signals after the feedback electronics have been saturated by moisture resulting in loss of response. Panels (a and b) are from Ekström, Dalton, and Nettles (2006). Panels (c and d) are from Hutt and Ringler (2011).

response degradation was from corroded components within the feedback electronics boxes in high humidity environments (Hutt & Ringler, 2011; Figure 14c). That is, when the feedback electronics or connectors became saturated with moisture they would produce degraded responses, with a loss of gain at the corner frequency (Hutt & Ringler, 2011; Figure 14d). With the Streckeisen STS-1 no longer being produced this brought into question the data quality of the GSN as well as other stations operating Streckeisen STS-1 instruments.

Additional quality control issues were raised in a series of reports written by the Lamont Waveform Quality Center <https://www.ldeo.columbia.edu/~ekstrom/Projects/WQC.html>. These reports indicated that the GSN might have been failing to meet its calibration design goals (Lay et al., 2002) and ultimately identified the need to improve quality control across the network. In response, the U.S. Geological Survey (USGS) developed the Data Quality Analyzer system (Ringler, Hagerty, et al., 2015) and IRIS developed the Modular Utility for STAtistical kNoWledge Gathering system with NSF support (Casey et al., 2018). Both packages were designed around metrics that are computed daily. By analyzing various metrics over long time spans it is possible to identify both slow and abrupt changes in station performance. For example, by looking at ratios between co-located sensors it is possible to identify slow changes in the gain of one instrument (Ringler et al., 2010) as well as rapid changes resulting from an inaccurately described instrument response in the metadata (Pedersen et al., 2019). Using long time running metrics also allows station operators to refine historical metadata (W. Xu et al., 2018).

3. Global Earthquake Monitoring

The telemetry of modern global seismographic data has allowed organizations relying on these data to attain almost instantaneous global monitoring of earthquakes and nuclear events. Data contributions from stations located in remote areas of the planet where few scientific observations are available allow for better location

accuracy and magnitude estimations. The long operational history commonly shared by seismic stations in global networks and quality of data from them enable more precise and robust historical earthquake (re)locations, and improves the rapid characteristics of events today. The earthquake catalogs generated using these data provide a foundation for much seismological research.

3.1. Earthquake Detection and Discrimination

Global seismic monitoring was developed in response to three needs:

1. the detection and source characterization of large earthquakes (e.g., Nissen et al., 2019);
2. detecting and discriminating seismic sources for nuclear monitoring purposes (e.g., Alvizuri & Tape, 2018); and
3. development of a comprehensive global catalog of earthquake source parameters (e.g., Ekström et al., 2012) for seismotectonic investigations and earthquake hazards assessment research.

The same basic analytic steps are followed in each of these uses. Thus, seismic phase arrivals are commonly first detected at individual stations with transient detection algorithms, most commonly using a class of automatic seismic phase arrival time pickers known as short-term-average/long-term-average algorithms (e.g., Allen, 1978; Withers et al., 1998). This class of detectors generically relies on changes in the power ratio between short and long-term (optimally filtered) data windows, and therefore detection capabilities are dependent on the background noise level present at a given seismic station. The high-quality installations and quality control of many seismic stations in global networks (Berger et al., 2004; Peterson, 1993) makes this data particularly attractive to national agency earthquake monitoring efforts (Hayes et al., 2019).

Once automatic picks are created at a single station, picks from multiple stations are aggregated into collections associated with potential seismic sources with a minimum of false associations. This is done using a travel time associator algorithm (Yeck et al., 2019). While the nuclear monitoring community and the earthquake monitoring have similar, though not entirely overlapping, monitoring goals, approaches vary in how they leverage stations from GSNs and other regional seismic stations in their processing. For example, nuclear monitoring tends to further rely on seismic arrays (e.g., NetVisa, GA; Arora et al., 2013) with supplemental data from other globally distributed seismic stations. This is reflected in the seismic stations utilized by the International Monitoring System (IMS). Of the 50 stations in the IMS primary seismic network and 120 station auxiliary seismic network (Gaebler & Ceranna, 2021), 48 are part of the GSN or GEOSCOPE. Further details about nuclear monitoring are discussed in Sections 7.2 and 8.

The priorities of different earthquake monitoring systems and organizations vary. For example, the U.S. Tsunami Warning System uses the GSN to provide basic source parameters (location and magnitude) within about 5 min of large, potential tsunamigenic earthquakes world-wide. Complementing this work, the USGS National Earthquake Information Center (NEIC) focuses on providing rapid and accurate estimates of earthquake location, magnitude and source mechanism needed in impact assessments used by the emergency response community. NEIC also builds complete global catalogs of earthquake source parameters (complete to M 4.5) for seismic hazards assessment research and mitigation activities. The NEIC uses most of the well-calibrated, publicly available seismic stations (as of the time of this writing about 2,100 3-component seismic stations) in its response and catalog production. The GSN plays a key role by providing NEIC a globally distributed set of well-maintained and calibrated stations, which ensure generally uniform detection and response capabilities for the oceans and continents in both hemispheres. NEIC global monitoring is complemented by using the small, but important, number of globally distributed stations in the GEOSCOPE and GEOFON networks. Importantly, these GSNs operate some of the most geographically isolated stations; of the 20 most isolated stations used by the USGS NEIC in their automatic detection and association algorithms, 13 are GSN stations and 5 are GEOSCOPE stations (Figure 15). By design, these remote stations ensure rapid and accurate source characterization of earthquakes that are common in the ocean basins (e.g., subduction zones and spreading centers).

3.2. Earthquake Location

High data availability, low noise characteristics, and well constrained response information ensure the routine use of GSN data in the determination of seismic source locations, magnitudes, and seismic moment tensor solutions (Figure 16). Importantly, the GSN and its predecessor networks (e.g., WWSSN; Oliver & Murphy, 1971;

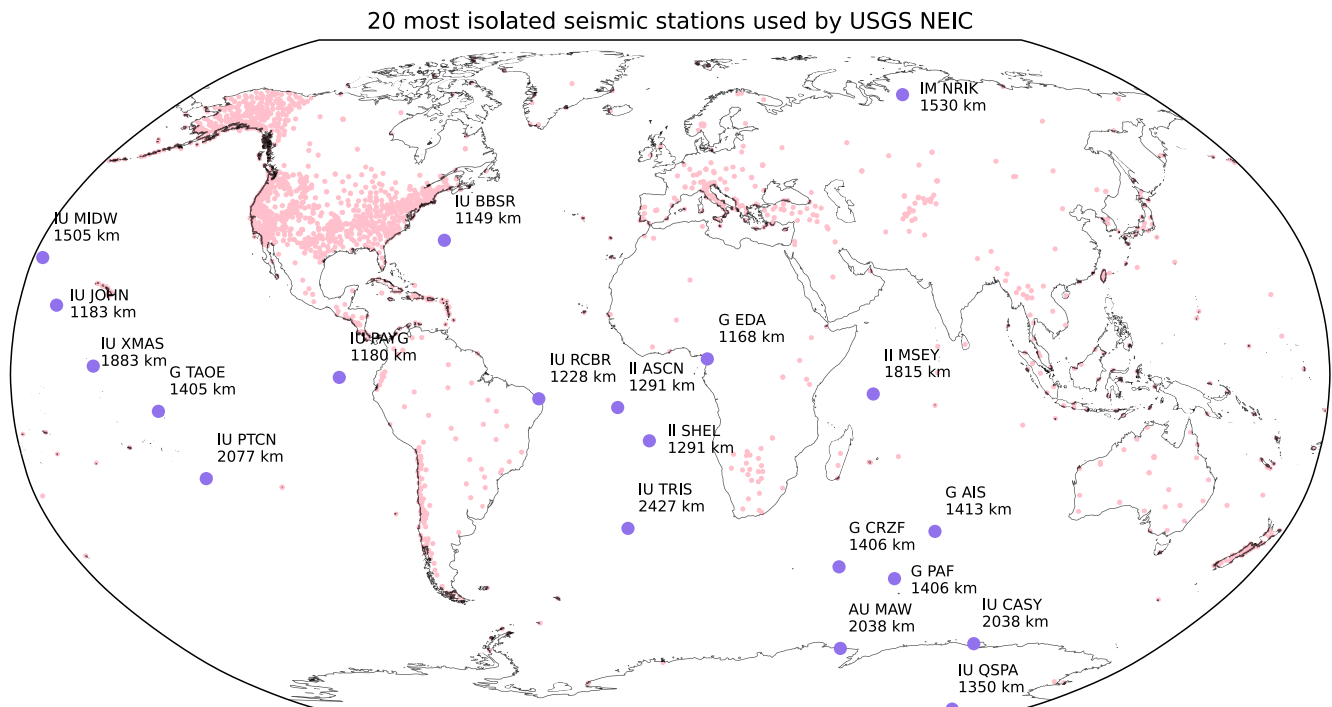


Figure 15. Map of stations used by the U.S. Geological Survey (USGS) National Earthquake Information Center (NEIC) in their automatic picking and association algorithms as of 24 June 2021. Seismic stations are shown as pink circles. The 20 most geographically isolated stations (furthest distance to a neighboring station) are highlighted as large purple circles, and the station network and name as well as distance to the next closest station are shown. The most remote station used by the NEIC is global seismographic network (GSN) station TRIS (Tristan da Cunha island).

Figure 1) provide the only consistent set of global arrival times for the last 60 years or more. Along with providing arrival times, these long running networks have enabled efforts such as the Global Centroid-Moment-Tensor Project (www.globalcmt.org). This project has focused on estimating moment tensors of $M > 5.5$ globally dating back to 1976 (Dziewonski et al., 1981; Ekström et al., 2012). This long record of recording becomes critical in reassessing older source locations in the context of newer source locations, which often have more arrival time data. This is principally due to the large increase of new local and regional seismic monitoring stations which enable arrival time picks at even finer resolution than the digital sampling rate at a single seismic station. A

Most Used Stations in Earthquake Catalogs

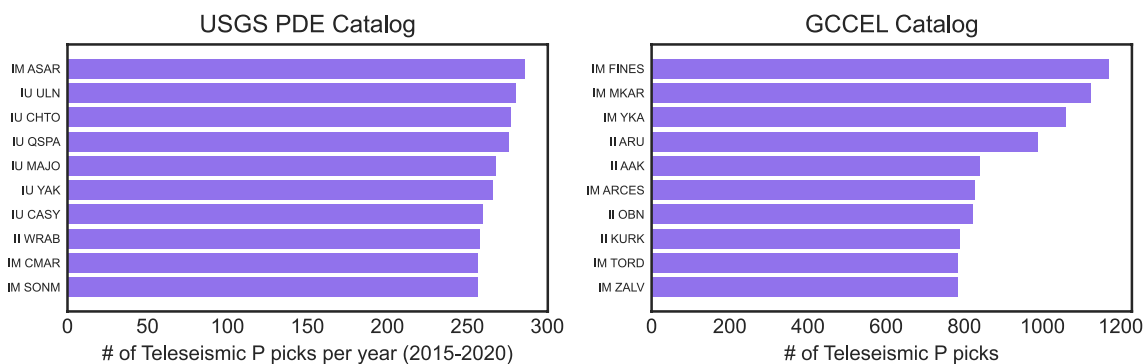


Figure 16. Ranked bar plot showing the most used stations when considering Teleseismic P picks for globally observable earthquakes ($M > 5.5$). (Left) The average number of Teleseismic P picks per year ($M > 5.5$) used in the U.S. Geological Survey (USGS) National Earthquake Information Center Preliminary Determination of Epicenters Catalog (PDE) from 2015 to 2020. (Right) The total number of Teleseismic P picks ($M > 5.5$) used in the Global Catalog of Calibrated Earthquake Locations (GCCEL).

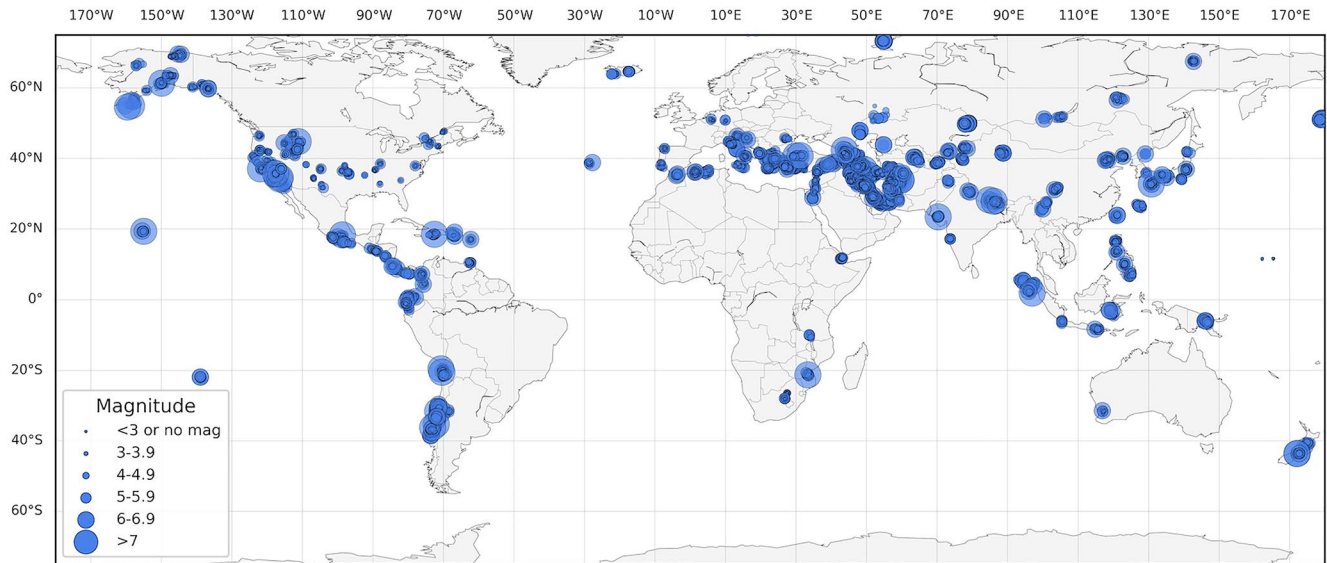


Figure 17. Calibrated earthquake relocations in the global data set of calibrated seismic source locations earthquake catalog. This is one of many earthquake relocation efforts that heavily leverages the exceptionally long observational period of global seismographic network stations to improve location estimates through joint observations.

comprehensive local or regional seismic hazards assessment often requires reexamining important historical events from the region. Such observations are best achieved using long running sites.

The NEIC has collaborated on the development of a Global Catalog of Calibrated Earthquake Locations that ensures minimally biased locations and estimates of ground truth uncertainty for all events. Thus far, 245 calibrated clusters (approximately 22,000 seismic events) have been determined using a combination of local, regional, and teleseismic arrival time data (dominated by the GSN, Figure 17). The local and regional data, often only available for more recent events, are used to develop a locally appropriate velocity model, which, in turn, results in a minimally biased initial location for a subset of seismic sources. These sources are then combined with other events and teleseismic observations. Older events often only have teleseismic observations. This process significantly improves the relative locations of all events and provides a baseline for accurately understanding systematic location bias and uncertainties of individual events. This work would be difficult to perform without the GSN, GEOSCOPE, and GEOFON networks providing a travel time link to pre-digital era stations.

Another important earthquake catalog, the ISC-GEM Global Instrumental Earthquake Catalogue (1904–2017; Di Giacomo et al., 2018; Storchak et al., 2013, 2015) represents a special effort to produce a uniform global catalog of locations for all M 5.5 and above earthquakes. This catalog of single event relocations serves as a reference for a wide range of applications that include studies of global seismicity, tectonics, Earth structure, nuclear test monitoring research and long-term hazard assessment. Like the NEIC ground truth catalog, the ISC-GEM catalog relies heavily on the fact that many GSN sites make use of vaults that were used for the WWSSN.

3.3. Operational Monitoring

Reliable moment tensor inversion (e.g., Ekström et al., 2012) and fault plane source estimation methods (e.g., Hayes, 2017) are reliant on well-distributed, well-calibrated and low noise (over a broad range of periods) stations. Consequently, the GSN is critical for the computation of NEIC moment tensor solutions and detailed earthquake source studies (i.e., “finite fault modeling”; see Section 6). Inclusions of VBB sensors at GSN stations have allowed for the development of novel and robust moment tensor techniques including those using (early arriving and up to 1,000 s period) W -phase observations (Kanamori & Rivera, 2008). Operationally, the W -phase is the standard for rapid and accurate moment tensor solutions at NEIC and within USGS-supported regional seismic networks.

M 7.2 – Nippes, Haiti

2021-08-14 12:29:08 (UTC) | 18.434°N 73.482°W | 10.0 km depth

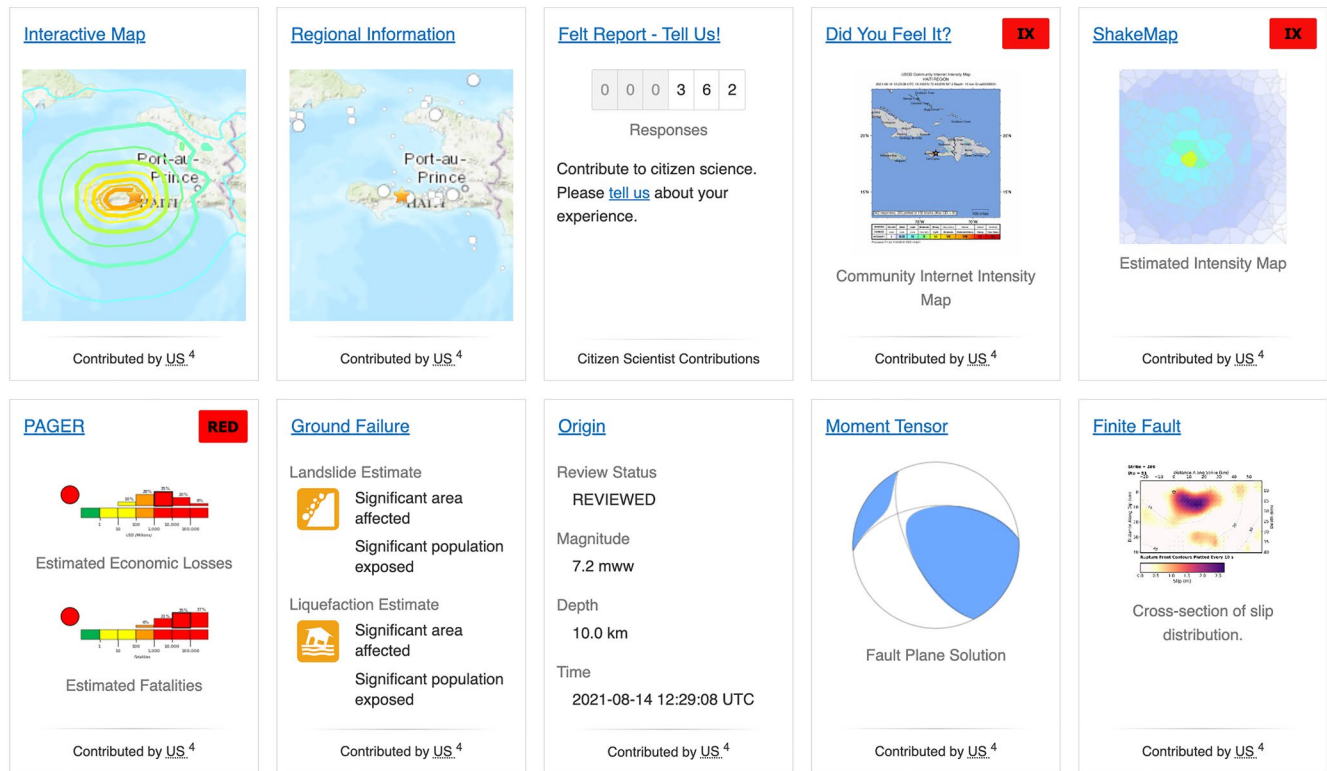


Figure 18. U.S. Geological Survey Event Page for August 2021 M7.2 Haiti earthquake. The event page rapidly disseminates key information about an earthquake including (clockwise from top left) hypocenter location, community felt reports of shaking, modeled shaking intensity, estimates of economic loss and fatalities, landslide and liquefaction hazard estimates, moment tensor solution, and a model of rupture. Figure from <https://earthquake.usgs.gov/earthquakes/eventpage/us6000f65h/executive>.

The data of the GSN and the complementary GEOFON and GEOSCOPE networks ensures that monitoring agencies like the NEIC can routinely and uniformly report W -phase magnitudes and mechanisms for all M_w 5.8 or larger events worldwide. This data also enables other projects to provide long running collections of event parameters (e.g., Lamont's Global CMT project provides focal mechanisms dating back to 1976 Dziewonski et al., 1981; Ekström et al., 2012). The European-Mediterranean Seismological Centre collects and distributes moment tensors from a number of other contributing monitoring agencies (Godey et al., 2013). The low-noise characteristics and long-period stability of GSN stations enables NEIC to routinely compute detailed earthquake source studies, such as “finite fault solution,” discussed in Section 6 for most shallow M_w 7 or larger events worldwide. Long-term high-quality catalogs of earthquake source parameters and kinematic descriptions of the rupture process enables scientist to better understand the physics of earthquakes. This leads to better seismotectonic characterization and associated seismic hazard assessment. Operational monitoring efforts has allowed for a number of routinely produced products such as the Prompt Assessment of Global Earthquakes for Response which enables emergency managers to get a quick estimate of the amount of damage and loss of life for a particular earthquake (Wald et al., 2010). Additionally, the hazard presented by landslides or liquefaction induced by the earthquake is characterized. Figure 18 illustrates how all of this information is rapidly disseminated to the public (2021 M 7.2 Haiti Event shown) on the U.S. Geological Survey's event page <https://earthquake.usgs.gov/earthquakes/eventpage/us6000f65h>.

4. Very Broadband Seismic Observations

Due to their global coverage and sensitivity across a broad range of frequencies, GSNs provide data sets that underpin tomographic imaging of whole Earth structure (for a recent review of tomography, see Ritsema and Lekić (2020)). Most studies further supplement these stations with regional networks to improve coverage. The low-noise and high-fidelity of GSN and GEOSCOPE recordings are crucial to estimating attenuation and detecting arrivals of deep Earth phases. The longevity of GSN and GEOSCOPE stations enables both the mapping of difficult-to-measure parameters like anisotropy, which can inform models of flow in the mantle (Montagner & Tanimoto, 1991), and the use of (auto)-correlation techniques for extracting subtle and time-varying signals.

Figure 19 shows the acceleration spectrum taken from the vertical component of the primary sensor at GSN station HRV (Adam Dziewonski Observatory, Massachusetts, USA) over a time window of 240 hr following the 2011 Tohoku earthquake. The spectrum spans five orders of magnitude in frequency. The largest signals lie in the tidal band and are associated with the diurnal and semidiurnal solid Earth tides. The lower left inset shows clusters of harmonics around 12 hr (0.023 mHz) and 24 hr (0.011 mHz) resolved by analysis of a longer, 60-day time span. At the other end of the seismic spectrum, teleseismic body waves (~0.1 to 1 Hz) would plot just off of the far right side of Figure 19.

Here, we discuss seismic observations that can be used to infer Earth structure, treating standing waves and traveling waves separately, due to the different methods that are used for their analysis, and focusing on the role of permanent, high-quality global networks, including the GSN and GEOSCOPE.

4.1. Normal Modes

At periods shorter than ~1 hr a forest of spectral peaks is visible, corresponding to the free oscillations (*normal modes*) of the Earth, with an example shown in Figure 19a. Because normal mode oscillations occur at periods of tens of minutes (Figures 6 and 19) and seismic data tends to become noisy at these periods (e.g., Peterson, 1993), exceptionally low station noise levels are required to observe them. Therefore, most normal mode studies heavily utilize observations from the GSN, GEOSCOPE, and other VBB stations.

Two different types of normal modes exist: (a) spheroidal modes, which involve vertical and horizontal motion, and (b) toroidal modes, which involve horizontal motions only. Spheroidal mode multiplets ${}_nS_l$ and toroidal mode multiplets ${}_nT_l$ are characterized by their radial order n and angular order l . Each multiplet consists of $2l + 1$ singlets with azimuthal order m with the same degenerate resonance (or center frequency). To account for the effects of lateral structure, rotation, and anelasticity, perturbation theory is typically applied, which predicts the splitting of spectral peaks into singlets relative to a background reference, 1D Earth model (typically, the radially varying preliminary reference Earth model [PREM]; Dziewonski & Anderson, 1981). For a comprehensive overview of this theory, see Dahlen and Tromp (1998) and Woodhouse and Deuss (2015).

Normal mode perturbation theory is often formulated by coupling modes with respect to the 1D Earth, where the coupling strength depends on lateral heterogeneity, spatial wavelengths, and on specific modes. Several levels of coupling approximation may be considered: self-coupling, narrow-band coupling, and full coupling. The first approximation accounts for coupling within an isolated multiplet only, which limits one to only consider even-degree structure in the Earth. The splitting of a given mode is conveniently described by the splitting function (Giardini et al., 1987), which may be thought of as the integrated effect of lateral Earth structure on a particular normal mode. By taking broadband seismic spectra one may employ a two-step procedure to determine splitting functions of individual modes, which can then be combined to constrain mantle structure in tomographic inversions (Giardini et al., 1988; Ritzwoller et al., 1986).

These standing waves possess distinct sensitivities to density, rigidity, and incompressibility across different depth regions within the Earth (Figure 19b through Figure 19g). Modal peaks undergo splitting (Woodhouse & Dahlen, 1978) in frequency due to the Earth's ellipticity, rotation, anisotropy, and lateral variations in structure; the middle inset shows the five singlets of the ${}_0S_2$ multiplet (Roult et al., 2006). This so-called “football” mode has a sensitivity kernel very similar to that of solid Earth tides (Figure 19b), while the nearby “breathing” mode, ${}_0S_0$, has strong sensitivity to P -wave velocity throughout the Earth (Figure 19c). Other selected modes highlight different regions of sensitivity: ${}_3S_2$ provides information regarding inner core S -wave velocities while ${}_7S_5$ is influenced by P -wave velocity in the outer core. Stoneley modes of the core are a special subset of normal modes

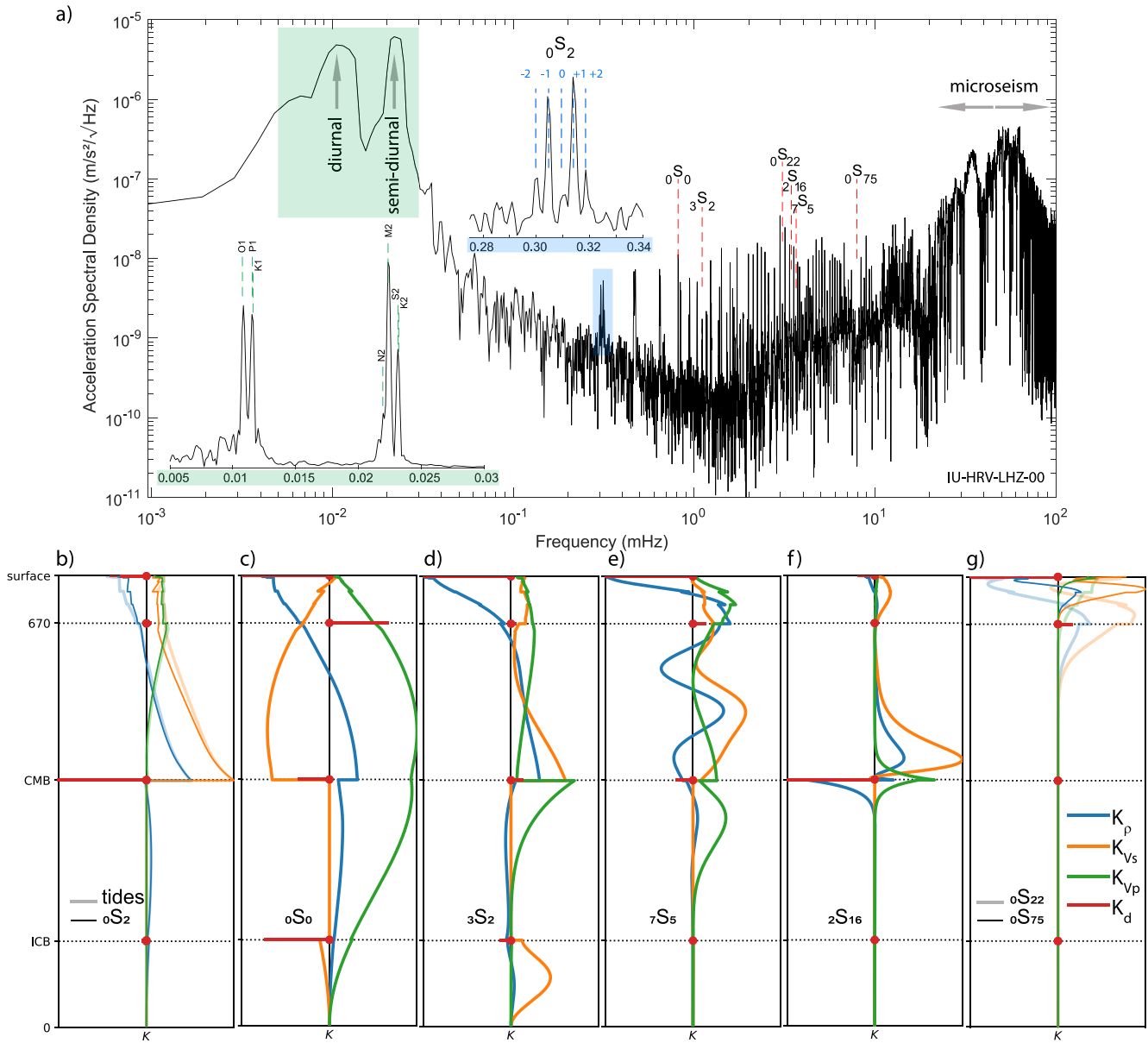


Figure 19. (a) Acceleration spectral density for the vertical component of the primary sensor at Global Seismographic Network station HRV (Massachusetts, USA), computed from 10 days of data starting at the time of the 2011 M_w 9.0 Tohoku earthquake. Dashed red lines denote frequencies of selected normal modes. The left inset, computed from a longer, 60-day time span, shows peaks corresponding to various tidal components. The right inset shows the fine structure of ${}_0S_2$, with singlet frequencies corresponding to $m < \ell$ (where m and ℓ are the spherical harmonic order and degree, respectively) measured by Roult et al. (2006) marked by blue dashed lines. (b) Sensitivity kernels for degree-zero perturbations of density, V_s , V_p , and discontinuity topography computed for degree-two tidal forcing and ${}_0S_2$. Panel (c–f) same as panel (b), but for modes ${}_0S_0$, ${}_3S_2$, ${}_7S_5$, and ${}_2S_{16}$ (tides not shown). Panel (g) same as panel (b), but comparing the sensitivity kernels of Rayleigh-wave equivalent modes ${}_0S_{22}$ and ${}_0S_{75}$.

whose energy is trapped along the core-mantle boundary (Stoneley, 1924), making these modes very sensitive to the deepest part of the mantle and the uppermost outer core (e.g., note the kernel for Stoneley mode ${}_2S_{16}$ in Figure 19). Fundamental branch modes at high frequencies are most sensitive to upper mantle structure, with modes being equivalent to Rayleigh waves with specific periods (e.g., ${}_0S_{22}$ and ${}_0S_{75}$ correspond to Rayleigh waves at ~ 325 and ~ 125 s [Figure 19g]).

Observations of normal mode degenerate frequencies have been made since the great (M_w 9.5) 1960 Chile earthquake struck (Benioff et al., 1961; Pekeris et al., 1961), just as algorithms to theoretically compute these frequencies started to exist. Several large earthquakes occurred in the 1960s while the WWSSN was in operation, leading

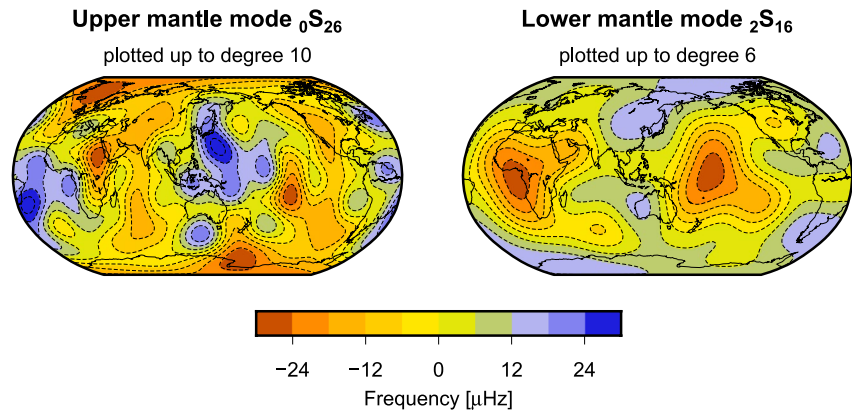


Figure 20. Splitting function maps of upper mantle mode ${}_0S_{26}$ and lower mantle mode ${}_2S_{16}$, which were measured jointly using 124 GSN stations (Koelemeijer et al., 2013). The frequency variations are due to lateral variations in Earth structure, as described by the sensitivity kernels (e.g., Figure 19). Although these maps resemble mantle tomography models, we have to remember that the variations are due to not only velocity, but also density and topography on internal boundaries.

to many further observations of mode resonance frequencies (summarized by Derr (1969)). Continued developments in both theory and the observations of long-period spectra facilitated by the GSN have given rise to large data sets of degenerate frequencies (e.g., T. Masters & Widmer, 1995) that underpin the development of 1D reference Earth models (particularly constraining density) (Dziewonski & Anderson, 1981; De Wit & Trampert, 2015; Irving et al., 2018; Montagner & Kennett, 1996) and have provided evidence of inner core solidity (Dziewonski & Gilbert, 1971).

Normal mode splitting observations were also made as early as the 1960s (Benioff et al., 1961), leading to early insights into aspherical Earth structure (G. Masters et al., 1982). Many studies set out to estimate normal mode splitting in the last century, which led to the development of splitting function databases, obtained using either iterative least squares inversion of spectra or multiplet stripping (e.g., G. Masters, Laske, & Gilbert, 2000; Woodhouse & Giardini, 1985; Resovsky & Ritzwoller, 1998; Ritzwoller et al., 1986). While most of these focused on self-coupled spheroidal mode splitting functions, Resovsky and Ritzwoller (1998) also estimated cross-coupled splitting functions that provide insights into odd-degree structure as well as toroidal mode splitting functions. Due to advances in data quality and the number of available stations, renewed efforts in the last decade have produced data sets of normal modes with higher frequency and more sensitivity to P -wave velocity (Deuss et al., 2013), as well as anelastic Earth structure (Mäkinen & Deuss, 2013) and lower mantle density (Koelemeijer et al., 2013). The stations of the GSN play a crucial role in our ability to make accurate measurements of normal mode splitting (i.e., with low uncertainties), with for example, data from 124 GSN stations used for the splitting function measurement of ${}_2S_{16}$ (Figure 20), an important Stoneley mode for constraining lower mantle density (Koelemeijer et al., 2013).

4.2. Surface Waves

Surface wave observations are for good reason heavily relied upon in studies imaging the Earth's crust and upper mantle (e.g., B. Romanowicz, 2002). The frequency-, polarization-, and directional-dependence of their propagation enables seismologists to estimate 3D velocity variations and map radial and azimuthal anisotropy. While velocity variations are directly linked to temperature and compositional variations associated with mantle convection, anisotropy provides a time-integrated measurement of strain (e.g., Park & Levin, 2002). Because they attenuate more slowly with distance than body waves and are strongly excited by Earth's frequent shallow earthquakes, the global ubiquity and strength of surface waves enables studies of crustal and upper mantle structure unrivaled using other methods, in particular below oceans devoid of seismic stations.

At increasing periods, surface waves become sensitive to increasingly deeper structures. This can be seen by comparing the sensitivity kernels of Rayleigh-wave equivalent modes (fundamental branch) at ~ 125 s (mode ${}_0S_{75}$) and ~ 325 s (mode ${}_0S_{22}$) in Figure 19g. The sensitivity of ${}_0S_{75}$ is constrained to the upper 200 km of the Earth while ${}_0S_{22}$ can sample transition zone structure at 410–660 km depth. Overtone branches provide sensitivity to

greater depths even at shorter periods (e.g., Ritsema et al., 2004), they are more difficult to analyze, requiring either non-linear inversion of the interference pattern of multiple overtone branches (e.g., Beucler et al., 2003; Visser et al., 2007), or iterative stripping procedures (van Heijst & Woodhouse, 1997). This results in generally higher measurement uncertainty compared to fundamental mode surface waves (for a recent comparison, see Moulik et al. (2022)).

Estimating the extent of isotropic structure below the so-called “heterosphere” (the upper 200–250 km of Earth; Dziewonski et al., 2010) requires observations at periods longer than 200 s, which are typically possible only at low-noise installations of VBB instruments. This is true whether the data are analyzed in the frequency domain through measurements of peak shifts (i.e., standing waves) or in the time domain through phase velocity measurements (i.e., traveling waves). When mapping radial anisotropy variations, long period observations are crucial even within the heterosphere. This is because mapping radial anisotropy requires the simultaneous inversion of Love and Rayleigh waves, and the sensitivity of Love waves is shallower than that of Rayleigh waves at a given period. As for mapping azimuthal anisotropy, excellent global azimuthal coverage is required (Montagner & Tanimoto, 1991; Tanimoto & Anderson, 1985). The azimuthal coverage is often improved using additional globally distributed stations from various regional networks.

Because seismic attenuation and velocities are affected differently by temperature, composition, and the presence of volatiles, attenuation estimates provide complementary information about the structure and dynamics of the mantle. Attenuation and lateral gradients of velocity, which can produce (de)-focusing (Woodhouse & Wong, 1986), both affect amplitudes of surface waves. Therefore, reliable measurements of amplitudes are crucial for mapping both attenuation and small-scale velocity variations, and for distinguishing between their competing effects. While the latest attenuation tomography models (see Dalton et al., 2008; H. Zhu et al., 2013; Karaoğlu & Romanowicz, 2018b) have higher resolution than the first models (B. Romanowicz, 1990), they continue to rely heavily on data from the GSN and GEOSCOPE. Indeed, modeling of amplitudes when mapping attenuation variations can identify station calibration issues (Ma et al., 2016), and such issues can introduce errors into models of attenuation (Ringler, Anthony, Dalton, & Wilson, 2021).

The generally poorer path coverage of surface wave data sets in the southern hemisphere can be remedied by including major-arc phases and measurements of surface wave trains that have circled the planet more than once (i.e., higher-orbit phases) (see Moulik et al., 2022). Relative amplitude changes between higher-orbit trains were used to construct the first tomographic models of upper mantle attenuation (e.g., B. Romanowicz, 1990). Reliable measurements of higher-orbit trains are typically feasible only at periods >150 s (e.g., Ekström, 2011). This is yet another reason that high-fidelity long-period observations are important for surface wave-based studies of structure.

Well-calibrated instrument responses, low-noise installations, and accurate sensor orientations are required to accurately measure the frequency-dependence of Rayleigh wave ellipticity (e.g., Ferreira & Woodhouse, 2007) and to reliably estimate the actual arrival angle of surface waves (e.g., Laske, 1995). Although most global tomographic inversions assume an arrival angle along the great circle path between the source (earthquake) and seismic station, using arrival angles that often deviate from this path can yield higher-resolution estimates on mantle velocity structure (e.g., Yoshizawa et al., 1999), and can help in estimating azimuthal anisotropy (Laske & Masters, 1999). Recently, Magrini et al. (2020) showed that corrections for deviations of arrival angles from the expected path are needed to reconcile phase velocity measurements from ambient noise correlations to those obtained with earthquake waveforms. Rayleigh wave ellipticity measurements can be inverted for profiles of shear wave speed beneath stations (Yano et al., 2009), and are routinely utilized in joint inversions (e.g., Lin et al., 2012). Their incorporation into global tomographic inversions can benefit from more realistic sensitivity kernels, which are needed to prevent spurious low velocity zones that can appear in joint inversions for velocity profiles (Maupin, 2017).

Strong lateral gradients in upper mantle anisotropy can convert long-period (100–200 s) Love waves to Rayleigh waves (Park & Yu, 1993); observations of this converted energy on the vertical component continue to be used to map out abrupt variations in anisotropy (e.g., Eakin, 2021; Levin & Park, 1998). At longer periods, coupling due to anisotropy can be studied in the frequency domain, and enables the probing of anisotropy at greater depths, particularly the transition zone (e.g., Beghein et al., 2008; Hu et al., 2009).

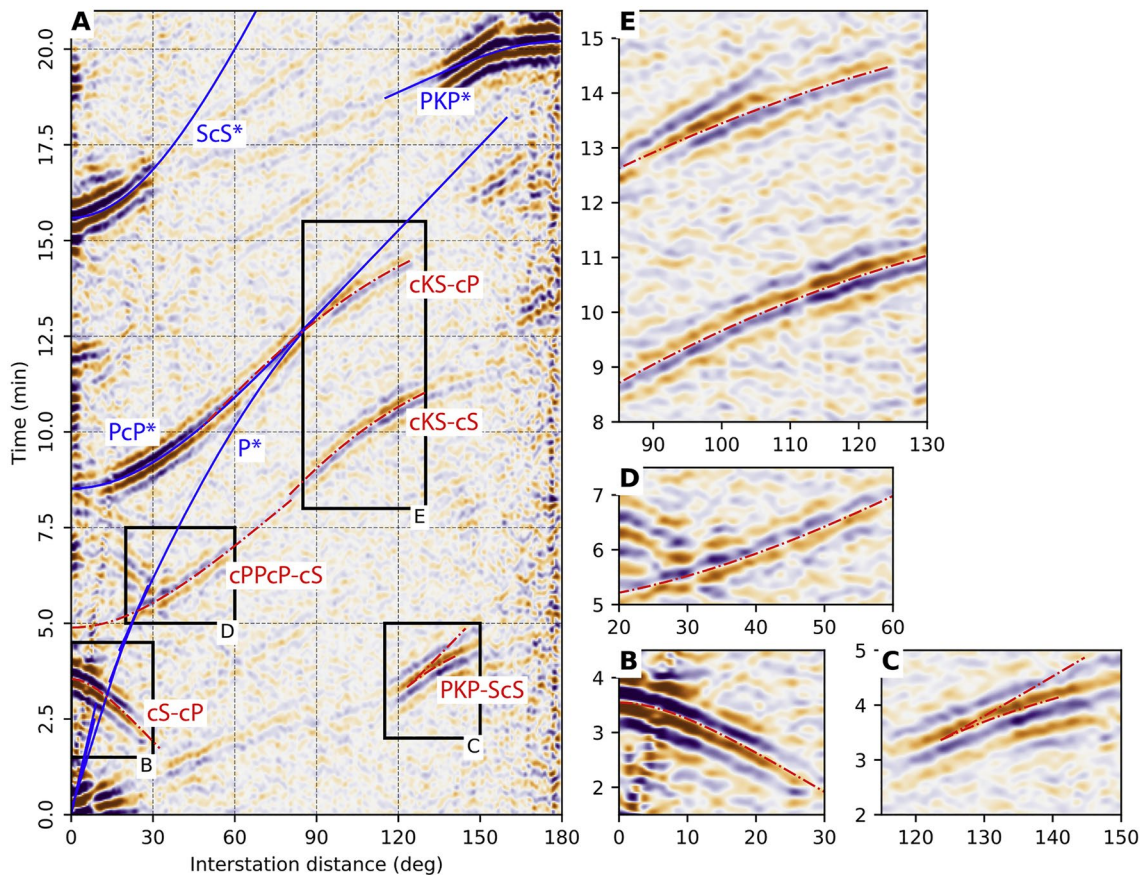


Figure 21. (a) The first 20 min of an observed cross-correlogram showing non-causative and causative (resembling regular phases from the seismic traveltime stacks) features in the Earth's correlation wavefield. The non-causative features are shown in red and the features resembling regular seismic phases are shown in blue. Enlarged sections showing: (b) *cS-cP*, (c) *PKP-ScS*, (d) *cPPcP-cS*, and (e) *cKS-cP* and *cKS-cS*. From Tkalčić et al. (2020), which was adopted from Pham et al. (2018).

4.3. Body Waves

Although *body wave* arrivals can be detected with temporary seismometer deployments, permanent networks like the GSN and GEOSCOPE provide a number of unique capabilities that continue to enable imaging of deep Earth structure. Indeed, GSN data contributes prominently in claims of detection of elusive seismic phases such as the *PKJKP* (inner core shear wave phase; Deuss et al., 2000; Julian et al., 1972; Okal & Cansi, 1998), which remains controversial (e.g., P. M. Shearer et al., 2011). They are also a major constituent of travel time data sets of core phases, which have enabled regional imaging of isotropic and anisotropic structure (e.g., Irving, 2016), tomography (Burdick et al., 2019; Pejić et al., 2017), and inferences of inner-core growth (e.g., Frost et al., 2021).

The advent of correlation-based techniques that extract body wave arrivals from seismic coda (Campillo & Paul, 2003) has provided a new means of studying differential travel times between pairs of seismic phases that are not readily identified with traditional methods (for a recent review, see Tkalčić et al. (2020)). These techniques are analogous to those based on cross-correlations of ambient noise recordings (e.g., Shapiro & Campillo, 2004). Though an early focus has been on identifying inner core phases with regional arrays (e.g., H.-H. Huang et al., 2015) as well as globally distributed seismic data (e.g., Tkalčić & Pham, 2018), the techniques can contribute to deep Earth imaging by providing new estimates on differential travel times of phases reverberating between and converting across mantle interfaces, although the full understanding and interpretation of global body wave coda correlations are an active area of current research (Lin et al., 2013; Poli et al., 2017; S. Wang & Tkalčić, 2020). Because these correlation-based techniques rely on stacking many earthquake coda correlograms, these studies benefit from stable, long-term installations provided by the GSN and GEOSCOPE networks. For example, Tkalčić et al. (2020) was able to identify a number of phases using this method (Figure 21). These

phases, which are described with a letter “*c*” were first described as exotic phases that originate from the Core Mantle Boundary (CMB) from various interference (Tkalčić et al., 2020).

Although *SKS* splitting studies (Silver & Chan, 1991; Vinnik et al., 1989) have been a primary body-wave technique for studying lithospheric and mantle anisotropy (e.g., Long & Silver, 2009), they have poor depth resolution due to the steep incidence of these ray paths. Because anisotropy can produce observable splitting of *P*-to-*S* (*P_s*) converted waves at mantle and crustal interfaces (Vinnikand & Montagner, 1996), it can also be studied using receiver function methods. However, the amplitude of waves converted across an interface depends on its impedance contrast, so that *P_s* waves produced within the mantle tend to have small amplitudes and their study thus benefits from extensive stacking of earthquake signals. Indeed, the azimuth-dependence of *P_s* conversions at long-operational seismographic stations has been used to estimate anisotropic structure of continental (e.g., Levin & Park, 1997) and oceanic (e.g., Olugboji & Park, 2016) lithosphere. Furthermore, distinguishing between the competing effects of anisotropy and dipping layers requires well-sampled azimuthal coverage (e.g., Savage, 1998). Therefore, such methods benefit from the high SNR and decadal-scale data acquired at long-lived stations.

The longevity and long-term stability of seismic observations enabled by high-quality permanent global networks are crucial for monitoring small temporal changes in subsurface properties (e.g., due to fluid migration, stress changes, and inner-core super-rotation). This has been done by exploiting so-called “repeating” earthquakes, whose waveforms are nearly identical between occurrences separated by years or decades (Uchida & Bürgmann, 2019). Alternatively, one can use changes in travel times of target phases on similar paths, which also requires the long-term operation of seismic stations (e.g., Souriau, 1998a). Recently, D. Kim and Lekic (2019) have shown that autocorrelation and receiver function techniques at a GSN station can be used to study inter-annual variations in subsurface velocity over decades. Together with recent progress in studying the global correlation wavefield (Tkalčić et al., 2020), this opens the potential for monitoring temporal changes within targeted regions of the Earth's interior, similar to how velocity variations in earthquake source regions are studied (Wegler & Sens-Schönfelder, 2007).

5. Global Seismic Imaging

5.1. Earth Parameters From Normal Modes

5.1.1. Mantle Structure

One key aspect of many tomography models is the incorporation of normal mode data into global Earth structure inversions. Given the global nature of these oscillations, analysis is not affected by heterogeneous geographic data coverage in the same manner as body wave and surface wave observations. In most studies of 3D mantle structure, normal mode data are parameterized as splitting functions, as discussed in Section 4. Observed splitting functions, rather than the spectra themselves, are then inverted for Earth structure, which drastically reduces the computational power required for the inversion.

Early splitting function data sets mostly contained normal modes with frequencies below ~3 mHz, which are primarily sensitive to shear-wave velocity. These data have been used in global tomographic inversions, providing important information on the long-wavelength structure of the mantle (e.g., Ishii & Tromp, 1999; Resovsky & Ritzwoller, 1999a; X.-D. Li et al., 1991). To obtain smaller-scale details, subsequent studies combined normal-mode observations with surface wave and body wave data, with studies also constraining estimates of independent variations in anisotropy and *P*-wave velocity in the last decade due to the advent of new data sets (e.g., Durand et al., 2016; Koelemeijer et al., 2016; Mosca et al., 2012; Moulik & Ekström, 2014; Ritsema et al., 1999, 2011).

Unlike the vast majority of seismic data types, normal modes are significantly sensitive to the effects of self-gravity, and thus density perturbations—an important parameter that dictates mantle dynamics. As a consequence, normal mode theory is the most reliable and efficient way to predict the long-period Earth response to earthquakes and tidal forces, with different levels of approximations being applied across decades of development. Ishii and Tromp (1999) produced early tomographic models focusing on deep mantle density, which laid the foundations for future studies of density variations in the mantle (e.g., G. Masters, Laske, Bolton, & Dziewonski, 2000; Moulik & Ekström, 2016; Trampert et al., 2004). Typically, these studies found an anti-correlation between

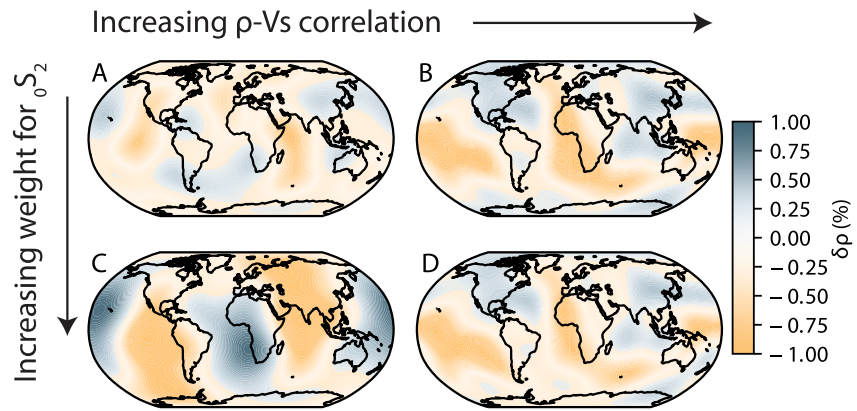


Figure 22. Density variations at 2,875 km depth describing structure for spherical harmonic degrees $l = 1-7$ from four tomographic inversions. Lateral variations in density ($\delta\rho$) in the lowermost mantle depend on the amount of imposed scaling between density and V_s structure and on the importance assigned to mode ${}_0S_2$ in the inversion. Modified from Rudolph et al. (2020). A, B, C, and D correspond to increasing ρ - V_s , increasing the weight for ${}_0S_2$, and increasing both, respectively.

variations in density and shear-wave velocity in the deep mantle, an observation that requires the presence of chemically anomalous material. Instead of inverting for mantle structure, Koelemeijer et al. (2017) used splitting function observations of Stoneley modes to obtain models of deep mantle buoyancy that best explained their data. Although their preferred models are consistent with a purely thermal interpretation and thus appear to contradict earlier results, this is readily explained by the choices of data selection and model parameters considered.

As is typical in Earth structure inversions, parameter trade-offs are an important consideration in normal mode inversions, particularly given the data are sensitive to multiple parameters. For example, B. Romanowicz (2001) already documented a strong trade-off between lower mantle density and CMB topography, and trade-offs with other parameters were studied extensively by Koelemeijer et al. (2012). Results for mantle density also strongly depend on which normal modes are included in the inversions (Koelemeijer et al., 2017; Moulik & Ekström, 2016). Figure 22 illustrates this for the longest period mode ${}_0S_2$, with a stronger weight on this mode leading to different models of mantle density. Finally, choices about how strongly the inversion is regularized (e.g., imposed correlation between V_s and ρ), also affect the retrieval of density structure (Figure 22), as explored early on by Resovsky and Ritzwoller (1999b).

Although normal mode studies have made important contributions to our overall understanding of Earth's long wavelength structure, there remain paths for improvement and innovation. In particular, no inversion thus far has included the full effects of full coupling, although some splitting functions are observed using group coupling (narrow band coupling). Several theoretical studies have explored the coupling approximations and indicate that it is important to consider (e.g., Akbarashrafi et al., 2018; Clevede et al., 2000; Deuss & Woodhouse, 2001; H.-Y. Yang & Tromp, 2015), particularly for density (Al-Attar et al., 2012). While traditionally splitting functions rather than spectra have been inverted for structure (motivated by the early investigations of X.-D. Li et al. (1991)), this has been questioned recently by Akbarashrafi et al. (2018) and Jagt and Deuss (2021). The former study suggests that substantial artefacts may arise in tomographic models when one uses splitting functions, while the latter study shows that the direct inversion of spectra does result in significantly lower misfits in their resultant models. Spectral inversions were attempted as early as 1991 (X.-D. Li et al., 1991), but it is only now that we have the computational power to also include full coupling in these spectral inversions. Combined with the availability of sufficient, long-period spectra with low noise levels, as provided by many global seismographic stations, this will allow us to put important constraints on odd-degree mantle structure.

These (and other) 3D studies of mantle structure require knowledge of the reference, or average, 1D background structure. Since many normal modes integrate large portions of the mantle, they are often useful in determining radial profiles of the mantle, and provide improved estimates on Earth's density profile (e.g., Dziewonski & Anderson, 1981; de Wit et al., 2014; G. Masters & Gubbins, 2003) and radial anisotropy (Montagner & Kennett, 1996). Another example of estimating 1D characteristics of the mantle includes Lau and Romanowicz (2021), who used long-period frequencies to characterize elastic and density properties of the mantle just

above and below the 660 km discontinuity. In such studies the center frequencies of normal modes (and not their splitting) are of interest. Radial modes (which are characterized as ${}_nS_0$) are of particular importance given their broad sensitivity (see kernel for ${}_0S_0$, Figure 19). A parameter of note is the attenuation of such modes, as this provides key estimates on the anelastic rheology of the Earth, resulting in the broadening of normal mode peaks. Important observations of normal mode attenuation have been made using globally distributed seismographic station data (e.g., Durek & Ekström, 1995; Durek & Romanowicz, 1999; Talavera-Soza & Deuss, 2020; Widmer et al., 1991).

5.1.2. Core Structure

There exists a distinct set of normal modes that are sensitive to the core (e.g., ${}_7S_5$ and ${}_3S_2$). Indeed, normal mode studies of core structure provide a distinct complement to body waves discussed above. One mystery that currently remains is to determine what light element(s) are present within the core. Mineral physicists attempt to estimate what iron alloy might explain the density deficit observed by seismic data, and key to this is refining the density profile of the Earth (Hirose et al., 2013). PREM remains one of the main density profiles used in these explorations, but more recent studies relying on normal mode data indicate that the inner core density might be $\sim 1\%$ lighter than that of PREM (A. J. S. Robson & Romanowicz, 2019). The low attenuation within the inner core has also been explored via normal modes (e.g., G. Masters & Gilbert, 1981). For the outer core, Irving et al. (2018) determined new elastic parameters by parameterizing the inversion using an equation of state and obtaining a velocity profile that partially reconciles a long-standing discrepancy between body wave and normal mode data.

Inner core anisotropy has also been observed with normal mode data as early as the 1980s (e.g., Woodhouse et al., 1986). Tromp (1995) theoretically predicted its effect within a normal mode framework and following work continues to explore its presence in normal mode data (Beghein & Trampert, 2003; Delbridge & Ishii, 2020; Durek & Romanowicz, 1999; Ishii et al., 2002; Laske & Masters, 1999). Several hypotheses have since been proposed to explain this anisotropy as arising from the alignment of iron crystals as the inner core deforms (see Deuss, 2014, for a comprehensive review).

5.2. The Earth's Inner Core, and Evidence From Seismograms of Time-Varying Features

Long-running stations have allowed us to record core-sensitive seismic phases over multiple decades. Song and Richards (1996) reported *PKP* phases at the COL station in Alaska from earthquakes in the South Sandwich Islands over a 28-year period, and showed that the travel-time of the *PKP(DF)* wave (also called *PKIKP*) appeared to have shortened over this time period. A typical comparison of the various *PKP* waves for two events separated by 15 years is shown in Figure 23.

Body-wave travel times will not change on fixed paths through a rotating spherical object that is homogeneous and isotropic. What features of the inner core can then generate changing travel times? Song and Richards took evidence available in 1996 that the inner core's anisotropy was not aligned with the rotation axis, and inferred an eastward differential rotation of the inner core amounting to about 1° per year to explain their observations. Creager (1997) was the first to obtain evidence of lateral heterogeneity in the inner core, which he estimated (and found to be quite strong) for the *PKIKP* paths used by (Song & Richards, 1996). He showed that a slower rotation rate was therefore more appropriate as an explanation of the observed travel-time changes for the earliest body wave in Figure 23.

Hundreds of studies were triggered by these and other early papers. As noted by Deuss (2014), a substantial range of estimated inner core rotation rates resulted, including several that saw no evidence of differential rotation. She cited estimates based on seismic body waves (A. Li & Richards, 2003; Cao et al., 2005; Collier & Helffrich, 2001; Creager, 1997; Isse & Nakanishi, 2002; J. Zhang et al., 2005, 2008; Lindner et al., 2010; Poupinet et al., 2000; Song, 2000; Song & Dai, 2008; Song & Li, 2000; Song & Poupinet, 2007; Souriau, 1998b; Souriau & Poupinet, 2000; Su et al., 1996; Tkalčić et al., 2013; Vidale & Earle, 2005; Vidale et al., 2000; Waszek et al., 2011; X. Xu & Song, 2003; Y. Yang & Song, 2020), for which the main improvements were due to the use of so-called earthquake doublets (two events occurring in essentially the same location but separated by several years—with seismograms that were almost identical except for phases that had interacted with the inner core). For example, J. Zhang et al. (2008) gave six doublet examples, showing that travel times changed or not, according to whether the path within the inner core was oriented such that heterogeneities in the inner core moved

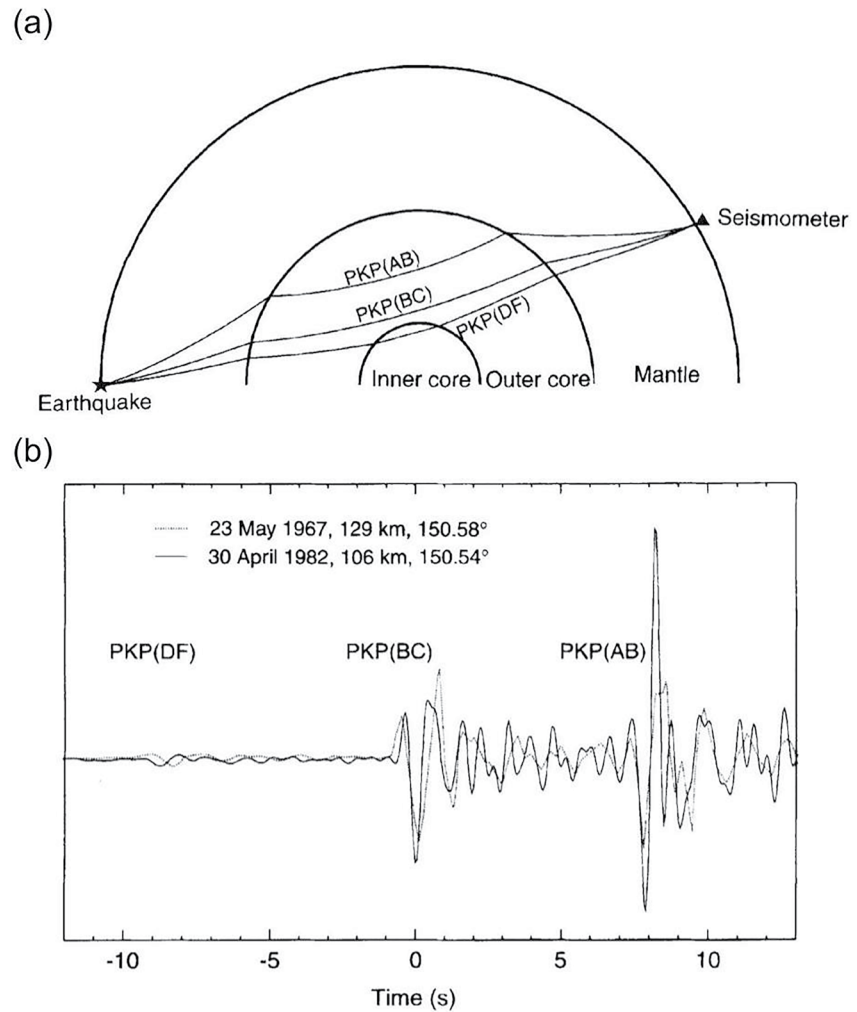


Figure 23. (a) Ray paths for a number of seismic phases that pass through the core of the Earth. (b) An overlay of two short-period *PKP* seismograms at global seismographic network station COL (College, Alaska) for two Sandwich Islands earthquakes. From Song and Richards (1996).

across the ray path (the travel time changed), or merely moved heterogeneities *along* the ray path (the travel time did not change). An example is shown in Figure 24, with its evidence for a travel-time change on the *PKIKP* path between the Aleutians and South Africa. In her review of published rotation rate estimates, Deuss (2014) also cited estimates based on normal mode studies (Laske & Masters, 1999, 2003; Sharrock & Woodhouse, 1998; Tomiyama & Oda, 2008), and on calculations from geodynamo modeling and coupling between mantle and inner core (Aubert & Dumberry, 2011; Aubert et al., 2008; Aurnou et al., 1998; Dumberry, 2010; Glatzmaier & Roberts, 1995).

Here, we can note that most papers exploring the possibility of inner-core rotation made the two simplifying assumptions (a) that the inner core moves as a rigid object on the time scale of the observations (papers by Lianxing Wen and his colleagues are an exception), and (b) that the rotation has been constant in recent decades. As reviewed by Voosen (2022), the inner core is very close to its melting temperature throughout its volume, and the eastward super-rotation rate reported in numerous early papers may have changed in the last 10 or so years. There may be the prospect of explaining all careful observations within the framework of an unsteady overall inner core rotation, but with some degree of superimposed deformations throughout its volume. Such a model would have many more parameters than just a single (albeit time-varying) rotation rate.

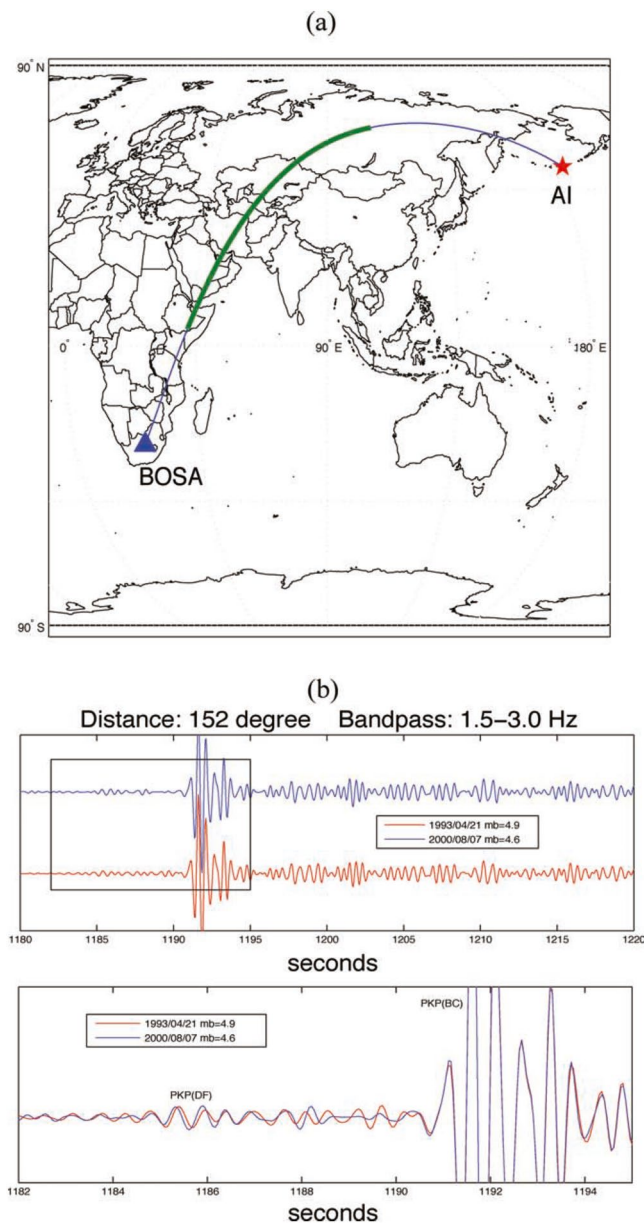


Figure 24. PKP arrivals at station BOSA (GT Network) in South Africa from a pair of nearly identical earthquakes in the Aleutian Islands (AI). They indicate an apparent temporal change (-0.1 s) of inner core travel times between the two events (which are approximately 7.3 years apart). (a) Map view of the ray path projected on the Earth's surface. Blue curve represents the ray path projected on Earth's surface. The green part of the curve represents the projected part of the ray path within the inner core. (b) Comparison of the highly similar waveforms of the AI doublet recorded at BOSA. PKP signals within the box in the upper panel are superimposed and enlarged in the lower panel, showing an apparent change of both inner core travel times and PKP(DF) coda. The orientation is such that an inner core differential rotation would move heterogeneities across the PKP(DF) path, explaining the observed travel-time change. From J. Zhang et al. (2008).

5.3. Global Earth Models

Global seismology has been essential for revealing the large scale structure of the Earth, including the discovery of the crust, mantle, and the outer and inner cores (e.g., D. L. Anderson, 2007). Because the global seismic wavefield is so rich, combining normal mode observations with body wave, surface wave, and other observables, in conjunction with a long history of observation, as well as theoretical and methodological advancements in tomography, has resulted in increasingly well resolved global Earth models. The seminal and widely used 1D reference model PREM (Dziewonski & Anderson, 1981) made use of body-wave arrivals as well as normal modes (Figure 25). A number of additional 1D models have also been widely applied such as AK-135F, which makes use of a diverse set of body wave arrivals and normal modes (Montagner & Kennett, 1996). These 1D models are widely used to calculate nominal seismic attributes consistent with general Earth structure and as references for higher-dimensional modeling efforts.

Methodological improvements, increasing computational power, and greater global seismometer station coverage spanning decades of earthquake recording have revealed Earth's anisotropic 3D velocity structure with steadily improved resolution. These models address fundamental questions of composition, structure, dynamics, and history that span the nature of seismic discontinuities; the plate tectonic system and the structure and dynamics of subducted slabs; the origin and geometry of mantle plumes (Figure 26); the roots of and persistence of continents; the inner and outer core; and the core-mantle boundary. Joint inversions incorporating a range of data types with different depth sensitivities have been essential in such efforts, for example, Ritsema et al. (2011) developed a degree-40 3D shear-wave velocity model to jointly fit body-wave, surface-wave, and normal-mode data. The advent of accurate numerical wave propagation software (Komatitsch & Tromp, 2002a; Komatitsch et al., 2002; Tromp et al., 2005) has enabled full-waveform tomographic inversions that model entire seismograms rather than extracted features such as phase arrival times and modal frequencies. As a community we have now moved beyond earlier efforts based on a normal mode perturbation formalism (e.g., Woodhouse & Dziewonski, 1984), resulting in a new generation of global (Bozdağ et al., 2016; French & Romanowicz, 2015; Lei et al., 2020; Lekić & Romanowicz, 2011), and regional or continent-scale (Blom et al., 2020; Fichtner et al., 2009; Gao et al., 2021; H. Zhu et al., 2012; Lloyd et al., 2019; Tape et al., 2009; Tao et al., 2018) models.

Increasing global coverage from regional networks and sustaining long running stations are critical for facilitating further tomographic progress, and full-waveform inversion workflows are being developed for the progressive and efficient incorporation of new data (e.g., Krischer et al., 2015), including an ever-larger data archive from globally distributed seismic stations (e.g., Afanasiev et al., 2015; Fichtner, van Herwaarden, et al., 2018; van Herwaarden et al., 2021). Computational advancements are driving the ability to calculate increasingly complete forward models within more finely parameterized model spaces, and thus utilize increasingly high frequency seismogram information, although computational capabilities may still remain insufficient to utilize the full observable seismic bandwidth for a decade or more. A representative of the recent state of the art in full-waveform global inversion is the transversely isotropic GLAD-M15 model of Lei et al. (2020) (Figure 27). This inversion incorporates globally distributed broadband data from 1,480

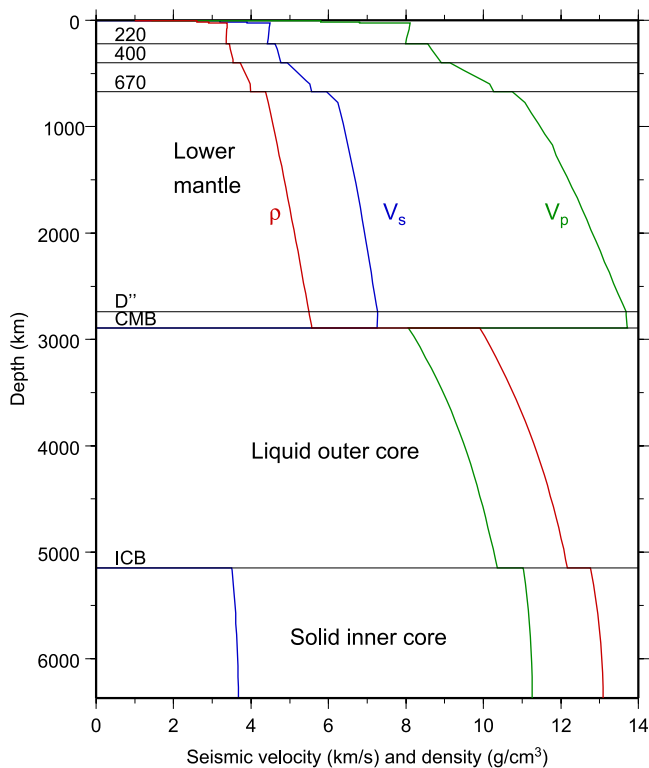


Figure 25. The preliminary reference Earth model (Dziewonski & Anderson, 1981). This was the first global reference model that included radial anisotropy in the top 220 km of the mantle as well as depth profiles of anelastic attenuation in shear and compression.

M_w 5.5–7.2 earthquakes recorded at 11,800 seismic stations retrieved from the FDSN federated IRIS, ORFEUS, INGV, IGP, ETH, and GEONET data centers. Broadband 3-component seismograms were modeled at periods between 250 and 17 s. The inversion incorporates a 3D anelastic crust and mantle structure, topography, bathymetry, ellipticity, rotation, ocean loading, and self-gravitation in its forward modeling, and was implemented on supercomputers at the U.S. Oak Ridge National Laboratory.

Global 3D seismic velocity models are showing progressive convergence (e.g., Figure 26), as indicated by quantitative comparative studies (e.g., de Viron et al., 2021) and associated model interrogation and inter-comparison tools (e.g., Becker & Boschi, 2002; Hosseini et al., 2018; Lekic et al., 2012). In contrast, global density and attenuation models currently show much greater variation, particularly in the lower mantle, that reflects resolution differences associated with the ill-posed nature of such inversions (e.g., Karaoğlu & Romanowicz, 2018a). For example, Karaoğlu and Romanowicz (2018b) showed correlations of less than 0.5 between a set of current surface wave attenuation models at depths below 250 km.

5.4. Future Directions for Investigating Earth Structure

Upgrades to GSNs and improved global coverage from regional networks continue to reveal new signals that can be incorporated into studies of Earth structure. Here, we highlight novel applications and propose future directions that further exploit the unique place of GSNs amongst seismological observatories.

One such notable area is in the further analysis of Earth tides (see lower left inset in Figure 19), which are some of the largest signals recorded by seismic instruments (displacements from the semi-diurnal tide exceed 0.5 m at the equator). An advantage of using Earth tides for imaging is that they are

continuously excited on daily cycles. In contrast, studies making use of normal mode observations must rely on relatively infrequent observations following large earthquakes. Additionally, Earth tides are recorded with high fidelity on a variety of different instruments including GPS receivers and gravimeters. Notably, Lau et al. (2017) used GPS observations of this tidal deformation to estimate models imaging deep mantle buoyancy structure, and it is promising that similar analysis could be performed using high-quality, very-broadband seismic data, such as from GEOSCOPE and GSN stations. We should note though that the tidal data predominantly are sensitive to degree two structure in the Earth due to their very long wavelengths, whereas normal modes have sensitivity to higher degree Earth structure.

Many seismic instruments have poorly constrained responses at tidal frequencies compared to gravimeters, uncertainty in ocean loading models, and contributions from local site effects have historically hindered the use of seismically recorded Earth tides for imaging purposes (Westerhaus & Zürn, 2001). Additionally seismic instruments are limited at tidal frequencies by self-noise levels of the seismic instruments (Ringler et al., 2019), and long-period noise caused by temperature (Doody et al., 2017), and pressure variations (Davis & Berger, 2007). In particular, pressure variations often cause tilting of the sensor which appear as large ground accelerations and obscure tidal signals on the horizontal components (Sorrells, 1971). However, the recent deployment of borehole Streckeisen STS-6 sensors at several GSN stations (Figure 7) has enabled high-fidelity tidal observations on the horizontal components of some stations (Ringler et al., 2019) and techniques have advanced to improve the calibration of seismic instruments to within 1% accuracy (Anthony, Ringler, & Wilson, 2017). Combined with improvements in ocean loading models (Boy et al., 2003) and techniques to correct for local site effects (Lambotte et al., 2006), inverting for Earth structure using seismic Earth tide observations may be expected to advance in the near-future.

The fields of ambient noise seismology and seismic interferometry, coupling both theoretical foundations (Aki, 1957; Jon, 1968; Schuster et al., 2004; Weaver & Lobkis, 2001) and the rapid growth of large volumes of

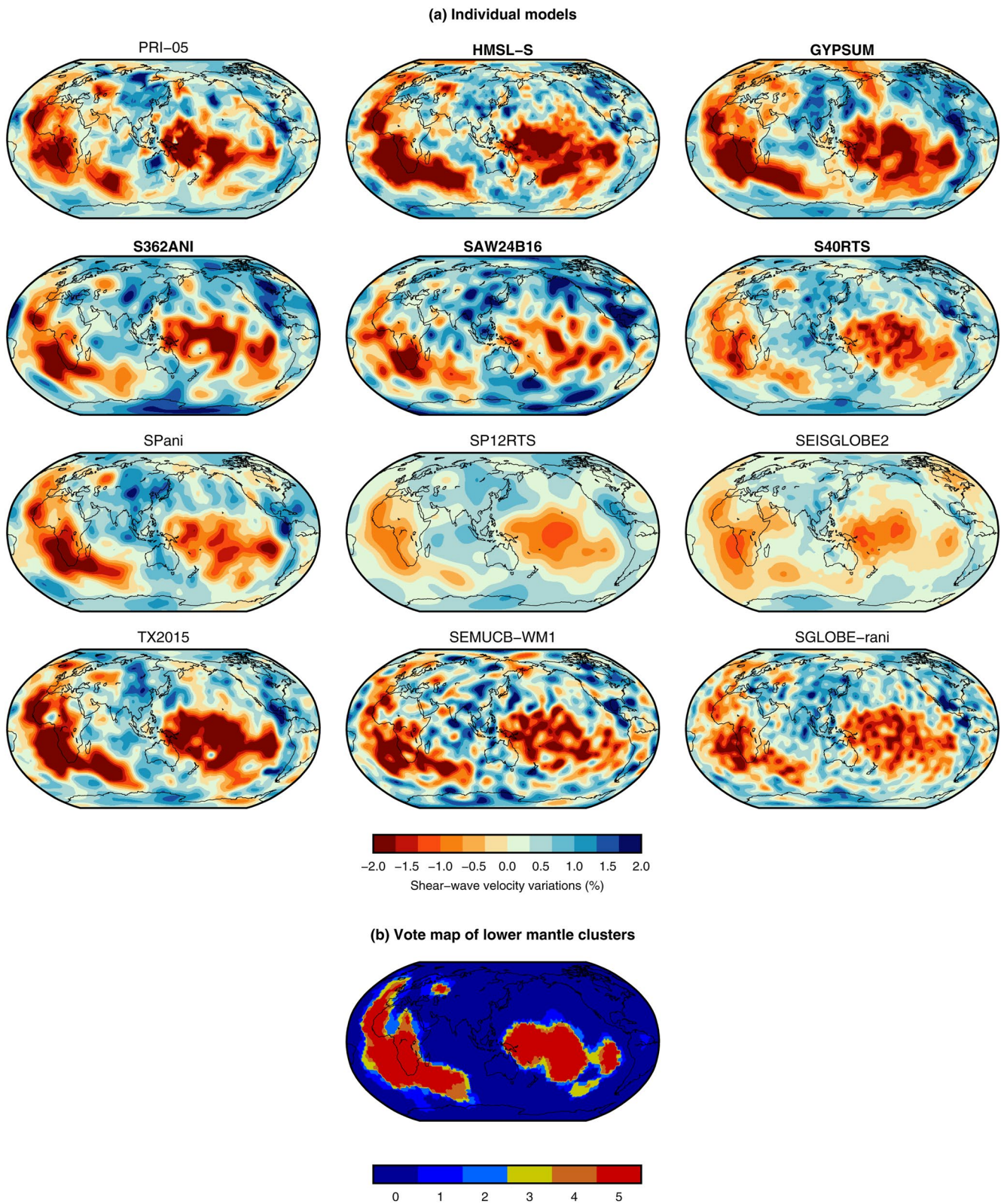


Figure 26.

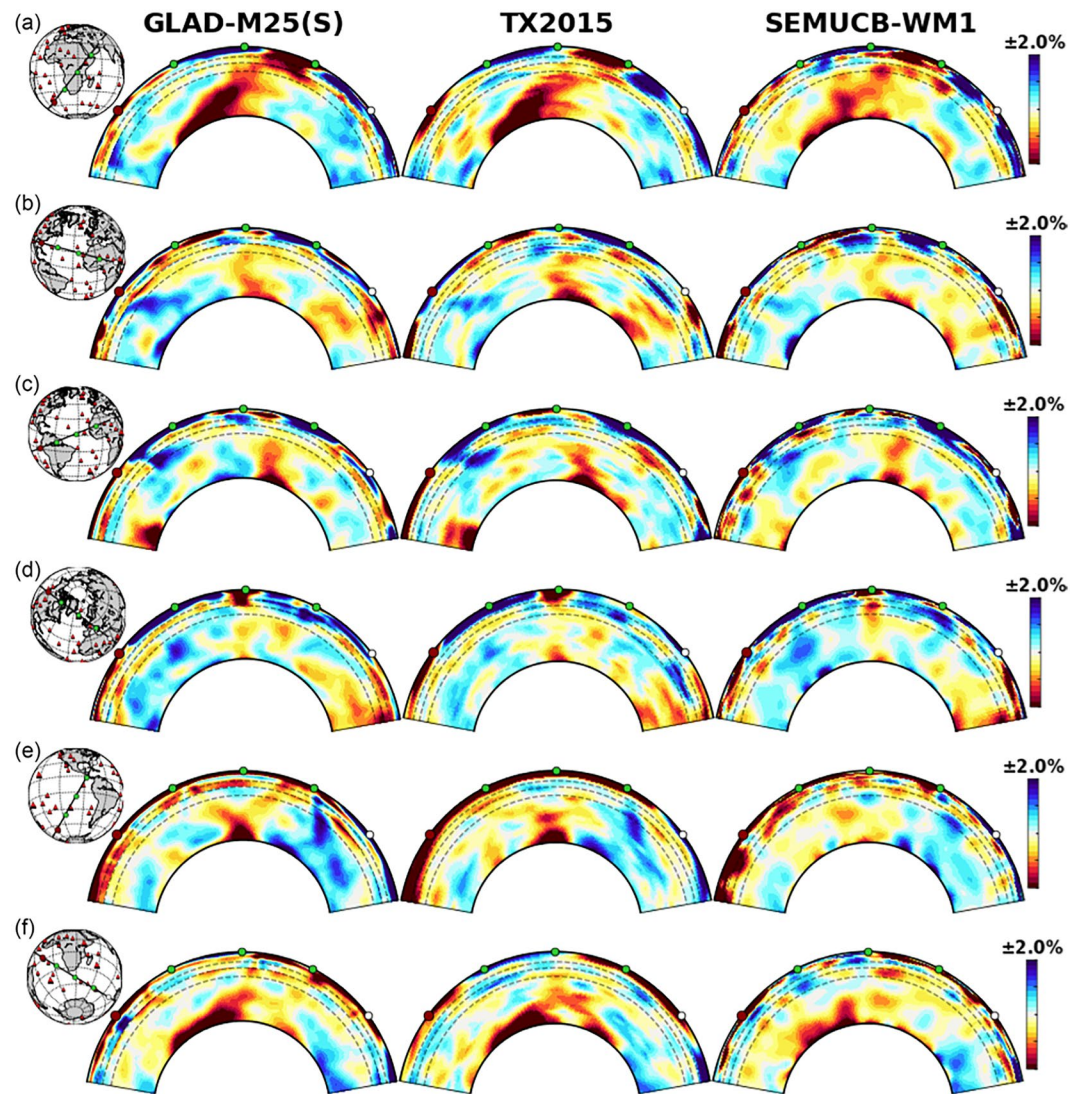


Figure 27. Shear wave velocity variations in Earth's mantle relative to a 1D radial reference model for three recent global shear-wave inversions GLAD-M25(S), Lei et al. (2020, left column); TX2015; TX2015, Lu and Grand (2016, middle column); and SEMUCB-WM1, French and Romanowicz (2015, right column) relative to the locations of major hot spots: (a) Afar; (b) Bermuda (left) and Canary (middle); (c) Cape Verde (middle) and Hoggar (right); (d) Iceland (middle) and Eifel (right); (e) Easter (left) and Galapagos (right); and (f) Marion (middle) and Kerguelen (right). Dashed depths indicate mantle depths of 410, 660, and 1,000 km. From Lei et al. (2020).

high-quality continuous seismic data distributed by global data centers, now routinely facilitate the recovery and analysis of empirical Green functions from cross-correlation operations applied to the ambient seismic wavefield (e.g., Curtis et al., 2006; Nakata et al., 2019; Shapiro & Campillo, 2004). Resultant Green function estimates are used to infer seismic velocity structure and in some cases, for example, using acoustic tomography in the oceans to observe seismic *T*-phases (Wunsch, 2020), to estimate changes in Earth's global-scale elastic properties. For

Figure 26. Global seismic tomography of the lower mantle, showing (a) individual models of shear-wave velocity variations near Earth's core-mantle boundary (CMB; 2,800 km depth) relative to a 1D radial reference model. Maps are plotted for shear-wave velocity models PRI-05 (Montelli et al., 2006), HMSL-S (Houser et al., 2008), GYPSUM (Simmons et al., 2010), S362ANI (Kustowski et al., 2008), SAW642ANb (Méglin & Romanowicz, 2000), S40RTS (Ritsema et al., 2011), SPani (Tesoniero et al., 2015), SP12RTS (Koelemeijer et al., 2016), SEISGLOBE2 (Durand et al., 2016), TX2015 (Lu & Grand, 2016), SEMUCB-WM1 (French & Romanowicz, 2015), and SGLOBE-rani (Chang et al., 2015). In panel (b), we illustrate the agreement in global tomography models by showing the vote map of Lekic et al. (2012) based on the long wavelength structures of five tomographic models (indicated in bold in panel (a)). A vote of "0" indicates agreement on fast velocities, a vote of "5" agreement on slow velocities. The two Large-Low-Seismic-Velocity-Provinces, roughly located beneath southern Africa and the SW Pacific Ocean, stand out clearly in this vote map and are imaged consistently in global tomography models (Garnero et al., 2016).

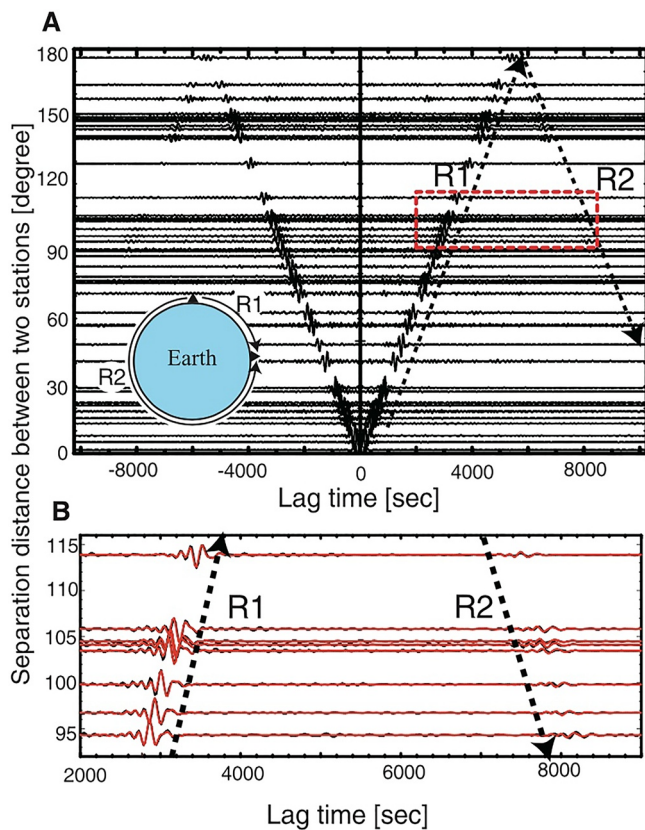


Figure 28. (a) Globally recovered vertical-component Rayleigh wavefield from the cross-correlation of ambient noise (100–400 s period). R1 and R2 indicate Rayleigh waves propagating along the minor and major great circle arcs, respectively, between pairs of stations with separation distances indicated on the y-axis. The correlation was performed for 54 International Federation of Digital Seismograph Networks stations using data collected between 1986 and 2003. (b) Comparison of observed (black) and synthetic (red, using the preliminary reference Earth model, Dziewonski & Anderson, 1981) cross-correlation Rayleigh wave signals for the region indicated by the red box in panel (a). From Nishida et al. (2009).

instance at 100–400 s period, surface wave Green functions are recoverable at station separations that span and exceed (i.e., for multiple Rayleigh wave passes) the circumference of the Earth (e.g., Nishida et al., 2009; Figure 28). Ambient noise methodologies are applicable across a broad range of frequencies given the broadband excitation of the seismic wavefield from continuous seismic sources such as ocean waves or wind (see Section 9).

Many variations of ambient noise methodologies and applications exist within this vibrant field, with the first-developed methods involving station-receiver pairs requiring the simultaneous recording of the noise sources. However, in recent years it has also become useful to process station autocorrelations, or to asynchronously process data, assuming a permanent station that acts as a virtual source (e.g., Chen & Saygin, 2020; Poli et al., 2017; Rao et al., 2021) or by redatuming data to retrieve old seismograms (e.g., Curtis et al., 2012). Stations of the GSNs, with their long operational history, provide ideal candidates for virtual sources in such studies, augmenting the scientific return from future temporary networks by tying their data to those from previous generations of data. Global-scale cross-correlation recovery of long-period body wave features has also been demonstrated (e.g., Nishida, 2013) using long-duration (hours to tens of hours) global coda wavefield of large earthquakes. However, such methods are at present difficult to implement in Earth structure studies. This is because the global body-wave coda is dominated by free surface to core-mantle boundary reverberations. This situation results in insufficient equipartition (diffusivity) of the ambient global body wavefield and global cross-correlations thus do not provide a direct access to accurate body-wave Green functions (Lin et al., 2013; Poli et al., 2017; S. Wang & Tkalčić, 2020).

Finally, the broadband nature of GSN and GEOSCOPE data offers a bridge to deformation captured by Global Navigation Satellite System (GNSS) geodesy, partially filling the so-called seismo-geodetic gap between long-period seismometry and short-period geodesy (e.g., Larson, 2009; Riquelme et al., 2016). In many applications it is increasingly evident that transient rheology governs key processes at intermediate timescales like post-seismic (e.g., Bürgmann & Dresen, 2008) and post-glacial rebound (e.g., Ivins et al., 2020; Lau & Holtzman, 2019). Seismic attenuation is expected to vary with frequency and may be represented by a variety of relaxation mechanisms that are active at different characteristic timescales. This frequency dependence is seen in experimental studies (e.g., Faul & Jackson, 2015)

and observational studies using GSN data (Lekić et al., 2009). Recently, Lau and Faul (2019) self-consistently compared attenuation from GSN normal mode observations to geodetic data spanning decades. Because of inherent trade-offs between frequency- and spatial-dependence of attenuation, much work remains to be done. Exploiting this unique aspect of GSNs as well as the increasing coverage of regional stations presents an opportunity to further refine our understanding of frequency dependent rheology.

6. Great Earthquakes and Fault Rupture Imaging

The largest earthquakes (“great” earthquakes with magnitudes of 8 or larger) occur on time scales of tens to hundreds of years, and our record of these infrequent events is sparse. For the years since 1900, a nearly complete record of all major earthquakes (Figure 29) exists, including most giant ($M_w \geq 8.5$) events (British Association for Advancement of Science Seismological Committee & Milne, 1912). The rate of large earthquake occurrence is irregular, with two temporal clusters of giant earthquakes, spanning roughly 1950–1965 and 2004–2011 (Figure 29). While large earthquakes occur at irregular frequencies, earthquake magnitudes are distributed exponentially as $\log_{10}N(M) = a - \beta M$, where $N(M)$ is the number of magnitude larger than or equal to M and β and a are constants (Godano & Pingue, 2000). This scaling relationship is known as the Gutenberg-Richter

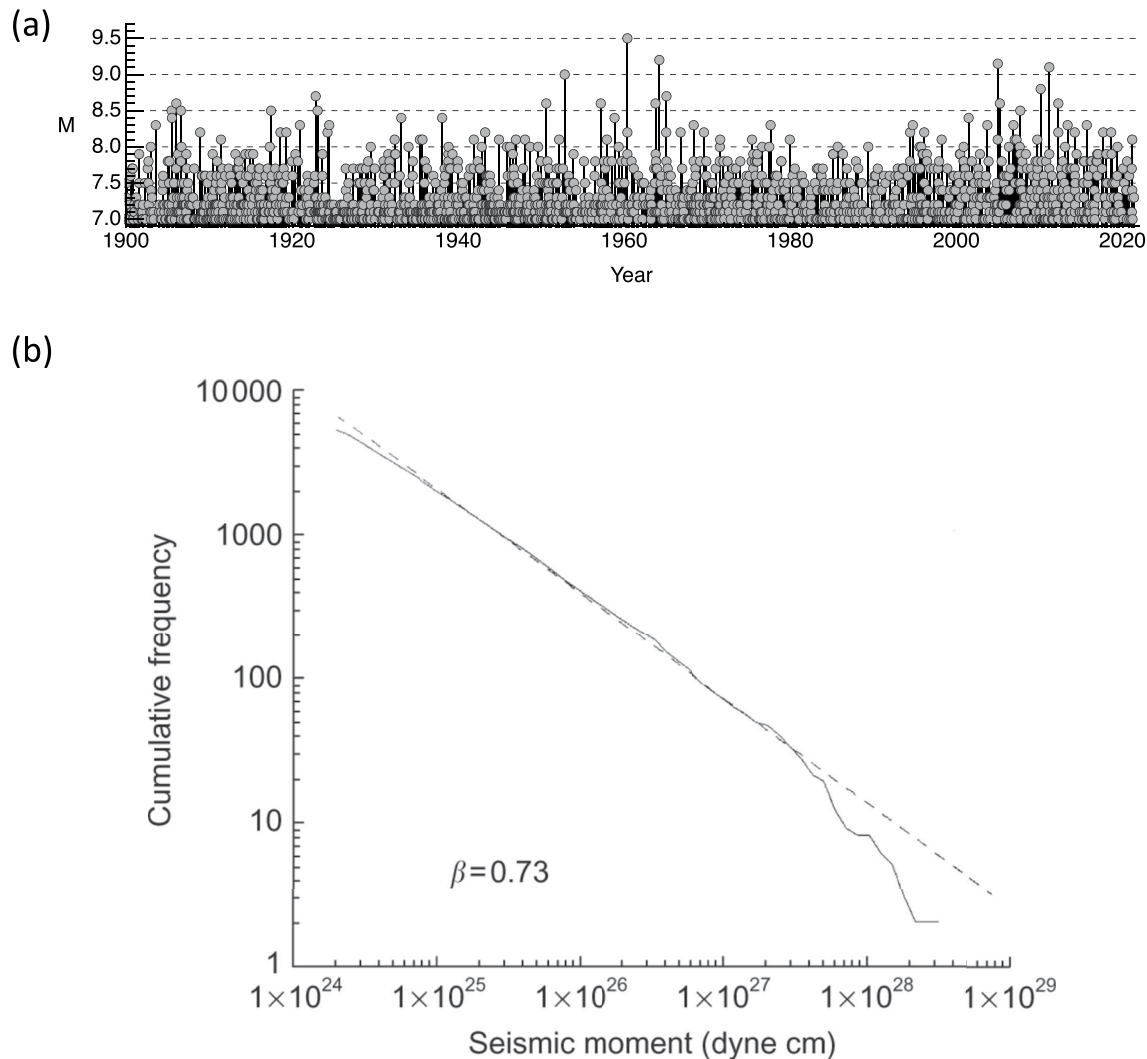


Figure 29. (a) Major ($M \geq 7$) and great ($M \geq 8$) earthquake timeline showing the occurrence pattern of large earthquakes for the past 120 years. The era of global digital seismographic networks since circa 1990 has captured one of the most active stretches in large earthquake history, providing valuable short- and long-period observations of several giant ($M_w \geq 8.5$) and many great earthquakes. (b) Gutenberg-Richter scaling relationship of the cumulative frequency of the seismic moment using the Global Centroid-Moment-Tensor catalog from 1977 to 1994. The dashed line represents the linear fit on the log-log scale in the range $5 \cdot 10^{24}$ to $5.2 \cdot 10^{27}$ dyne-cm ($5 \cdot 10^{17}$ to $5.2 \cdot 10^{20}$ N-m). Panel (a) was reproduced from International Seismological Centre (2021) and panel (b) was reproduced from Godano and Pingue (2000).

(GR) law (Gutenberg & Richter, 1944). Short-term (minutes to weeks) dynamic and static stress changes are known to trigger solid Earth and cryospheric seismicity at regional and teleseismic ranges (C. Li et al., 2021; D. P. Hill et al., 1993; Freed, 2005; Peng et al., 2014), as do local stress and hydrological perturbations (Johnson et al., 2017). However, temporal clustering between the sparse data set of Earth's largest instrumentally recorded earthquakes, and temporal correlations with other geophysical activity (e.g., solar cycles), remain both intriguing and speculative, with most researchers concluding that the global occurrence of large earthquakes, once declustered for aftershocks, is consistent with a Poissonian random process (e.g., Bendick & Bilham, 2017; Beroza, 2012; Jenkins et al., 2021; Marchitelli et al., 2020; McCaffrey, 2008; P. M. Shearer & Stark, 2012).

Fortuitously, modern GSNs have provided on-scale, high-quality VBB ground motion records across the episode of great earthquake activity that began in the early 2000s, and that followed an approximately 35-year period with relatively few large events (Figure 29). The collection of these data is a major achievement in the field, and successfully satisfied one of the key goals of global digital network designers and operators (Butler et al., 2004; Park et al., 2005). Thus, present modern GSNs have now yielded invaluable records of some of the largest

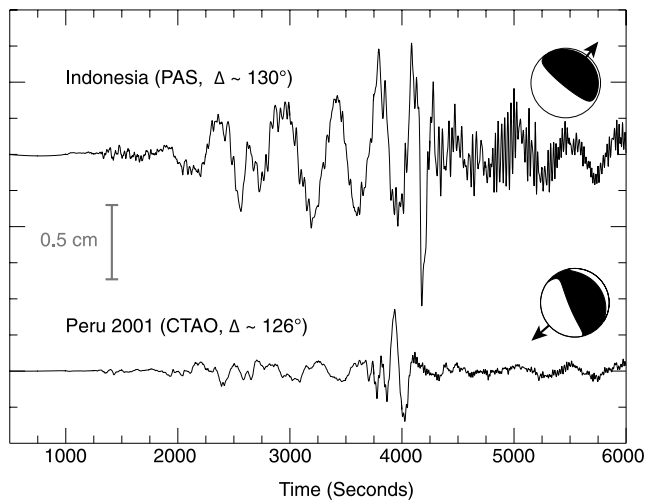


Figure 30. Observed displacement seismograms for the 2004 M_w 9.1–9.3 Sumatra-Andaman Islands earthquake observed at PAS (Pasadena, CA, USA; California Integrated Seismic Network; CI) and for the 2001 M_w 8.4 southern Peru earthquake observed at GSN station CTAO (Charters Towers, Australia). The long-period character of these large earthquakes is apparent in the records, and is only observable with very broadband instrumentation. Insets display the global centroid moment tensor focal polarity (Ekström et al., 2012) for the two events and the direction from the source to the station (arrows). The signals were chosen to equalize radiation pattern and distance effects on the signals to facilitate comparison. Reproduced from Lay et al. (2005).

earthquakes in history. Of particular interest and the focus of many investigations were the 2004 (M_w 9.1–9.3, Lay et al., 2005), 2005 (M_w 8.6), and 2007 Sumatra (M_w 8.4); 2010 Maule, Chile (M_w 8.8); 2011 Tohoku-Oki (M_w 9.0, M. Simons et al., 2011); and 2012 off-the coast of Sumatra earthquakes (M_w 8.6 and 8.2). Besides these exceptional events, global networks have ensured worldwide accurate recordings of all $M_w > 8$ (on average 1 per year), $M_w > 7$ (10–20 per year) and $M_w > 6$ (100–200 per year) earthquakes. These observations have been further improved by being supplemented with regional network data.

We first describe how GSNs were able to characterize both giant and large earthquakes, using a large variety of techniques that often can be implemented in near-real time. Then we emphasize that teleseismic broadband data are complementary with other data (in particular GNSS) to provide accurate imaging of the space-time evolution of the large earthquakes rupture. Finally, we document the ability of GSNs to record tiny and valuable signals generated by the largest earthquakes, such as the early gravity-induced wavefield.

6.1. Large Earthquake Rupture Modeling From Global Seismic Observations

The reliable quantification and characterization of large earthquakes, in a minimum amount of time, is an important scientific and societal task which was discussed in Section 3.3. At the local scale, where seismic waves and associated deformation arrive first and are the strongest, several elements make providing accurate and robust information on the characteristics of the event challenging. In particular, when source dimensions are on the same order as the distances to the stations, even the determination of first order

earthquake characteristics, such as moment magnitude, requires complex modeling taking into account fault geometry and dimensions of the causative rupture. Moreover, algorithms have to be made robust as the observation configuration (e.g., azimuthal coverage) can differ significantly between successive events. Finally, methods that have been implemented in these contexts (e.g., Delouis, 2014) obviously rely on the presence of local or regional networks.

At the global scale, however, such difficulties are largely avoided and systematic methods based on simple source representations have been developed (Section 3.3). All these approaches rely on the geographical distribution, real-time transmission and broadband character of globally distributed seismic stations. The difference in the radiated wavefield from the largest earthquakes from more modest magnitude earthquakes is substantial. The long duration of the largest earthquakes and large seismic moment excite a long-period dominated global wavefield (Figure 30). These features are well captured by the VBB instruments often operated by GSN stations, and make possible the implementation of *W*-phase inversion for rapid source characterization (Kanamori & Rivera, 2008).

Use of the *W*-phase and the earliest arriving body waves allows for the robust global estimation of key parameters (location, focal mechanism and magnitude) of the largest earthquakes within 15–20 min of origin time. This information is of high interest to quantify the event's tsunamigenic potential, especially when the event exhibits indications of being a shallow sub-sea rupture with a large seismic moment. So-called “tsunami earthquakes,” an exceptional class of tsunamigenic earthquakes, are characterized by ruptures long and anomalously slow, and radiate seismic energy depleted in high frequencies (Kanamori, 1972). These events can be quickly and globally discriminated by the “slowness” parameter (Θ), the logarithmic ratio between an earthquake's estimated radiated energy and its moment (Lomax et al., 2007; Newman & Okal, 1998). In the twenty-first century, notable examples of such events are the 17 July 2006 M_w 7.8 Java earthquake (Ammon et al., 2006) and the 5 October 2010 M_w 7.8 Mentawai earthquake (Newman et al., 2011), which generated tsunamis that were greater than predicted by their seismic magnitude.

Globally distributed seismic data can be used to robustly retrieve the fault rupture space-time evolution of large earthquakes. The high frequency (>1 Hz) content of a teleseismic record is almost fully carried by the direct

P wave, which offers a way to estimate the source duration (Lomax & Michelini, 2009; Ni et al., 2005). The exceptional duration (>500 s) of the M_w 9.1–9.3 2004 Sumatra earthquake was first determined by such an approach. More sophisticated methods have used deconvolution (L. J. Ruff, 1989; Tanioka & Ruff, 1997; Vallée & Douet, 2016) to extract source time functions of large earthquakes from *P* and *S* teleseismic body waves. In addition to their practical use in illuminating earthquakes with anomalously long duration, with respect to their magnitude, such methods can be applied to a large collection of earthquakes to search for generic properties of the rupture processes. An important result, also supported by corner frequency measurements (Allmann & Shearer, 2009), is that earthquake duration globally scales with magnitude as expected for a constant stress drop source process. This global invariance, however, hides some specific trends. Subduction interface earthquakes tend to have a longer duration than earthquakes in other tectonic contexts (Chounet & Vallée, 2018; Houston, 2001), suggesting that repeated ruptures or the hydrated nature of the subduction interface result in a lower stress drop and/or rupture velocity. Bilek and Lay (1999) and Bilek et al. (2004) showed that shallow subduction interface events have longer durations than earthquakes located deeper in the seismogenic zone. This can be interpreted either by different source characteristics or by lower medium rigidity, the latter hypothesis being favored by subduction dynamics. Over the full seismogenic depth extent (0–700 km), source time functions also show that shallow earthquakes (<70 km) have lower stress drop than intermediate depth (70–300 km) and deep earthquakes (300–700 km) (Houston, 2001). These differences can be attributed to rigidity increase from the surface to the transition zone (Vallée, 2013).

Globally distributed seismic data also provide key elements on the space-time features of the rupture process. Several approaches, including multiple point-source inversions (Duputel et al., 2012; Fukao, 1972; Tsai et al., 2005) or continuous line source analysis have been applied to data from global seismograph networks. Most of these techniques track the relative differences between stations with different azimuths (often referred to as directivity effects) to retrieve the main characteristics of large earthquakes. One of the findings of the last two decades was that some large earthquakes propagate at supershear speeds (i.e., faster than the shear-wave velocity) over long distances (e.g., Bouchon & Vallée, 2003; Das, 2015; Zhan et al., 2014). Such supershear earthquakes require long strike-slip faults with low friction as necessary, but not necessarily sufficient conditions (Das, 2015). The determination of the detailed space-time slip evolution of large earthquakes is a challenging task because of the large number of free parameters, uncertainties in fault geometry, and the fact that Green's functions typically vary little over the rupture zone. Finite fault approaches such as those proposed by Olson and Apsel (1982), Hartzell and Heaton (1983), or Ji et al. (2002) can, however, be applied to teleseismic data, with improved resolution when jointly inverting body waves and surface waves (e.g., Hayes, 2017). Determining the rupture process of the M_w 9.1–9.3 Sumatra-Andaman earthquake relied heavily on matching synthetic waveforms from different slip models to seismic observations made predominantly on GEOSCOPE and GSN stations (Ammon et al., 2005). Illustrative results for the 11 March 2011, M_w 9.1, Tohoku earthquake, shown in Figure 31, both illuminate the strengths and the limitations and the finite fault teleseismic inversions. All inversions show the dominantly updip rupture propagation, resulting in very large slip close to the trench, at the origin of the devastating tsunami. However, maximum slip value as well as the southern extent of the rupture zone significantly differ between inversions. Global databases of teleseismic finite-fault models (Hayes, 2017; Mai & Thingbaijam, 2014; Ye et al., 2016) are therefore mostly used to analyze their main features, and details are best discussed on earthquakes that benefit local and teleseismic observations (Section 6.2). We refer the reader to Ide et al. (2005) for an overview on finite-fault inversions as well as Mai et al. (2016) for details on estimating uncertainties in finite-fault inversions.

Besides their use in waveform inversion, which is generally limited to periods down to a few seconds, the data from global and regional seismographic networks have been helpful in mapping high-frequency (around and above 1 Hz) radiation patterns of large earthquakes. For such applications, a seismographic network is considered an antenna, and backprojection (or time-reversal) techniques (Ishii et al., 2005; Krüger & Ohrnberger, 2005; Larmat et al., 2006) allow one to locate in space and time the strongest radiators (Walker et al., 2005; Y. Xu et al., 2009). Here also, the use of the GSN data is complementary to dense local or regional arrays (where the required correlation between waveforms is higher but the measured time shifts are smaller). This approach, which does not require any inversion or definition of a source model, has been extensively used to determine the rupture extent and rupture velocity of large earthquakes (e.g., Meng et al., 2012; Satriano et al., 2012; Walker & Shearer, 2009). Careful analysis of high-frequency seismic radiation from megathrust earthquakes further revealed that this energy tends to originate at the bottom of the rupture zone (rather than in the areas of maximum

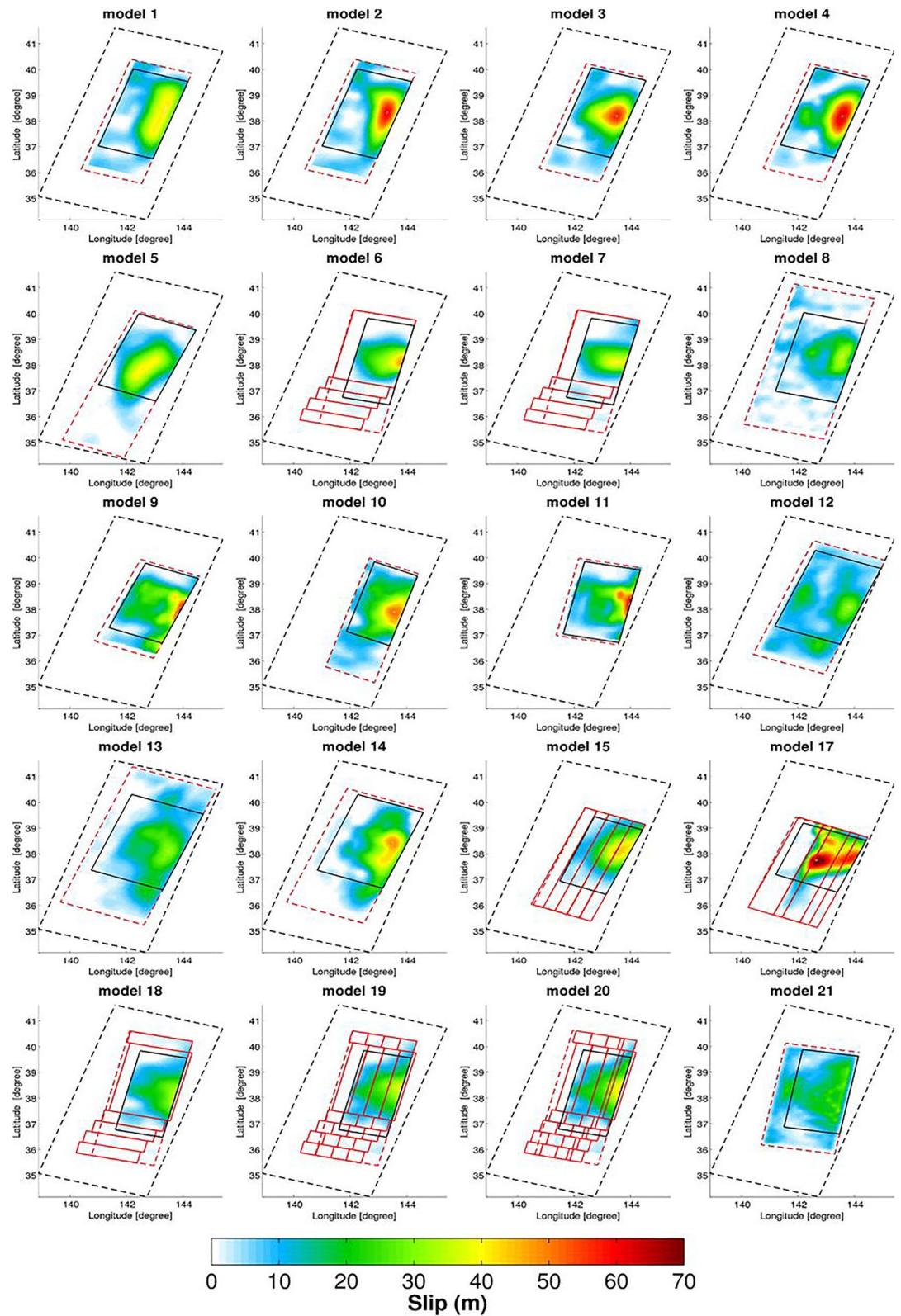


Figure 31. Twenty slip models for the 2011 Tohoku earthquake (excluding Model 16 that has a similar pattern to Model 15). The original fault geometry is indicated with red lines. The red dashed lines outline single plane representations of the corresponding model. The smallest and largest areas used in the slip-model comparison are denoted by black lines and black dashed lines, respectively. Reproduced from Razafindrakoto et al. (2015).

slip), suggesting that the frictional properties of the subduction interface are depth dependent (H. Yao et al., 2013; Lay et al., 2012).

6.2. Large Earthquake Rupture Processes and Joint Analyses of Seismic and Geodetic Observations

For large earthquakes occurring onshore or in well instrumented areas, data from GSNs complement other geophysical observations, and the most comprehensive and detailed analyses are now performed jointly with these other data types. Strong motion records and high-rate GNSS-derived displacements (Ge et al., 2000; Larson et al., 2003) are highly sensitive to the closest source emissions, and their addition to teleseismic data thus improves local resolution. Static geodetic data (GNSS and Interferometric Synthetic Aperture Radar; InSAR) have proved to be very useful for understanding large earthquake rupture processes. Even if they allow access to only the final earthquake slip, they have the advantage of a higher dynamic range, producing faithful recordings of large (e.g., up to many meters of displacement) ground motions in the near-field (C. Xu et al., 2016). While there can be relatively large uncertainty in the vertical components of GNSS measurements, they have been shown to be consistent with traditional seismic recordings and can be utilized in critical early assessment measurements such as *W*-phase moment tensor inversion (Riquelme et al., 2016), as well as to resolve high-amplitude normal modes in certain situations (Mitsui & Heki, 2012). Since many GNSS sites provide data in real time and do not directly overlap with global seismographic stations they also provide valuable complementary spatial sampling to be incorporated into seismic studies.

InSAR provides spatially dense surface measurements of near-source surface deformations created by large and shallow earthquakes (e.g., Funning & Garcia, 2018; Massonnet et al., 1993). One such case in recent years is the 25 April 2015 M_w 7.8, Gorkha (Nepal) earthquake (Barnhart et al., 2019; Grandin et al., 2015). Even for megathrust earthquakes like the 2010 Maule and 2011 Tohoku events, the pattern of deformation observed inland provided strong estimates on the slip location along the plate interface and on its downdip extent. With the advent of the Sentinel-1 program, the revisit time for forming InSAR images has now significantly decreased down to a few days, and the anticipated 2023 launch of the NISAR system will further expand resources <https://nisar.jpl.nasa.gov/mission/quick-facts/>. Even if this latency still precludes near-real-time applications, InSAR results are invaluable in refining seismic observations.

Both GNSS (static and high-rate) and InSAR data sets have increasingly become integrated with seismic data to realize joint inversions that greatly increase resolution of the slip on large faults or fault systems following earthquakes. Wald et al. (1996) demonstrated the value of this approach by attaining a rupture model of the 1994 M_w 6.7 Northridge (California) earthquake using near-source strong motion data, teleseismic body waves recorded at GSN seismic stations, and static regional geodetic (GNSS and leveling) observations. This study, and a number of other ones which also integrate InSAR and/or high-rate GNSS for the 2011 Tohoku earthquake (e.g., Ammon et al., 2011) and the 2015 Gorkha earthquake (e.g., Grandin et al., 2015; Yi et al., 2017) highlighted the enhanced understanding of rupture history that arises from a combined analysis of seismic and geodetic data. These studies suggest that continued expansion of high-rate GNSS observations at and near global seismographic stations (particularly those in close proximity to plate boundaries) will be valuable to future source studies.

For subduction megathrust earthquakes, the addition of marine and seafloor measurements helps to estimate the rupture characteristics, particularly close to the trench. Tsunami amplitudes, mostly measured by tide gauges and the DART system (Meinig et al., 2005), have also been integrated into source inversions to better resolve shallow slip (e.g., Heidarzadeh et al., 2016). The near-trench static offsets generated by the 2011 Tohoku earthquake were captured by seafloor geodetic techniques (Kido et al., 2011; Sato et al., 2011). Huge horizontal displacements observed there (25–30 m) show that large differences in finite-fault models exist (Figure 31) and it is necessary to quantitatively compare such rupture models (Razafindrakoto et al., 2015). For large events like the Tohoku earthquake it is possible to use data beyond that provided by GSNs to better estimate the large-scale space-time slip distribution (Bletery et al., 2014).

Collectively, the broadband analyses of recent large events produced a number of important observations and required the community to reevaluate a number of assumptions of the likely environments of the largest earthquakes (e.g., Bilek & Lay, 2018 and references therein). For example, previous hypotheses suggesting that young subducting plates favor the occurrence of megathrust earthquakes (L. Ruff & Kanamori, 1980) were challenged by the 2004 Sumatra Andaman Islands and the 2011 Tohoku earthquakes (e.g., Morra et al., 2013;

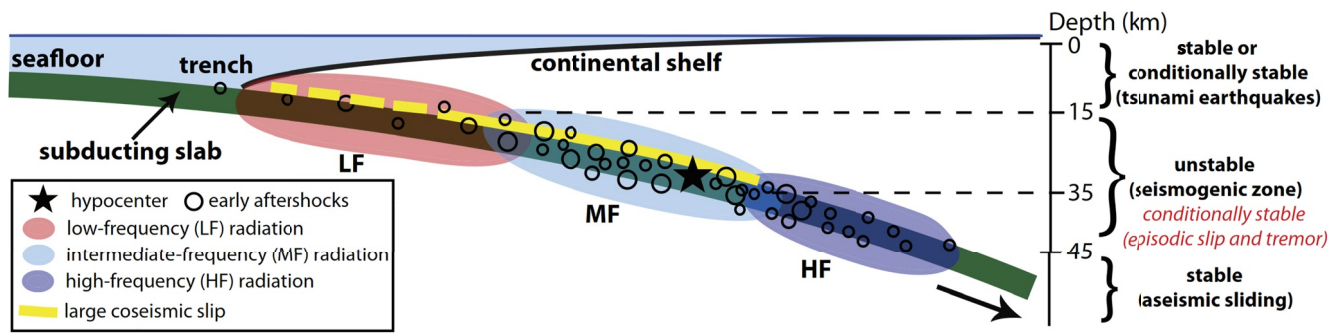


Figure 32. Seismic observations of subduction zone megathrust earthquakes and frictional stability regimes of the subducting plate interface. The yellow dashed line suggests possible large coseismic slip in the shallow portion of the slab interface in the case of tsunami earthquakes. From H. Yao et al. (2013).

Stein et al., 2012). The diversity of rupture processes of these great earthquakes as well as the availability of VBB observations has led to a number of advances in our characterizations of large earthquakes (e.g., Kanamori, 2014; Lavallée & Archuleta, 2005; Lavallée et al., 2006; Lay, 2015; Mai & Beroza, 2002). VBB imaging of these large earthquakes has demonstrated the importance of both along-strike and along-dip variations in rupture processes. The more novel results are subduction systems along-dip variations that span the range of slow rupture at the shallowest depths (all the way to the trench) to high-frequency radiation from the deeper seismogenic zone and still deeper to the region of slow-slip and seismic tremor (Figure 32, H. Yao et al., 2013; Kanamori, 2014; Lay et al., 2012).

The sequence of large earthquakes that began in 2004 along the eastern Indian Ocean Region (Sumatra and off-shore Sumatra) has demonstrated the interaction and clustering of Earth's large earthquakes along subduction boundaries, and their interaction with a nascent plate boundary region beneath the central Indian Ocean (e.g., Delescluse et al., 2012; Lay, 2015). The sequence is somewhat similar in style to the events of the 1950s and 1960s that ruptured along the Alaska-Aleutian boundary (e.g., P. Shearer & Bürgmann, 2010). Also clear are interplate stress transfers between nearby large inter- and intra-plate earthquakes such as those that struck the Kuril Islands in 2006–2007 (Ammon et al., 2008; Lay, Kanamori, et al., 2009; Steblov et al., 2008) and Samoa in 2009 (Beavan et al., 2010; Lay et al., 2010). Events have also clearly re-ruptured parts of previous ruptures showing the substantial overlap of ruptures that may occur along boundaries during large earthquakes decades later (e.g., Lorito et al., 2011; Natawidjaja et al., 2006; Nocquet et al., 2017). Such observations lead to the emergence of the concept of supercycles (Goldfinger et al., 2013; Sieh et al., 2008), where centuries-long accumulated strain is released through clusters of large earthquakes. Such a behavior biases the inferences of earthquake occurrence based on strain accumulated between two successive large earthquakes. Without a doubt, the collection and analysis of VBB observations has led to important developments in our understanding of large earthquake processes. The resulting picture remains complex but future observations are sure to lead to new patterns and advances in our understanding.

6.3. Elastogravity Signals From Large Earthquakes Observed by Global Networks

In the period range between several tens to thousands of seconds, high-quality VBB sensors installed at low noise globally distributed sites (Figure 6) allow for the detection of new classes of signals, including those associated with Earth's largest earthquakes. Classical earthquake signals observed in this period range include Earth normal modes, which, as discussed above in Section 2, were a foundational motivation for global VBB network initiatives (Agnew et al., 1976). Normal modes are significantly affected by the coupling between medium deformation and gravity changes, and self-gravitating Earth models are required to accurately predict the gravest of these modes (e.g., Dahlen & Tromp, 1998).

With the exception of very long-period normal mode signals, dynamic gravity perturbations generated by earthquakes have been sparsely studied. However, a large earthquake, together with the *P* waves that it radiates, affect the Earth density distribution in such a way that tiny changes of the gravity direction and amplitude are expected (Harms et al., 2015). Due to the speed-of-light propagation of gravity perturbations, an intriguing aspect of these gravity-induced signals is their near-immediate appearance anywhere on Earth as soon as the earthquake

starts. This provides a potential monitoring tool or early warning tool which is observationally favorable since such signals can be detected during a time window without other seismic phases between the origin time and the P -wave arrival (Montagner et al., 2016). When recorded by a broadband seismic station, these early signals were coined Prompt Elasto-Gravity Signals (PEGS). PEGS are created by two contributing processes, the first coming from density perturbation induced gravity changes themselves and the second from the elastic readjustment of the gravitationally perturbed Earth (Figure 33; Heaton, 2017). PEGS synthetic calculations show that their peak amplitude is on the order of 10^{-9} m/s² in the 30–500 s period range for the largest earthquakes, while the best VBB sensors have an RMS noise level of one to several 10^{-10} m/s² in this period range.

The first high signal-to-noise observation of PEGS was made at GSN station MDJ (Northeast China) during the 2011 M_w 9.1 Tohoku earthquake (Figure 33), and was complemented by other observations at global and regional networks (Vallée et al., 2017). PEGS from five other earthquakes with M_w 7.9–8.8 were subsequently observed (Vallée & Juhel, 2019). Global networks provided key observations of elastogravity signals for most of these earthquakes, and PEGS observations for the 2018 M_w 8.2 deep Fiji earthquake relied only on GSN and GEOSCOPE stations. In all these cases, observed signals can be accurately modeled using several complementary approaches (Juhel et al., 2019; S. Zhang et al., 2020; Vallée et al., 2017). Modeling shows that the low frequency nature of PEGS makes them insensitive to the details of the earthquake source; in contrast, they are sensitive to first-order source characteristics, in particular the seismic moment time evolution and focal mechanism. Together with the early arriving nature of these signals, this illuminates a potential for very rapid earthquake information. A current limitation is that the SNR limits PEGS observations to the vertical component and prevents observations for earthquakes of $M_w < 7.8$. In the future, signal-to-noise improvement provided by deep borehole VBB instruments should allow for these signals to be observed on horizontal components. Better understanding of seismic noise in the 30–500 s period range, as well as more advanced signal processing techniques (including machine learning) should also lower the magnitude threshold and ability to infer source information. Finally, additional instruments such as gravity gradiometers (e.g., Ando et al., 2010) are also envisioned to better detect and utilize these signals (Juhel et al., 2018).

7. Nuclear Discrimination and Monitoring

7.1. A Brief History of Monitoring Nuclear Tests With Seismology

Following the Trinity nuclear test explosion of 16 July 1945 by the U.S. and the use of nuclear weapons against Japan, seven additional countries have acknowledged conducting nuclear test explosions: the Soviet Union (beginning in 1949); the United Kingdom (1952); France (1960); China (1964); India (1974); Pakistan (1998); and the Democratic People's Republic of Korea (DPRK, 2006). Burr et al. (2019) discuss evidence for a small nuclear test in the atmosphere on 22 September 1979, reportedly by Israel though this has not been acknowledged. More than 10 additional countries began the pursuit of nuclear weapons technology, but eventually pulled back without conducting nuclear test explosions and chose to join the Treaty on the Non-Proliferation of Nuclear Weapons (NPTs) as non-nuclear weapons states. The NPT, intended to impede the “horizontal” spread of nuclear weapons between countries, entered into force in 1970, initially for a 25-year period. It is linked politically to the CTBT (to impede “vertical” proliferation of nuclear weapons technology within the nuclear weapons states). In the early 1990s the resumption of CTBT negotiations was deemed of sufficient promise that the NPT member states voted in May 1995 to remove the 25-year limitation—making the NPT of indefinite extent. As of March 2022, a total of 191 countries have become NPT members—more than have signed any other treaty. The text of the CTBT was finalized in 1996, and as of 2022 it has been signed by 186 states. However, as of this writing, it has not entered into force because it has not been ratified by some key countries, including China, the DPRK, India, Israel, Pakistan, and the U.S. Nevertheless extensive monitoring experience has been built up since 1996 with the installation and operation of global geophysical networks intended to verify CTBT compliance. Details of their operation and capabilities are described in National Academy of Sciences (2002); National Research Council (2012). An overview of seismological efforts is given by Richards et al. (2021).

The CTBT will in practice be monitored by the international CTBT Organization (CTBTO, headquartered in Vienna, Austria) which operates the IMS (it includes two networks of seismic monitoring stations), and the International Data Centre (IDC). The work is also carried out by the national efforts of member states and by the loosely organized efforts of numerous institutions that acquire and process data originally recorded for purposes other than treaty monitoring. The IDC provides basic analysis such as bulletins of seismic event locations,

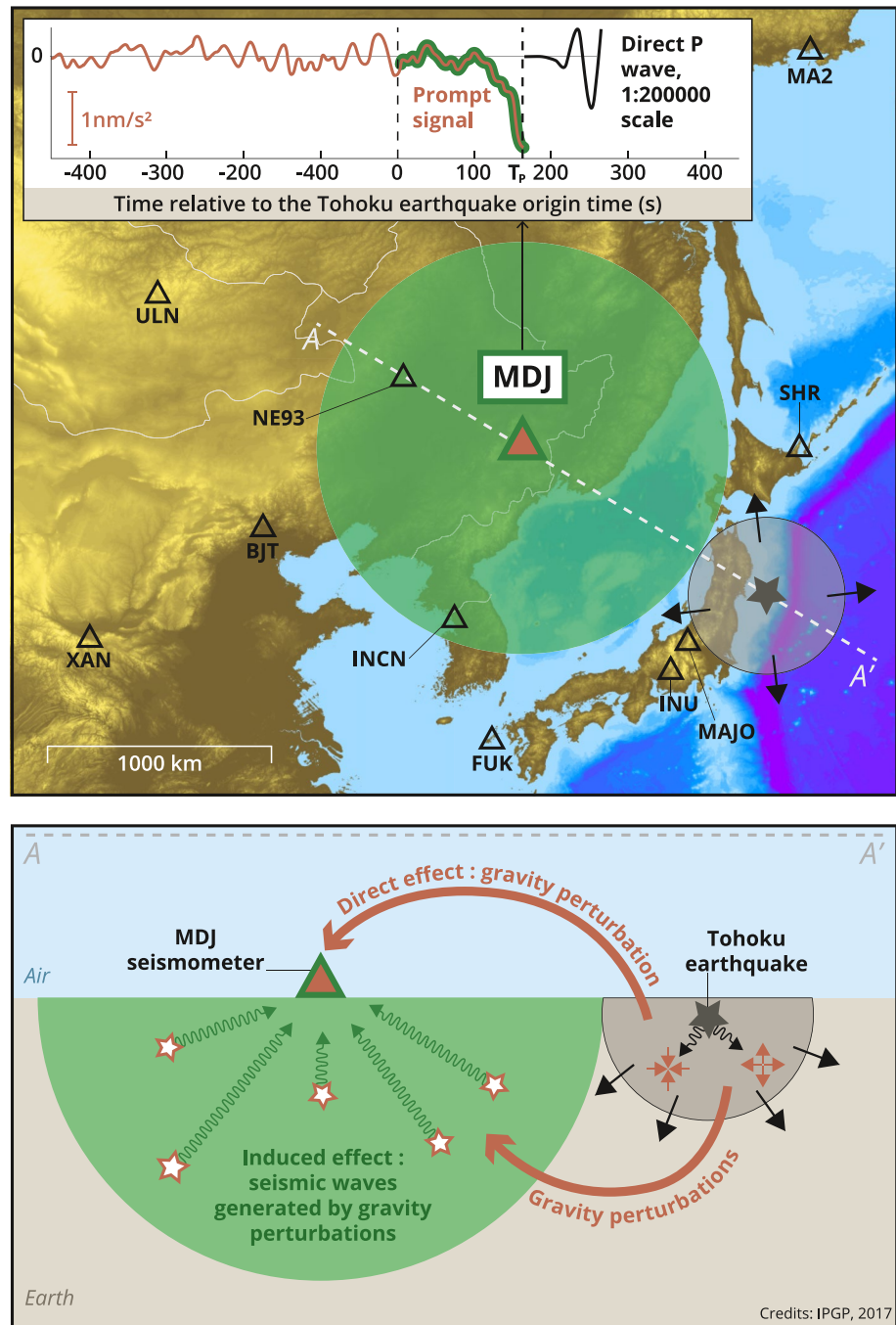


Figure 33. Observation and origin of the prompt elastogravity signals illustrated using data from global seismographic network station MDJ in northeast China, 1,280 km from the Tohoku earthquake epicentral region (black star). At such distances, direct seismic waves arrive about 165 s after origin time, as shown in the inset showing the MDJ vertical acceleration in the 33–500 s period range. However, a clear, even if much weaker, acceleration signal is detected by the seismometer before the direct waves arrive. The origin of this signal can be understood by considering the interval after the earthquake occurs but before the arrival of the direct seismic waves. For example, by about 55 s after the origin time, direct waves have propagated inside the volume shown by the gray area, but are still far from arriving at MDJ. Within this volume, seismic waves have caused compression and dilation of the medium to create density perturbations, as further indicated in the bottom cross-section. The global contribution of all such density perturbations gives rise to a gravity perturbation that is effectively immediately detected by the seismometer as an apparent acceleration (direct effect). The gravitational field is also modified everywhere on Earth, and each mass element affected by these perturbations becomes a secondary source of seismic waves (induced effect). Within the green volume around the seismometer this secondary seismic wavefield arrives before the direct waves.

including a procedure for screening out events deemed unlikely to be explosive. Unscreened events thus come to the attention of member states and may be studied in detail—with such members conducting independent analysis and identification. Although becoming effective only with entry into force, the CTBT specifies procedures for member states to make a formal request to conduct on-site inspection of regions in which nuclear testing has been suspected of taking place. In this context the quality of seismic event locations is particularly important because of the following treaty text: “The area of an on-site inspection shall be continuous and its size shall not exceed 1,000 km². There shall be no linear distance greater than 50 km in any direction.”

When global CTBT monitoring began in the late 1990s, the work could build upon decades of practical experience that some member states had acquired from teleseismic monitoring of more than 2,000 nuclear test explosions conducted prior to 1996. Limited experience with monitoring at regional distances using P_n , P_g , S_n , and R_g phases out to about 1,000 km—and L_g out to greater distances—had indicated by the 1980s that access to regional phases permitted significant improvement upon solely teleseismic monitoring performance, that is, providing capability to detect smaller seismic events, to locate them precisely, and to characterize them as an earthquake or explosion. With more than 25 years of additional experience using regional signals since the CTBT text was finalized in 1996, it has indeed turned out that regional signals facilitate improved monitoring. In the next section we give examples where particular GSN stations have provided key data that enable confident interpretations of events that had originally appeared problematic. We also summarize the current capability of seismic monitoring methods applied to nuclear testing in North Korea up to March 2022, where seismic monitoring today is characterizing remarkably small events (down at the $M 2$ level and occasionally even lower). Section 8 reviews progress in seismic event location, indicating the potential to achieve orders-of-magnitude better precision in source locations for active regions spanning broad areas using regional waves recorded by sparse networks such as the GSN. Improving monitoring efforts is particularly important for treaty verification, and has application to all types of seismic source.

7.2. Developments in Explosion Monitoring Promoted by Global Seismographic Networks

Following World War II, nuclear test explosions from the 1940s to the early 1980s were monitored first by detection and analysis of diagnostic radioisotopes and later—as the Limited Test Ban Treaty of 1963 took hold and nuclear tests moved into the underground environment—by their seismic signals. For the most part, detailed analysis was based on teleseismic records and led to the sequential steps of: detection; association of all the signals from separate stations that are due to a particular event; locating that event; identifying it (as a natural earthquake, a chemical explosion, a nuclear test, or something else); estimating its size; and (if nuclear) attributing it to a particular country.

The background of practical experience with teleseismic signals sometimes proved inadequate, as became apparent on 16 August 1997 when seismic signals indicated a small event near the islands of Novaya Zemlya, once used by the USSR to conduct its largest nuclear test explosions and still today used for nuclear weapons research (Figure 34). The event was too weak to generate usable long-period surface waves (and thus prevented teleseismic use of the $m_b - M_s$ discriminant). According to news reports at the time, questions arose as to whether the Russian Federation had carried out a small nuclear explosion on land at its former test site.

The event was well recorded regionally at the GSN station KEV (Kevo, Finland), which had previously recorded several known nuclear test explosions. Inspection of the spectral ratios between P -waves and S -waves (Figure 35) of the unknown event and these prior nuclear tests showed that the unknown event contained substantially more S -wave energy per unit of P -wave energy than the nuclear tests and was therefore likely an earthquake.

The ratio of the Fourier amplitude spectra of P -waves compared to those of S -waves had been developed in the 1980s as a discriminant, but the 1997 event near Novaya Zemlya gave it prominence as an effective way to discriminate earthquake and explosion signals. The ratio is typically higher for explosions than for earthquakes. Though often based on data only from the vertical component of recorded ground motions, W.-Y. Kim et al. (1997), showed that the ratio can more effectively discriminate when the amplitudes of P - and S -motions are based on all three components of ground motion. The discriminant is effective also for small events—a point that has emerged from detailed studies of small earthquakes and explosions, for example, one using GSN data from station WMQ (Urumqi, Xinjiang Province, China) and MAKZ (Makanchi, Kazakhstan) (Pan et al., 2007). Additionally, when North Korea (DPRK) conducted its first explosion on 9 October 2006, the P -to- S spectral

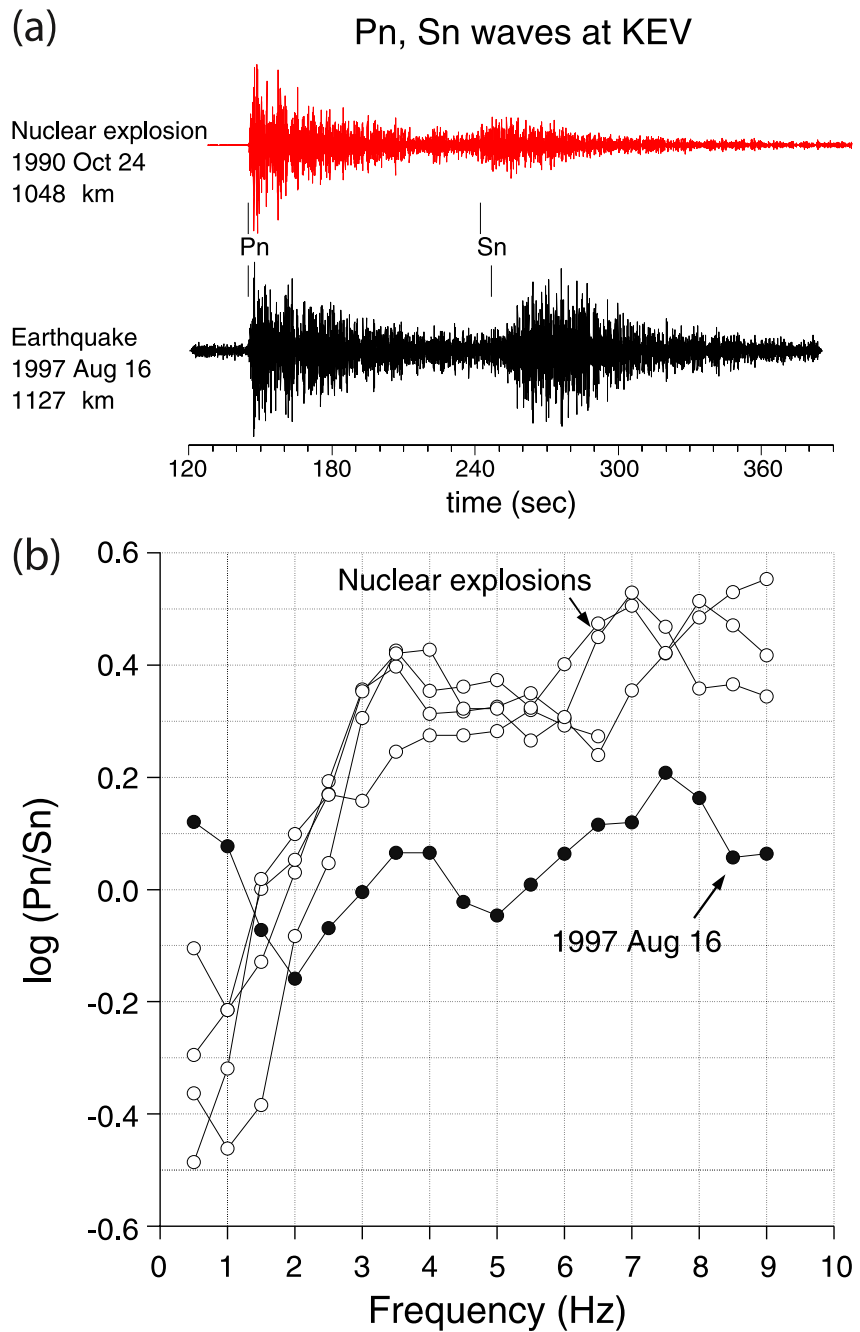


Figure 35. (a) Waveforms for a Soviet-era nuclear explosion at the Novaya Zemlya test site (top red trace, 24 October 1990, 1,048 km) and for the 16 August event (bottom black trace, 1,127 km), recorded at the same station, KEV (Kevo, in northern Finland). (b) P -to- S spectral ratios for a few nuclear explosions (white), and for the 16 August 1997 event (black), at KEV. From Richards and Kim (1997).

with InSAR as discussed in Section 6.2, has helped to better estimate the moment tensor of events based on a relatively limited number of recordings.

In practice, there is no perfect “silver bullet” discriminant that can be applied to seismic data to distinguish between earthquake and explosion sources; and there are additional specialized questions of how to distinguish between the seismic signals of nuclear explosions and those from chemical explosions, which in most cases are conducted as a ripple-fired series of small charges to achieve the commercial purpose of breaking and moving rock (Khalturin et al., 1998). As new discriminants are proposed, they are critically evaluated and some survive

Vertical Records from Nuclear Tests in North Korea, 2006-2017 at MDJ (Mudanjiang, China)

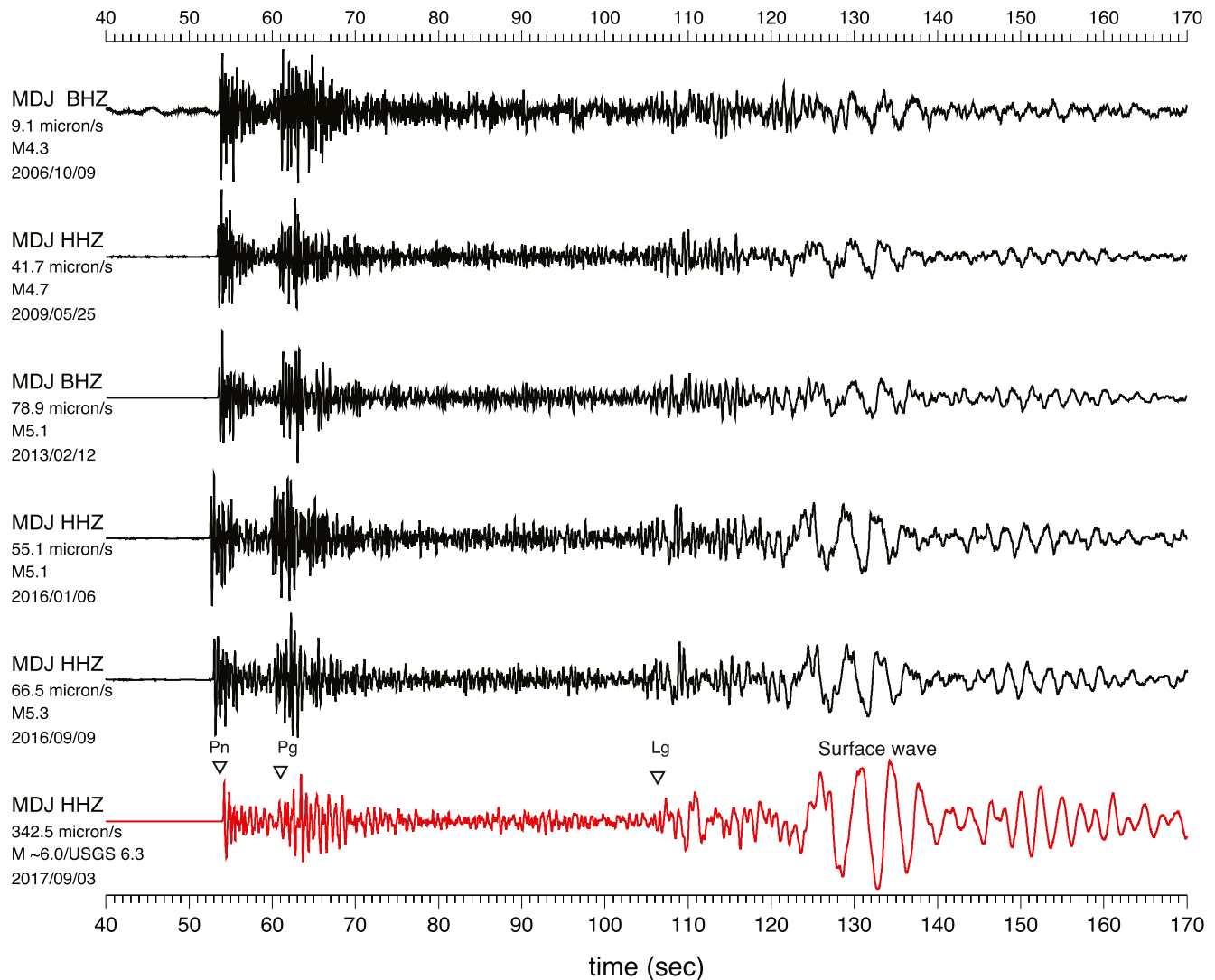


Figure 36. Vertical ground velocity due to the six nuclear test explosions conducted by the Democratic People's Republic of Korea between 2006 (top trace) to 2017 (bottom trace) recorded at MDJ (Mudanjiang, Heilongjiang Province, China), located about 335 km to the north of these events. Note that the y-axis changes scale for each event.

to become particularly useful. An overall point which emerges from experience with monitoring DPRK nuclear tests through 2022, 26 years after the CTBT text was finalized, is that capabilities to monitor underground nuclear testing today are orders-of-magnitude better than was generally anticipated when the CTBT was opened for signature in 1996. As illustrated above, many of these capabilities directly resulted from observations made from long-running, high-quality GSN stations. Regional signals are particularly useful because they can have the best SNR for small events.

8. Progress in Seismic Event Location Promoted by Global Seismographic Networks

When seismologists speak of “seismic data” they typically mean seismograms. However, for much wider communities of Earth scientists, engineers, and stakeholders, including policymakers, journalists, emergency managers, nuclear test-ban monitoring communities, and for insurance and other commercial-sector interests, the “seismic data” of greatest interest are various data products that are derived from seismograms (e.g., Hutko et al., 2017; Trabant et al., 2012). Of these, the most fundamental are lists of earthquake and explosion locations, origin times,

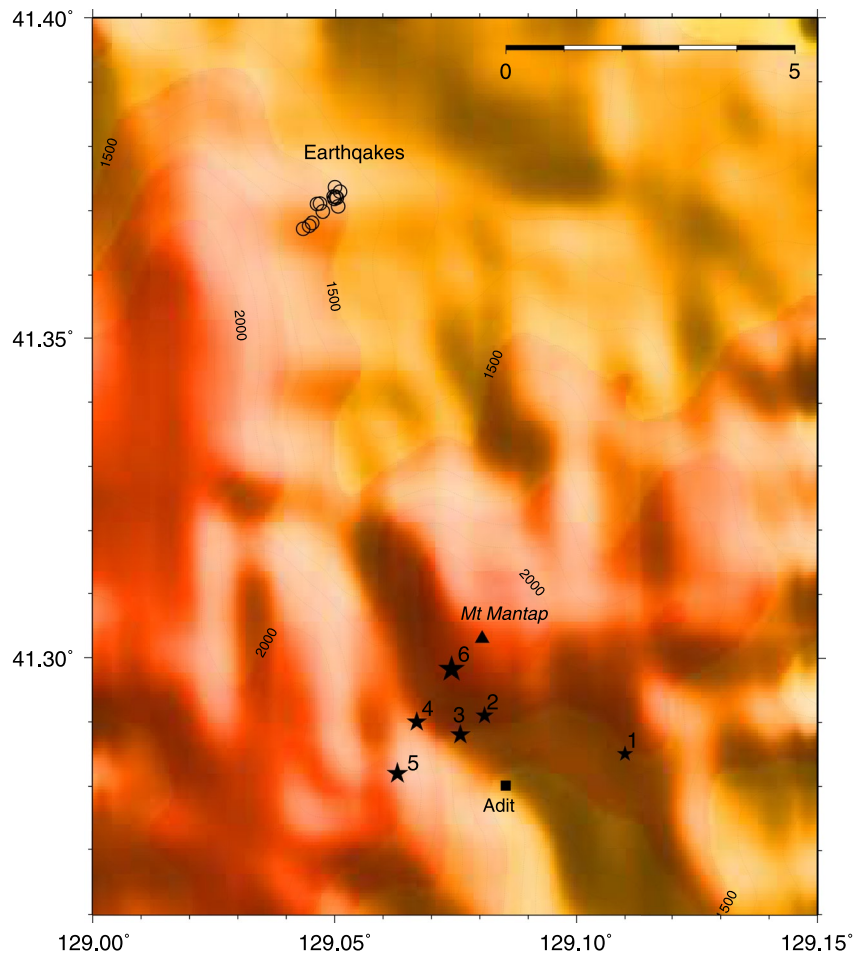


Figure 37. A map showing locations for the summit of Mount Mantap (black triangle); the first Democratic People's Republic of Korea underground nuclear explosion (UNE; small star), to the east and south of this summit; five subsequent UNEs conducted within the mountain (larger stars) including the large test explosion of 3 September 2017; and a series of small aftershocks aligned over several hundred m, about 8 km to the north of the peak (black circles). Adapted from W.-Y. Kim et al. (2018).

magnitudes and other source characteristics, and intensity information. Hypocenter lists, or event catalogs, are often backed up by a published *bulletin of seismicity* that summarizes local, regional, or teleseismic phase arrival time reports, and other fundamental observations made at stations.

In 2009, the U.S. National Science Foundation accepted a report on grand challenges in seismology and understanding Earth's dynamic systems (Lay, Aster, et al., 2009). It noted that, "Recent advances in data quality and availability, advanced processing methods, and computational capabilities enable significant improvements in earthquake catalogs and Earth models, yet there is not a dedicated effort to systematically enhance these fundamental seismological products. It is realistic to commit to monitoring almost all seismicity on all continents down to $M \sim 3$ events, and beneath the oceans down to $M \sim 4$, over the next decade. Event location accuracy can be systematically improved on large and even global scales, with relative locations as accurate as a few hundred meters rather than current levels of a few to tens of kilometers. Integration of catalogs ... would benefit basic research, applied research, and many societal applications that use seismicity distributions."

In practice, national and international mission agencies charged with providing catalogs and assessments of seismic events have to support major efforts to maintain stations and to incorporate increasing data volumes associated with increasing numbers of stations. Progress toward the "grand challenges" goal stated above has therefore been slow, although special studies of particular regions with active seismicity have shown that monitoring

capabilities can be extended down to magnitudes lower than three for extensive continental regions, and we note examples below.

Seismicity bulletins, whether produced on a local, regional, national, or global scale, have the potential for significant improvement—that is, better event locations, better completeness to lower magnitudes, better characterization of focal mechanisms, and estimates of finite source size for the larger events. Improved characterization of seismic events has often been the key to new insights into earthquake processes and structures, and drives new levels of confidence in the ability to accurately monitor a region of interest. Of course, new seismicity insights and improved monitoring capabilities are the very rationales upon which much work in seismology is funded. For some users, prompt reporting on all types of seismicity is essential. For others, the most complete catalog of earthquakes or explosions is needed, even if this information is not finalized until long after the events occur. Since different user community needs will not be met with a single catalog and bulletin, a range of products exists for different interests that include geophysical research, quantitative estimation of seismic hazard, and monitoring arms control treaties, and tracking the weapons-development programs of a potential adversary.

Seismic event location is a nonlinear optimization problem. In sections below, we first comment briefly on aspects of a traditional method in which events are located one-at-a-time using phase picks, noting that such location estimates have improved because of substantial growth in globally distributed stations reporting. We then discuss a series of developments in the use of regional waveforms, and waveform archives associated with global networks, that can provide complementary results.

8.1. Locations Based on Phase Picks for Each Seismic Event, Contrasted With Methods Using Waveform Segments

The traditional approach to event location uses iterative, linearized least squares methods and was introduced by Geiger (1910, 1912). The data are the arrival times, measured on seismograms, of particular seismic phases, most commonly *P*-waves, and these observations are best fit to a theoretical model of travel times and source origin time to minimize differences with measurements quantified by an objective function. Such methodologies are associated with three difficulties.

1. They use only a small fraction of the information contained in seismograms.
2. Phase arrival information is measured where the signal is typically quite small, which can lead to inaccuracies in picking signal onsets (e.g., from emergent signals).
3. They require a forward model to predict observed phase arrival times (e.g., ray-tracing through an assumed Earth seismic velocity structure) that will in general be 3D, complex, and will differ between regions.

Extensive efforts have been made to get around the third difficulty, for example, by developing source-specific station corrections for each seismographic station in a network (Murphy et al., 2005), or by use of methods for rapidly calculating regional seismic travel times in a simplified 3D Earth model (Myers et al., 2010). The speed of *P_n*-waves can vary by more than 10% between different regions, so it is indeed worthwhile to use better regional travel-times for purposes of interpreting the times at which signals arrive. But the first two difficulties remain. To address them both, recorded waveforms can be used rather than arrival times. And then numerous choices must be addressed such as what time window and frequency band to use to improve event detection and location; and what methods to apply to the waveforms.

Ideally, as with Geiger's method, one would develop a model of seismic-wave velocities within the Earth together with source models for candidate seismic events under study—and adjust parameters of these models to fit observed waveforms. The challenges of that approach are daunting, as indicated for example, by K. B. Olsen et al. (2018) in their finite difference simulations of regional seismic waves at stations in the Republic of Korea (South Korea) from the DPRK nuclear test of 2009.

K. B. Olsen et al. (2018) pushed simulation of wave propagation in state-of-the-art 3D crustal models, using a fairly smooth 3D model with 24 billion points at uniform spacing (100 m), noting that modern capabilities enable synthetics up to 4 Hz out to distances of several hundred km. They included anelastic attenuation parameterized by a variety of *Q* models, and achieved some success with synthetics that matched the timing of observed regional wave arrivals; but they at first grossly overpredicted Rayleigh-wave amplitudes and under-predicted the coda. After adjustment to *Q* values, their key to achieving better fits between synthetics and observations—of *P_n*, *P_g*,

Sn, *Lg*, and Rayleigh waves—for seismograms that are broadly similar to those shown in Figure 36—was to add small-scale perturbations of the *P*- and *S*-velocities according to statistical rules that are summarized by the strength and length scale of inhomogeneities. It is satisfying that computations and modeling are at last able to confirm a speculation of Jeffreys (1931a), who also noted oscillations after the arrival of *P*- and *S*-waves and before the arrival of surface waves. He examined and rejected a host of explanations, concluding that “the only suggestion which survives is that the oscillations are due to reflexions of the original pulse within the surface layers.”

Porritt and Conley (2021) have also explored the effects of stochastic scattering on synthetic waveforms, but using 2D and 2.5D finite difference methods. Their focus was on the regional seismograms of earthquakes in Oklahoma recorded by USArray stations. Remarkably, the observed spectra of the smaller events (M2.9 and M3.7) have much of their signal above 1 Hz with an apparently increasing frequency with distance, from 200 to 1,000 km, and beyond; and signals that can extend up to about 10 Hz.

Regional waves for example, at the GSN station MDJ (Mudanjiang, China) and at the IMS arrays Ussuriysk in Russia and KSRS in the Republic of Korea, from DPRK explosions, are recorded (to about 10 Hz and above) after propagating hundreds of wavelengths; and the duration of substantial amplitudes in such seismograms can be tens of seconds. The community cannot generate 3D synthetics that are a good fit to such observations although we have described significant progress. It is well worth pushing hard, to fit details of synthetics to observations across as broad a band of frequencies as possible, with associated benefits of improving our knowledge of Earth structure, of the statistical features of stochastic scattering, and of source properties such as stress drop and details of the distribution of slip over a finite fault region. But the observed band in practice extends to high frequencies that cannot be fully modeled today.

Fortunately, as we next discuss, empirical methods have been developed that work quite well to access waveform information pertinent to event location and discrimination. Such empirical methods improve event detection and location in regions of high seismicity—that is, in areas where many events take place. Each event can be compared with its neighbors, to obtain relative locations and sizes of seismic events in active regions. It is preferable to work with absolute locations rather than relative ones, but for studies in earthquake physics and patterns of stress, relative locations can be adequate. And relative locations may, over time, be promoted to absolute ones on the basis of special information on some of the events.

8.2. Empirical Methods of Event Location Applied Using Regional Waveforms From Sparse Station Networks

Many different groups have contributed practical methods of monitoring regions of active seismicity, where the emphasis is on comparative analysis of two signals at each station that recorded both signals from a neighboring pair of events. In particular, the relative time of arrival, ΔT , of a whole waveform can be measured from waveform pairs at a common station. Precision that had been on the order of a few tenths of a second (in measurement of the arrival time of weak *P*-waves) is significantly improved, in measuring the relative time of a common waveform from two events at the same station. Obtaining the relative location for each event within an event cluster can then be done using double-difference methods, as described by Waldhauser and Ellsworth (2000), again with significant improvement in precision—since what is sought is the relative location of event pairs, and ignorance of the velocity of seismic waves in the region between a group of events and each recording station does not matter when the input measurement from each station is ΔT for each event pair. Only the horizontal velocity in the source region—of the phase of interest, enters the relationship between ΔT measurements at different stations and the relative vector location of the two events.

Waveform correlation was applied to digital seismic data for the first time on a significant scale in the 1980s in Iceland (Slunga et al., 1995), using empirical methods rather than synthetics, to detect, locate, and characterize seismic events. Many authors, often working independently, have developed these methods for application to diverse regions. Here, we review successes with the empirical approach in application to the seismicity of seismic events in continental regions of Central Asia and East Asia. We describe techniques evaluated for limited regions and then applied on much larger scales. For practical results in broad regions with data from a sparse network of stations, we focus on estimating epicentral locations only—that is, for shallow sources with no indication of significant depth.

Thus, Schaff and Richards (2004a) used data from five GSN stations in China and South Korea to study in detail the relative location of 28 events in Liaoning Province, China that occurred in 1999. Cross correlation of *Lg*-wave windows provided highly accurate differential travel-times—the associated location precision was about 150 m even though stations were typically at distances 500–1,000 km from the source region. Epicenter estimates were not substantially affected by the paucity of stations nor by large azimuthal gaps. Much larger studies of the seismicity of China and nearby regions for the 21-year period 1985 to 2005 were shown by Schaff and Richards (2004b, 2011) to have a significant fraction of repeating events. Such event pairs had seismograms that looked highly similar at each station recording them both — indeed so similar that the events must be within one km of each other. The repeat events comprised more than 10% of the seismicity of China, and more than 2,000 pairs of them, broadly distributed, were used by Jiang et al. (2014) to assess the quality of locations published in seismicity bulletins based on the China National Seismograph Network and the Beijing Capital Region Seismograph Network (for which each event was separately located using traditional methods). Event pairs that had to be within 1 km (from their waveform similarity at common stations), were located on the order of a few km apart even in the best monitored regions with high station density, and were typically reported a few tens of km apart in remote regions such as the Tibetan Plateau. It is remarkable that cross-correlation methodologies applied to high-quality but sparse global networks can resolve event locations better than traditional methods applied to networks of local and regional stations.

Successes with repeats among known events raises questions about finding additional repeats using seismograms from known events as templates, and by searching continuous recorded ground motion for new events with similar but smaller signals. Slinkard et al. (2016) evaluated methods for searching continuous data for a large region of central Asia for 2006–2008. They used data from three high-quality stations: BVAR and MKAR (small arrays), and the GSN station KURK (Kurchatov, Kazakhstan; a 3-component station). Underlying issues were: what quality of templates is needed for effective detection; and how could newly detected events be validated? They confirmed over 6,500 unique detections that are not in event bulletins for the region, most of them validated by detection of the same event at different stations.

This study identified mistakes, easily made at first, that need to be avoided when processing many thousands of seismograms (too many to inspect individually). For example, it was found that a template for an earthquake recorded at a distance of about 1,000 km would be problematic if it also included the signal from a local mine blast, since this could lead to many detections due to cross-correlation with other blasts from the same local mine—but none of these detections should be taken as detections of additional earthquakes near the one which provided the earthquake signal in the template. Slinkard et al. (2014) also obtained practical experience with detection methods by exploring different types of seismic signals to use as templates. The relatively simple choice of just the main part of the *Lg*-wave, for 25 s, was found to be most effective. Presumably this is because the *Lg*-wave for the region being studied had the highest SNR. Slinkard et al. (2014) used the pass-band from 0.5 to 5 Hz. This paper also introduced a method for choosing correlation-detection thresholds tailored for each template applied to each station channel, to achieve a pre-determined false alarm rate.

Supplementing these results on event detection for a large region, case studies reported by Richards et al. (2015) explored the capability of locating seismic events precisely using GSN *Lg*-waveforms recorded at far-regional distances from event clusters. An underlying issue is how well can the work be done when the events within a sub-cluster are very close to each other. Cross-correlation methods were applied to measure ΔT values of pairs of events within sub-clusters, within a region of dense seismicity several hundred km west of station BJT; and these values were then used to obtain relative epicenters. The first relocated cluster, shown in Figure 38a, consisted of 10 events near (39.0°N and 110.6°E) spread out over about 10 km. It was relocated with precision at the level of about one km. Contributing to each of the measurements ΔT of the relative arrival times of signals from each pair of events, as recorded at a common station, is a small uncertainty presumably due to the fact that the waveforms are slightly different. The second cluster, consisting of nine events near (39.2°N and 112.5°E), spread out over only about 1.5 km, and in this case their signals are so similar at each of the stations recording them, that sub-sample measurements of ΔT are essentially due only to the slight differences in event location. The resulting confidence ellipses in Figure 38b are then only a few tens of meters across, a remarkably precise result for such a sparse regional network.

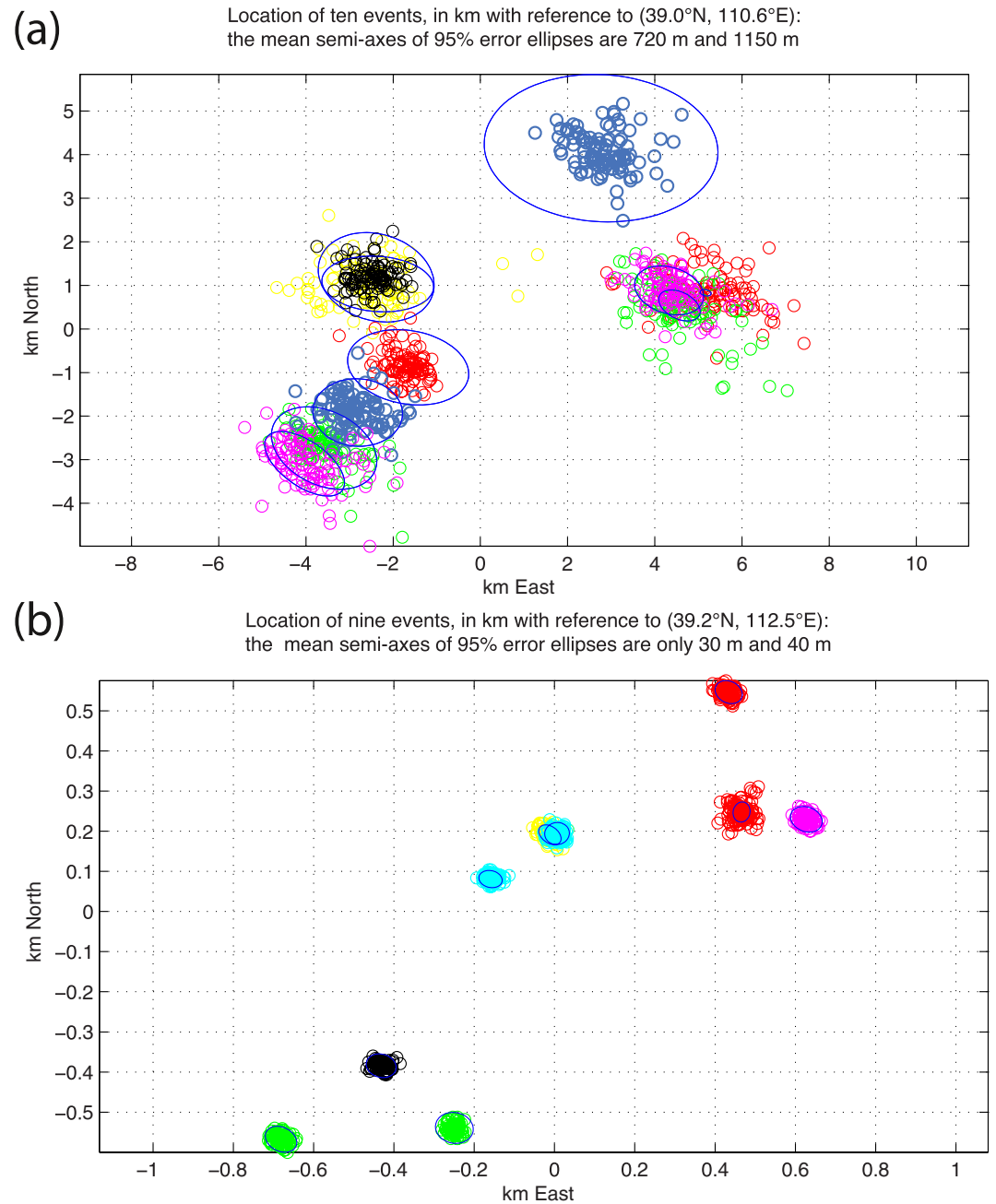


Figure 38. Estimates of the relative location of two clusters of seismic events, and the precision of these estimates. (a) Ten events clustered in the time period from December 2009 to August 2012, using the method of Schaff and Richards (2004a). These locations are more than 300 km from BJT, 1,000 km from ULN, and 600 km from XAN (the three stations at which L_g signals from these events were cross-correlated to obtain precise relative arrival times). The bootstrap errors (distribution of small circles) agree well with the error ellipses. Panel (b) similar to panel (a), but now for the relative location of nine events clustered in the time period from April 2006 to August 2006. These locations are about 500, 1,000, and 550 km, from stations BJT, ULN, and XAN, respectively. The relocation of events within a cluster can be remarkably precise if the cluster is small, because then their waveforms are so similar, as recorded at common stations. Note the scale differences between panels (a) and (b).

We note that aftershocks can be a challenge to monitoring agencies, since they may occur at the rate of hundreds per day in the hours and days after a major earthquake. Characterizing them well, is a part of understanding the process by which stress release occurs throughout the overall source volume of the main event.

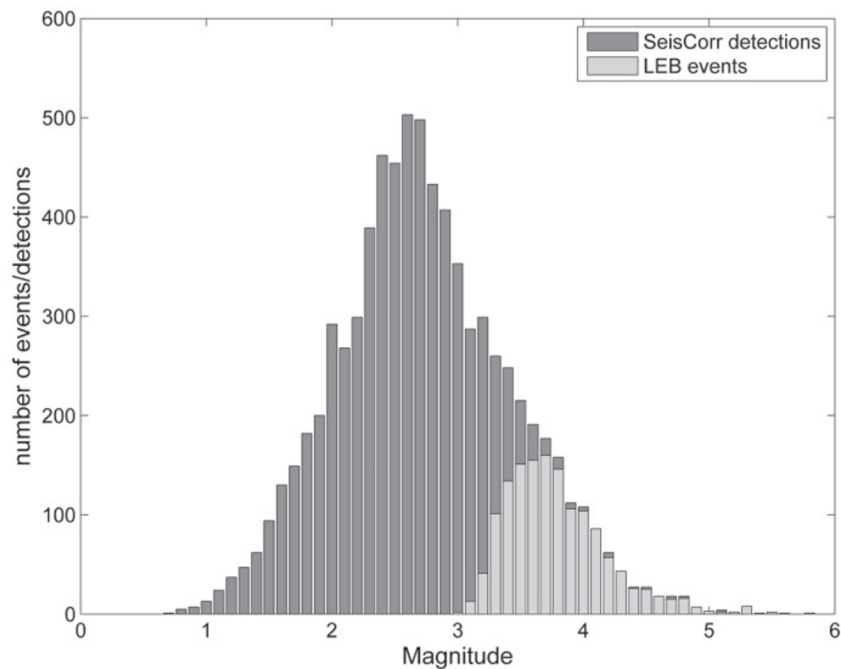


Figure 39. Distribution of magnitudes for newly detected aftershocks of the Wenchuan earthquake (dark gray). Event Bulletin of the International Data Centre of the Comprehensive Test-ban Treaty Organization magnitudes are also shown for template events (light gray). Adapted from Slinkard et al. (2016).

A case study by Slinkard et al. (2016) used a set of template waveforms from known aftershocks of the Wenchuan earthquake (12 May 2008, M_s 7.9), as listed in a seismicity bulletin from the CTBTO IDC, and searched for these same waveforms in continuous data recorded by three GSN stations at regional distance (XAN, EMH, and KMI), plus five temporary stations deployed as part of the Array Seismology Collaborative Experiments in Northeastern Tibet. Slinkard et al. (2016) detected more than 6,000 additional events in the mainshock source region from 1 May to 12 August 2008. These new detections are distributed in magnitude in the way expected for aftershocks, as shown in Figure 39. They extend the magnitude of completeness downward by 1.1 magnitude units. And they lead to a more than fivefold increase in number of known aftershocks compared with the global bulletins published by the IDC and the International Seismological Centre. Moreover, more $M > 2$ events were detected than were reported by the nearby Sichuan Seismograph Network. Several clusters of these detections were then relocated by Slinkard et al. (2016) using the double-difference method, yielding locations that reduced travel-time residuals by a factor of 32 compared with the initial bulletin locations. These results suggest that using waveform correlation on a few regional stations can find aftershock events very effectively, and can locate them with precision.

Experience acquired from these case studies was applied by Schaff, Richards, et al. (2018) to see how well relocation could be done for a broad area. Epicentral relocations for all of mainland China and surrounding areas using cross-correlation measurements (about 111 million of them) were made on Lg waves recorded at regional distances on a sparse station network (Figure 40). Using a two-step procedure (pairwise locations and cluster locations), they obtained high-quality locations for 5,623 events comprising 20% of a starting catalog for all of China for 21 years and 25% of a catalog for Wenchuan aftershocks. The average semi-major axes of the 95% confidence ellipses are 420 m for all of China and 370 m for Wenchuan. It is remarkable that such good relocations were obtained in view of the large azimuthal gaps and station distances (98% of the station distances for all of China are over 200 km, and the mean and maximum station distances are 898 and 2,174 km). These results provide order-of-magnitude improvements in locations for event clusters, using waveforms from a very sparse far-regional network for which data are openly available. Two examples are shown in Figure 41, where each cluster located precisely is quite small and has a lineation that conforms to one plane of the focal mechanism for one of the events. Also important, is that the percentage of events which can be relocated with high precision is

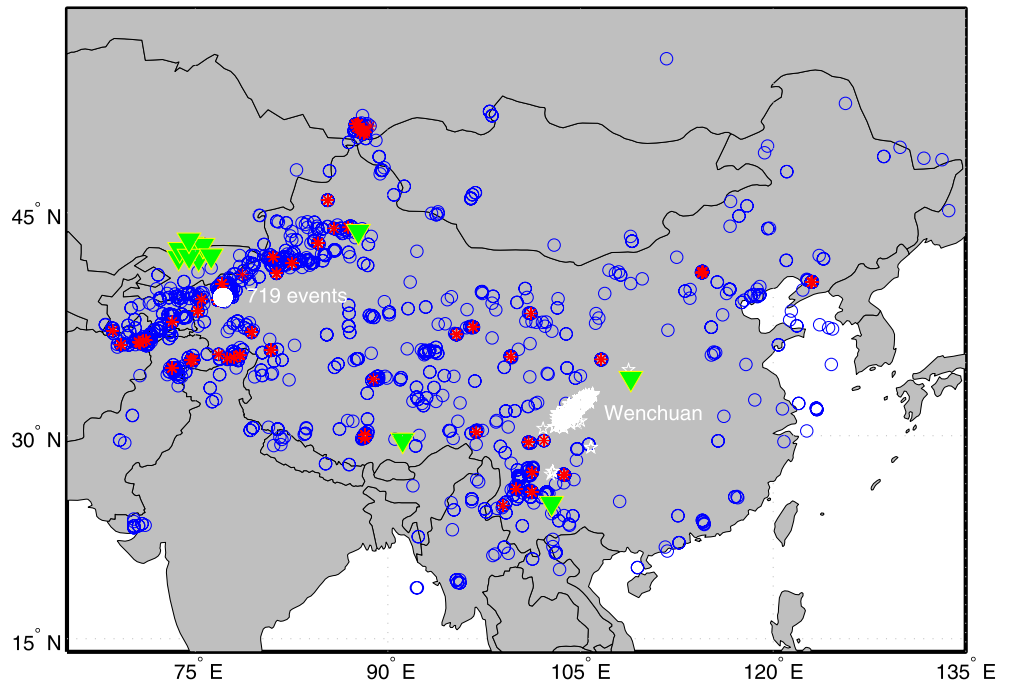


Figure 40. A map of location estimates based on Lg -waveforms for 5,623 seismic events well distributed throughout China; 3,689 for all of China from 1985 to 2005 and 1934 for the Wenchuan area from May to August 2008. Green triangles show the only 14 stations that recorded more than 33% of the Annual Bulletin of Chinese Earthquakes events for the 21-year time period. Location of Wenchuan events (mostly aftershocks) is given by white stars; a 719 event cluster is given by a white dot. Red stars indicate locations of the 64 clusters having seven or more events. Single circles denote two or more superimposed events (collocated at this scale). Adapted from Schaff, Richards, et al. (2018).

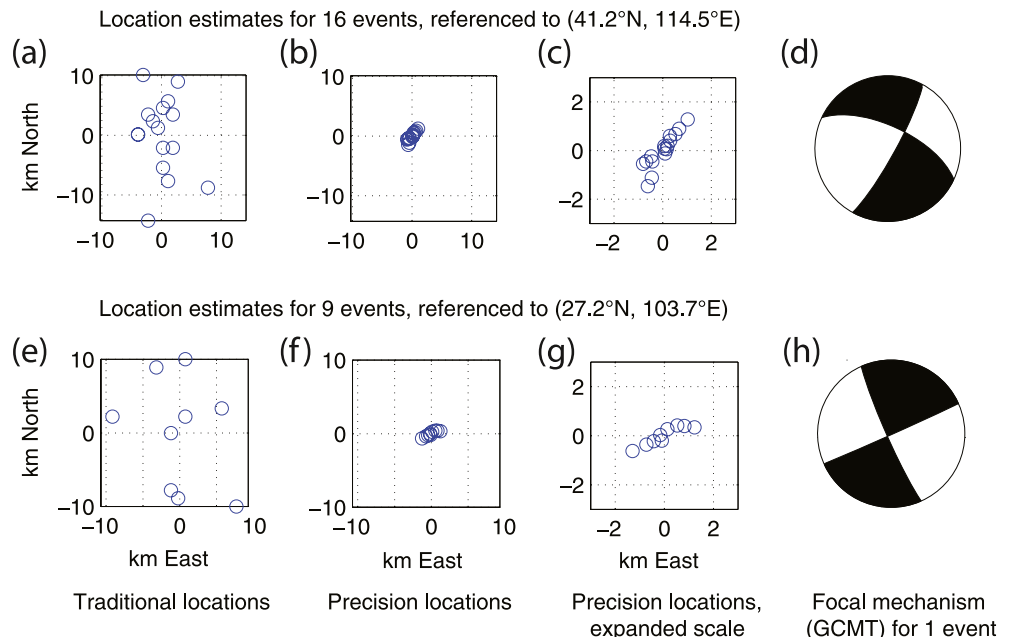


Figure 41. (a) Location of an event cluster, as reported in the Annual Bulletin of Chinese Earthquakes (obtained via the traditional method of locating events one-at-a-time from phase picks). (b) Final location of epicenters from the same cluster (based on cross-correlation measurement of ΔT between event pairs recorded at common stations). (c) Zoomed in view of panel (b). (d) Moment tensor for an event in the cluster. Panels (e–h) are the same as panels (a–d), respectively, but for a different cluster. Adapted from Schaff, Richards, et al. (2018).

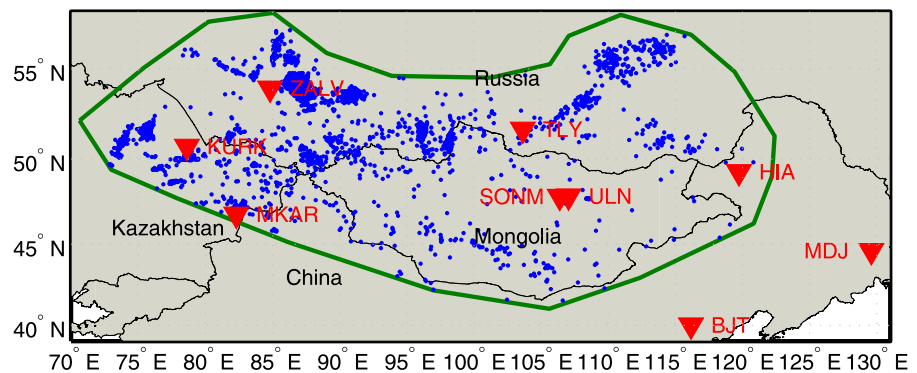


Figure 42. A study of seismicity in Mongolia and neighboring regions from 2012 to 2016 that implements template-searching of continuous data to detect new events and relocation of events using regional L_g waveforms recorded at common stations.

about double the number of repeating events reported earlier, enabling better insight into the underlying tectonic structures associated with seismic events whose relative locations can now be well-estimated.

Schaff, Richards, et al. (2018) used only the events reported from 1985 to 2005 in the Annual Bulletin of Chinese Earthquakes. With the prospect of being able to detect (and then relocate) many more events if modern methods of template searching were applied over a broad region, these authors proposed a six-step scheme to apply modern methods of event location in a particular region of space and time:

1. identify seismic events likely to be well recorded, using, for example, a regional bulletin or detailed global bulletin;
2. extract waveforms to serve as templates (a few tens of seconds of the L_g -wave had been identified as suitable);
3. cross correlate the template for each channel against the continuous archive for that channel, and note detections (e.g., via cross-correlation values greater than a value identified via a predetermined false alarm rate, as discussed in Slinkard et al., 2014);
4. validate such detections (via an association approach or against a local bulletin); after a review of the quality of the detections;
5. measure the relative arrival times (via cross correlation) of pairs of events that were not far apart from each other and were recorded at common stations; and
6. relocate as many events as possible using double-difference methods.

Preliminary results are now emerging, for example, for the 5 years encompassing 2012 to 2016 for seismicity in the polygonal region shown in Figure 42 which includes all of Mongolia, plus large regions of China, Kazakhstan, and Russia, including the Kuzbass region of southern Siberia where extensive blasting is conducted to mine coal and iron ore. Using about a thousand templates per station, cross-correlation detections were made on searches of continuous data for a sparse network of IMS array stations, plus six long-running 3-component open stations. More than 30,000 events were detected, for which initially there were too few stations in the detection network to perform locations. Fortunately a temporary Portable Array Seismic Studies of the Continental Lithosphere (Aster et al., 2005) network with many stations had been deployed in Mongolia during the 5-year time period of this study. Adding data from that network, based on expected arrival times for L_g -waves based on the sparse network of Figure 42, allowed measured differential travel times to be estimated at enough stations to make location estimates. Preliminary results reported by Schaff in July 2021 at the Science and Technology conference sponsored by CTBTO in Vienna included location results similar to those obtained in a previous study for all of China (Schaff, Richards, et al., 2018), with very low residuals (~ 0.02 s) and small confidence ellipses (a few 100 m across). As shown with an example in Figure 43, it is obvious from their daily and weekly time-of-occurrence statistics that many of these events are mining blasts from the Kuzbass region just east of station ZALV (Figure 42).

To conclude this section, we see that recent decades of research on seismic event detection and location have produced results that offer far more detailed information on spatial and temporal patterns of seismicity than can be derived from the traditional single event approaches which dominate today's seismicity bulletins. Catalogs in

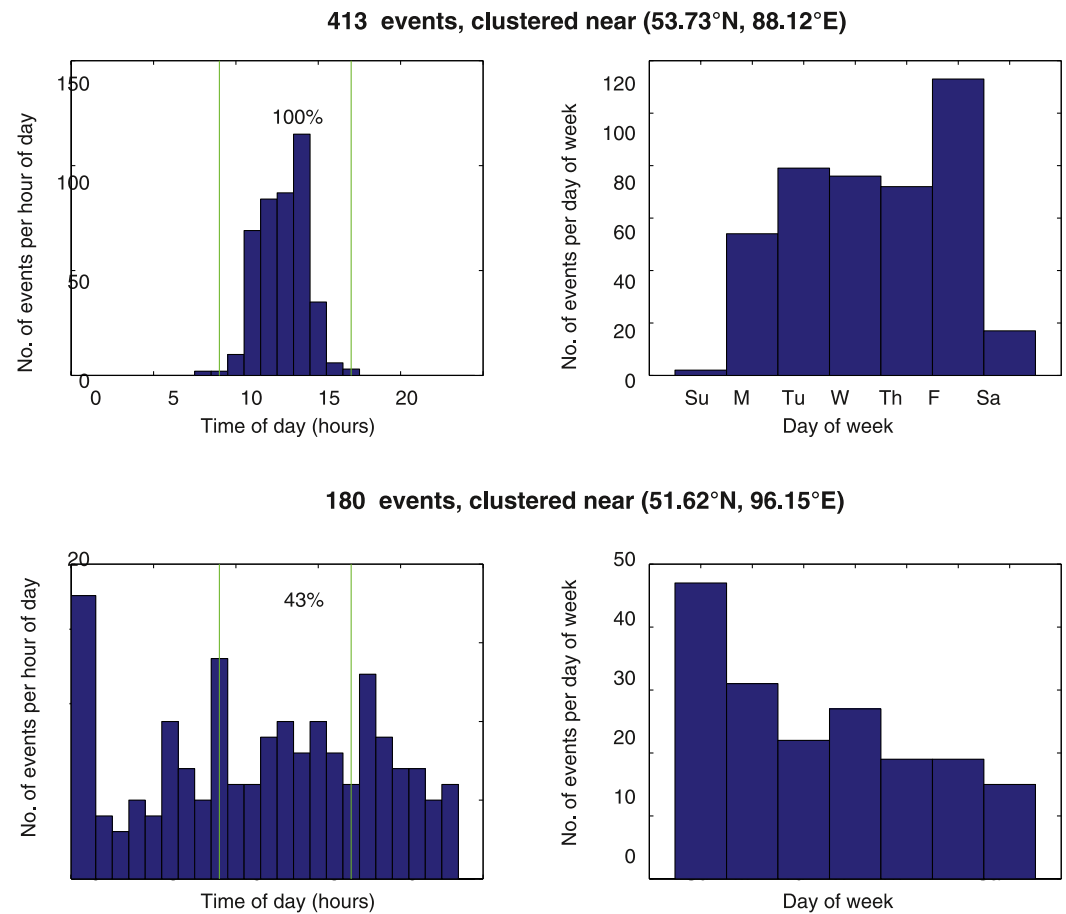


Figure 43. Examples of clusters of seismic events, detected and relocated in the vast polygon shown in Figure 42 including Mongolia and the Kuzbass region of southern Siberia. Shown here are bar charts for two clusters, indicating the distribution of local time-of-day and day-of-week for the events in each cluster. The upper pair of more than 400 events exhibit the timing of blasts in a mining operation. The lower pair includes the cluster of aftershocks of a significant earthquake that occurred on Sunday, 26 February 2012.

which events are located one-at-a-time with phase picks continue to be good starting estimates, and will continue to be critical for reporting events in areas of sparse seismicity. The very name long-used by the USGS for its bulletin using such methods (the “Preliminary Determination of Epicenters”) is informative in that it is indeed preliminary. Monitoring communities today are beginning to appreciate and implement methods to systematically realize more accurate catalogs. The new methods leverage continuous archives of high-quality waveforms and require attention to effective computational strategies, since the percentage of events amenable to analysis via modern methods gets larger as archives extend over time, and as smaller events are added to the catalog. In turn these improvements raise questions about whether the development and application of modern methods of event detection and location should be done as a community service by a centrally organized unit, or should be left to scientists who apply the new methods on smaller scales to enable higher-quality analysis of particular regions of interest.

9. Environmental Seismology

Greatly expanded globally distributed broadband seismic data acquisition and analysis have coincided with increasing motivations and interest in “Environmental Seismology,” in which seismic records are utilized to study near-surface processes arising in and coupling the solid Earth (notably including the cryosphere), atmosphere, and hydrosphere (Larose et al., 2015), including effects associated with climate change. Networks of broadly

distributed seismic stations have enabled development of this field by providing low-noise records of ground motion in oceanic and ice-covered regions.

In this section, we review key advances in environmental seismology, emphasizing those that have utilized data from GSNs as well as a broader perspective on the expanding scope of this subfield.

9.1. Global Seismic Excitation by Ocean Waves

The cumulative forces of ocean gravity waves on the solid Earth produce the most globally continuous and ubiquitously observed seismic signals. Every broadband seismometer that is deployed in a quiet environment on Earth records two spectral peaks in seismic energy that are referred to as the “primary” and “secondary” microseisms (Figure 6).

Ocean-generated seismic signals, or microseisms, arise from nonlinear ocean wave interactions (Ardhuin et al., 2011, 2015; Hasselmann, 1963; Longuet-Higgins, 1950; Nakata et al., 2019) that create spatial and temporal varying forces at the sea floor and along continental and island coasts. The predominant global microseism wavefield consists primarily of Rayleigh waves spanning, with increasing period range, the secondary, primary and “Earth hum” (Bromirski & Gerstoft, 2009; Suda et al., 1998; Traer et al., 2012) bands (Section 2.1). In recent decades much weaker *P* and *S* body waves of ocean microseism origin have been globally recognized and studied using array (Gerstoft et al., 2008; Landes et al., 2010; Nishida & Takagi, 2022) and correlation methods (L. Li et al., 2020). Ocean gravity waves additionally excite elastic waves in the atmosphere (see Section 10.1). The microseism bands create a globally observed ambient seismic wavefield that can be processed using the methods of seismic interferometry (e.g., Curtis et al., 2006; Nakata et al., 2019; Schuster, 2009) to recover seismic Green functions for Earth structure and temporal variation (e.g., Mordret et al., 2016; S. Wang & Tkalčić, 2020) studies.

The primary microseism, which is observed at periods between approximately 6 and 25 s (0.04–0.17 Hz), reflects the action of waves generated by winds over the oceans, particularly by large storms with extensive fetches that excite large deep-water wave systems (Elfouhaily et al., 1997). The primary microseism represents the most direct proxy for ocean wave amplitudes and direct wave impacts on coastal regions, since it is generated by wave forces that are applied in coastal regions in shallow water, but is strongly dependent on wave direction and coastal bathymetry (Aster et al., 2008; Cessaro, 1994; Gerstoft & Tanimoto, 2007).

The secondary microseism, observed at periods between approximately 3 and 12.5 s (0.08–0.34 Hz) and thus occupying about half the period range of that of the primary microseism, is commonly ~30 dB stronger in acceleration power (Figure 6). The secondary microseism arises from nonlinear interactions of superimposed and opposite-traveling waves that create ocean floor pressure variations, and its amplitude and period reflects wave amplitude, directional wave number, and spectrum (Ardhuin et al., 2011). Because it is excited by pressure variations that span the ocean water column and elastically couple with sub-seafloor structure, secondary microseism generation is also affected by water depth (Longuet-Higgins, 1950) and local Earth structure (Kedar et al., 2008). Ocean sedimentary basins, bathymetry and other structural complexities may also facilitate the excitation of higher mode Rayleigh waves, Love waves (Gualtieri et al., 2020, 2021; Le Pape et al., 2021), and *S* waves (Xiao et al., 2021).

Relative and absolute ocean wave metrics can be extracted from the microseism wavefield (Bromirski & Duennebier, 2002; Bromirski & Flick, 2020; Moschella et al., 2020) and wave effects due to variations in climate indices, sea ice, and other environmental drivers can be discerned across decade-scale time periods using data from long-duration globally distributed seismographic stations (Anthony, Aster, & McGrath, 2017; Aster et al., 2010; Tsai & McNamara, 2011). The data quality and long-running history of GSNs and the prominent generation of microseism signals has been exploited to examine hurricanes, typhoons, and other extreme storm events (Ebeling & Stein, 2011; Gerstoft et al., 2006; Retailleau & Gualtieri, 2019) across the world's oceans over the last 30 years, as well as decade-scale secular changes in ocean wave intensity and location (Aster et al., 2008, 2010; Grevemeyer et al., 2000), and interactions between climate indices, ocean state, and the cryosphere (sea ice) (Anthony, Aster, & McGrath, 2017; Cannata et al., 2019). Because many GSN sites occupy former WWSSN sites (Figure 1), the opportunity exists to deploy or analyze co-located buoys at select, coastal GSN stations, where comparisons could be performed, and to reconstruct historical wave states dating back to the 1960s (Bromirski & Flick, 2020). One hurdle is that WWSSN seismograms were recorded on paper drums (Peterson & Hutt, 2014) which complicates analysis. However, advances in digitization of paper records (e.g.,

M. Wang et al., 2014) have started to be leveraged to extract historical microseism properties (Lecocq, Arduin, et al., 2020). Improvements in modeling of microseism source processes, verified through microseism observations made predominantly at GEOSCOPE and GSN stations, has increasingly facilitated validation of global wave hindcast estimates (Arduin et al., 2011; Kedar et al., 2008).

Although the microseism wavefield was viewed as a source of undesired noise for many decades, a twenty-first century revolution in the widespread of use of correlation-based background noise methods, driven by continuously recorded high-quality seismic data, has resulted in widespread utilization of this ambient wavefield for Earth imaging at the crust to uppermost mantle scale, particularly via Rayleigh wave inversion (Nakata et al., 2019; Shapiro et al., 2005; Stehly et al., 2006). The ubiquitous and long-wavelength microseism signal can also be used as a test signal to estimate relative seismometer sensitivities (Ringler, Storm, et al., 2015).

Global and regional seismograph stations play a pivotal role in detecting and understanding signals generated by the oceans at periods longer than the strong primary and secondary microseism bands. For instance, although observations of a third global microseism peak near 26 s had been made as early as 1961 (Oliver, 1962), later recording of this signal at GSN stations and its predecessor networks were able to show that the signal arose though oceanic excitation within the Gulf of Guinea, Africa (Holcomb, 1998; Shapiro et al., 2005).

A fourth globally observed ambient noise signal associated with ocean gravity wave activity, commonly referred to as “Earth hum,” occurs between 50 and 300 s period (0.003 and 0.02 Hz) (Bromirski & Gerstoft, 2009; Nishida, 2014). Earth hum was first observed in seismic records on vertical component, Streckeisen STS-1 sensors located at quiet GEOSCOPE and GSN stations (e.g., Nishida & Kobayashi, 1999). Later, the first observations of Earth hum on the seismometer horizontal components were made by Kurrle and Widmer-Schmidrig (2008) at four low noise global seismograph stations including the GSN stations BFO (Black Forest Observatory, Germany) and MAJO (Matsushiro, Japan). Modeling of Earth hum generation benchmarked against observations made at GEOSCOPE and GSN stations suggests that it arises in a manner similar to the primary microseism through solid-Earth forcing of infragravity waves (Arduin et al., 2015; Bromirski & Gerstoft, 2009). The Earth hum source process generates both Rayleigh and Love waves (Deen et al., 2018) and continuously excites Earth's spheroidal and toroidal normal modes (Kurrle & Widmer-Schmidrig, 2008; Nishida & Kobayashi, 1999; Tanimoto, 2007; Webb, 2008). Due to the long-period nature of the signal, ambient noise cross-correlations at sufficiently quiet seismic stations have been used to extract long-period surface waves for tomographic imaging of the upper mantle (Haned et al., 2016; Nishida et al., 2009; Ventosa et al., 2017).

9.2. Acoustic Ocean Tomography

The potential of large-scale ocean acoustic tomography using the oceanic long-range sound propagation wave guide has long been recognized (ATOC Consortium, 1998; Behringer et al., 1982; Wunsch, 2020). Seismic data from long-running seismographic stations have recently been used to estimate changes in ocean temperature (Wu et al., 2020) using global network-facilitated high-accuracy earthquake catalogs to identify near-repeating events near Sumatra. Associated hydroacoustic *T*-phases (Buehler & Shearer, 2015; Talandier & Okal, 1998) recorded on the GSN station at DGAR (Diego Garcia, Chagos Islands) were cross-correlated between 1.5 and 2.5 Hz to produce differential travel time measurements with a corresponding ocean depth sensitivity kernel that is maximal near 1,700 m (Figure 44). Such measurements are of both general oceanographic interest but are also of particular importance given the decades-long record of global network recording because in excess of 90% of recent anthropogenic surface warming is absorbed by the oceans (Zanna et al., 2019).

9.3. Cryoseismology

Glacial systems are prolifically seismogenic, and data from global seismographic networks were among the first to be used to identify seismic signals arising from large glacial sources in the polar regions and continue to play key roles in their study (Aster & Winberry, 2017; Pirli & Voss, 2021; Podolskiy & Walter, 2016). Seismic waves propagate readily through compact ice. Seismic stations sited adjacent to or atop glaciers and icebergs facilitate the monitoring of cryospheric seismic activity, and of temporal changes in source phenomenology, location, and occurrence in response to climate-driven or other changes. A growing body of seismic observations is being utilized to detect brittle failure, basal slip, and temporal changes in elastic response (Aster et al., 2021; Mordret

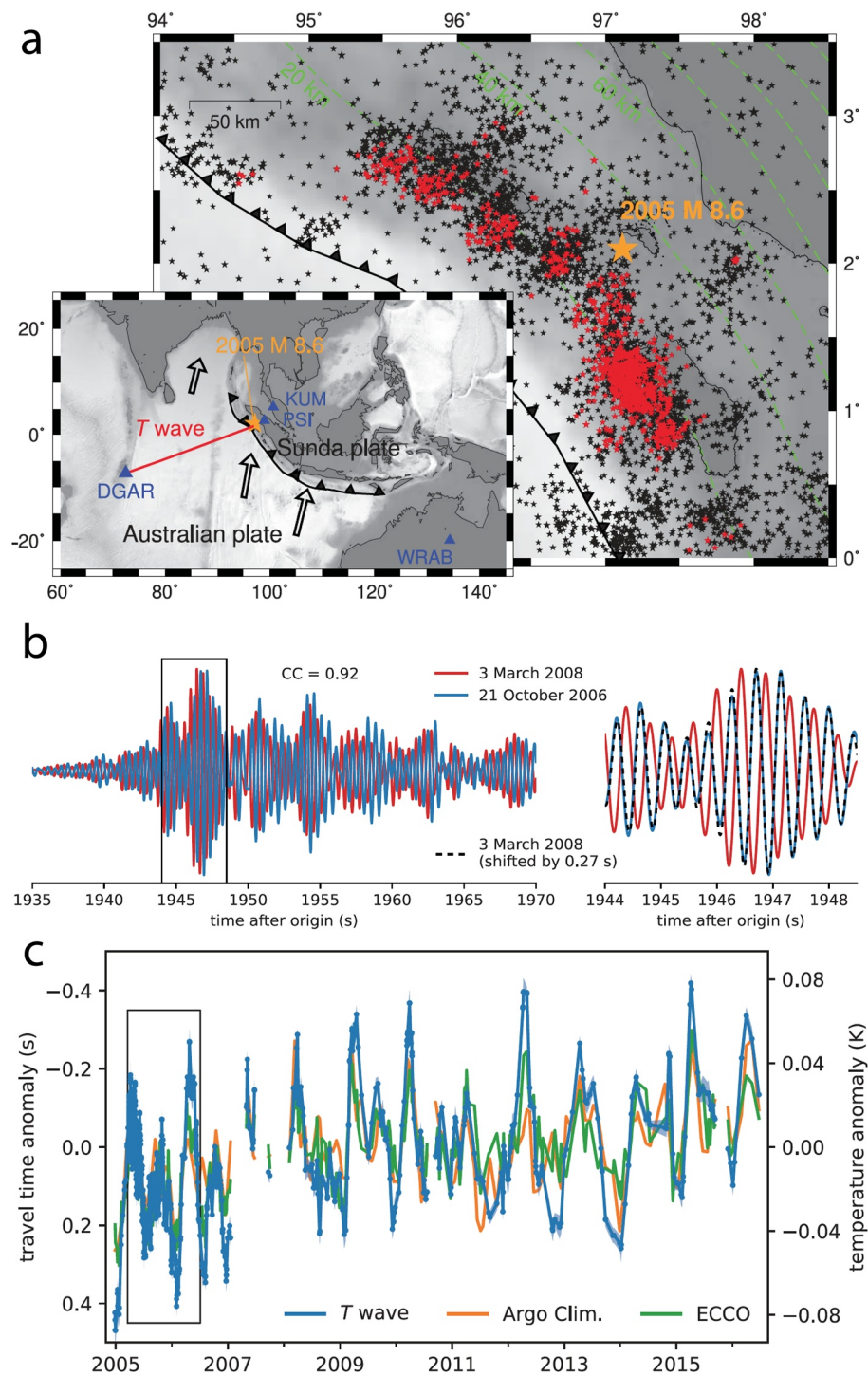


Figure 44. Ocean acoustic thermometry facilitated by seismology. (a) Study area of Wu et al. (2020) showing the aftershock zone of the 2005 M_w 8.6 Nias-Simeulue earthquake (orange epicenter star) and quasi-repeating aftershocks used in the study (red stars). Inset shows the oceanic T -phase ray path to GSN seismic station DGAR on Diego Garcia. (b) T -phase waveforms (1.5–2.5 Hz bandpass) for example, events in October 2006 (blue) and March 2008 (red), showing a cross-correlation best lag of 0.27 s (a uniform warming of 0.02°K corresponds to a -0.1 s travel time change for the $\sim 3,000$ km path). (c) Travel time anomalies and inferred temperature changes over a 10-year period compared to that predicted independently by Argo float climatology (orange; Riser et al., 2016) and ECCO (Estimating the Circulation and Climate of the Ocean, version 4, release 4; Forget et al. (2015); green) results. Boxed time period shows a particularly well-sampled period due to the numerous aftershocks during that time. Note that seismically estimated temperature excursions to depths greater than 1.5 km often exceed those from shallower sensitivity oceanographic methods. Reproduced from Wu et al. (2020).

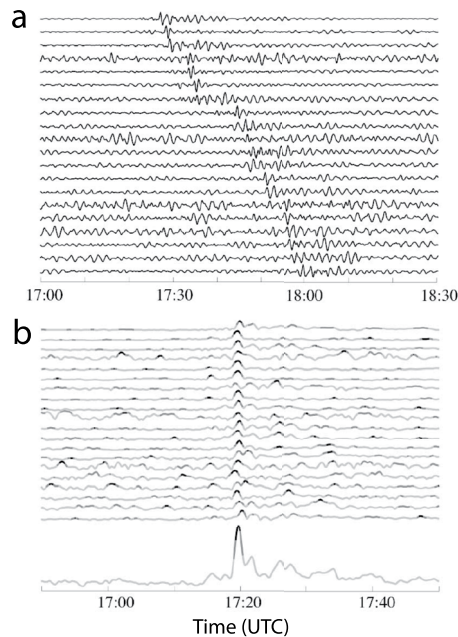


Figure 45. (a) Global long-period vertical-component 35–150 s period Rayleigh waves observed at ranges varying from (top to bottom) 19°–154° (~2,100–17,000 km) from a surface wave magnitude M_S 5.0 glacial earthquake in Greenland (68.75°N and 33.25°W) on 28 December 2001. (b) Corresponding envelope-processed and propagation lag-compensated signals, with the signal stack shown at the bottom. After Ekström, Nettles, and Tsai (2006).

et al., 2016; Olinger et al., 2019; Zhan, 2019) and provide analogs for seismic studies of icy bodies elsewhere in the solar system (K. G. Olsen et al., 2021; Vance et al., 2018).

Large-scale glacial calving (Ekström, Nettles, & Tsai, 2006; Ekström et al., 2003; Nettles & Ekstrom, 2010; Podolskiy et al., 2021; Tsai et al., 2008; Winberry et al., 2020) of icebergs with volumes up to $\approx 1 \text{ km}^3$ in Greenland, Alaska, and Antarctica radiates globally observable surface wave energy between about 10–150 s that is comparable to that produced by up to $M_s = 5$ earthquakes (Figure 45). These events exhibit anomalously long source duration relative to earthquakes of similar magnitudes, in some cases exceeding 60 s. Seismogenic forces generated during calving, collapse, and buoyant overturn of icebergs are multiple and complex. However, inferences of the principal long-period source forcing, estimated by non double-couple moment tensor inversions, visual observations, and by computational and laboratory modeling, are consistent with a superposition of horizontal reaction force applied to the glacial front and hydrodynamic vertical force applied to the sea bed (Murray et al., 2015; Veitch & Nettles, 2017). Secular changes in the location and occurrence of seismogenic calving events in Greenland indicate that they have increased in occurrence and advanced northward in recent decades due to warming-driven changes in ocean temperature and glacial state and dynamics (Ekström, Nettles, & Tsai, 2006; K. G. Olsen & Nettles, 2017; Veitch & Nettles, 2012). However, the complex source history and multiple seismogenic forces generated during iceberg calving complicate efforts to tightly estimate mass flux and other glacial metrics from far-field seismic observations alone (Bonnet et al., 2020; Sergeant et al., 2016; Winberry et al., 2020). These events appear to be most seismically efficient when the glacier terminus is near to the grounding line (Veitch & Nettles, 2012), a condition that has recently become more common in Greenland (Nettles &

Ekström, 2010) and (M. Nettles, written personal communication, 2021) due to widespread retreat of glacial ice tongues (E. A. Hill et al., 2017). This retreat and weakening process is also accelerating for some tidewater glacial systems and ice shelves in Antarctica (Lhermitte et al., 2020; Paolo et al., 2015). Conditions favoring these large calving-associated events are relevant to the important Marine Ice Cliff Instability process (Parizek et al., 2019) and prospective future Antarctic ice loss and attendant global sea level rise (DeConto et al., 2021; Joughin & Alley, 2011). These conditions become enhanced when marginal and/or ice shelf back stress is reduced (as by ice shelf weakening or collapse), inland glaciers accelerate and thin to near flotation, and the marine glacial terminus becomes subject to tidal and flexural bending stresses, basal crevasse formation, and other factors that favor repeated large-scale calving (Amundson et al., 2010; T. D. James et al., 2014).

Long-period and regionally visible glacial seismic events also can originate from slow basal stick-slip events on asperities beneath Antarctica's ice streams, with the most thoroughly studied region to date being the Whillans Ice Stream (Bindschadler et al., 2003; Guerin et al., 2021; Wiens et al., 2008) draining the West Antarctic Ice Sheet with a long-term interevent stable sliding velocity of approximately 0.5 m/day (Walter et al., 2011). Long-operational GSN far-field stations in Antarctica (especially the low background noise stations QSPA and VNDA, which have sensors installed in the ice sheet and rock boreholes, respectively (Anthony et al., 2015)) have played a key role in the discovery and understanding of these slow events through their recording of Love and Rayleigh waves at periods between approximately 20–150 s. High surface wave amplitudes radiated in this period band occur during intervals of rapid moment rate change (e.g., at the start and end phases of these events). Slow ice stream basal events have seismic moments that approach those of M_w 7 earthquakes produced by an approximately $2 \times 10^4 \text{ km}^2$ slip patch undergoing up to $\sim 70 \text{ cm}$ of total slip, and using the rigidity of glacial ice ($3.5 \times 10^9 \text{ Pa}$) in the moment estimation. These events feature much slower slip propagation and stress drops than tectonic earthquakes, with basal rupture propagation velocity near 150 m/s and a stress drop near 250 Pa (Walter et al., 2011), and slip durations of tens of minutes. Because of the near-horizontal basal slip plane geometry and slow rupture, these events are most comprehensively observed with a combination of near- and far-field seismometry, combined with GNSS positioning atop or close to the rupture plane. These events are tidally modulated,

despite being over 600 km from open ocean, with quasi-repeating events typically occurring twice per day (once just after high tide and one just before low tide). The seismogenic slip behavior of the Whillans Ice Stream system is modulated by the flow rate of the ice stream, and has shown temporal variations that reflect changes in flow rates (Joughin et al., 2005; Winberry et al., 2017), and has undergone a long-term deceleration since the mid-1980s (Winberry et al., 2017).

Antarctic ice shelves and ice tongues calve Earth's largest icebergs, the greatest of which have masses near 10^{15} kg and surface areas exceeding 10,000 km² (MacAyeal, Okal, Thom, et al., 2008). Collisions of large icebergs (MacAyeal, Okal, Aster, & Bassis, 2008) amongst themselves and with the seafloor under the influence of tidal forces and ocean currents (e.g., Martin et al., 2010) can produce powerful and long-duration seismic signals ($f \gtrsim 0.1$ Hz and persisting for many minutes to hours) that are detected on seismographs at local, regional, and teleseismic distances (MacAyeal, Okal, Aster, & Bassis, 2008; Martin et al., 2010; Talandier et al., 2002, 2006; Tanaka et al., 2019). At the greatest ranges, the transmission of elastic energy is facilitated through the intermediary of short period ($> \sim 1$ Hz) ocean *T*-phases (Buehler & Shearer, 2015) that convert to local seismic phases near coasts (Talandier & Okal, 1998) and may be detected by island and near-coastal seismographs (Talandier et al., 2002, 2006) to teleseismic distances. The signals include up to hours-long “songs” (Müller et al., 2005) with evolving multi-voiced harmonic and/or broadband spectral signatures. The principal, if not necessarily exclusive, causative mechanism for iceberg tremor is repetitive stick-slip and the associated generation of spectral lines via a Dirac comb effect (Figure 46; Aster et al., 2021; Powell & Neuberg, 2003). Iceberg seismoacoustic sources contribute significantly to the ocean acoustic noise environment at frequencies from about 1–50 Hz, particularly in the Southern Ocean (Dziak et al., 2013; Matsumoto et al., 2014).

9.4. Environmental Seismology Beyond Global Networks

In addition to globally and regionally visible processes discussed above, isolated stations and regional seismographic networks observe a wide range of more local environmental phenomena. Notable areas of study include seismicity in frozen ground and frozen lake systems (e.g., Kavanaugh et al., 2019; Ruzhich et al., 2009); fluvial seismic radiation from water and sediment load transport in rivers, glacial outburst floods, and within and/or beneath glaciers (e.g., Burtin et al., 2008, 2010, 2016; Cook et al., 2018; Eibl et al., 2020; Roth et al., 2016, 2014; Schmandt et al., 2013; Tsai et al., 2012); snow avalanches (e.g., Lacroix et al., 2012; Marchetti et al., 2020; Suriñach et al., 2001; van Herwijnen & Schweizer, 2011), rockfalls and landslides (e.g., Bontemps et al., 2020; Norris, 1994); and resonant and other elastic and anelastic site effects excited in topographic features such as mountain massifs, cliffs and rock towers (e.g., Moore et al., 2018; Weber et al., 2022). Seismic interferometry using ambient noise may in principle be scaled across all seismic wavelength and length scales to study localized and near-surface temporal material changes due to environmental and climate forcing, including in permafrost (e.g., Albaric et al., 2021; S. R. James et al., 2019); glacial firn and snow (Chaput et al., 2018, 2022; MacAyeal, 2018; MacAyeal et al., 2018); water table and vadose zone saturation in aquifers (e.g., Clements & Denolle, 2018; Lecocq et al., 2017; Voisin et al., 2017), and crustal weakening and strength recovery at depths from the near-surface to tens of kilometers in response to earthquake strong ground motion (e.g., Q. Wang et al., 2019; Rubinstein & Beroza, 2004).

In recent years, there is increasing interest to analyze seismic data to study anthropogenic signals (different from nuclear tests and explosions as described in Section 7). Particularly on seismometers in urban environments, the amalgamation of everyday human activity is recorded as a near-continuous signal, with characteristic weekly and daily variations (e.g., Boese et al., 2015; Diaz et al., 2020; D. N. Green et al., 2017). With an understanding of anthropogenic seismic noise, it becomes viable to use this seismic signal for ambient noise tomography (Groos & Ritter, 2009). Global government-imposed lockdowns to combat the COVID-19 pandemic have intensified the study of anthropogenic seismic noise, as the staggered easing of restrictions would aid the characterization of dominant noise sources. At the same time, the reduced noise levels during lockdowns make it possible to detect natural events that otherwise drown in the noise (De Plaen et al., 2021; Grecu et al., 2021) and thus improve seismic hazard estimates. Notably, in a global study of lockdown effects on seismic amplitudes, Lecocq, Hicks, et al. (2020) also observed a significant reduction in seismic noise at 20 GSN stations.

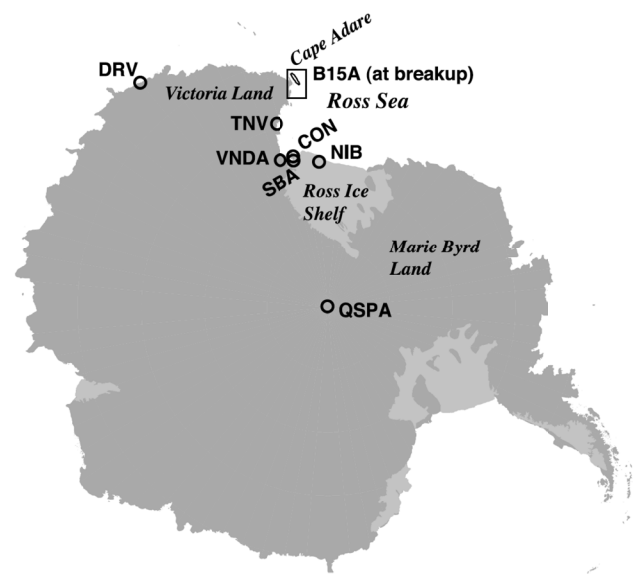
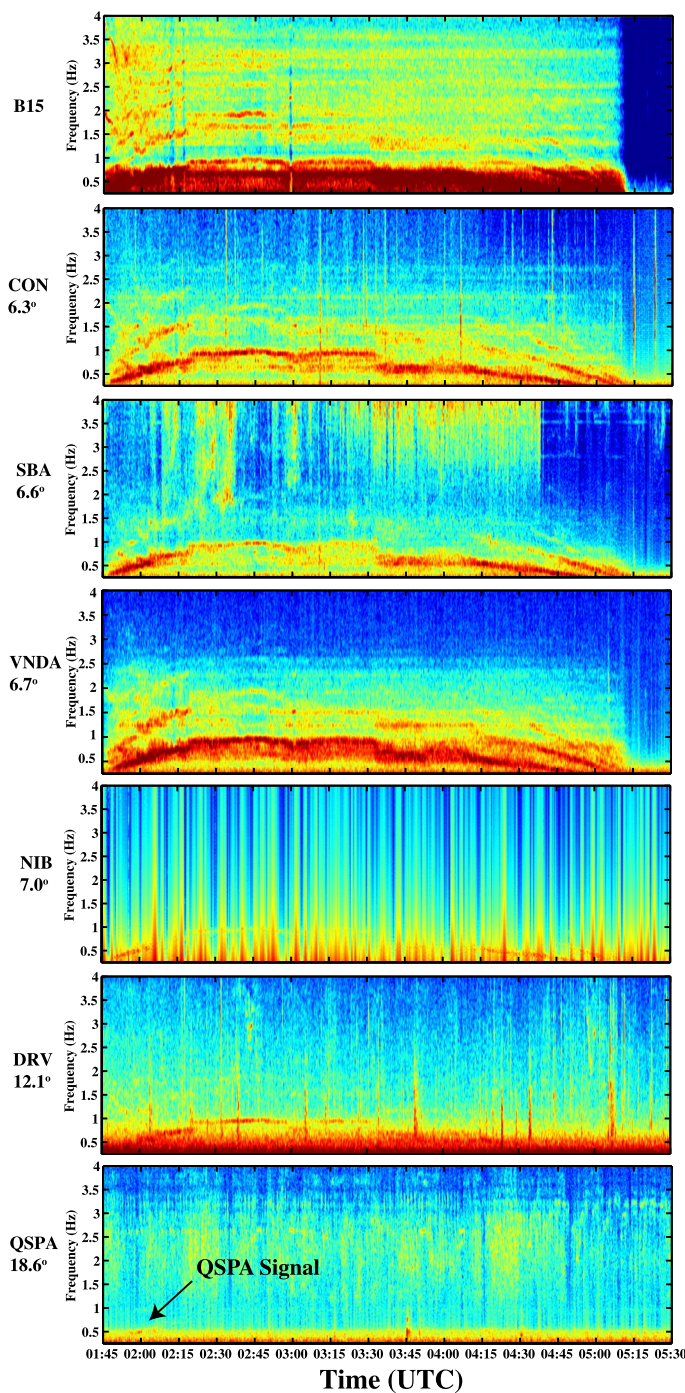


Figure 46. Vertical-component seismic velocity spectrograms of iceberg harmonic tremor during the seafloor grounding-induced breakup of iceberg B15A (pre-breakup areal extent of ≈ 120 by 70 km) on 27 October 2005, observed at Antarctic stations (inset). B15: Temporary station installed on a surviving B15A fragment; CON: Station near the summit of Mount Erebus Volcano, Ross Island (Aster et al., 2004); SBA: GSN station near Scott Base (New Zealand), Ross Island; VNDA: Global Telemetered Seismographic Network (GTSN) station near Lake Vanda, Dry Valleys; NIB: Temporary station near the front the Ross Ice Shelf; DRV: GEOSCOPE station near Dumont D’Urville Station (France); QSPA: GSN station near the Amundsen-Scott South Pole Station (US) (Anthony et al., 2021). Intervals of non-harmonic line spacing likely reflect multiple simultaneous sources during the complex breakup episode. Source-receiver distances are given in degrees. Reproduced from Martin et al. (2010).

10. Non-Seismic Signals

The high sensitivity and large dynamic range of modern seismographic systems confers on them an ability to measure many signals arising from non-seismic wave processes. Seismographic systems can be sensitive to atmospheric pressure at a wide variety of periods, ranging from the sonic band to atmospheric-Earth coupled normal modes (Alejandro et al., 2020; Beauclin et al., 1996; Edwards et al., 2007; Lognonné et al., 1998; Tauzin et al., 2013; Zürn & Wielandt, 2007; Figure 47), temperature (Doody et al., 2017), and magnetic field variations (Forbriger, 2007). To help identify these effects as well as mitigate them, many seismic stations are equipped with auxiliary sensors which record other environmental and geophysical phenomena. Although these non-seismic sensors are often considered secondary to the seismic channels, they provide data which can be utilized for other studies. It is also possible to deterministically subtract non-seismic signals from seismic data when these effects can be sufficiently modeled (e.g., Zürn et al., 2015).

10.1. Infrasond and Pressure

The combined deployment of infrasond transducers with seismometers opens up opportunities for better characterization of geophysical and anthropogenic noise sources, the study of elastic and gravity wave coupling between the solid Earth and atmosphere, and to improve our understanding of the atmosphere (Arrowsmith et al., 2010; Hedlin et al., 2012). In comparison with the rich history of GSNs, there has not been a comparably extensive legacy of global networks in infrasond science. However, following the decision to deploy a global network of infrasond arrays as part of the CTBT verification system in 1996, there has been significant growth in infrasond research. In the past 20 years, the IMS global network has grown from inception to become the first modern global infrasond network (Che et al., 2014; Kebeasy, 2008). As described at <https://www.ctbto.org/specials/vdec/>, a virtual Data Exploitation Centre provides scientists with a procedure for accessing CTBTO data, to conduct and publish their own research findings.

The research enabled by the IMS network has subsequently motivated the deployment of local and regional infrasond networks, which are typically co-located with seismometers (Arrowsmith et al., 2008; Che et al., 2019). These seismo-acoustic stations have been used to study how both natural and anthropogenic infrasond sources (including large industrial accidents) propagate in the atmosphere and couple into the solid Earth (Fuchs et al., 2019; Koper et al., 2003). The success of the initial infrasond signals recorded on TA motivated a much larger scale deployment throughout the remainder of the project (Tytell et al., 2016). Infrasond transducers have recently been added to 21 GSN stations (Wilson et al., 2018).

At global scales, most infrasond signals observed at multiple stations are generated by bolides (e.g., Figure 47), volcanoes, earthquakes, and the infrasonic equivalent of the secondary microseisms, microbaroms (Donn & Naini, 1973). For a description of the wider variety of possible sources observed at closer distances, the reader is referred to Bedard and Georges (2000). Infrasond observations of bolides on the IMS network have provided important estimates on impact size and can detect many previously unknown impactors (Silber & Brown, 2019). For example, infrasond observations of bolide airbursts recorded on the IMS network have suggested that the flux of impactors with diameters of tens of meters is greater than previously estimated (Brown et al., 2013). Energetic infrasond from explosive volcanism can propagate hundreds to thousands of kilometers in atmospheric wave guides and large explosive eruptions are routinely recorded by the IMS infrasond network (see the summary in Matoza et al. (2017)). In remote volcanic regions, infrasond is sometimes the only ground-based technology to record an explosive eruption. Infrasond has been observed on the IMS network from earthquakes, particularly from large events (Le Pichon et al., 2006). Back projection techniques can characterize the distributed source of infrasond from distant earthquakes, enabling non-seismographic estimates of ground shaking in remote regions (Shani-Kadmiel et al., 2021). The most ubiquitous signal observed on infrasond arrays are the ocean microbaroms. Data from the IMS network and other recent deployments have enabled the ocean microbaroms to be mapped (Landès et al., 2012), generation models to be explored (De Carlo et al., 2021), and have advanced the use of microbaroms as an ambient noise interferometry source to retrieve atmospheric state (Haney, 2009) and to extend understanding of the coupled microseism-microbarom system (Bowen et al., 2003).

In addition to the study of geophysical and anthropogenic sources, global infrasond networks provide the opportunity to study wave propagation, with applications to investigating the atmosphere and coupling of waves between the solid Earth and atmosphere. The atmosphere is a dynamic component of the Earth system, and atmospheric

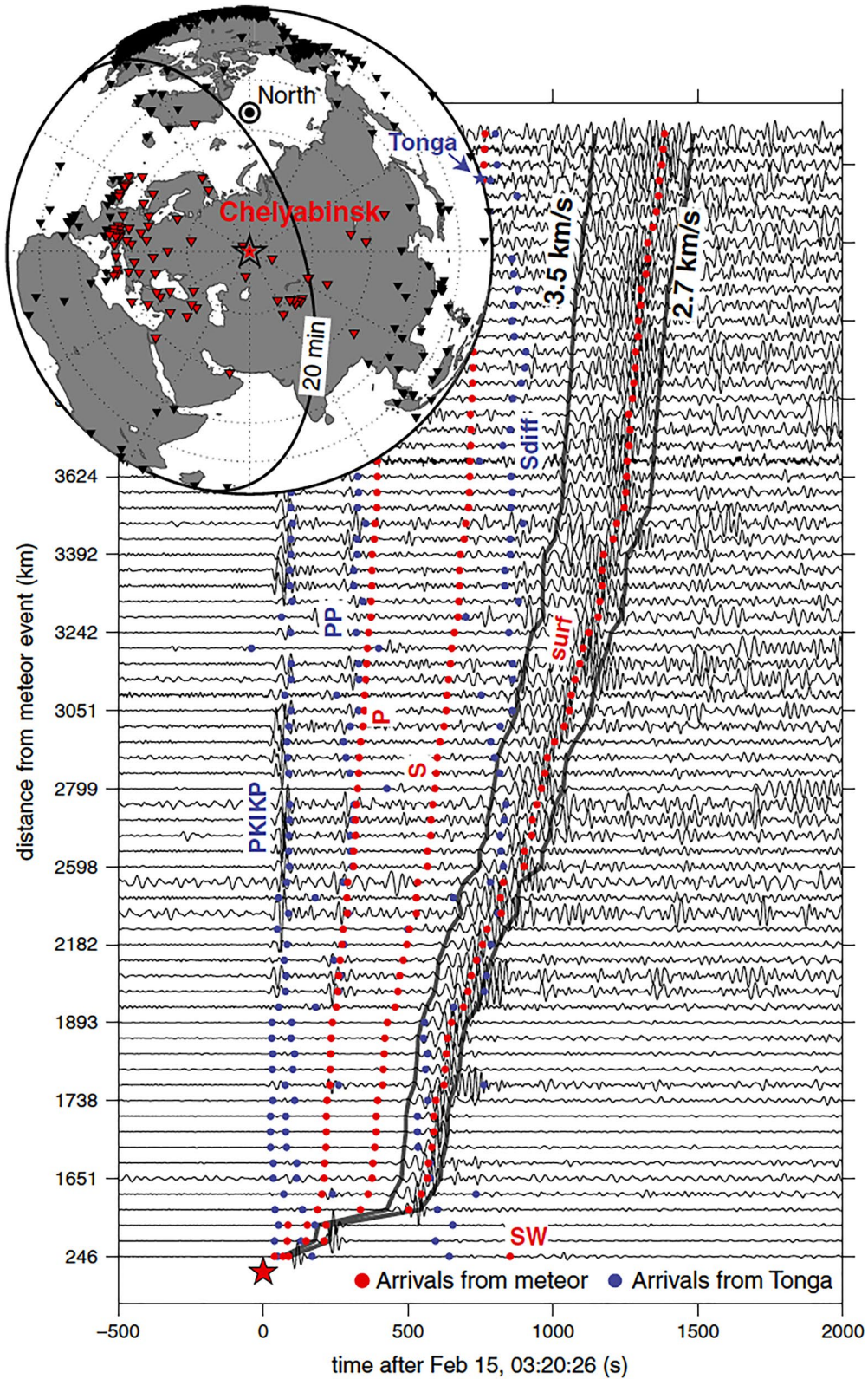


Figure 47.

variability covers an extremely wide range of temporal and spatial scales (Williams et al., 2017). Recent work based on IMS data and other temporary deployments is demonstrating that infrasound data can provide unique insights into these phenomena, ranging in time scales from minutes to years, and over spatial scales that include the boundary layer, troposphere, middle atmosphere, and thermosphere (e.g., de Groot-Hedlin & Hedlin, 2014). At short spatial-temporal scales, recent analysis of infrasound data from the IMS (Hupe et al., 2019) and other networks (de Groot-Hedlin et al., 2017) have shown that infrasound can provide unique and important measurements of key atmospheric gravity wave parameters (e.g., amplitude, frequency, direction, and vertical wavenumber spectra). At longer time and space scales, infrasound measurements can provide important information on synoptic and global-scale circulation patterns, particularly in the stratosphere and lower thermosphere. Researchers have begun to explore how infrasound can be used to infer information about temperature and wind profiles in the middle atmosphere, and how these unique data points might be assimilated in state-of-the-art atmospheric models (for a recent review see Assink et al. (2019)).

Beyond providing a mechanism to study atmospheric phenomena, pressure sensors provide data which can be used to correct seismic data that has been contaminated by local atmospheric pressure changes (e.g., Alejandro et al., 2020; Beauduin et al., 1996; Zürn & Widmer, 1995; Zürn et al., 2015, 2007). It is generally accepted that at periods greater than 20 s the elevated horizontal component seismic noise is largely generated by atmospheric pressure variations inducing local ground tilt (e.g., Sorrells, 1971). Current models suggest these tilts can be described by a Local Deformation Model, which characterizes deformation around the seismometer as a function of varying pressure as well as a Travelling Wave Model that models the pressure disturbance as an acoustic gravity wave (Zürn et al., 2007). The effect of pressure changes on vertical seismic data is better understood (Zürn & Wielandt, 2007), but these corrections are isolated to improving noise levels in a band between 3 and 10 mHz (Forbriger et al., 2021). This is in contrast to the pressure corrections applied to gravimeters where it is possible to obtain noise reductions at frequencies below 1 mHz (Freybourger et al., 1997).

10.2. Geomagnetic

The sensitivity of seismographs to magnetic field variations has been noted since the 1970s (Tape et al., 2020), particularly at high latitudes where large magnetic field variations during space weather events are easily resolved across multiple global stations (Díaz et al., 2020; Ringler et al., 2020). This makes it advisable to shield seismometers from magnetic field fluctuations using μ -metal (a nickel-iron alloy with high magnetic permeability), or other ferromagnetic material, and/or to record the local magnetic field to remove unwanted magnetic signal from the seismic data stream. Both of which are routinely done at most stations operating Streckeisen STS-1 seismometers (Forbriger, 2007). Figure 48 demonstrates that broadband seismometers across the globe recorded Sudden Storm Commencement geomagnetic events between 2008 and 2019.

A co-located fluxgate magnetometer can be used to remove unwanted magnetic field signals in seismic data, and also provides an independent record of the magnetic field at the station site (Ringler et al., 2020). As of this writing, 10 GSN stations (typically at high latitudes) have co-located magnetometers. While the drift of these magnetometers used in the GSN is not well known and the calibration procedures do not conform with those required by the International Real-time Magnetic Observatory Network (INTERMAGNET; Love & Chulliat, 2013), it has been shown that these could help increase the spatial resolution of space weather event detection (Tape et al., 2020). As seismologists make further use of long-term records provided from globally distributed seismograph stations it might be necessary for seismic station operators to adopt some of the INTERMAGNET practices for improving the characterization of amplitude drift, as identified at some long-running global seismic stations (Ringler, Evans, & Hutt, 2015). Therefore, future collaboration between the geomagnetic and global seismographic communities has the potential to improve observations and data quality in both fields.

Figure 47. Band pass filtered (20–60 s) vertical component seismograms retrieved from the Incorporated Research Institutions for Seismology and GEOSCOPE data centers, displaying seismic phases excited by infrasonic air waves from the exceptionally large Chelyabinsk bolide of 15 February 2013, for broadband seismograph stations within 4,000 km of Chelyabinsk, Russia, indicated by the red triangles and star on the map inset, respectively (note the nonlinear vertical distance axis). Predicted times for indicated seismic phases excited by atmospheric infrasound and teleseismic signals from a M 5.8 earthquake in the Tonga region (with the epicenter indicated along with its 20-min (1,200-s) P -wave arrival contour in the map inset) are indicated by red and blue dots, respectively. “North” indicates the geographic North Pole. Rayleigh surface wave amplitude correspond to an $M_s = 3.7$ near-surface seismic source. Reproduced from Tauzin et al. (2013).

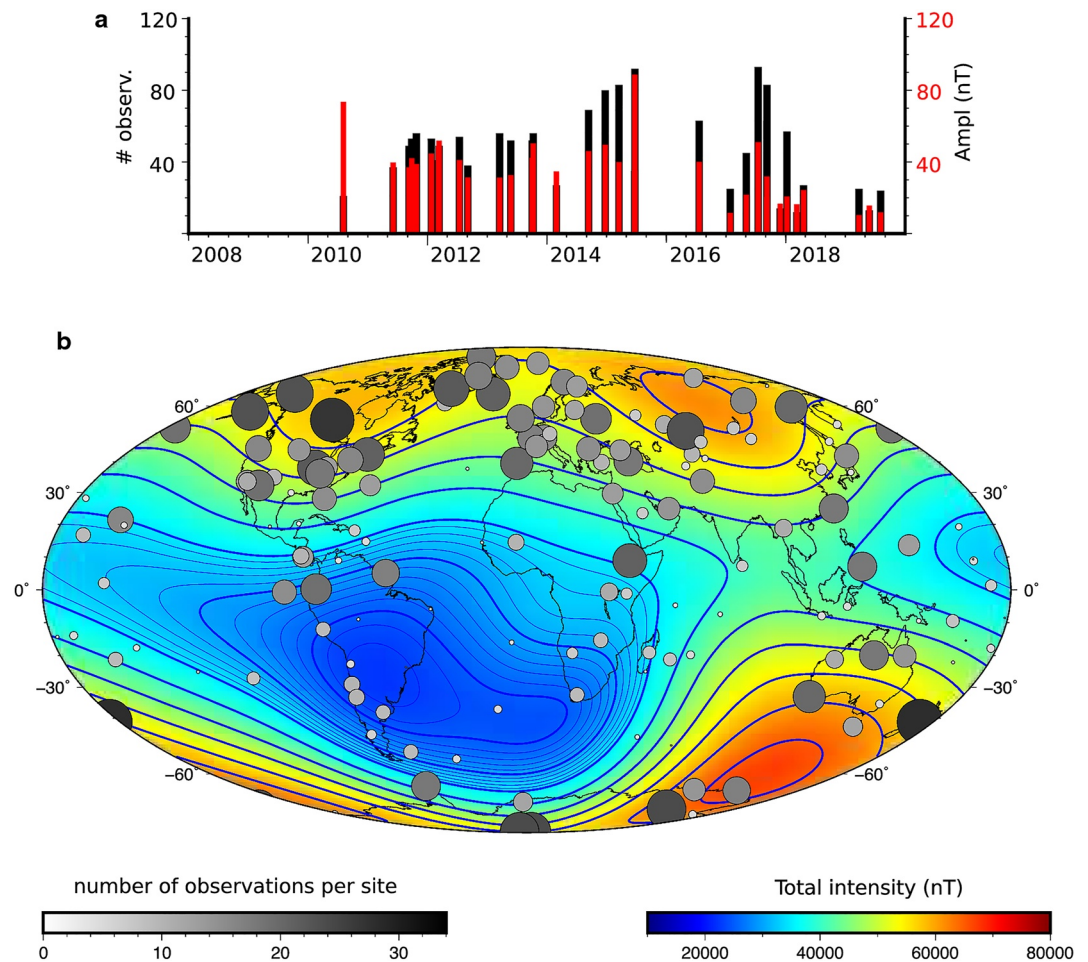


Figure 48. Magnetic amplitude of Sudden Storm Commencement (SSC) events compared with corresponding inductive signals detected by seismic stations. (a) Mean amplitude of the significant SSC events during the 24th solar cycle (red bars) compared with the number of observations of each event in the broadband stations (black bars). (b) Total magnetic intensity (NOAA National Centers for Environmental Information (NCEI) Geomagnetic Modeling Team and British Geological Survey, 2019) for 2018 compared to the number of SSC observations for each investigated broadband seismic station. Isolines are shown every 1,000 nT below 35,000 nT and every 5,000 nT above this value to better estimate the South Atlantic Anomaly. The size and gray saturation of the circles indicates the number of observations at each seismic site. Reproduced from Díaz et al. (2020).

10.3. Meteorological

Many global seismograph stations are supplemented with meteorological instrumentation (e.g., wind speed and direction, humidity, temperature, rainfall, and total precipitation). While the detailed seismic signatures of local to regional meteorological phenomena are areas of recent research (e.g., Valovcin & Tanimoto, 2017), many station operators have made an effort to record these additional observations for site awareness and for their future scientific potential (Tytell et al., 2016). For example, force-feedback broadband seismometers are extremely sensitive to changes in temperature (Melton, 1979). While correcting seismic data that is affected by temperature variation-induced noise in otherwise low-noise environments has not been generally incorporated yet, recording temperature can help to identify sensors that are not adequate thermally isolated (Doody et al., 2017). For example, in Figure 49 we show that the STS-1 (blue) and Streckeisen STS-6 (green) record the diurnal Earth tides while the secondary Streckeisen STS-2 sensor (orange) at GSN station TUC (Tucson, Arizona) is insufficiently thermally isolated to recover this signal with high fidelity.

It is not clear if seismic noise due to local wind can be removed as well as the removal of noise due to temperature effects. This difficulty reflects the highly site-dependent and nonlinear spatial and directional variability of wind

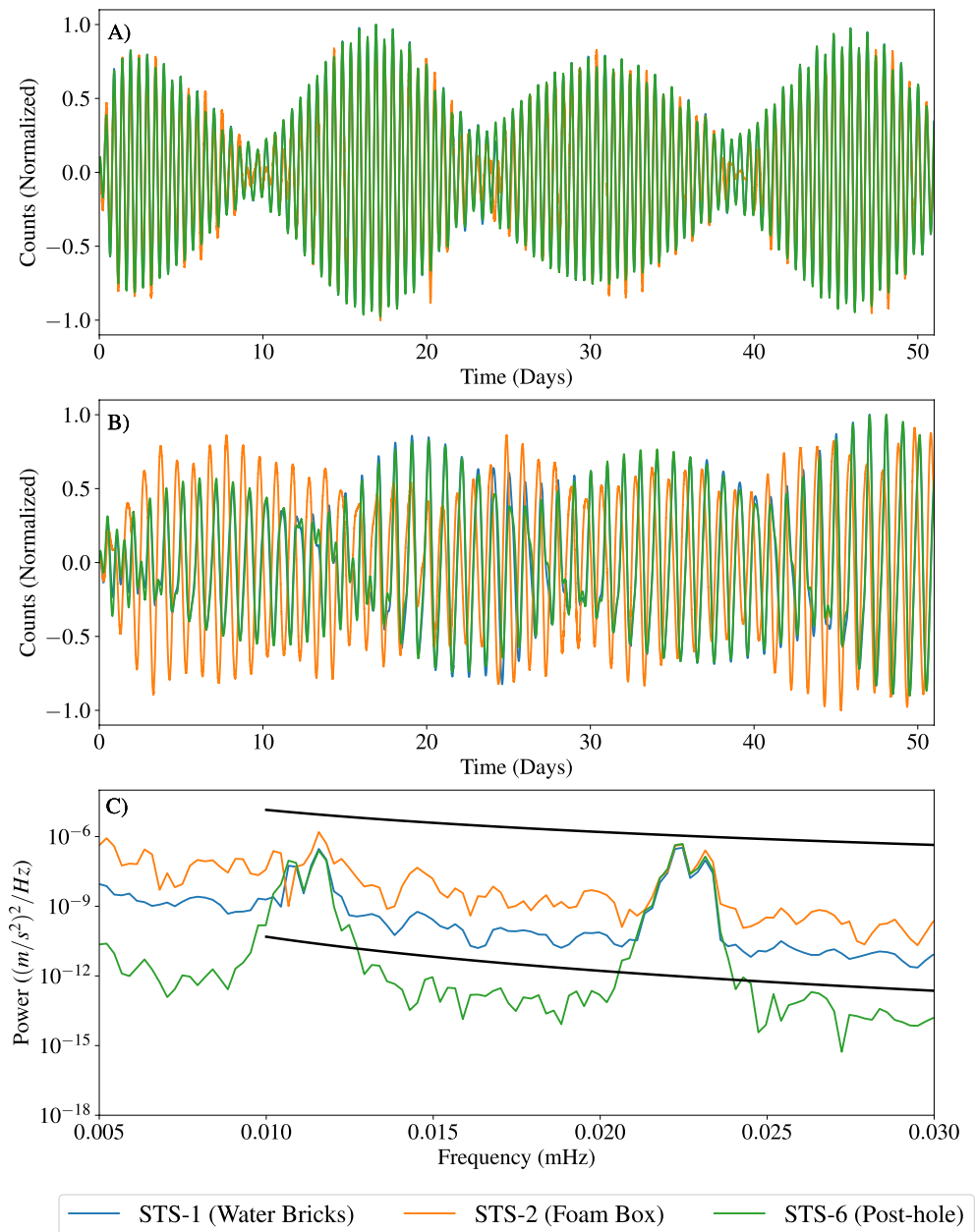


Figure 49. Time series comparison of (a) semi-diurnal Earth tides band-pass filtered from 10 to 13 hr period and (b) diurnal Earth tides band-pass filtered from 22 to 25 hr on the Streckeisen STS-2 (orange), the Streckeisen STS-6 (green), and the Streckeisen STS-1 (blue) at global seismographic network station TUC (Tucson, Arizona) over a 50-day time period beginning on 11 April 2017. (c) The Power Spectral Density over a 50-day window is also shown, with black lines representing the low and high global noise models of Peterson (1993). Reproduced from Doody et al. (2017).

(e.g., Dybing et al., 2019; Withers et al., 1996). However, the impact of wind speed and direction has helped to identify installation practices that mitigate these unwanted signals. For example, installing instruments at depth in competent materials (e.g., large Young's modulus) can mitigate wind induced seismic noise (Dybing et al., 2019; Hutt et al., 2017).

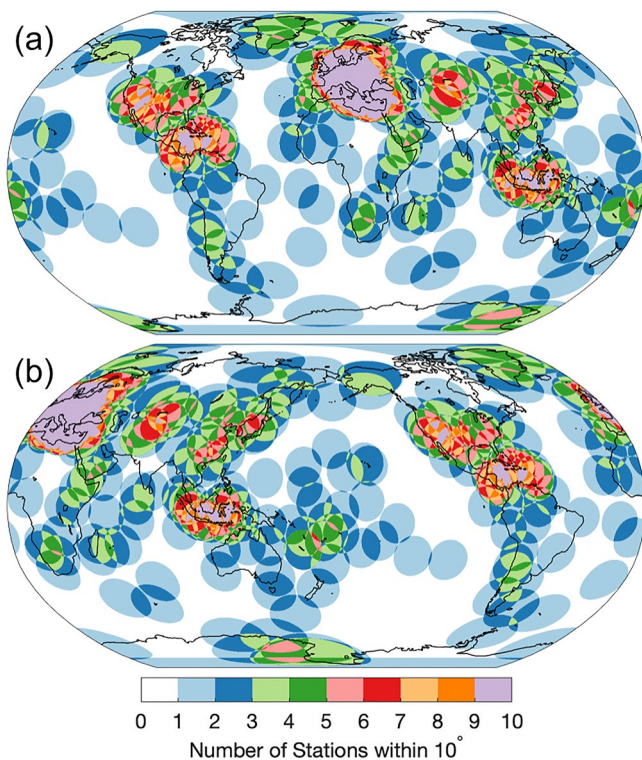


Figure 50. Stations from the global seismographic network (GSN), GEOSCOPE, GeoFon, and Mediterranean networks showing the geographical density of stations. (a) Africa centered and (b) Pacific centered. Color contours show the number of stations within 10° of any global location. Figure modified from Kohler et al. (2020).

11. Future Opportunities and Challenges

11.1. Instrument Calibrations

The design goal of the GSN is to calibrate across the entire usable seismic bandwidth of an instrument to within 1% (Lay et al., 2002). Studies attempting to verify how well the GSN is calibrated suggest that this goal has not been met, but that steady improvements have been made over time (Bernard et al., 1991; Davis & Berger, 2007, 2012; Davis et al., 2005; Ringler, Storm, et al., 2015). As scientists continue to analyze and model increasingly subtle seismic signals, improvements in calibration methods will be necessary.

In situ instrument responses are typically calibrated by injecting a (force) signal into the instrument through a calibration coil. It is then possible to invert for the poles and zeros that describe the linear transfer function in a least squares sense (Fels & Berger, 1994; Ringler et al., 2012). Because the forcing constant of the calibration coil is not known to high accuracy, these methods only provide information about the relative response across the excited frequency band. To calibrate the mid-band sensitivity of an instrument it is necessary to move the sensor with a known motion. One method is to use a step-table to input a known displacement into the seismometer (Wielandt, 2012), but this method has an uncertainty larger than 1% (Anthony, Ringler, & Wilson, 2017). Using absolute gravity measurements, Anthony, Ringler, and Wilson (2017) developed a methodology to absolutely calibrate an accelerometer to within 0.06% and then, through a string of relative calibrations, calibrate the vertical component of a VBB seismometer to within 0.14%.

However, applying these methods operationally across a large network of seismographs poses additional challenges. For instance, the methodology has yet to be fully vetted for the horizontal components and it remains unclear how responses may change over time and in different environmental conditions. We note that methods exist that can calibrate superconducting gravimeters to much better than 1% (Van Camp et al., 2016) so there should not be fundamental limitations preventing further calibration improvements from being implemented at GSN stations.

ers to much better than 1% (Van Camp et al., 2016) so there should not be fundamental limitations preventing further calibration improvements from being implemented at GSN stations.

11.2. Improved Station Distribution and Multiscale Distribution

Despite the International Ocean Network I.O.N. initiative (Purdy et al., 1995; Suyehiro et al., 2006), there are relatively few oceanic island sites and only a couple cabled sea-floor observatories (Delaney et al., 2016; Duennebieber et al., 2002). The technical and geographic challenges associated with developing sea-floor infrastructure have precluded the establishment of a uniform, long-term broadband global seismographic distribution (Figure 50). The restriction of almost all seismic stations to continents and islands has resulted in highly nonuniform detection capabilities and seismic interrogation of Earth structure since the earliest days of global seismology. For example, limited ray path coverage along with the difficulty in recording 150 s period Rayleigh waves globally fundamentally limits resolution of inversions for attenuation structure in the lower mantle (Ringler, Anthony, Dalton, & Wilson, 2021). Short-term (up to a few years) Ocean Bottom Seismograph (OBS) instruments and methodologies are well developed, but the technological advances and resources necessary for the widespread establishment of long-term OBS stations in remote oceans regions remain elusive (Kohler et al., 2020).

One promising approach for improving global seismic resolution is ocean hydrophone recording, particularly at ocean depths where the background noise for a drifting instrument can be sufficiently low for P and other seismic phases. The development and deployment of autonomous floating Mobile Earthquake Recording in Marine Areas by Independent Divers hydrophone systems (F. J. Simons et al., 2009; Nolet et al., 2019; Sukhovich et al., 2015; Simon et al., 2021a, 2021b) is a notable achievement in this regard. The Pacific Array has also shown promise in improving station spacing in the Ocean (<http://eri-ndc.eri.u-tokyo.ac.jp/PacificArray/>). Cabled seafloor

observatories (Delaney et al., 2016; Duennebier et al., 2002) have also demonstrated that this approach can be effectively implemented, but to date these installations have been few, and are much more costly than land-sited stations. A recent development with substantial geophysical and seismological potential for global and general instrumentation has been the advancement of VBB Distributed Acoustic Sensing technologies utilizing optical fiber scattering and polarization to employ special use and existing undersea or land-sited fiber-containing cables as massively multi-channel strainmeters (e.g., Lindsey et al., 2020; Sladen et al., 2019; Y. Yang et al., 2021; Zhan et al., 2021). A further approach leveraging a vast and growing international transoceanic fiber optic system is the Science Monitoring And Reliable Telecommunications initiative (Howe et al., 2019), which seeks to integrate seismic and other sensors into undersea repeater infrastructure.

On land, developing a next generation of high-quality seismograph stations with lower equipment and logistical cost provides pathways to improved station coverage, particularly in regions that remain relatively sparsely sampled (e.g., Africa and Antarctica; Figure 50). Increased station coverage could not only improve ray path coverage across a large bandwidth, but also decrease uncertainty in normal mode splitting function measurements (Majstorović et al., 2018). A notable development has been the advancement of broadband seismic station technology as a result of continent-spanning EarthScope TA efforts in the conterminous United States, southern and northwestern Canada, and Alaska (Section 2.3) as well as the SKIPPY project across Australia (Zielhuis & van der Hilst, 1996). EarthScope catalyzed the development of mass-produced, high-quality, logistically efficient, and low-footprint telemetered broadband seismic systems incorporating shallow posthole sensors, optimized power and telemetry systems, and a readily air- or land-transportable drill for seismometer installation (Busby & Aderhold, 2020). Parallel technical development of telemetered broadband seismograph stations for extreme polar conditions, notably in Antarctica (Anthony et al., 2015; Shen et al., 2020) and Greenland (K. G. Olsen & Nettles, 2017; Toyokuni et al., 2020), have similarly made the expansion of high latitude seismic stations and other geophysical instrumentation realizable.

11.3. Increasing Bandwidth and Multi-Instrumental Integration

GSNs have naturally focused on the principal “seismic spectrum” of approximately 1 mHz–100 Hz. However, increasing the effective bandwidth of global elastic and nonelastic deformation through multi-instrumental approaches offers exceptional opportunities for further study and understanding of a wide range of dynamic processes of the Earth and to estimate Earth structure. For example, Lau et al. (2017) used Earth tide measurements from GNSS stations to invert for Large Low Shear Velocity Province (LLSVP) structure. Along with a growing global near-real-time GNSS geodetic capability (Melbourne et al., 2021) that can, for example, augment rapid near-field characterization of major earthquake sources (Bock et al., 2011; Melgar et al., 2013; Nie et al., 2016), strain sensitive instrumentation, including borehole strain meters (Hodgkinson et al., 2013) and rapidly emerging optical fiber-based technologies (Lindsey et al., 2020) offer further paths to extending the global observational bandwidth to extremely long-periods (in theory, to zero frequency). Merging seismic and non-seismic multi-instrument data streams to realize extremely broadband strain and displacement data time series necessitates careful instrumental co-calibration and consistency evaluation (e.g., Nie et al., 2016).

11.4. Rotational Seismology

Rotational seismology is a scientific and observational field with deep historical roots that observes and utilizes inertial frame rotations that occur during both strong and weak seismic excitation, but that are not detected by inertial and translational sensors such as single seismometers (Lee et al., 2009). The rotational (curl) field is, however, detectable at point locations using specialized (e.g., ring laser gyroscope) instrumentation (e.g., Igel et al., 2005, 2021). Substantial progress has been made in realizing such rotational instruments in recent decades, notably including the operation of a 4-m ring laser at Wettzell Observatory in Germany since 2002 (e.g., Igel et al., 2007). Integrated interpretation of seismic and rotational data allows for the selective discrimination of shear and Love wave energy and enhances the estimation of the source back-azimuth from a single observation site, and can facilitate enhanced resolution of local shear velocity structure (e.g., Ferreira & Igel, 2009; Sollberger et al., 2020; Yuan et al., 2020). Recent developments in low-noise rotational sensors provide a path forward for a globally distributed network of rotational data streams, which could improve understanding of global seismic phenomena such as the ratio of Rayleigh to Love wave microseism energy (Tanimoto et al., 2015), local slowness estimation to enhance tomographic and source studies, tilt correction to horizontal inertial sensors (Bernauer

et al., 2020), toroidal mode splitting and mode coupling (Nader et al., 2012) as well as other analyses benefiting from local shear wavefield separation (Schmelzbach et al., 2018).

11.5. Broadband Arrays

Beginning in the early 1960s, seismologists began constructing seismic arrays (Rost & Thomas, 2002) incorporating seismometers deployed in primarily L-shaped patterns and spanning distances of a few tens of kilometers (Schweitzer et al., 2012). By examining wavefield arrivals across multiple sensors, seismologists were able to improve characterization of both earthquakes and underground nuclear tests compared to single station observations. By the late 1960s, larger arrays had been constructed, notably including the 525-element and 200 km-aperture Large Aperture Seismic Array (LASA) in Montana, United States (P. Green et al., 1965). These early arrays were predominantly comprised of short-period, vertical component sensors. Experimentation with broadband arrays began in the late 1970s, with the Gräfenberg array incorporating 13 Streckeisen STS-1 sensors being a seminal example (e.g., Friedrich et al., 1998).

With continued developments in seismic instrumentation, additional arrays of 3-component, broadband seismometers have been emplaced across the globe during the last 30 years and have driven advances in understanding fault rupture dynamics (e.g., Ishii et al., 2005), improved resolution in seismic mantle imaging (e.g., Schmandt & Lin, 2014), and helped reveal the global source regions of ambient noise (e.g., Friedrich et al., 1998; Z. Wang et al., 2021). However, seismic arrays have been, and are today, overwhelmingly located in the northern hemisphere and long periods of operation are often required to both calibrate them and to attain maximal resolution in seismic imaging (Schweitzer et al., 2012). Incorporation of small-aperture arrays at select global seismographic station sites was proposed by the GSN design committee in 2002 (Lay et al., 2002) and larger aperture (>100 km) broadband arrays distributed across the globe were proposed by the Global Arrays in Broadband Seismology (GABBA) focus group in 2013 (Koper & Ammon, 2013). GABBA-type arrays were noted as being crucial to attaining the necessary imaging resolution for broad questions regarding the dynamics of both interior of the Earth and fault mechanics. Promising conceptualizations of low-noise ice cap-emplaced borehole seismic arrays near South Pole have also received recent attention (Anthony et al., 2021), and small-aperture (~1 km), broadband posthole sensor arrays have been installed at a few GSN station sites in a further investigatory capacity (Anthony, Ringler, Wilson, Zebulon Maharrey, et al., 2020; Donner et al., 2017) but the potential of long-term networks of global broadband research arrays has yet to be realized.

11.6. Improved Signal-to-Noise at Long Periods

Long-period self-noise levels of seismic instruments have been slow to improve, but our understanding of shielding instruments from unwanted non-seismic noise sources has seen progress. For example, the recently available Streckeisen STS-6 and the Nanometrics T-360-GSN borehole instruments have allowed network operators to replace older technology GeoTech KS-54000 sensors to reduce noise levels in GSN instrumentation as a whole (Ringler et al., 2019). Although the GeoTech KS-54000 instruments were installed in boreholes, long-period horizontal noise levels never matched those of vault-sited Streckeisen STS-1, suggesting that instrument noise was limiting the performance at such stations (Berger et al., 2004). Along with improved instrumental noise characteristics and isolation from surface noise sources, boreholes allow operators to mitigate unwanted local tilt noise (Hutt et al., 2017) and provide improved thermal capacity and stability (Doody et al., 2017) to the instrumental environment.

While it is presently unclear if the vertical component of the Streckeisen STS-6 can meet the performance of the Streckeisen STS-1 in certain frequency bands (Forbriger et al., 2021), data from the M_w 8.1 Kermadec Island earthquake of 4 March 2021 suggests that the Streckeisen STS-6 instruments observed more high fidelity normal modes (Ringler, Anthony, Davis, et al., 2022) at frequencies below 1 mHz than Streckeisen STS-1 seismometers during this event (Figure 51). The installation of Streckeisen STS-6 instruments in shallow postholes, by way of drilling into the vault pier, can also improve long-period horizontal data (Ringler et al., 2019). This suggests that while individual Streckeisen STS-1 instruments in certain locations could provide superior data in some frequency bands, the Streckeisen STS-6 installed in shallow vaults provides superior typical data network-wide. By increasing the sensitivity of the Streckeisen STS-6, at the cost of also decreasing the clip level, it may be possible to further improve instrumental noise levels. While it has been shown that superconducting gravimeters

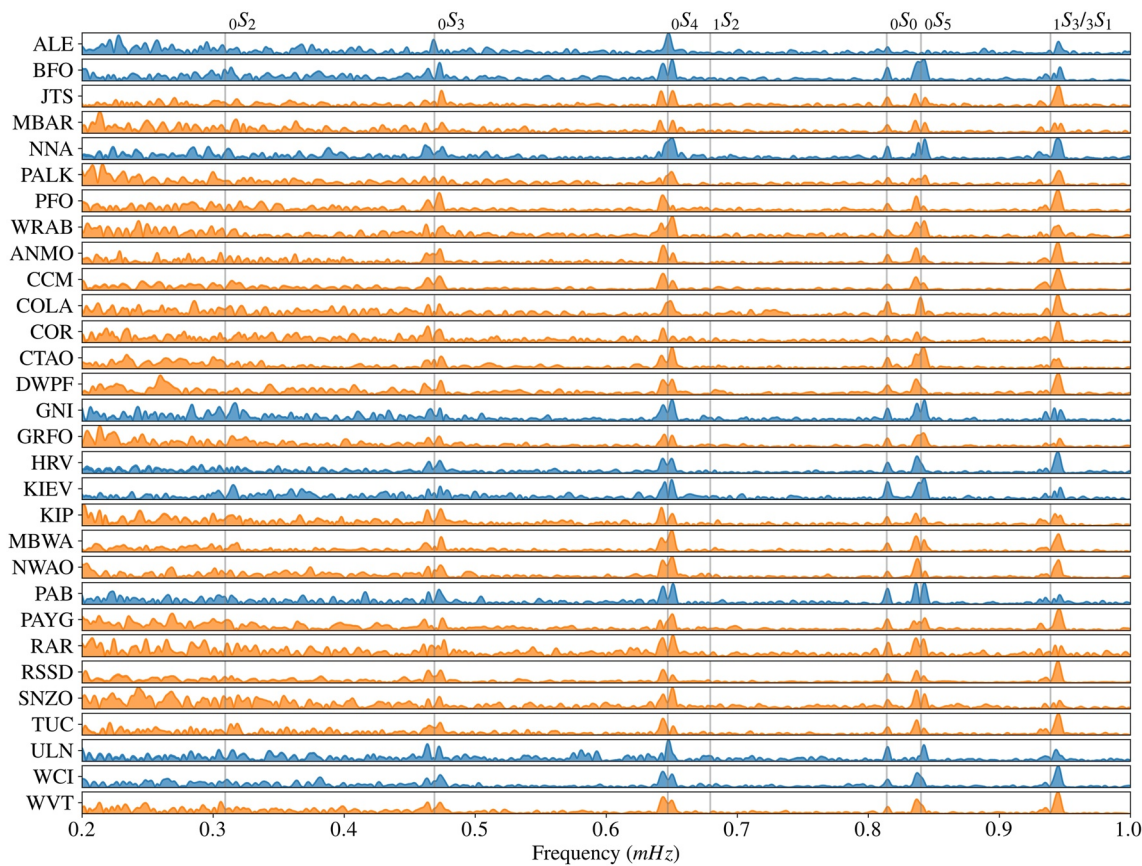


Figure 51. Global seismicographic network (GSN) station vertical-component spectra (Streckeisen STS-6: orange; Streckeisen STS-1: blue) resolving normal modes below 1 mHz excited by the M_w 8.1 Kermadec Island earthquake of 4 March 2021. Spectra were calculated using 126 hr of data following the event origin time. The amplitudes of each station are individually scaled. Figure modified from Ringler, Anthony, Davis, et al. (2022).

are capable of producing superior spectra below 1 mHz (Widmer-Schmidrig, 2003), relatively few of these instruments have been deployed to date for this purpose (Häfner & Widmer-Schmidrig, 2012). Such instrumentation improvements are a subject of current research.

11.7. Improved Timing

Modern seismic data is time-tagged through GPS-conditioned crystal oscillators, which has allowed many seismologists to assume all timestamps are accurate and extremely precise. This is in contrast to the large number of corrections that were necessary in historical seismic data, implemented via a variety of timekeeping and calibration mechanisms (Agnew, 2020). With GNSS timing, it has been shown that precision is better than 10 ms across the GSN (Ringler, Anthony, Wilson, et al., 2021), in accordance with GSN design goals (Lay et al., 2002).

However, current timing precision may not be sufficient for future studies of the interior of the Earth. For example, improved estimation of changes in inner core rotation could require improved timing accuracy at the ms level or better (Deuss, 2014; J. Yao et al., 2021; Lythgoe et al., 2020; Y. Yang & Song, 2020, 2021). As noted earlier, consensus on the rate of inner core differential rotation and possibly its variability is lacking. Most basically, there is currently a lack of agreement on the evidence for travel-time changes based on details of time-dependent features of waves, such as the coda of *PKIKP* waves scattered within the inner core. Accurate absolute timing is good to have though Lythgoe et al. (2020) suggest that temporal variations in inner core phases are not in dispute, but properly accounting for uncertainties in absolute timing is needed for robust data interpretation. Reasons for a lack of consensus may include the use of differential phase measurements that were picked by eye rather than through the use of cross-correlation or other more objective methods; and the use of normal mode techniques where differential rotation is inconsistent because of different modes being analyzed (Laske & Masters, 1999).

11.8. Station Site Conditions

Local strain-tilt coupling has plagued the Earth tide community as a strong noise source for many years and produced anomalous horizontal seismic records at periods greater than ~ 25 s (e.g., Kohl & Levine, 1995). The highly local processes associated with this effect can even produce resolvable differences in long-period signals between sensors that are located in the same vault (Zürn et al., 2015). However, using local strain-tilt corrections could help to reduce these unwanted effects (Lambotte et al., 2006). Strain-tilt coupling should be frequency independent at periods greater than ~ 25 s (King et al., 1976) so if these coefficients can be calculated at Earth tide frequencies (e.g., Lambotte et al., 2006) it might be possible to use these corrections for horizontal to vertical ratio estimates, which have shown considerable scatter (Ferreira & Woodhouse, 2007). Although several methods to help reduce the uncertainty in surface wave amplitude estimates have been proposed (Tanimoto & Rivera, 2008) it is likely that there is an azimuthal component as well as significant scatter coming from strain-tilt coupling that has not yet been fully modeled or corrected for (Ringler et al., 2018).

11.9. Resolution of Normal Modes

Recent work on normal mode splitting functions, which are sensitive to Earth's structure after accounting for ellipticity and rotation, has suggested new opportunities to better resolve density (Akbarashrafi et al., 2018; A. Robson et al., 2022). These studies indicate that splitting functions of modes with frequencies below ~ 3 mHz are limited in reliably retrieving the density structure of the mantle. However, recent splitting function data sets include modes with frequencies up to ~ 10 mHz (Deuss et al., 2013; Koelemeijer et al., 2013) that still need to be analyzed in the same way, particular the higher frequency Stoneley modes used by (Koelemeijer et al., 2017). Understanding the uncertainty arising from various coupling approximations (e.g., self-coupling, group-coupling, and full-coupling) for how different modes interact with one another, as well as the data used to recover splitting functions, will be important for increasing the number of useful observations. A particular focus in future studies should be given to more reliable measurements of odd-degree coefficients, which requires good-quality, low-noise spectra as provided by GSN stations. Such odd-degree observations are vital for constraining the odd-degree structure of the deep mantle and for example, investigate differences between the African and Pacific LLSVP. At the same time, increased efforts to measure toroidal mode splitting functions from horizontal data (such as those reported by Schneider and Deuss (2020)) are necessary to constrain estimates of mantle anisotropy. Improved understanding and correction of modal horizontal noise levels could also help to explain some of the amplitude anomalies identified in the gravest of horizontal normal models (Park et al., 2008).

11.10. Computational Seismology

While GSNs are able to produce high-quality globally distributed seismic data to better image the interior of the Earth, many techniques rely on our ability to compute realistic synthetic seismograms from a given Earth model. Historically, computing power has limited the field to using 1D “normal mode summation” seismograms from numerical integration (e.g., MINEOS, G. Masters et al., 2014), with wavefield simulations offering a modern alternative (Nissen-Meyer et al., 2014; van Driel et al., 2015).

Along with improvements in global coverage of seismic stations there have been recent advances in numerical methods as well as computational infrastructure. A number of these advances have directly improved the field of global seismology. For example, the package SPEC-FEM3D Globe uses the spectral element method (SEM) to produce synthetic seismograms for a 3D Earth model (see Komatitsch and Tromp (1999) and Igel (2016), for an introduction to the SEM). With the advance in computational power and access it is now possible to produce 3D synthetic seismograms in the 17–500 s period band (Tromp et al., 2010).

Improvements in synthetic seismograms have in conjunction with adjoint-methods (see Fichtner et al., 2006a, 2006b for an introduction)—which enables vastly more efficient estimates of various derivatives used in optimization problems—enabled higher resolution 3D global Earth models via full waveform inversion (e.g., Bozdağ et al., 2016; Fichtner, van Herwaarden, et al., 2018). While these methods have greatly improved our ability to image the interior of the Earth, they are still limited to relatively longer period phases (e.g., 17 s body waves and 45 s surface waves Bozdağ et al. (2016)).

Along with improvements in computing power and methods there has also been a trend in improving access to 3D seismograms or the computation of them, one such package is the AxiSEM package for producing 2.5D and 3D synthetics (Nissen-Meyer et al., 2014). AxiSEM has been used to produce on demand broadband synthetic seismograms (van Driel et al., 2015) that can be downloaded from IRIS together with observed waveforms. While 3D synthetic seismograms have shown much promise in improving our understanding of Earth structure, there are still challenges in estimating the density structure of the Earth. For example, it will be necessary to include self-gravity in the weak-formulation of the wave equation used in SEM (Komatitsch & Tromp, 1999, 2002b). It will also be necessary to improve computing power and algorithms so that we can further refine global simulations of earthquakes on a routine basis, with high-resolution (e.g., Komatitsch et al., 2002).

11.11. Machine Learning

One of the most recent advances in network seismology on local, regional, and global scales is the reemergence of machine-learning as a viable tool to process seismic data. Machine-learning algorithms are so named because they learn (or are trained) directly from input data sets. The recent focus on these tools is in part because of the broad accessibility of machine-learning tools and the accessibility of seismic data sets, including seismic-wave forms and labeled information (e.g., earthquake catalogs).

A primary focus of applying machine learning to seismology has been the development of tools to assist in seismic monitoring, including event-detection (e.g., Perol et al., 2018; W. Zhu & Beroza, 2018; Ross, Meier, Hauksson, & Heaton, 2018), seismic-arrival characterization (e.g., Mousavi & Beroza, 2020; Ross, Meier, & Hauksson, 2018; Yeck et al., 2020), association (Ross et al., 2019), denoising (W. Zhu et al., 2019), condensing seismic data (Valentine & Trampert, 2012) or tools which combine various tasks of seismic processing into a single model architecture (e.g., Mousavi et al., 2020). These tasks generally rely on supervised learning, leveraging curated labeled data sets to train models to perform a task. Machine learning is also being leveraged to extract unknown features from large data sets (unsupervised learning), such as identifying reoccurring signal types (e.g., Seydoux et al., 2020; Yoon et al., 2015). These approaches allow researchers to extract novel observations from archived continuous wave forms. The applications of machine-learning to seismology, and seismic network data, are diverse and an emergent field. Kong et al. (2019) gives a more complete look at the current state of applying machine learning to seismology.

11.12. Planetary Seismology

As of this writing, the VBB seismometer deployed by the InSight mission to Mars (Banerdt et al., 2020) has been transmitting ground motion data from the red planet for over 1,200 Martian days (Sols). During this time, its low self-noise and extensive thermal protection allowed VBB to record accelerations approaching $10^{-10} m/s^2 / \sqrt{Hz}$ in the 0.1–1 Hz frequency range, 2–3 orders of magnitude below the Earth Low Noise Model (Lognonné et al., 2020). The extremely low environmental noise on Mars reflects the absence of oceans, a much thinner atmosphere, and lack of anthropogenic signals. Developing the VBB and establishing its noise requirements benefited from preliminary testing using GSN sites, but posed challenges regarding station installation, temperature stability, and magnetic shielding distinct from those encountered in the controlled environment of permanent broadband installations on Earth (Lognonné et al., 2019). To locate marsquakes and aid in the identification of arrivals of interest, processing of InSight data relies heavily on techniques developed and validated on data from the GSNs (e.g., Böse et al., 2017; Marusiak et al., 2020; Panning et al., 2015), many of which involve extracting polarization information from 3-component waveforms recorded at a single-station. Thus far, InSight VBB data has led to many first-order discoveries about the Martian interior and seismicity. For example, it has been used to establish seismicity rates and types (Giardini et al., 2020), characterize crustal structure beneath the lander with receiver functions and autocorrelations (D. Kim, Lekić, et al., 2021; Knapmeyer-Endrun et al., 2021), develop radial models of mantle from body wave traveltimes (Khan et al., 2021), determined the depth to the mantle transition zone (Q. Huang et al., 2020) and detected core-reflected waves constraining the size and density of the core (Stähler et al., 2021). Work to detect impacts, surface waves, and core-transiting phases continues. The latest Mars Seismic Catalog (InSight Marsquake Service, 2021) contains 951 marsquakes, which are classified into families according to their dominant frequency content and graded according to their signal quality. Of these, 6 has multiple identifiable phases and clear polarization (quality A) and an additional 133 have multiple

identifiable phases but lack polarization (quality B). As was pioneered by the GSN, GEOSCOPE and other global seismic networks on Earth, the waveform data collected by InSight are publicly available from the IRIS DMS, under the network code XB and station name ELSYE.

Extracting robust structural and source constraints from seismograms requires a thorough understanding of the sources of noise (e.g., Ringler, Sleeman, et al., 2014), which, in the case of data from Mars, may be unfamiliar to a seismologist working primarily on records from Earth. A comprehensive description of transient and sustained idiosyncratic signals arising from coupling between InSight sensors and spacecraft can be found in D. Kim, Davis, et al. (2021). They show that systematic variations in sustained spacecraft-sensor instrument noise, such as lander modes that vary with temperature, can be misinterpreted as structural signals in techniques relying on the (auto)correlation of environmental noise. In light of the enormous scientific return of the InSight mission, the future of planetary seismology is bright. NASA's Farside Seismic Suite (Panning et al., 2022) is expected to place a VBB vertical component seismometer and a compact 3-component short period seismometer in Schrödinger crater on the far side of the Moon. In addition to resolving crustal thickness and layering beneath the crater itself, the mission is expected to constrain the rate of micrometeorite impacts, and to expand on the detection of deep moonquake clusters beyond the nearside, where all Apollo-era seismometers were deployed (Nakamura et al., 1982). Geophones on NASA's Dragonfly mission to Titan, expected to launch in 2027, will bring the first seismic measurements from an icy world, enabling the characterization of tidally induced seismicity and the determination of ice shell thickness (Lorenz et al., 2019). Finally, the Lunar Geophysical Network concept (Haviland et al., 2022) seeks to deploy a global network of four multi-geophysics stations that would map out the Moon's seismic activity, mantle and crustal structure and heterogeneity, and address fundamental questions about the Moon's initial differentiation, its present-day heat budget, and core evolution.

12. Conclusions

Over the past century, GSNs have evolved from a sparse collection of analog instruments (e.g., Milne, 1900) to more than 150+ globally distributed VBB stations that are capable of recording the entire seismic spectrum, from Earth tides to high-frequency seismic waves at tens of Hz, along with a number of other geophysical and environmental measurements (e.g., temperature, pressure, infrasound, total electron content from GPS, and magnetic field variations). GSNs have been essential drivers for the development of robust calibrated and curated international data centers with worldwide real-time and open access to scientific and broader users. These stations have been further supplemented by regional networks. While most GSNs are no longer in their deployment phase, there exist many opportunities for instrumental and networked improvements.

The establishment of a global interconnected system of diverse seismographic and other geophysical and environmental (both long-established and temporary) instrumentation linked with federated data and metadata archival and distribution creates a universal Earth-spanning sensor network that both complements and transcends science motivations for long-established uniformly engineered global networks. For example, tomographic studies of Earth structure routinely utilize all available and suitable data regardless of network affiliation and operational attribution. Large-scale geophysical events, such as the eruption of Hunga Tong—Hunga Ha'apai volcano in the south Pacific Ocean, with its remote sensing observations and global seismic, sonic, tsunami, and infra-sonic signatures (including atmospheric shock waves that have no modern analog; Matoza et al., 2022; Ringler, Anthony, Aster, et al., 2022; Witze, 2022), is currently being analyzed using a comprehensive array of geophysical data types.

Globally distributed seismic data and methodologies are capable at locating and characterizing Earth's seismic sources. Being able to rapidly determine the location, size, and source characteristics of sizeable events anywhere on Earth (currently this is routine for events larger than approximately M_w 5, but can be done for much lower magnitudes in many regions of the world) has value in mitigating loss of life and property by way of enabling timely earthquake impact assessments and tsunami warnings, as well as in characterizing the complex statistical patterns of global seismicity in time and space. Recent decades of research on detecting and locating multiple events in the same general region have produced results with far more detailed information on spatial and temporal patterns of seismicity than can be derived from the traditional single event approaches which dominate today's seismicity bulletins. Above and beyond their sensitive monitoring capabilities, seismographic networks

are essential to steadily advance the imaging of the Earth's interior. The seismological signature of the heterogeneous Earth can be used to help resolve the planet's interior state, structure, composition, and dynamics.

The dynamic range and bandwidth of instrumentation in modern seismographic networks facilitate the rapid characterization of fault rupture during large earthquakes on multiple spatial and temporal scales, and facilitate the recording of seismic phenomena ranging from very long-period elastogravity and normal modes to regional high-frequency crustal guided phases. GSNs have played an historic and continuing role in nuclear explosion monitoring and assessment, which provided strong motivation for early network development. Global and regional seismology is today a core component to realizing necessary technical capabilities for international treaties limiting the vertical and horizontal proliferation of nuclear weapons.

A principal and community sanctioned goal of GSNs is to freely distribute and promote the wide and diverse use of high-quality data to the widest international and scientific user community, including for non-traditional users of seismic data. For example, seismic data exhibit sensitivity to changes in ocean, hydrological, cryospheric, atmospheric, anthropogenic noise in urban settings, and other dynamic Earth processes and is increasingly leveraged to identify and interrogate long-term process and material changes in Earth systems. Identifying and interpreting temporal changes and validating increasingly small signals within the seismic wavefield motivates continual calibration improvement, which is aided by the co-siting of multiple seismic and other geophysical instruments at station sites.

Although land-based seismic networks and their technologies have reached a relative plateau of maturity, increasing worldwide integration of global, regional, and local seismographic network data from many data providers continues to densify the spatial sampling of Earth's elastic wavefield, and multidisciplinary uses and joint analyses of diverse geophysical data streams continue to expand. A major frontier that remains is the need to substantially improve the density and quality of seismic data from the oceans, with both ocean-bottom and water column (e.g., floating) sensing capabilities being advanced towards this goal. With sustained resources allocated to the operation, densification, and instrumental diversification of global seismograph stations and continued scientific discovery, we anticipate a bright future for global network seismology for a broad global user community.

Glossary

- Advanced Seismic Research Observatory (ASRO)** Network of five digital stations that formed part of the GDSN. Also referred to as the modified high gain long-period observatory (network code AS).
- Albuquerque Seismological Laboratory (ASL)** Field office of the U.S. Geological survey that operates the CU, IC, and IU networks as well as a number a number of other long-term networks.
- Array Aperture** Greatest horizontal distance between any two seismometers in a seismic array.
- Associator** Algorithm used to associate seismic phase picks recorded across a seismograph network to particular seismic events.
- Cavity Effect** Seismic signature caused by vault wall deformation, commonly contributing to tilt noise.
- Clip Level** Largest signal that an instrument can record before it is no longer able to provide an output that is linearly proportional to the input.
- Comprehensive Nuclear-Test-Ban Treaty (CTBT)** Multilateral international treaty that bans all critical nuclear tests for both civilian and military purposes. As of 2021, 170 states have ratified and an additional 15 states have signed, but not ratified, the CTBT.
- Comprehensive Nuclear-Test-Ban Treaty Organization (CTBTO)** International organization to be established upon entry into force of the CTBT, currently provisionally established under the CTBTO Preparatory Commission headquartered in Vienna, Austria, which operates the International Monitoring System (IMS).
- Computational Seismology** The field of seismology that deals with solving the wave equation numerically or attempts to model various observed phenomena.
- Data Quality Analyzer (DQA)** Software packaged used and developed at ASL for in situ data quality monitoring.
- Datalogger or Digitizer** Instrument used to convert an analog signal, usually a voltage, into a time-tagged digital time series.
- Degenerate Resonance** The center frequency of a normal mode multiplet.

- Digital Acoustic Sensing (DAS)** Optoelectronic instrumentation of communication fibers to facilitate broadband distributed strain sensing, typically utilizing Rayleigh scattering.
- Dynamic Range** Ratio between the smallest instrumentally observable signal and the largest observable signal, usually expressed in dB.
- Earth Hum** Continuous excitation of normal modes by atmosphere and ocean processes.
- Elastogravity Signals** Elastic changes in the gravity field of the Earth caused by large changes in mass, such as those associated with a great earthquake.
- Full coupling** A term in normal mode seismology that indicates the interaction (or resonance) between modes (generally up to a specified frequency) is taken into account.
- Global Arrays in Broadband Seismology (GABBA)** Seismological community focus group aimed at evaluating how global seismic arrays can supplement sparse global station coverage.
- Glacial Earthquake** Seismic event attributed to glacial processes.
- GEOFON** GEOForchungsNetz; German global network of seismograph stations (network code GE).
- GEOSCOPE** French global network of seismograph stations (network code G).
- Global Seismographic Network (GSN)** U.S. global network of seismograph stations. This network includes the Caribbean USGS Network (network code CU), the New China Digital Seismograph Network (network code IC), the IRIS/IDA network (network code II), and the IRIS/USGS network (network code IU).
- Global Digital Seismograph Network (GDSN)** Digital successor network to the analog WWSSN; included the Seismic Research Observatory (SRO), the Digital World Wide Standardized Seismographic Network (DW), and the Abbreviated Seismic Research Observatory (ASRO).
- Global Telemetered Seismograph Network (GTSN)** Network of 12 stations developed by the USGS and U.S. Air Force to supplementing global monitoring and research (network code GT).
- Global Network Satellite Systems (GNSSs)** Satellite geodetic systems for precise positioning, including the GPS, GLONASS, BDS, and Galileo constellations.
- Gravimeter** Instrument used to measure gravity or its changes. Gravimeters act as excellent low-frequency vertical seismometers.
- Heterosphere** Uppermost 200–250 km of the Earth; initially proposed by Dziewonski et al. (2010).
- Incorporated Research Institutions for Seismology (IRIS)** U.S. headquartered university consortium dedicated to the advancement of seismology and seismological data, including co-management of the Global Seismographic Network in partnership with the USGS.
- Instrument Self-Noise** Intrinsic noise of an instrument in the absence of signal.
- Interferometric Synthetic-Aperture Radar (InSAR)** Geodetic methods to generate interferometric images using phase differences between multiple satellite- or aircraft-acquired radar images.
- International Deployment of Accelerometers (IDAs)** Globally distributed network of gravimeters focused on recording long-period seismic signals (network code ID). IDA currently operates approximately one third of the broadband stations of the GSN (network code II).
- International Monitoring System (IMS)** Globally distributed geophysical sensing system of seismographs, hydroacoustic stations, infrasound stations, radionuclide detectors, and laboratories operated by the CTBT Preparatory Commission.
- International Federation of Digital Seismograph Networks (FDSNs)** Global organization of digital broadband seismograph network operators.
- Japan Meteorological Agency (JMA)** Japanese agency charged with collecting data and providing public results of geophysical phenomena, including earthquakes.
- LaCoste-Romberg Gravimeter** the gravimeter used in the IDA (ID) network.
- Large Low Shear Velocity Province (LLSVP)** Regions of lower-than-average seismic velocity that have been seismically identified in the lowermost part of the mantle.
- Local (seismic distance range)** Source-receiver distance range at which seismograms are dominated by direct crustal phases ($\lesssim 1^\circ$, or 111 km).
- Magnitude (seismic)** One of a number of measures of inherent (logarithmic) seismic source size derived from seismic wave observations. Widely used scales include body wave (m_b), surface wave (M_s), and moment M_w magnitude.
- MedNet** Network of VBB seismograph stations in the Mediterranean region operated by Istituto Nazionale di Geofisica e Vulcanologia (INGV), Italy (network code MN).

- Microseism** Globally observed background seismic signal (between approximately 3–25 s period) arising due to forces from ocean gravity waves acting on the solid Earth.
- Mode Coupling** Energy transfer (resonance) between distinct normal modes of the Earth.
- Mode Splitting** Separation of degenerate normal mode frequencies into distinct frequencies (singlets) due to the rotation, ellipticity, and heterogeneity of the Earth.
- Modular Utility for STATistical kNowledge Gathering (MUSTANG)** IRIS-developed and maintained software package for in-situ monitoring of data quality for all networks that contribute data to the IRIS Data Management System.
- Moment Tensor** Tensor representation of a point-equivalent (or best approximation to such) seismic source; generalizable to a planar or spatial moment tensor density.
- Multiplet** The $2l + 1$ singlets associated with a given normal mode ${}_nS_l$ or ${}_nT_l$.
- Nanometrics T-360** Vault or borehole VBB seismometer produced by Nanometrics, Inc., including for the purpose of succeeding the Streckeisen STS-1.
- Narrow Band Coupling** An approximation used in normal mode seismology where modes interact within a given frequency band.
- National Earthquake Information Center (NEIC)** U.S. Geological Survey center headquartered in Golden, Colorado, U.S. NEIC's principal missions include estimating locations and sizes of all significant global earthquakes, and the rapid communication of this information; and the curation and distribution of seismic and associated data; and the advancement of earthquake monitoring, risk management, and scientific research.
- New Low-/High-Noise Model (NLNM/NHNM)** Power spectral density model produced by Peterson (1993) characterizing the lowest and highest background seismic noise levels on Earth for culturally isolated seismographic sites ranging from continental interiors to oceanic islands.
- Normal Modes** Elastic free motion eigenfunctions of the Earth; also referred to as free oscillations.
- Power Spectral Density (PSD)** Distribution of power for a given signal in the Fourier frequency domain; commonly expressed in dB relative to acceleration ($[m/s^2]^2/Hz$) in global seismology (e.g., Peterson, 1993).
- Preliminary Reference Earth Model (PREM)** Widely utilized 1D Earth model for seismic velocity and density as a function of radius inverted from seismic wave observations (Dziewonski & Anderson, 1981).
- Prompt Elasto-Gravity Signals (PEGSSs)** Earthquake-associated signals created by density-perturbation-induced gravity field changes, and by the associated elastic readjustment of the gravitationally perturbed Earth.
- Regional (seismic distance range)** Source-receiver distances between local and teleseismic, for which seismograms contain a mixture of crustal and mantle phases ($\gtrsim 1^\circ$, or 111 km and $\lesssim 30^\circ$, or 3,330 km).
- Rotational Seismology** Study of rotational motions produced by seismic phenomena, often utilizing specialized (non-translational) instrumentation.
- Seismic Research Observatory (SRO)** Network of 13 globally distributed stations which made up part of the GDSN (network code SR).
- Instrument Self-Noise** Intrinsic noise of seismographic and recording equipment, usually displayed as a function of frequency.
- Self-Coupling** An approximation used in normal mode seismology where only interaction within a mode multiplet is considered (i.e., no resonance with other modes).
- Sensitivity Kernel** Sensitivity of a seismic phase to Earth structure as a multi-valued function of space.
- Standard for the Exchange of Earthquake Data (SEED)** Digital standard for encoding and distributing seismic data. This format was initially developed by the FDSN and has been adopted by IRIS as well as a number of other data centers.
- StationXML** Extendable markup language schema for seismic metadata. StationXML is planned to eventually replace the metadata portion of SEED.
- Stoneley Modes** Subset of Earth normal modes that are trapped along solid-liquid interfaces, such as the core-mantle boundary.
- Streckeisen STS-1 Seismometer** Pioneering VBB seismometer deployed in a large number of global seismograph networks.
- Streckeisen STS-6 Seismometer** VBB seismometer used as a successor to the Streckeisen STS-1 in global seismograph networks. The STS-6 is installed in a borehole or posthole.

Acknowledgments

The authors acknowledge the seminal and historic contributions of global seismologists over the past 140 years, notably including Don Anderson, Jon Berger, Keith Edward Bullen, Adam Dziewonski, Beno Gutenberg, Inge Lehmann, Harold Jeffreys, John Milne, Jack Oliver, Jon Peterson, and Frank Press. The authors thank Bob Hutt, David Simpson, and Joseph Stein for identifying important historical references and for helpful discussions regarding the initial build out of the Global Seismographic Network (GSN). The authors thank an anonymous reviewer, Adria Elskus, Ryan Gold, Bob Hutt, Martin Mai, Rob Mellors, Barbara Romanowicz, Joseph Stein, and Justin Wilgus for reviews of this work. The authors thank Valerio AcoCELLA for help handling the manuscript. This work has benefited from discussions with Peter Davis, Lind Gee, Katrin Hafner, Bob Hutt, Rob Mellors, Joseph Stein, Tyler Storm, Bob Woodward, and David Wilson. The authors also thank the staff at the USGS Albuquerque Seismological Laboratory, at Project International Deployment of Accelerometer, Institut de Physique du Globe de Paris, GFZ, and the many other institutions who are essential to sustaining global station operations and data quality. The authors thank Michel Van Camp for encouraging us to write this review article as well as provide a number of additional comments. The authors additionally thank Kent Anderson and Katrin Hafner for the use of Figure 8. The authors thank Rob Mellors for parts of Figure 9. The authors thank Barbara Romanowicz for suggesting Figure 11. The authors thank Carl Tape for providing some additional references and comments. The authors thank Molly Staats for providing a list of GSN references available at: www.iris.edu/hq/programs/gsn/citations. The authors used the Python package ObsPy for seismic data processing (Beyreuther et al., 2010), Matplotlib for figures (Hunter, 2007) as well as Generic Mapping Tools (Wessel et al., 2019), and Cartopy for maps (UK Meteorological Office, 2010). The GSN is a cooperative scientific facility operated jointly by the Incorporated Research Institutions for Seismology (IRIS), the United States Geological Survey (USGS), and the Seismological Facilities for the Advancement of Geoscience (SAGE) Award of the National Science Foundation (NSF), under Cooperative Support Agreement EAR-1851048. The facilities of IRIS Data Services, and specifically the IRIS Data Management Center, were used for access to waveforms, related metadata, and/or derived products used in this study. IRIS Data Services are funded through the Seismological Facilities for the Advancement of Geoscience (SAGE) Award of the National Science Foundation under Cooperative Support Agreement EAR-1851048. The work of

- Strain-Tilt Coupling** Tilt induced by local strain, usually within or adjacent to a seismic sensor vault.
- T-phase** Acoustic phase in the ocean (or similar water column) that is converted to seismic energy (typically at a shoreline).
- Teleseismic (seismic distance range)** Source-receiver distances for which seismograms are dominated by mantle phases ($\gtrsim 30^\circ$, or 3,330 km).
- Tilt Noise** Primarily horizontal component noise generated seismometer tilt within Earth's gravity field and recorded as an apparent horizontal acceleration.
- Treaty on the Non-Proliferation of Nuclear Weapons (NPTs)** International treaty with the objective to prevent the spread of nuclear weapons that opened for signatures in 1968 and went into force in 1970.
- Tsunami Warning System** U.S. system for warning coastal locations of possible tsunamis generated by earthquakes.
- Very Broad Band (VBB)** Seismographic system with a flat amplitude response velocity across a bandwidth that encompasses a large fraction of Earth's available seismic spectrum (e.g., 50 Hz to 360 s period).
- World-Wide Standardized Seismograph Network (WWSSN)** US analog network of 120 uniform stations built out in the 1960s. The geographic footprint of much of this network evolved into the GDSN and GSN.

Data Availability Statement

Data from the networks discussed in this work are freely available through the FDSN request tools implemented in numerous data centers (e.g., IRIS, RESIF, ORFEUS, and GEOFON). See for example, <https://service.iris.edu/fdsnws/dataselect/1/> for an access via web services. This work discussed or made use from the following networks: Albuquerque Seismological Laboratory (ASL)/USGS (1974, 1976, 1980, 1988, 1992, 1993, 2006), Scripps Institution of Oceanography (1975, 1986), Institut De Physique Du Globe De Paris (IPGP) and École et Observatoire des Sciences de la Terre de Strasbourg (EOST) (1982), MedNet Project Partner Institutions (1988), GEOFON Data Centre (1993), and California Institute of Technology and United States Geological Survey Pasadena (1926).

References

- Adushkin, V. V., Bobrov, D. I., Kitov, I. O., Rozhkov, M. V., & Sanina, I. A. (2017). Remote detection of aftershock activity as a new method of seismic monitoring. *Doklady Earth Sciences*, 473(1), 303–307. <https://doi.org/10.1134/S1028334X17030011>
- Afanasyev, M., Peter, D., Sager, K., Simut, S., Ermert, L., Krischer, L., & Fichtner, A. (2015). Foundations for a multiscale collaborative Earth model. *Geophysical Journal International*, 204(1), 39–58. <https://doi.org/10.1093/gji/ggv439>
- Agnew, D., Berger, J., Buland, R., Farrell, W., & Gilbert, F. (1976). International Deployment of Accelerometers: A network for very long period seismology. *EOS, Transactions American Geophysical Union*, 57(4), 180–188. <https://doi.org/10.1029/EO057i004p00180>
- Agnew, D. C. (2020). Time marks and clock corrections: A century of seismological timekeeping. *Seismological Research Letters*, 91(3), 1417–1429. <https://doi.org/10.1785/0220190284>
- Agnew, D. C., Berger, J., Farrell, W., Gilbert, J., Masters, G., & Miller, D. (1986). Project IDA: A decade in review. *Eos, Transactions American Geophysical Union*, 67(16), 203–212. <https://doi.org/10.1029/EO067i016p00203>
- Ahern, T., Casey, R., Barnes, D., Benson, R., Knight, T., & Trabant, C. (2012). *SEED reference manual version 2.4*. IRIS.
- Akbarashrafi, F., Al-Attar, D., Deuss, A., Trampert, J., & Valentine, A. P. (2018). Exact free oscillation spectra, splitting functions and the resolvability of Earth's density structure. *Geophysical Journal International*, 213(1), 58–76. <https://doi.org/10.1093/gji/ggx539>
- Aki, K. (1957). Space and time spectra of stationary stochastic waves, with special reference to microtremors. *Bulletin of the Earthquake Research Institute*, 35, 415–456.
- Aki, K., & Richards, P. G. (1980). *Quantitative seismology volume 1: Theory and methods*. Freeman and Company. <https://doi.org/10.1515/9780691216157>
- Al-Attar, D., Woodhouse, J. H., & Deuss, A. (2012). Calculation of normal mode spectra in laterally heterogeneous Earth models using an iterative direct solution method. *Geophysical Journal International*, 189(2), 1038–1046. <https://doi.org/10.1111/j.1365-246X.2012.05406.x>
- Albaric, J., Kühn, D., Ohnberger, M., Langet, N., Harris, D., Polom, U., et al. (2021). Seismic monitoring of permafrost in Svalbard, Arctic Norway. *Seismological Research Letters*, 92(5), 2891–2904. <https://doi.org/10.1785/0220200470>
- Albuquerque Seismological Laboratory (ASL)/USGS. (1974). *Seismic Research Observatory*. International Federation of Digital Seismograph Networks. <https://doi.org/10.7914/SN/SR>
- Albuquerque Seismological Laboratory (ASL)/USGS. (1976). *Modified High Gain Long Period Observatory*. International Federation of Digital Seismograph Networks. <https://doi.org/10.7914/SN/AS>
- Albuquerque Seismological Laboratory (ASL)/USGS. (1980). *Digital World-Wide Standardized Seismograph Network*. International Federation of Digital Seismograph Networks. <https://doi.org/10.7914/SN/DW>
- Albuquerque Seismological Laboratory (ASL)/USGS. (1988). *Global seismograph network – IRIS/USGS*. International Federation of Digital Seismograph Networks. <https://doi.org/10.7914/SN/IU>

Won-Young Kim, David P. Schaff, and Paul G. Richards at Lamont-Doherty Earth Observatory was supported in part by the US Defense Threat Reduction Agency under award number HDTRA1-11-1-00027 to Columbia University, and by two awards from the Department of Energy's National Nuclear Security Administration to the University of Michigan: DE-NA0002534 to the Consortium for Verification Technology and DE-NA0003920 to the Consortium on Monitoring, Technology, and Verification. V. Lekić acknowledges support from NSF EAR-1345082. H. C. P. Lau acknowledges support from NSF EAR-1923865. P. Koelemeijer acknowledges support from a Royal Society University Research Fellowship (URF R1\180377). Any use of trade, product, or firm names is for descriptive purposes only and does not imply endorsement by the U.S. Government.

- Albuquerque Seismological Laboratory (ASL)/USGS. (1992). *New China Digital Seismograph Network*. International Federation of Digital Seismograph Networks. <https://doi.org/10.7914/SN/IC>
- Albuquerque Seismological Laboratory (ASL)/USGS. (1993). *Global Telemetered Seismograph Network (USAF/USGS)*. International Federation of Digital Seismograph Networks. <https://doi.org/10.7914/SN/GT>
- Albuquerque Seismological Laboratory (ASL)/USGS. (2006). *Caribbean USGS Network*. International Federation of Digital Seismograph Networks. <https://doi.org/10.7914/SN/CU>
- Alejandro, A. C. B., Ringler, A. T., Wilson, D. C., Anthony, R. E., & Moore, S. V. (2020). Towards understanding relationships between atmospheric pressure variations and long-period horizontal seismic data: A case study. *Geophysical Journal International*, 223(1), 676–691. <https://doi.org/10.1093/gji/ggaa340>
- Allen, R. (1978). Automatic earthquake recognition and timing from single traces. *Bulletin of the Seismological Society of America*, 68(5), 1521–1532. <https://doi.org/10.1785/bssa0680051521>
- Allmann, B. P., & Shearer, P. M. (2009). Global variations of stress drop for moderate to large earthquakes. *Journal of Geophysical Research*, 114(B1), B01310. <https://doi.org/10.1029/2008JB005821>
- Alvizuri, C., & Tape, C. (2018). Full moment tensor analysis of nuclear explosions in North Korea. *Seismological Research Letters*, 89(6), 2139–2151. <https://doi.org/10.1785/0220180158>
- Ammon, C. J., Ji, C., Thio, H.-K., Robinson, D., Ni, S., Hjorleifsdottir, V., et al. (2005). Rupture process of the 2004 Sumatra-Andaman earthquake. *Science*, 308(5725), 1133–1139. <https://doi.org/10.1126/science.1112260>
- Ammon, C. J., Kanamori, H., & Lay, T. (2008). A great earthquake doublet and seismic stress transfer cycle in the central Kuril islands. *Nature*, 451(7178), 561–565. <https://doi.org/10.1038/nature06521>
- Ammon, C. J., Kanamori, H., Lay, T., & Velasco, A. A. (2006). The 17 July 2006 Java tsunami earthquake. *Geophysical Research Letters*, 33(24), L24308. <https://doi.org/10.1029/2006GL028005>
- Ammon, C. J., Lay, T., Kanamori, H., & Cleveland, M. (2011). A rupture model of the 2011 off the Pacific coast of Tohoku Earthquake. *Earth Planets and Space*, 63(7), 693–696. <https://doi.org/10.5047/eps.2011.05.015>
- Amundson, J. M., Fahnestock, M., Truffer, M., Brown, J., Luthi, M. P., & Motyka, R. J. (2010). Ice melange dynamics and implications for terminus stability, Jakobshavn Isbrae, Greenland. *Journal of Geophysical Research*, 115(F1), F01005. <https://doi.org/10.1029/2009JF001405>
- Anderson, D., Anderson, J., Ford, D., Gee, L. S., Gyure, G., Hutt, C. R., et al. (2015). Upgrade of the New China Digital Seismograph Network. *Seismological Research Letters*, 86(5), 1364–1373. <https://doi.org/10.1785/0220140182>
- Anderson, D. L. (2007). *New theory of the Earth* (2nd ed.). Cambridge University Press. <https://doi.org/10.1017/CBO9781139167291>
- Ando, M., Ishidoshiro, K., Yamamoto, K., Yagi, K., Kokuyama, W., Tsubono, K., & Takamori, A. (2010). Torsion-bar antenna for low-frequency gravitational-wave observations. *Physical Review Letters*, 105(16), 161101. <https://doi.org/10.1103/PhysRevLett.105.161101>
- Anthony, R. E., Aster, R., & McGrath, D. (2017). Links between atmosphere, ocean, and cryosphere from two decades of microseism observations on the Antarctic Peninsula. *Journal of Geophysical Research: Earth Surface*, 121(1), 153–166. <https://doi.org/10.1002/2016JF004098>
- Anthony, R. E., Aster, R., Wiens, D., Anandakrishnan, S., Huerta, A. D., Winberry, J. P., et al. (2015). The seismic noise environment of Antarctica. *Seismological Research Letters*, 86(1), 89–100. <https://doi.org/10.1785/0220140109>
- Anthony, R. E., Ringler, A. T., DuVernois, M., Anderson, K. R., & Wilson, D. C. (2021). Six decades of seismology at South Pole, Antarctica: Current limitations and future opportunities to facilitate new geophysical observations. *Seismological Research Letters*, 92(5), 2718–2735. <https://doi.org/10.1785/0220200448>
- Anthony, R. E., Ringler, A. T., & Wilson, D. C. (2017). Improvements in absolute seismometer sensitivity calibration using local Earth gravity measurements. *Bulletin of the Seismological Society of America*, 108(1), 503–510. <https://doi.org/10.1785/0120170218>
- Anthony, R. E., Ringler, A. T., Wilson, D. C., Bahavar, M., & Koper, K. D. (2020). How processing methodologies can distort and bias power spectral density estimates of seismic background noise. *Seismological Research Letters*, 91(3), 1694–1706. <https://doi.org/10.1785/0220190212>
- Anthony, R. E., Ringler, A. T., Wilson, D. C., Zebulon Maharrey, J., Gyure, G., Pepiot, A., et al. (2020). Installation and performance of the Albuquerque Seismological Laboratory small-aperture posthole array. *Seismological Research Letters*, 91(4), 2425–2437. <https://doi.org/10.1785/0220200080>
- Arduhin, F., Gualtieri, L., & Stutzmann, E. (2015). How ocean waves rock the Earth: Two mechanisms explain microseisms with periods 3 to 300 s. *Geophysical Research Letters*, 42, 765–772. <https://doi.org/10.1002/2014GL026272>
- Arduhin, F., Stutzmann, E., Schimmel, M., & Mangeny, A. (2011). Ocean wave sources of seismic noise. *Journal of Geophysical Research*, 116(C9), C09004. <https://doi.org/10.1029/2011JC006952>
- Arora, N. S., Russell, S., & Sudderth, E. B. (2013). NET-VISA: Network processing vertically integrated seismic analysis. *Bulletin of the Seismological Society of America*, 103(2A), 709–729. <https://doi.org/10.1785/0120120107>
- Arrowsmith, S. J., Johnson, J. B., Drob, D. P., & Hedlin, M. A. (2010). The seismoacoustic wavefield: A new paradigm in studying geophysical phenomena. *Reviews of Geophysics*, 48(4), RG4003. <https://doi.org/10.1029/2010RG000335>
- Arrowsmith, S. J., Whitaker, R., Taylor, S. R., Burlacu, R., Stump, B., Hedlin, M., et al. (2008). Regional monitoring of infrasound events using multiple arrays: Application to Utah and Washington State. *Geophysical Journal International*, 175(1), 291–300. <https://doi.org/10.1111/j.1365-246X.2008.03912.x>
- Assink, J., Smets, P., Marcillo, O., Weemstra, C., Lalande, J.-M., Waxler, R., & Evers, L. (2019). Advances in infrasonic remote sensing methods. In *Infrasound monitoring for atmospheric studies* (pp. 605–632). Springer.
- Aster, R., Beaudoin, B., Hole, J., Fouch, M. J., Fowler, J., & James, D. (2005). IRIS PASSCAL program marks 20 years of scientific discovery. *EOS Transactions of the American Geophysical Union*, 86(17), 171–172. <https://doi.org/10.1029/2005EO170002>
- Aster, R., Lipovsky, B., Cole, H., Bromirski, P., Gerstoft, P., Nyblade, A., et al. (2021). Swell-triggered seismicity at the near-front damage zone of the Ross Ice Shelf. *Seismological Research Letters*, 92(5), 2768–2792. <https://doi.org/10.1785/0220200478>
- Aster, R., McIntosh, B., Kyle, P., Esser, R., Bartel, B., Dunbar, N., et al. (2004). Real-time data received from Mount Erebus volcano, Antarctica. *EOS, Transactions of the American Geophysical Union*, 85(10), 97–104. <https://doi.org/10.1029/2004EO100001>
- Aster, R., McNamara, D. E., & Bromirski, P. D. (2008). Multidecadal climate-induced variability in microseisms. *Seismological Research Letters*, 79(2), 194–202. <https://doi.org/10.1785/gssrl.79.2.194>
- Aster, R., McNamara, D. E., & Bromirski, P. D. (2010). Global trends in extremal microseism intensity. *Geophysical Research Letters*, 37(14), L14303. <https://doi.org/10.1029/2010gl043472>
- Aster, R., & Winberry, J. P. (2017). Glacial seismology. *Reports on Progress in Physics*, 80(12), 126801. <https://doi.org/10.1088/1361-6633/aa8473>
- ATOC Consortium. (1998). Ocean climate change: Comparison of acoustic tomography, satellite altimetry, and modeling. *Science*, 281(5381), 1327–1332. <https://doi.org/10.1126/science.281.5381.1327>

- Aubert, J., Amit, H., Hulot, G., & Olson, P. (2008). Thermochemical flows couple the Earth's inner core growth to mantle heterogeneity. *Nature*, 454(7205), 758–761. <https://doi.org/10.1038/nature07109>
- Aubert, J., & Dumberry, M. (2011). Steady and fluctuating inner core rotation in numerical geodynamo models. *Geophysical Journal International*, 184(1), 162–170. <https://doi.org/10.1111/j.1365-246X.2010.04842.x>
- Aurnou, J., Brito, D., & Olson, P. (1998). Anomalous rotation of the inner core and the toroidal magnetic field. *Journal of Geophysical Research*, 103(B5), 9721–9738. <https://doi.org/10.1029/97JB03618>
- Banerdt, W. B., Smrekar, S. E., Banfield, D., Giardini, D., Golombek, M., Johnson, C. L., et al. (2020). Initial results from the insight mission on Mars. *Nature Geoscience*, 13(3), 183–189. <https://doi.org/10.1038/s41561-020-0544-y>
- Barnhart, W. D., Hayes, G. P., & Wald, D. J. (2019). Global earthquake response with imaging geodesy: Recent examples from the USGS NEIC. *Remote Sensing*, 11(11), 1357. <https://doi.org/10.3390/rs11111357>
- Beauduin, R., Lognonné, P., Montagner, J. P., Cacho, S., Karczewski, J. F., & Morand, M. (1996). The effects of the atmospheric pressure changes on seismic signals or how to improve the quality of a station. *Bulletin of the Seismological Society of America*, 86(6), 1760–1769. <https://doi.org/10.1785/bssa0860061760>
- Beavan, J., Wang, X., Holden, C., Wilson, K., Power, W., Prasetya, G., et al. (2010). Near-simultaneous great earthquakes at Tongan megathrust and outer rise in September 2009. *Nature*, 466(7309), 959–963. <https://doi.org/10.1038/nature09292>
- Becker, T. W., & Boschi, L. (2002). A comparison of tomographic and geodynamic mantle models. *Geochemistry, Geophysics, Geosystems*, 3(1), 1003. <https://doi.org/10.1029/2001GC000168>
- Bedard, A., & Georges, T. (2000). Atmospheric infrasound. *Acoustics Australia*, 28(2), 47–52.
- Beghein, C., Resovsky, J., & Van Der Hilst, R. D. (2008). The signal of mantle anisotropy in the coupling of normal modes. *Geophysical Journal International*, 175(3), 1209–1234. <https://doi.org/10.1111/j.1365-246X.2008.03970.x>
- Beghein, C., & Trampert, J. (2003). Robust normal mode constraints on inner-core anisotropy from model space search. *Science*, 299(5606), 552–555. <https://doi.org/10.1126/science.1078159>
- Behringer, D., Birdsall, T., Brown, M., Cornuelle, B., Heinmiller, R., Knox, R., et al. (1982). A demonstration of ocean acoustic tomography. *Nature*, 299(5879), 121–125. <https://doi.org/10.1038/299121a0>
- Bell, R. W. (2018). CTBTO science and technology for a safer world. In L. Maiani, S. Aousahl, & W. Plastino (Eds.), *International cooperation for enhancing nuclear safety, security, safeguards and non-proliferation—60 years of IAEA and EURATOM* (pp. 167–174). Springer Berlin Heidelberg.
- Bendick, R., & Bilham, R. (2017). Do weak global stresses synchronize earthquakes? *Geophysical Research Letters*, 44(16), 8320–8327. <https://doi.org/10.1002/2017gl074934>
- Benioff, H., Press, F., & Smith, S. (1961). Excitation of the free oscillations of the Earth by earthquakes. *Journal of Geophysical Research*, 66(2), 605–619. <https://doi.org/10.1029/jz066i002p00605>
- Berger, J., Davis, P., & Ekström, G. (2004). Ambient Earth noise: A survey of the global seismographic network. *Journal of Geophysical Research*, 109(B11), B11307. <https://doi.org/10.1029/2004JB003408>
- Bernard, P., Karczewski, J.-F., Morand, M., Dole, B., & Romanowicz, B. (1991). The G-calibration: A new method for an absolute in situ calibration of long-period accelerometers, tested on the Streckeisen instruments of the GEOSCOPE network. *Bulletin of the Seismological Society of America*, 81(4), 1360–1372. <https://doi.org/10.1785/bssa0810041360>
- Bernauer, F., Wassermann, J., & Igel, H. (2020). Dynamic tilt correction using direct rotational motion measurements. *Seismological Research Letters*, 91(5), 2872–2880. <https://doi.org/10.1785/0220200132>
- Beroza, G. C. (2012). How many great earthquakes should we expect? *Proceedings of the National Academy of Science*, 109(3), 651–652. <https://doi.org/10.1073/pnas.1120744109>
- Beucler, E., Stutzmann, E., & Montagner, J.-P. (2003). Surface wave higher-mode phase velocity measurements using a roller-coaster-type algorithm. *Geophysical Journal International*, 155(1), 289–307. <https://doi.org/10.1046/j.1365-246x.2003.02041.x>
- Beyreuther, M., Barsch, R., Krischer, L., Megies, T., Behr, Y., & Wassermann, J. (2010). ObsPy: A python toolbox for seismology. *Seismological Research Letters*, 81(3), 530–533. <https://doi.org/10.1785/gssrl.81.3.530>
- Bilek, S. L., & Lay, T. (1999). Rigidity variations with depth along interplate megathrust faults in subduction zones. *Nature*, 400(6743), 443–446. <https://doi.org/10.1038/22739>
- Bilek, S. L., & Lay, T. (2018). Subduction zone megathrust earthquakes. *Geosphere*, 14(4), 1468–1500. <https://doi.org/10.1130/ges01608.1>
- Bilek, S. L., Lay, T., & Ruff, L. J. (2004). Radiated seismic energy and earthquake source duration variations from teleseismic source time functions for shallow subduction zone thrust earthquakes. *Journal of Geophysical Research*, 109(B9), B09308. <https://doi.org/10.1029/2004jb003039>
- Bindschadler, R. A., King, M. A., Alley, R. B., Anandakrishnan, S., & Padman, L. (2003). Tidally controlled stick-slip discharge of a West Antarctic ice stream. *Science*, 301(5636), 1087–1089. <https://doi.org/10.1126/science.1087231>
- Bletery, Q., Sladen, A., Delouis, B., Vallée, M., Nocquet, J.-M., Rolland, L., & Jiang, J. (2014). A detailed source model for the M_w 9.0 Tohoku-Oki earthquake reconciling geodesy, seismology, and tsunami records. *Journal of Geophysical Research: Solid Earth*, 119(10), 7636–7653. <https://doi.org/10.1002/2014jb011261>
- Blom, N., Gokhberg, A., & Fichtner, A. (2020). Seismic waveform tomography of the central and eastern Mediterranean upper mantle. *Solid Earth*, 11(2), 669–690. <https://doi.org/10.5194/se-11-669-2020>
- Bock, Y., Melgar, D., & Crowell, B. W. (2011). Real-time strong-motion broadband displacements from collocated GPS and accelerometers. *Bulletin of the Seismological Society of America*, 101(6), 2904–2925. <https://doi.org/10.1785/0120110007>
- Boese, C., Wotherspoon, L., Alvarez, M., & Malin, P. (2015). Analysis of anthropogenic and natural noise from multilevel borehole seismometers in an urban environment, Auckland, New Zealand. *Bulletin of the Seismological Society of America*, 105(1), 285–299. <https://doi.org/10.1785/0120130288>
- Bonnet, P., Yastrebov, V. A., Queutey, P., Leroyer, A., Mangeny, A., Castelnau, O., et al. (2020). Modelling capsizing icebergs in the open ocean. *Geophysical Journal International*, 223(2), 1265–1287. <https://doi.org/10.1093/gji/ggaa353>
- Bontemps, N., Lacroix, P., Larose, E., Jara, J., & Taïpe, E. (2020). Rain and small earthquakes maintain a slow-moving landslide in a persistent critical state. *Nature Communications*, 11(1), 780. <https://doi.org/10.1038/s41467-020-14445-3>
- Boschi, E., Giardini, D., & Morelli, A. (1991). MedNet: The very broad-band seismic network for the Mediterranean. *Il Nuovo Cimento C*, 14(1), 79–99. <https://doi.org/10.1007/BF02509260>
- Böse, M., Clinton, J. F., Ceylan, S., Euchner, F., van Driel, M., Khan, A., et al. (2017). A probabilistic framework for single-station location of seismicity on Earth and Mars. *Physics of the Earth and Planetary Interiors*, 262, 48–65. <https://doi.org/10.1016/j.pepi.2016.11.003>
- Bouchon, M., & Vallée, M. (2003). Observation of long supershear rupture during the magnitude 8.1 Kunlunshan earthquake. *Science*, 301(5634), 824–826. <https://doi.org/10.1126/science.1086832>

- Bowen, S. P., Richard, J. C., Mancini, J. D., Fessatidis, V., & Crooker, B. (2003). Microseism and infrasound generation by cyclones. *Journal of the Acoustical Society of America*, 113(5), 2562–2573. <https://doi.org/10.1121/1.1567277>
- Boy, J.-P., Llubes, M., Hinderer, J., & Florsch, N. (2003). A comparison of tidal ocean loading models using superconducting gravimeter data. *Journal of Geophysical Research*, 108(B4). <https://doi.org/10.1029/2002JB002050>
- Bozdağ, E., Peter, D., Lefebvre, M., Komatitsch, D., Tromp, J., Hill, J., et al. (2016). Global adjoint tomography: First-generation model. *Geophysical Journal International*, 207(3), 1739–1766. <https://doi.org/10.1093/gji/ggw356>
- British Association for Advancement of Science Seismological Committee, & Milne, J. (1912). *A catalogue of destructive earthquakes, A.D. 7 to A.D. 1899*. The Association.
- Bromirski, P. D., & Duennebier, F. K. (2002). The near-coastal microseism spectrum: Spatial and temporal wave climate relationships. *Journal of Geophysical Research*, 107(B8), 2166. <https://doi.org/10.1029/2001jb000265>
- Bromirski, P. D., & Flick, R. E. (2020). Near-coastal winter waves from microseisms. *Geophysical Research Letters*, 47(18), e2020GL089831. <https://doi.org/10.1029/2020gl089831>
- Bromirski, P. D., & Gerstoft, P. (2009). Dominant source regions of the Earth's "hum" are coastal. *Geophysical Research Letters*, 36(13), L13303. <https://doi.org/10.1029/2009gl038903>
- Brown, P. G., Assink, J. D., Astiz, L., Blaauw, R., Boslough, M. B., Borovička, J., et al. (2013). A 500-kiloton airburst over Chelyabinsk and an enhanced hazard from small impactors. *Nature*, 503(7475), 238–241. <https://doi.org/10.1038/nature12741>
- Brush, S. G. (1980). Discovery of the Earth's core. *American Journal of Physics*, 48(9), 705–724. <https://doi.org/10.1119/1.12026>
- Buehler, J. S., & Shearer, P. M. (2015). T phase observations in global seismogram stacks. *Geophysical Research Letters*, 42(16), 6607–6613. <https://doi.org/10.1002/2015gl064721>
- Buland, R., Berger, J., & Gilbert, F. (1979). Observations from the IDA network of attenuation and splitting during a recent earthquake. *Nature*, 277(5695), 358–362. <https://doi.org/10.1038/277358a0>
- Burdick, S., Waszek, L., & Lekić, V. (2019). Seismic tomography of the uppermost inner core. *Earth and Planetary Science Letters*, 528, 115789. <https://doi.org/10.1016/j.epsl.2019.115789>
- Bürgmann, R., & Dresen, G. (2008). Rheology of the lower crust and upper mantle: Evidence from rock mechanics, geodesy, and field observations. *Annual Review of Earth and Planetary Sciences*, 36(1), 531–567. <https://doi.org/10.1146/annurev.earth.36.031207.124326>
- Burr, W., Cohen, A., De Geer, L.-E., Gilinsky, V., Polakow-Suransky, S., Sokolski, H., et al. (2019). Blast from the past. *Foreign Policy*. Retrieved from <https://foreignpolicy.com/2019/09/22/blast-from-the-past-vela-satellite-israel-nuclear-double-flash-1979-ptbt-south-atlantic-south-africa/>
- Burtin, A., Bollinger, L., Vergne, J., Cattin, R., & Nábělek, J. L. (2008). Spectral analysis of seismic noise induced by rivers: A new tool to monitor spatiotemporal changes in stream hydrodynamics. *Journal of Geophysical Research*, 113(B5), B05301. <https://doi.org/10.1029/2007jb005034>
- Burtin, A., Hovius, N., & Turowski, J. (2016). Seismic monitoring of torrential and fluvial processes. *Earth Surface Dynamics*, 4(2), 285–307. <https://doi.org/10.5194/esurf-4-285-2016>
- Burtin, A., Vergne, J., Rivera, L., & Dubernet, P. (2010). Location of river-induced seismic signal from noise correlation functions. *Geophysical Journal International*, 182(3), 1161–1173. <https://doi.org/10.1111/j.1365-246X.2010.04701.x>
- Busby, R. W., & Aderhold, K. (2020). The Alaska Transportable Array: As built. *Seismological Research Letters*, 91(6), 3017–3027. <https://doi.org/10.1785/0220200154>
- Busby, R. W., Woodward, R. L., Hafner, K. A., Vernon, V. F., & Frassetto, A. M. (2018). The design and implementation of EarthScope's USArray Transportable Array. *IRIS Consortium*, (pp. 64).
- Butler, R., Lay, T., Creager, K., Earle, P., Fischer, K., Gaherty, J., et al. (2004). The global seismographic network surpasses its design goal. *Eos, Transactions American Geophysical Union*, 85(23), 225–229. <https://doi.org/10.1029/2004EO230001>
- California Institute of Technology and United States Geological Survey Pasadena. (1926). *Southern California Seismic Network*. International Federation of Digital Seismograph Networks. <https://doi.org/10.7914/SN/CI>
- Campillo, M., & Paul, A. (2003). Long-range correlations in the diffuse seismic coda. *Science*, 299(5606), 547–549. <https://doi.org/10.1126/science.1078551>
- Cannata, A., Cannavo, F., Moschella, S., Gresta, S., & Spina, L. (2019). Exploring the link between microseism and sea ice in Antarctica by using machine learning. *Scientific Reports*, 9(1), 13050. <https://doi.org/10.1038/s41598-019-49586-z>
- Cao, A., Romanowicz, B. A., & Takeuchi, N. (2005). An observation of PKJKP: Inferences on inner core shear properties. *Science*, 308(5727), 1453–1455. <https://doi.org/10.1126/science.1109134>
- Casey, R., Templeton, M. E., Sharer, G., Keyson, L., Weertman, B. R., & Ahern, T. (2018). Assuring the quality of IRIS data with MUSTANG. *Seismological Research Letters*, 89(2A), 630–639. <https://doi.org/10.1785/0220170191>
- Cessaro, R. (1994). Sources of primary and secondary microseisms. *Bulletin of the Seismological Society of America*, 84(1), 142–148. <https://doi.org/10.1785/bssa0840010142>
- Chang, S.-J., Ferreira, A. M., Ritsema, J., Heijst, H. J., & Woodhouse, J. H. (2015). Joint inversion for global isotropic and radially anisotropic mantle structure including crustal thickness perturbations. *Journal of Geophysical Research: Solid Earth*, 120(6), 4278–4300. <https://doi.org/10.1002/2014JB011824>
- Chaput, J., Aster, R., Karplus, M., & Nakata, N. (2022). Ambient high-frequency seismic surface waves in the firn column of central west Antarctica. *Journal of Glaciology*, 1–14. <https://doi.org/10.1017/jog.2021.135>
- Chaput, J., Aster, R. C., McGrath, D., Baker, M., Anthony, R. E., Gerstoft, P., et al. (2018). Near-surface environmentally forced changes in the Ross Ice Shelf observed with ambient seismic noise. *Geophysical Research Letters*, 45(20), 11187–11196. <https://doi.org/10.1029/2018gl079665>
- Che, I.-Y., Park, J., Kim, I., Kim, T. S., & Lee, H.-I. (2014). Infrasound signals from the underground nuclear explosions of North Korea. *Geophysical Journal International*, 198(1), 495–503. <https://doi.org/10.1093/gji/ggu150>
- Che, I.-Y., Park, J., Kim, T. S., Hayward, C., & Stump, B. (2019). On the use of a dense network of seismo-acoustic arrays for near-regional environmental monitoring. In *Infrasound monitoring for atmospheric studies* (pp. 409–448). Springer.
- Chen, Y., & Saygin, E. (2020). Empirical Green's function retrieval using ambient noise source-receiver interferometry. *Journal of Geophysical Research: Solid Earth*, 125(2), e18261. <https://doi.org/10.1029/2019JB018261>
- Chounet, A., & Vallée, M. (2018). Global and interregion characterization of subduction interface earthquakes derived from source time functions properties. *Journal of Geophysical Research: Solid Earth*, 123(7), 5831–5852. <https://doi.org/10.1029/2018jb015932>
- Clements, T., & Denolle, M. A. (2018). Tracking groundwater levels using the ambient seismic field. *Geophysical Research Letters*, 45(13), 6459–6465. <https://doi.org/10.1029/2018gl077706>
- Clevede, E., Megnin, C., Romanowicz, B., & Lognonne, P. (2000). Seismic waveform modeling and surface wave tomography in a three-dimensional Earth: Asymptotic and non-asymptotic approaches. *Physics of the Earth and Planetary Interiors*, 119(1–2), 37–56. [https://doi.org/10.1016/s0031-9201\(99\)00152-1](https://doi.org/10.1016/s0031-9201(99)00152-1)

- Clinton, J. F., & Heaton, T. H. (2002). Potential advantages of a strong-motion velocity meter over a strong-motion accelerometer. *Seismological Research Letters*, 73(3), 332–342. <https://doi.org/10.1785/gssrl.73.3.332>
- Collier, J. D., & Helffrich, G. (2001). Estimate of inner core rotation rate from United Kingdom regional seismic network data and consequences for inner core dynamical behaviour. *Earth and Planetary Science Letters*, 193(3), 523–537. [https://doi.org/10.1016/S0012-821X\(01\)00520-9](https://doi.org/10.1016/S0012-821X(01)00520-9)
- Cook, K. L., Andermann, C., Gimbert, F., Adhikari, B. R., & Hovius, N. (2018). Glacial lake outburst floods as drivers of fluvial erosion in the Himalaya. *Science*, 362(6410), 53–57. <https://doi.org/10.1126/science.aat4981>
- Creager, K. C. (1997). Inner core rotation rate from small-scale heterogeneity and time-varying travel times. *Science*, 278(5341), 1284–1288. <https://doi.org/10.1126/science.278.5341.1284>
- Curtis, A., Behr, Y., Entwistle, E., Galetti, E., Townend, J., & Bannister, S. (2012). The benefit of hindsight in observational science: Retrospective seismological observations. *Earth and Planetary Science Letters*, 345–348, 212–220. <https://doi.org/10.1016/j.epsl.2012.06.008>
- Curtis, A., Gerstoft, P., Sato, H., Snieder, R., & Wapenaar, K. (2006). Seismic interferometry—Turning noise into signal. *The Leading Edge*, 25(9), 1082–1092. <https://doi.org/10.1190/1.2349814>
- Dahlen, F. A. (1968). The normal modes of a rotating elliptical Earth. *Geophysical Journal of the Royal Astronomical Society*, 16(4), 329–367. <https://doi.org/10.1111/j.1365-246X.1968.tb00229.x>
- Dahlen, F. A., & Tromp, J. (1998). *Theoretical global seismology*. Princeton University Press. <https://doi.org/10.1515/9780691216157>
- Dalton, C. A., Ekström, G., & Dziewoński, A. M. (2008). The global attenuation structure of the upper mantle. *Journal of Geophysical Research*, 113(B9), B09303. <https://doi.org/10.1029/2007JB005429>
- Das, S. (2015). Supershear earthquake ruptures – Theory, methods, laboratory experiments and fault superhighways: An update. In A. Ansal (Ed.), *Perspectives on European earthquake engineering and seismology* (pp. 1–20). Springer International Publishing.
- Davis, P., & Berger, J. (2007). Calibration of the global seismographic network using tides. *Seismological Research Letters*, 78(4), 454–459. <https://doi.org/10.1785/gssrl.78.4.454>
- Davis, P., & Berger, J. (2012). Initial impact of the global seismographic network quality initiative on metadata accuracy. *Seismological Research Letters*, 83(4), 697–703. <https://doi.org/10.1785/02201120021>
- Davis, P., Ishii, M., & Masters, G. (2005). An assessment of the accuracy of GSN sensor response information. *Seismological Research Letters*, 76(6), 678–683. <https://doi.org/10.1785/gssrl.76.6.678>
- de Groot-Hedlin, C. D., Hedlin, M. A., Hoffmann, L., Alexander, M. J., & Stephan, C. C. (2017). Relationships between gravity waves observed at Earth's surface and in the stratosphere over the central and eastern United States. *Journal of Geophysical Research: Atmospheres*, 122(21), 11–482. <https://doi.org/10.1002/2017jd027159>
- de Groot-Hedlin, C. D., & Hedlin, M. A. H. (2014). Infrasound detection of the Chelyabinsk meteor at the USArray. *Earth and Planetary Science Letters*, 402, 337–345. <https://doi.org/10.1016/j.epsl.2014.01.031>
- De Carlo, M., Hupe, P., Le Pichon, A., Ceranna, L., & Arduhin, F. (2021). Global microbarom patterns: A first confirmation of the theory for source and propagation. *Geophysical Research Letters*, 48(3), e2020GL090163. <https://doi.org/10.1029/2020GL090163>
- DeConto, R. M., Pollard, D., Alley, R. B., Velicogna, I., Gasson, E., Gomez, N., et al. (2021). The Paris climate agreement and future sea-level rise from Antarctica. *Nature*, 593(7857), 83–89. <https://doi.org/10.1038/s41586-021-03427-0>
- Deen, M., Stutzmann, E., & Arduhin, F. (2018). The Earth's hum variations from a global model and seismic recordings around the Indian Ocean. *Geochemistry, Geophysics, Geosystems*, 19(10), 4006–4020. <https://doi.org/10.1029/2018gc007478>
- Delaney, J., Kelley, D., Marburg, A., Stroemer, M., Hadaway, H., Juniper, K., & Knuth, F. (2016). Axial Seamount – Wired and restless: A cabled submarine network enables real-time, tracking of a mid-ocean ridge eruption and live video of an active hydrothermal system Juan de Fuca ridge, NE Pacific. In *IEEE, Proceedings OCEANS 2016 MTS/IEEE Monterey*. <https://doi.org/10.1109/OCEANS.2016.7761484>
- Delbridge, B. G., & Ishii, M. (2020). Reconciling elasticity tensor constraints from mineral physics and seismological observations: Applications to the Earth's inner core. *Geophysical Journal International*, 222(2), 1135–1145. <https://doi.org/10.1093/gji/ggaa220>
- Delescluse, M., Chamot-Rooke, N., Cattin, R., Fleitout, L., Trubienko, O., & Vigny, C. (2012). April 2012 intra-oceanic seismicity off Sumatra boosted by the Banda-Aceh megathrust. *Nature*, 490(7419), 240–244. <https://doi.org/10.1038/nature11520>
- Delouis, B. (2014). FMNEAR: Determination of focal mechanism and first estimate of rupture directivity using near-source records and a linear distribution of point sources. *Bulletin of the Seismological Society of America*, 104(3), 1479–1500. <https://doi.org/10.1785/0120130151>
- De Plaen, R. S., Márquez-Ramírez, V. H., Pérez-Campos, X., Zúñiga, F. R., Rodríguez-Pérez, Q., Gómez González, J. M., & Capra, L. (2021). Seismic signature of the COVID-19 lockdown at the city scale: A case study with low-cost seismometers in the city of Querétaro, Mexico. *Solid Earth*, 12(3), 713–724. <https://doi.org/10.5194/se-12-713-2021>
- Derr, J. S. (1969). Free oscillation observations through 1968. *Bulletin of the Seismological Society of America*, 59(5), 2079–2099. <https://doi.org/10.1785/BSSA0590052079>
- Deuss, A. (2014). Heterogeneity and anisotropy of Earth's inner core. *Annual Review of Earth and Planetary Sciences*, 42(1), 103–126. <https://doi.org/10.1146/annurev-earth-060313-054658>
- Deuss, A., Ritsema, J., & van Heijst, H. (2013). A new catalogue of normal-mode splitting function measurements up to 10 mHz. *Geophysical Journal International*, 193(2), 920–937. <https://doi.org/10.1093/gji/ggt010>
- Deuss, A., & Woodhouse, J. H. (2001). Theoretical free-oscillation spectra: The importance of wide band coupling. *Geophysical Journal International*, 146(3), 833–842. <https://doi.org/10.1046/j.1365-246X.2001.00502.x>
- Deuss, A., Woodhouse, J. H., Paulssen, H., & Trampert, J. (2000). The observation of inner core shear waves. *Geophysical Journal International*, 142(1), 67–73. <https://doi.org/10.1046/j.1365-246X.2000.00147.x>
- de Viron, O., Van Camp, M., Grabkowiak, A., & Ferreira, A. M. G. (2021). Comparing global seismic tomography models using varimax principal component analysis. *Solid Earth*, 12(7), 1601–1634. <https://doi.org/10.5194/se-12-1601-2021>
- Dewey, J., & Byerly, P. (1969). The early history of seismology (to 1900). *Bulletin of the Seismological Society of America*, 59, 183–227.
- de Wit, R., Käufel, P., Valentine, A., & Trampert, J. (2014). Bayesian inversion of free oscillations for Earth's radial (an) elastic structure. *Physics of the Earth and Planetary Interiors*, 237, 1–17. <https://doi.org/10.1016/j.pepi.2014.09.004>
- De Wit, R., & Trampert, J. (2015). Robust constraints on average radial lower mantle anisotropy and consequences for composition and texture. *Earth and Planetary Science Letters*, 429, 101–109. <https://doi.org/10.1016/j.epsl.2015.07.057>
- Díaz, J., Ruiz, M., Curto, J. J., Torta, J. M., Ledo, J., Marcuello, A., & Queralt, P. (2020). On the observation of magnetic events on broad-band seismometers. *Earth Planets and Space*, 72(1), 109. <https://doi.org/10.1186/s40623-020-01236-9>
- Díaz, J., Schimmel, M., Ruiz, M., & Carbonell, R. (2020). Seismometers within cities: A tool to connect Earth sciences and society. *Frontiers of Earth Science*, 8, 9. <https://doi.org/10.3389/feart.2020.00009>
- Di Giacomo, D., Engdahl, E. R., & Storchak, D. A. (2018). The ISC-GEM earthquake catalogue (1904–2014): Status after the extension project. *Earth System Science Data*, 10(4), 1877–1899. <https://doi.org/10.5194/essd-10-1877-2018>
- Dirks, P. (2006). AfricaArray: Building a scientific workforce for Africa's natural resources sector. *Traders African Business Journal*, 25, 54–55.

- Donn, W. L., & Naini, B. (1973). Sea wave origin of microbaroms and microseisms. *Journal of Geophysical Research*, 78(21), 4482–4488. <https://doi.org/10.1029/JC078i021p04482>
- Donner, S., Lin, C.-J., Hadziioannou, C., Gebauer, A., Vernon, F., Agnew, D. C., et al. (2017). Comparing direct observation of strain, rotation, and displacement with array estimates at Piñon Flat Observatory, California. *Seismological Research Letters*, 88(4), 1107–1116. <https://doi.org/10.1785/0220160216>
- Doody, C. D., Ringler, A. T., Anthony, R. E., Wilson, D. C., Holland, A. A., Hutt, C. R., & Sandoval, L. D. (2017). Effects of thermal variability on broadband seismometers: Controlled experiments, observations, and implications. *Bulletin of the Seismological Society of America*, 108(1), 493–502. <https://doi.org/10.1785/0120170233>
- Duennebier, F. K., Harris, D., Jolly, J., Baibinec, J., Copson, D., & Stiffel, K. (2002). The Hawaii-2 observatory seismic system. *IEEE Journal of Oceanic Engineering*, 27(2), 212–217. <https://doi.org/10.1109/joe.2002.1002475>
- Dumberry, M. (2010). Gravitationally driven inner core differential rotation. *Earth and Planetary Science Letters*, 297(3), 387–394. <https://doi.org/10.1016/j.epsl.2010.06.040>
- DuPutel, Z., Kanamori, H., Tsai, V. C., Rivera, L., Meng, L., Ampuero, J.-P., & Stock, J. M. (2012). The 2012 Sumatra great earthquake sequence. *Earth and Planetary Science Letters*, 351, 247–257. <https://doi.org/10.1016/j.epsl.2012.07.017>
- Durand, S., Debayle, E., Ricard, Y., & Lambotte, S. (2016). Seismic evidence for a change in the large-scale tomographic pattern across the D" layer. *Geophysical Research Letters*, 43(15), 7928–7936. <https://doi.org/10.1002/2016GL069650>
- Durek, J. J., & Ekström, G. (1995). Evidence of bulk attenuation in the asthenosphere from recordings of the Bolivia Earthquake. *Geophysical Research Letters*, 22(16), 2309–2312. <https://doi.org/10.1029/95GL01434>
- Durek, J. J., & Romanowicz, B. A. (1999). Inner core anisotropy inferred by direct inversion of normal mode spectra. *Geophysical Journal International*, 139(3), 599–622. <https://doi.org/10.1046/j.1365-246x.1999.00961.x>
- Dybing, S. N., Ringler, A. T., Wilson, D. C., & Anthony, R. E. (2019). Characteristics and spatial variability of wind noise on near-surface broadband seismometers. *Bulletin of the Seismological Society of America*, 109(3), 1082–1098. <https://doi.org/10.1785/0120180227>
- Dziak, R., Fowler, M., Matsumoto, H., Bohnenstiehl, D., Park, M., Warren, K., & Lee, W. S. (2013). Life and death sounds of iceberg A53a. *Oceanography*, 26(2), 10–13. <https://doi.org/10.5670/oceanog.2013.20>
- Dziewonski, A. M., & Anderson, D. L. (1981). Preliminary reference Earth model. *Physics of the Earth and Planetary Interiors*, 25(4), 297–356. [https://doi.org/10.1016/0031-9201\(81\)90046-7](https://doi.org/10.1016/0031-9201(81)90046-7)
- Dziewonski, A. M., Chou, T.-A., & Woodhouse, J. H. (1981). Determination of earthquake source parameters from waveform data for studies of global and regional seismicity. *Journal of Geophysical Research*, 86(B4), 2825–2852. <https://doi.org/10.1029/JB086iB04p02825>
- Dziewonski, A. M., & Gilbert, F. (1971). Solidity of the inner core of the Earth inferred from normal mode observations. *Nature*, 234(5330), 465–466. <https://doi.org/10.1038/234465a0>
- Dziewonski, A. M., Lekic, V., & Romanowicz, B. A. (2010). Mantle anchor structure: An argument for bottom up tectonics. *Earth and Planetary Science Letters*, 299(1–2), 69–79. <https://doi.org/10.1016/j.epsl.2010.08.013>
- Eakin, C. (2021). The deep roots of geology: Tectonic history of Australia and its margins expressed by mantle anisotropy. *Research Square*. <https://doi.org/10.21203/rs.3.rs-121788/v2>
- Ebeling, C. W., & Stein, S. (2011). Seismological identification and characterization of a large hurricane. *Bulletin of the Seismological Society of America*, 101(1), 399–403. <https://doi.org/10.1785/0120100175>
- Edwards, W. N., Eaton, D. W., McCausland, P. J., ReVelle, D. O., & Brown, P. G. (2007). Calibrating infrasonic to seismic coupling using the stardust sample return capsule shockwave: Implications for seismic observations of meteors. *Journal of Geophysical Research*, 112(B10), B10306. <https://doi.org/10.1029/2006jb004621>
- Eibl, E. P. S., Bean, C. J., Einarsson, B., Pálsson, F., & Vogfjörð, K. S. (2020). Seismic ground vibrations give advanced early-warning of subglacial floods. *Nature Communications*, 11(1), 2504. <https://doi.org/10.1038/s41467-020-15744-5>
- Ekström, G. (2011). A global model of Love and Rayleigh surface wave dispersion and anisotropy, 25–250 s. *Geophysical Journal International*, 187(3), 1668–1686. <https://doi.org/10.1111/j.1365-246X.2011.05225.x>
- Ekström, G., Dalton, C. A., & Nettles, M. (2006). Observations of time-dependent errors in long-period instrument gain at global seismic stations. *Seismological Research Letters*, 77(1), 12–22. <https://doi.org/10.1785/gssrl.77.1.12>
- Ekström, G., Nettles, M., & Abers, G. (2003). Glacial earthquakes. *Science*, 302(622), 624. <https://doi.org/10.1126/science.1088057>
- Ekström, G., Nettles, M., & Dziewoński, A. (2012). The global CMT project 2004–2010: Centroid-moment tensors for 13,017 earthquakes. *Physics of the Earth and Planetary Interiors*, 200–201, 1–9. <https://doi.org/10.1016/j.pepi.2012.04.002>
- Ekström, G., Nettles, M., & Tsai, V. C. (2006). Seasonality and increasing frequency of Greenland glacial earthquakes. *Science*, 311(5768), 1756–1758. <https://doi.org/10.1126/science.1122112>
- Elfouhaily, T., Chapron, B., Katsaros, K., & Vandemark, D. (1997). A unified directional spectrum for long and short wind-driven waves. *Journal of Geophysical Research*, 102(C7), 15781–15796. <https://doi.org/10.1029/97jc00467>
- Engdahl, E. R., Peterson, J., & Orsini, N. A. (1982). Global digital networks – Current status and future directions. *Bulletin of the Seismological Society of America*, 72(6B), S243–S259. <https://doi.org/10.1785/bssa07206b0243>
- Faul, U., & Jackson, I. (2015). Transient creep and strain energy dissipation: An experimental perspective. *Annual Review of Earth and Planetary Sciences*, 43(1), 541–569. <https://doi.org/10.1146/annurev-earth-060313-054732>
- Fels, J.-F., & Berger, J. (1994). Parametric analysis and calibration of the STS-1 seismometer of the IRIS/IDA Seismographic Network. *Bulletin of the Seismological Society of America*, 84(5), 1580–1592. <https://doi.org/10.1785/bssa0840051580>
- Ferreira, A. M. G., & Igel, H. (2009). Rotational motions of seismic surface waves in a laterally heterogeneous Earth. *Bulletin of the Seismological Society of America*, 99(2B), 1429–1436. <https://doi.org/10.1785/0120080149>
- Ferreira, A. M. G., & Woodhouse, J. H. (2007). Observations of long period Rayleigh wave ellipticity. *Geophysical Journal International*, 169(1), 161–169. <https://doi.org/10.1111/j.1365-246X.2006.03276.x>
- Fichtner, A., Bunge, H.-P., & Igel, H. (2006a). The adjoint method in seismology: I. Theory. *Physics of the Earth and Planetary Interiors*, 157(1), 86–104. <https://doi.org/10.1016/j.pepi.2006.03.016>
- Fichtner, A., Bunge, H.-P., & Igel, H. (2006b). The adjoint method in seismology: II. Applications: Traveltimes and sensitivity functionals. *Physics of the Earth and Planetary Interiors*, 157(1), 105–123. <https://doi.org/10.1016/j.pepi.2006.03.018>
- Fichtner, A., Kennett, B. L., Igel, H., & Bunge, H.-P. (2009). Full seismic waveform tomography for upper-mantle structure in the Australasian region using adjoint methods. *Geophysical Journal International*, 179(3), 1703–1725. <https://doi.org/10.1111/j.1365-246X.2009.04368.x>
- Fichtner, A., van Herwaarden, D. P., Afanasiev, M., Simute, S., Krischer, L., Cubuk-Sabuncu, Y., et al. (2018). The collaborative seismic Earth model: Generation 1. *Geophysical Research Letters*, 45(9), 4007–4016. <https://doi.org/10.1029/2018GL077338>
- Forbriger, T. (2007). Reducing magnetic field induced noise in broad-band seismic recordings. *Geophysical Journal International*, 169(1), 240–258. <https://doi.org/10.1111/j.1365-246X.2006.03295.x>

- Forbriger, T., Zürn, W., & Widmer-Schmidrig, R. (2021). Challenges and perspectives for lowering the vertical-component long-period detection level. *Seismological Research Letters*, 92(4), 2498–2512. <https://doi.org/10.1785/0220200399>
- Forget, G., Campin, J.-M., Heimbach, P., Hill, C. N., Ponte, R. M., & Wunsch, C. (2015). ECCO version 4: An integrated framework for non-linear inverse modeling and global ocean state estimation. *Geoscientific Model Development*, 8(10), 3071–3104. <https://doi.org/10.5194/gmd-8-3071-2015>
- Freed, A. M. (2005). Earthquake triggering by static, dynamic, and postseismic stress transfer. *Annual Review of Earth and Planetary Sciences*, 33(1), 335–367. <https://doi.org/10.1146/annurev.earth.33.092203.122505>
- French, S. W., & Romanowicz, B. A. (2015). Broad plumes rooted at the base of the Earth's mantle beneath major hotspots. *Nature*, 525(7567), 95–99. <https://doi.org/10.1038/nature14876>
- Freybourger, M., Hinderer, J., & Trampert, J. (1997). Comparative study of superconducting gravimeters and broadband seismometers STS-1/Z in seismic and subseismic frequency bands. *Physics of the Earth and Planetary Interiors*, 101(3), 203–217. [https://doi.org/10.1016/S0031-9201\(97\)00003-4](https://doi.org/10.1016/S0031-9201(97)00003-4)
- Friedrich, A., Krüger, F., & Klinge, K. (1998). Ocean-generated microseismic noise located with the Gräfenberg array. *Journal of Seismology*, 2(1), 47–64. <https://doi.org/10.1023/A:1009788904007>
- Frost, D. A., Lasbleis, M., Chandler, B., & Romanowicz, B. A. (2021). Dynamic history of the inner core constrained by seismic anisotropy. *Nature Geoscience*, 14(7), 531–535. <https://doi.org/10.1038/s41561-021-00761-w>
- Fuchs, F., Schneider, F. M., Kolinsky, P., Serafin, S., & Bokelmann, G. (2019). Rich observations of local and regional infrasound phases made by the AlpArray seismic network after refinery explosion. *Scientific Reports*, 9(1), 13027. <https://doi.org/10.1038/s41598-019-49494-2>
- Fukao, Y. (1972). Source process of a large deep-focus earthquake and its tectonic implications—The western Brazil earthquake of 1963. *Physics of the Earth and Planetary Interiors*, 5, 61–76. [https://doi.org/10.1016/0031-9201\(72\)90074-x](https://doi.org/10.1016/0031-9201(72)90074-x)
- Funning, G. J., & Garcia, A. (2018). A systematic study of earthquake detectability using Sentinel-1 interferometric wide-swath data. *Geophysical Journal International*, 216(1), 332–349. <https://doi.org/10.1093/gji/ggy426>
- Gaebler, P. J., & Ceranna, L. (2021). Performance of the International Monitoring System seismic network based on ambient seismic noise measurements. *Pure and Applied Geophysics*, 178(7), 2419–2436. <https://doi.org/10.1007/s00024-020-02604-y>
- Gao, Y., Tilmann, F., Herwaarden, D., Thrastarson, S., Fichtner, A., Heit, B., et al. (2021). Full waveform inversion beneath the Central Andes: Insight into the dehydration of the Nazca slab and delamination of the back-arc lithosphere. *Journal of Geophysical Research: Solid Earth*, 126(7), e2021JB021984. <https://doi.org/10.1029/2021jb021984>
- Garnero, E. J., McNamara, A. K., & Shim, S.-H. (2016). Continent-sized anomalous zones with low seismic velocity at the base of Earth's mantle. *Nature Geoscience*, 9(7), 481–489. <https://doi.org/10.1038/ngeo2733>
- Ge, L., Han, S., Rizos, C., Ishikawa, Y., Hoshiba, M., Yoshida, Y., et al. (2000). GPS seismometers with up to 20 Hz sampling rate. *Earth Planets and Space*, 52(10), 881–884. <https://doi.org/10.1186/bf03352300>
- Geer, L.-E. D. (2012). Radionuclide evidence for low-yield nuclear testing in North Korea in April/May 2010. *Science and Global Security*, 20(1), 1–29. <https://doi.org/10.1080/08929882.2012.652558>
- Geiger, L. (1910). Herdbestimmung bei erdbeben aus den ankunftszeiten. Nachrichten von der Gesellschaft der Wissenschaften zu Göttingen. *Mathematisch-Physikalische Klasse*, 1910, 331–349.
- Geiger, L. (1912). Probability method for the determination of earthquake epicenters from the arrival time only. *Bulletin of St. Louis University*, 8, 56–71. (Translated from Geiger's 1910 German article).
- GEOFON Data Centre. (1993). *GEOFON Seismic Network*. Deutsches GeoForschungsZentrum GFZ. <https://doi.org/10.14470/TR560404>
- Gerstoft, P., Fehler, M. C., & Sabra, K. G. (2006). When Katrina hit California. *Geophysical Research Letters*, 33(17), L17308. <https://doi.org/10.1029/2006gl027270>
- Gerstoft, P., Shearer, P. M., Harmon, N., & Zhang, J. (2008). Global P, PP, and PKP wave microseisms observed from distant storms. *Geophysical Research Letters*, 35(23), L23306. <https://doi.org/10.1029/2008gl036111>
- Gerstoft, P., & Tanimoto, T. (2007). A year of microseisms in southern California. *Geophysical Research Letters*, 34(20), L20304. <https://doi.org/10.1029/2007gl031091>
- Giardini, D., Li, X.-D., & Woodhouse, J. H. (1987). Three-dimensional structure of the Earth from splitting in free-oscillation spectra. *Nature*, 325(6103), 404–411. <https://doi.org/10.1038/325405a0>
- Giardini, D., Li, X.-D., & Woodhouse, J. H. (1988). Splitting functions of long-period normal modes of the Earth. *Journal of Geophysical Research*, 93(B11), 13716–13742. <https://doi.org/10.1029/JB093iB11p13716>
- Giardini, D., Lognonné, P., Banerdt, W. B., Pike, W. T., Christensen, U., Ceylan, S., et al. (2020). The seismicity of Mars. *Nature Geoscience*, 13(3), 205–212. <https://doi.org/10.1038/s41561-020-0539-8>
- Gilbert, F. (1971). Excitation of the normal modes of the Earth by earthquake sources. *Geophysical Journal of the Royal Astronomical Society*, 22(2), 223–226. <https://doi.org/10.1111/j.1365-246X.1971.tb03593.x>
- Glatzmaier, G. A., & Roberts, P. H. (1995). A three-dimensional convective dynamo solution with rotating and finitely conducting inner core and mantle. *Physics of the Earth and Planetary Interiors*, 91(1), 63–75. [https://doi.org/10.1016/0031-9201\(95\)03049-3](https://doi.org/10.1016/0031-9201(95)03049-3)
- Godano, C., & Pingue, F. (2000). Is the seismic moment–frequency relation universal? *Geophysical Journal International*, 142(1), 193–198. <https://doi.org/10.1046/j.1365-246x.2000.00149.x>
- Godey, S., Bossu, R., & Guilbert, J. (2013). Improving the Mediterranean seismicity picture thanks to international collaborations. *Physics and Chemistry of the Earth, Parts A/B/C*, 63, 3–11. (Seismicity of the Mediterranean region and mitigation of earthquake losses). <https://doi.org/10.1016/j.pce.2013.04.012>
- Goldfinger, C., Ikeda, Y., Yeats, R. S., & Ren, J. (2013). Superquakes and supercycles. *Seismological Research Letters*, 84(1), 24–32. <https://doi.org/10.1785/0220110135>
- Grandin, R., Vallée, M., Satriano, C., Lacassin, R., Klinger, Y., Simoes, M., & Bollinger, L. (2015). Rupture process of the $M_w = 7.9$ 2015 Gorkha earthquake (Nepal): Insights into Himalayan megathrust segmentation. *Geophysical Research Letters*, 42(20), 8373–8382. <https://doi.org/10.1002/2015gl066044>
- Greco, B., Borleanu, F., Tiganescu, A., Poiata, N., Dinescu, R., & Tataru, D. (2021). The effect of 2020 COVID-19 lockdown measures on seismic noise recorded in Romania. *Solid Earth*, 12(10), 2351–2368. <https://doi.org/10.5194/se-12-2351-2021>
- Green, D. N., Bastow, I. D., Dashwood, B., & Nippress, S. E. (2017). Characterizing broadband seismic noise in Central London. *Seismological Research Letters*, 88(1), 113–124. <https://doi.org/10.1785/0220160128>
- Green, P., Frosch, R., & Romney, C. (1965). Principles of an experimental large aperture seismic array (LASA). *Proceedings of the IEEE*, 53(12), 1821–1833. <https://doi.org/10.1109/PROC.1965.4453>
- Grevemeyer, I., Herber, R., & Essen, H. H. (2000). Microseismological evidence for a changing wave climate in the northeast Atlantic Ocean. *Nature*, 408(6810), 349–352. <https://doi.org/10.1038/35042558>

- Groos, J., & Ritter, J. (2009). Time domain classification and quantification of seismic noise in an urban environment. *Geophysical Journal International*, 179(2), 1213–1231. <https://doi.org/10.1111/j.1365-246X.2009.04343.x>
- Gualtieri, L., Bachmann, E., Simons, F. J., & Tromp, J. (2020). The origin of secondary microseism Love waves. *Proceedings of the National Academy of Sciences of the United States of America*, 117(47), 29504–29511. <https://doi.org/10.1073/pnas.2013806117>
- Gualtieri, L., Bachmann, E., Simons, F. J., & Tromp, J. (2021). Generation of secondary microseism Love waves: Effects of bathymetry, 3-D structure and source seasonality. *Geophysical Journal International*, 226(1), 192–219. <https://doi.org/10.1093/gji/ggab095>
- Guerin, G., Mordret, A., Rivet, D., Lipovsky, B. P., & Minchew, B. M. (2021). Frictional origin of slip events of the Whillans Ice Stream, Antarctica. *Geophysical Research Letters*, 48(11), e2021GL092950. <https://doi.org/10.1029/2021GL092950>
- Gutenberg, B., & Richter, C. F. (1944). Frequency of earthquakes in California. *Bulletin of the Seismological Society of America*, 34(4), 185–188. <https://doi.org/10.1785/BSSA0340040185>
- Häfner, R., & Widmer-Schmidrig, R. (2012). Signature of 3-D density structure in spectra of the spheroidal free oscillation ${}_0S_2$. *Geophysical Journal International*, 192(1), 285–294. <https://doi.org/10.1093/gji/ggs013>
- Haned, A., Stutzmann, E., Schimmel, M., Kiselev, S., Davaille, A., & Yelles-Chaouche, A. (2016). Global tomography using seismic hum. *Geophysical Journal International*, 204(2), 1222–1236. <https://doi.org/10.1093/gji/ggv516>
- Haney, M. M. (2009). Infrasonic ambient noise interferometry from correlations of microbaroms. *Geophysical Research Letters*, 36(19), L19808. <https://doi.org/10.1029/2009GL040179>
- Hanka, W., & Kind, R. (1994). The GEOFON program. *Annals of Geophysics*, 37(5). <https://doi.org/10.4401/ag-4196>
- Hanka, W., & Saul, J. (2008). GEOFON and its role in earthquake monitoring and tsunami warning. In E. S. Husebye (Ed.), *Earthquake monitoring and seismic hazard mitigation in Balkan countries* (pp. 151–162). Springer Netherlands.
- Harms, J., Ampuero, J.-P., Barsuglia, M., Chassande-Mottin, E., Montagner, J.-P., Somala, S., & Whiting, B. (2015). Transient gravity perturbations induced by earthquake rupture. *Geophysical Journal International*, 201(3), 1416–1425. <https://doi.org/10.1093/gji/ggv090>
- Hartzell, S. H., & Heaton, T. H. (1983). Inversion of strong ground motion and teleseismic waveform data for the fault rupture history of the 1979 Imperial Valley, California, earthquake. *Bulletin of the Seismological Society of America*, 73(6A), 1553–1583. <https://doi.org/10.1785/bssa07306a1553>
- Hasselmann, K. (1963). A statistical analysis of the generation of microseisms. *Reviews of Geophysics*, 1(2), 177–210. <https://doi.org/10.1029/RG001i002p00177>
- Haviland, H. F., Weber, R. C., Neal, C. R., Lognonné, P., Garcia, R. F., Schmerr, N., et al. (2022). The lunar geophysical network landing sites science rationale. *The Planetary Science Journal*, 3(2), 40. <https://doi.org/10.3847/psj/ac0f82>
- Hayes, G. P. (2017). The finite, kinematic rupture properties of great-sized earthquakes since 1990. *Earth and Planetary Science Letters*, 468, 94–100. <https://doi.org/10.1016/j.epsl.2017.04.003>
- Hayes, G. P., Earle, P. S., Benz, H. M., Wald, D. J., & Yeck, W. L. (2019). National Earthquake Information Center strategic plan, 2019–23 (Tech. Rep.). <https://doi.org/10.3133/cir1457>
- Hayes, G. P., Moore, G. L., Portner, D. E., Hearne, M., Flamme, H., Furtney, M., & Smoczyk, G. M. (2018). Slab2, a comprehensive subduction zone geometry model. *Science*, 362(6410), 58–61. <https://doi.org/10.1126/science.aat4723>
- Heaton, T. H. (2017). Correspondence: Response of a gravimeter to an instantaneous step in gravity. *Nature Communications*, 8(1), 1–3. <https://doi.org/10.1038/s41467-017-01348-z>
- Hedlin, M. A. H., Walker, K., Drob, D. P., & de Groot-Hedlin, C. D. (2012). Infrasond: Connecting the solid Earth, oceans, and atmosphere. *Annual Review of Earth and Planetary Sciences*, 40(1), 327–354. <https://doi.org/10.1146/annurev-earth-042711-105508>
- Heidarzadeh, M., Murotani, S., Satake, K., Ishibe, T., & Gusman, A. R. (2016). Source model of the 16 September 2015 Illapel, Chile, M_w 8.4 earthquake based on teleseismic and tsunami data. *Geophysical Research Letters*, 43(2), 643–650. <https://doi.org/10.1002/2015gl067297>
- Hetényi, G., Molinari, I., Clinton, J., Bokelmann, G., Bondár, I., Crawford, W. C., et al. (2018). The AlpArray seismic network: A large-scale European experiment to image the Alpine orogen. *Surveys in Geophysics*, 39(5), 1009–1033. <https://doi.org/10.1007/s10712-018-9472-4>
- Hill, D. P., Reasenber, P. A., Michael, A., Arabaz, W. J., Beroza, G., Brumbaugh, D., et al. (1993). Seismicity remotely triggered by the magnitude 7.3 Landers, California, earthquake. *Science*, 260(5114), 1617–1623. <https://doi.org/10.1126/science.260.5114.1617>
- Hill, E. A., Carr, J. R., & Stokes, C. R. (2017). A review of recent changes in major marine-terminating outlet glaciers in Northern Greenland. *Frontiers of Earth Science*, 4, 111. <https://doi.org/10.3389/feart.2016.00111>
- Hirose, K., Labrosse, S., & Hernlund, J. (2013). Composition and state of the core. *Annual Review of Earth and Planetary Sciences*, 41(1), 657–691. <https://doi.org/10.1146/annurev-earth-050212-124007>
- Hodgkinson, K., Langbein, J., Henderson, B., Mencin, D., & Borsa, A. (2013). Tidal calibration of plate boundary observatory borehole strainmeters. *Journal of Geophysical Research: Solid Earth*, 118(1), 447–458. <https://doi.org/10.1029/2012jb009651>
- Holcomb, L. (1998). Spectral structure in the Earth's microseismic background between 20 and 40 seconds. *Bulletin of the Seismological Society of America*, 88(3), 744–757. <https://doi.org/10.1785/bssa0880030744>
- Hosseini, K., Matthews, K. J., Sigloch, K., Shephard, G. E., Domeier, M., & Tsekhmistrenko, M. (2018). Submachine: Web-based tools for exploring seismic tomography and other models of Earth's deep interior. *Geochemistry, Geophysics, Geosystems*, 19(5), 1464–1483. <https://doi.org/10.1029/2018GC007431>
- Houser, C., Masters, G., Shearer, P., & Laske, G. (2008). Shear and compressional velocity models of the mantle from cluster analysis of long-period waveforms. *Geophysical Journal International*, 174(1), 195–212. <https://doi.org/10.1111/j.1365-246X.2008.03763.x>
- Houston, H. (2001). Influence of depth, focal mechanism, and tectonic setting on the shape and duration of earthquake source time functions. *Journal of Geophysical Research*, 106(B6), 11137–11150. <https://doi.org/10.1029/2000jb900468>
- Howe, B. M., Arbic, B. K., Aucan, J., Barnes, C. R., Bayliff, N., Becker, N., et al. (2019). SMART cables for observing the global ocean: Science and implementation. *Frontiers in Marine Science*, 6, 424. <https://doi.org/10.3389/fmars.2019.00424>
- Hu, X., Liu, L., Kroner, C., & Sun, H. (2009). Observation of the seismic anisotropy effects on free oscillations below 4 mHz. *Journal of Geophysical Research*, 114(B7), B07301. <https://doi.org/10.1029/2008JB005713>
- Huang, H.-H., Lin, F.-C., Tsai, V. C., & Koper, K. D. (2015). High-resolution probing of inner core structure with seismic interferometry. *Geophysical Research Letters*, 42(24), 10–622. <https://doi.org/10.1002/2015GL066390>
- Huang, Q., Schmerr, N., Maguire, R., Antonangeli, D., Fernando, B., Leng, K., et al. (2020). Detecting the mantle transition zone of mars from seismic triplicated and reflected waves. In *Agu Fall Meeting* (Vol. 2020, pp. D1024-0011).
- Hunter, J. D. (2007). Matplotlib: A 2D graphics environment. *Computing in Science & Engineering*, 9(3), 90–95. <https://doi.org/10.1109/MCSE.2007.55>
- Hupe, P., Ceranna, L., & Le Pichon, A. (2019). How can the International Monitoring System infrasond network contribute to gravity wave measurements? *Atmosphere*, 10(7), 399. <https://doi.org/10.3390/atmos10070399>

- Hutko, A. R., Bahavar, M., Trabant, C., Weekly, R. T., Fossen, M. V., & Ahern, T. (2017). Data products at the IRIS-DMC: Growth and usage. *Seismological Research Letters*, 88(3), 892–903. <https://doi.org/10.1785/0220160190>
- Hutt, C. R., & Ringler, A. T. (2011). Some possible causes of and corrections for STS-1 response changes in the Global Seismographic Network. *Seismological Research Letters*, 82(4), 560–571. <https://doi.org/10.1785/gssrl.82.4.560>
- Hutt, C. R., Ringler, A. T., & Gee, L. S. (2017). Broadband seismic noise attenuation versus depth at the Albuquerque Seismological Laboratory. *Bulletin of the Seismological Society of America*, 107(3), 1402–1412. <https://doi.org/10.1785/0120160187>
- Ide, S., Beroza, G. C., & Mcguire, J. J. (2005). *Imaging earthquake source complexity* (pp. 117–135). American Geophysical Union (AGU).
- Igel, H. (2016). *Computational seismology: A practical introduction*. Oxford University Press.
- Igel, H., Cochard, A., Wassermann, J., Flaws, A., Schreiber, U., Velikoseltsev, A., & Pham Dinh, N. (2007). Broad-band observations of earthquake-induced rotational ground motions. *Geophysical Journal International*, 168(1), 182–196. <https://doi.org/10.1111/j.1365-246X.2006.03146.x>
- Igel, H., Schreiber, K. U., Gebauer, A., Bernauer, F., Egdorf, S., Simonelli, A., et al. (2021). ROMY: A multicomponent ring laser for geodesy and geophysics. *Geophysical Journal International*, 225(1), 684–698. <https://doi.org/10.1093/gji/ggaa614>
- Igel, H., Schreiber, U., Flaws, A., Schuberth, G., Velikoseltsev, A., & Cochard, A. (2005). Rotational motions induced by the M8.1 Tokachi-oki earthquake, September 25, 2003. *Geophysical Research Letters*, 32(8), L08309. <https://doi.org/10.1029/2004gl022336>
- InSight Marsquake Service. (2021). *Mars seismic catalogue, insight mission; v7 2021-07-01*. ETHZ, IPGP, JPL, ICL, University of Bristol. <https://doi.org/10.12686/a12>
- Institut De Physique Du Globe De Paris (IPGP)Ecole Et Observatoire Des Sciences De La Terre De Strasbourg (EOST). (1982). *GEOSCOPE, French Global Network of broad band seismic stations*. Institut De Physique Du Globe De Paris (IPGP), Université de Paris. <https://doi.org/10.18715/GEOSCOPE.G>
- International Seismological Centre. (2021). On-line bulletin. Retrieved from <http://www.isc.ac.uk/iscbulletin/>
- IRIS. (1984). *The IRIS proposal* (p. 83). IRIS.
- Irving, J. C. E. (2016). Imaging the inner core under Africa and Europe. *Physics of the Earth and Planetary Interiors*, 254, 12–24. <https://doi.org/10.1016/j.pepi.2016.03.001>
- Irving, J. C. E., Cottaar, S., & Lekić, V. (2018). Seismically determined elastic parameters for Earth's outer core. *Science Advances*, 4(6), eaar2538. <https://doi.org/10.1126/sciadv.aar2538>
- Ishii, M., Shearer, P. M., Houston, H., & Vidale, J. E. (2005). Extent, duration and speed of the 2004 Sumatra-Andaman earthquake imaged by the Hi-Net array. *Nature*, 435(7044), 933–936. <https://doi.org/10.1038/nature03675>
- Ishii, M., & Tromp, J. (1999). Normal-mode and free-air gravity constraints on lateral variations in velocity and density of Earth's mantle. *Science*, 285(5431), 1231–1236. <https://doi.org/10.1126/science.285.5431.1231>
- Ishii, M., Tromp, J., Dziewoński, A. M., & Ekström, G. (2002). Joint inversion of normal mode and body wave data for inner core anisotropy I. Laterally homogeneous anisotropy. *Journal of Geophysical Research*, 107(B12), ESE20–16. <https://doi.org/10.1029/2001JB000712>
- Isse, T., & Nakanishi, I. (2002). Inner-core anisotropy beneath Australia and differential rotation. *Geophysical Journal International*, 151(1), 255–263. <https://doi.org/10.1046/j.1365-246X.2002.01780.x>
- Ivins, E. R., Caron, L., Adhikari, S., Larour, E., & Scheinert, M. (2020). A linear viscoelasticity for decadal to centennial time scale mantle deformation. *Reports on Progress in Physics*, 83(10), 106801. <https://doi.org/10.1088/1361-6633/aba346>
- Jagt, L., & Deuss, A. (2021). Comparing one-step full-spectrum inversion with two-step splitting function inversion in normal mode tomography. *Geophysical Journal International*, 227(1), 559–575. <https://doi.org/10.1093/gji/ggab240>
- James, S. R., Knox, H. A., Abbott, R. E., Panning, M. P., & Screamor, E. J. (2019). Insights into permafrost and seasonal active-layer dynamics from ambient seismic noise monitoring. *Journal of Geophysical Research: Earth Surface*, 124(7), 1798–1816. <https://doi.org/10.1029/2019jfe005051>
- James, T. D., Murray, T., Selmes, N., Scharrer, K., & O'Leary, M. (2014). Buoyant flexure and basal crevassing in dynamic mass loss at Helheim Glacier. *Nature Geoscience*, 7(8), 593–596. <https://doi.org/10.1038/ngeo2204>
- Jeffreys, H. (1931a). On the cause of oscillatory movement in seismograms. *Geophysical Supplements to the Monthly Notices of the Royal Astronomical Society*, 2(8), 407–416. <https://doi.org/10.1111/j.1365-246X.1931.tb04462.x>
- Jeffreys, H. (1931b). The revision of seismological tables. *Geophysical Supplements to the Monthly Notices of the Royal Astronomical Society*, 2(7), 329–348. <https://doi.org/10.1111/j.1365-246X.1931.tb05419.x>
- Jenkins, A. P., Biggs, J., Rust, A. C., & Rougier, J. C. (2021). Decadal timescale correlations between global earthquake activity and volcanic eruption rates. *Geophysical Research Letters*, 48(16), e2021GL093550. <https://doi.org/10.1029/2021gl093550>
- Ji, C., Wald, D. J., & Helmberger, D. V. (2002). Source description of the 1999 Hector Mine, California, Earthquake, Part I: Wavelet domain inversion theory and resolution analysis. *Bulletin of the Seismological Society of America*, 92(4), 1192–1207. <https://doi.org/10.1785/0120000916>
- Jiang, C., Wu, Z., Li, Y., & Ma, T. (2014). Repeating events as estimator of location precision: The China national seismograph network. *Pure and Applied Geophysics*, 171(3), 413–423. <https://doi.org/10.1007/s00024-012-0508-2>
- Johnson, C., Fu, Y., & Burgmann, R. (2017). Seasonal water storage, stress modulation, and California seismicity. *Science*, 356(6343), 1161–1164. <https://doi.org/10.1126/science.aak9547>
- Jon, F. C. (1968). Synthesis of a layered medium from its acoustic transmission response. *Geophysics*, 33(2), 264–269. <https://doi.org/10.1190/1.1439927>
- Joughin, I., & Alley, R. B. (2011). Stability of the West Antarctic ice sheet in a warming world. *Nature Geoscience*, 4(8), 506–513. <https://doi.org/10.1038/ngeo1194>
- Joughin, I., Bindschadler, R. A., King, M. A., Voigt, D., Alley, R. B., Anandakrishnan, S., et al. (2005). Continued deceleration of Whillans Ice Stream, West Antarctica. *Geophysical Research Letters*, 32(22), L22501. <https://doi.org/10.1029/2005gl024319>
- Juhel, K., Ampuero, J.-P., Barsuglia, M., Bernard, P., Chassande-Mottin, E., Fiorucci, D., et al. (2018). Earthquake early warning using future generation gravity strainmeters. *Journal of Geophysical Research: Solid Earth*, 123(12), 10–889. <https://doi.org/10.1029/2018JB016698>
- Juhel, K., Montagner, J., Vallée, M., Ampuero, J.-P., Barsuglia, M., Bernard, P., et al. (2019). Normal mode simulation of prompt elastogravity signals induced by an earthquake rupture. *Geophysical Journal International*, 216(2), 935–947. <https://doi.org/10.1093/gji/ggy436>
- Julian, B. R., Davies, D., & Sheppard, R. M. (1972). Pkjkp. *Nature*, 235(5337), 317–318. <https://doi.org/10.1038/235317a0>
- Kanamori, H. (1972). Mechanism of tsunami earthquakes. *Physics of the Earth and Planetary Interiors*, 6(5), 346–359. [https://doi.org/10.1016/0031-9201\(72\)90058-1](https://doi.org/10.1016/0031-9201(72)90058-1)
- Kanamori, H. (2014). The diversity of large earthquakes and its implications for hazard mitigation. *Annual Review of Earth and Planetary Sciences*, 42(1), 7–26. <https://doi.org/10.1146/annurev-earth-060313-055034>
- Kanamori, H., & Rivera, L. (2008). Source inversion of W phase: Speeding up seismic tsunami warning. *Geophysical Journal International*, 175(1), 222–238. <https://doi.org/10.1111/j.1365-246x.2008.03887.x>

- Karaoğlu, H., & Romanowicz, B. A. (2018a). Global seismic attenuation imaging using full-waveform inversion: A comparative assessment of different choices of misfit functionals. *Geophysical Journal International*, 212(2), 807–826. <https://doi.org/10.1093/gji/ggx442>
- Karaoğlu, H., & Romanowicz, B. A. (2018b). Inferring global upper-mantle shear attenuation structure by waveform tomography using the spectral element method. *Geophysical Journal International*, 213(3), 1536–1558. <https://doi.org/10.1093/gji/ggy030>
- Kavanaugh, J., Schultz, R., Andriashek, L. D., van der Baan, M., Ghofrani, H., Atkinson, G., & Utting, D. J. (2019). A New Year's Day icebreaker: Icequakes on lakes in Alberta, Canada. *Canadian Journal of Earth Sciences*, 56(2), 183–200. <https://doi.org/10.1139/cjes-2018-0196>
- Kebeasy, R. (2008). The CTBTO International Monitoring System and global seismicity. In E. S. Husebye (Ed.), *Earthquake monitoring and seismic hazard mitigation in Balkan countries* (pp. 113–120). Springer Netherlands.
- Kedar, S., Longuet-Higgins, M., Webb, F., Graham, N., Clayton, R., & Jones, C. (2008). The origin of deep ocean microseisms in the North Atlantic Ocean. *Proceedings of the Royal Society A: Mathematical, Physical & Engineering Sciences*, 464(2091), 777–793. <https://doi.org/10.1098/Rspa.2007.0277>
- Kennett, B. L. N., Engdahl, E. R., & Buland, R. (1995). Constraints on seismic velocities in the Earth from traveltimes. *Geophysical Journal International*, 122(1), 108–124. <https://doi.org/10.1111/j.1365-246X.1995.tb03540.x>
- Khalturin, V. I., Rautian, T. G., & Richards, P. G. (1998). The seismic signal strength of chemical explosions. *Bulletin of the Seismological Society of America*, 88, 1511–1524. <https://doi.org/10.1785/BSSA0880061511>
- Khan, A., Ceylan, S., van Driel, M., Giardini, D., Lognonné, P., Samuel, H., et al. (2021). Upper mantle structure of Mars from insight seismic data. *Science*, 373(6553), 434–438. <https://doi.org/10.1126/science.abf2966>
- Kido, M., Osada, Y., Fujimoto, H., Hino, R., & Ito, Y. (2011). Trench-normal variation in observed seafloor displacements associated with the 2011 Tohoku-Oki earthquake. *Geophysical Research Letters*, 38(24), L24303. <https://doi.org/10.1029/2011gl050057>
- Kim, D., Davis, P., Lekić, V., Maguire, R., Compaire, N., Schimmel, M., et al. (2021). Potential pitfalls in the analysis and structural interpretation of seismic data from the Mars insight mission. *Bulletin of the Seismological Society of America*, 111(6), 2982–3002. <https://doi.org/10.1785/0120210123>
- Kim, D., & Lekić, V. (2019). Groundwater variations from autocorrelation and receiver functions. *Geophysical Research Letters*, 46(23), 13722–13729. <https://doi.org/10.1029/2019GL084719>
- Kim, D., Lekić, V., Irving, J. C., Schmerr, N., Knapmeyer-Endrun, B., Joshi, R., et al. (2021). Improving constraints on planetary interiors with pps receiver functions. *Journal of Geophysical Research: Planets*, 126(11), e2021JE006983. <https://doi.org/10.1029/2021JE006983>
- Kim, W.-Y., Aharonian, V., Lerner-Lam, A. L., & Richards, P. G. (1997). Discrimination of earthquakes and explosions in southern Russia using regional high-frequency three-component data from the IRIS/JSP Caucasus network. *Bulletin of the Seismological Society of America*, 87(3), 569–588. <https://doi.org/10.1785/BSSA0870030569>
- Kim, W.-Y., Richards, P. G., Schaff, D., Jo, E., & Ryoo, Y. (2018). Identification of seismic events on and near the North Korean Test Site after the underground nuclear test explosion of 3 September 2017. *Seismological Research Letters*, 89, 2120–2130. <https://doi.org/10.1785/0220180133>
- Kim, W.-Y., Richards, P. G., Schaff, D. P., & Koch, K. (2017). Evaluation of a seismic event, 12 May 2010 in North Korea. *Seismological Research Letters*, 107, 1–21. <https://doi.org/10.1785/0120160111>
- King, G., Zürn, W., Evans, R., & Emter, D. (1976). Site correction for long period seismometers, tiltmeters and strainmeters. *Geophysical Journal International*, 44(2), 405–411. <https://doi.org/10.1111/j.1365-246X.1976.tb03664.x>
- Knapmeyer-Endrun, B., Panning, M. P., Bissig, F., Joshi, R., Khan, A., Kim, D., et al. (2021). Thickness and structure of the Martian crust from insight seismic data. *Science*, 373(6553), 438–443. <https://doi.org/10.1126/science.abf8966>
- Knopoff, L. (1999). *Beno Gutenberg 1889–1960*. National Academy of Sciences, Biographical Memoir.
- Koelmeijer, P., Deuss, A., & Ritsema, J. (2013). Observations of core-mantle boundary Stoneley modes. *Geophysical Research Letters*, 40(11), 2557–2561. <https://doi.org/10.1002/grl.50514>
- Koelmeijer, P., Deuss, A., & Ritsema, J. (2017). Density structure of Earth's lowermost mantle from Stoneley mode splitting observations. *Nature Communications*, 8(1), 15241. <https://doi.org/10.1038/ncomms15241>
- Koelmeijer, P., Deuss, A., & Trampert, J. (2012). Normal mode sensitivity to Earth's D' layer and topography on the core-mantle boundary: What we can and cannot see. *Geophysical Journal International*, 190(1), 553–568. <https://doi.org/10.1111/j.1365-246X.2012.05499.x>
- Koelmeijer, P., Ritsema, J., Deuss, A., & van Heijst, H. J. (2016). SP12RTS: A degree-12 model of shear- and compressional-wave velocity for Earth's mantle. *Geophysical Journal International*, 204(2), 1024–1039. <https://doi.org/10.1093/gji/ggv481>
- Kohl, M. L., & Levine, J. (1995). Measurement and interpretation of tidal tilts in a small array. *Journal of Geophysical Research*, 100(B3), 3929–3941. <https://doi.org/10.1029/94JB02773>
- Kohler, M. D., Hafner, K., Park, J., Irving, J. C. E., Caplan-Auerbach, J., Collins, J., et al. (2020). A plan for a long-term, automated, broadband seismic monitoring network on the global seafloor. *Seismological Research Letters*, 91(3), 1343–1355. <https://doi.org/10.1785/0220190123>
- Kolář, P. (2020). The KHC seismic station: The birthplace of broadband seismology. *Seismological Research Letters*, 91(2A), 1057–1063. <https://doi.org/10.1785/0220190326>
- Komatitsch, D., Ritsema, J., & Tromp, J. (2002). The spectral-element method, Beowulf computing, and global seismology. *Science*, 298(5599), 1737–1742. <https://doi.org/10.1126/science.1076024>
- Komatitsch, D., & Tromp, J. (1999). Introduction to the spectral element method for three-dimensional seismic wave propagation. *Geophysical Journal International*, 139(3), 806–822. <https://doi.org/10.1046/j.1365-246x.1999.00967.x>
- Komatitsch, D., & Tromp, J. (2002a). Spectral-element simulations of global seismic wave propagation—I. Validation. *Geophysical Journal International*, 149(2), 390–412. <https://doi.org/10.1046/j.1365-246X.2002.01653.x>
- Komatitsch, D., & Tromp, J. (2002b). Spectral-element simulations of global seismic wave propagation—II. Three-dimensional models, oceans, rotation and self-gravitation. *Geophysical Journal International*, 150(1), 308–318. <https://doi.org/10.1046/j.1365-246X.2002.01716.x>
- Kong, Q., Trugman, D. T., Ross, Z. E., Bianco, M. J., Meade, B. J., & Gerstoft, P. (2019). Machine learning in seismology: Turning data into insights. *Seismological Research Letters*, 90(1), 3–14. <https://doi.org/10.1785/0220180259>
- Koper, K. D., & Ammon, C. J. (2013). Planning a global array of broadband seismic arrays. *Eos, Transactions American Geophysical Union*, 94(34), 300. <https://doi.org/10.1002/2013EO3400005>
- Koper, K. D., Wallace, T. C., & Aster, R. C. (2003). Seismic recordings of the Carlsbad, New Mexico, pipeline explosion of 19 August 2000. *Bulletin of the Seismological Society of America*, 93(4), 1427–1432. <https://doi.org/10.1785/0120020192>
- Krischer, L., Fichtner, A., Zukauskaitė, S., & Igel, H. (2015). Large-scale seismic inversion framework. *Seismological Research Letters*, 86(4), 1198–1207. <https://doi.org/10.1785/0220140248>
- Krischer, L., Smith, J., Lei, W., Lefebvre, M., Ruan, Y., de Andrade, E. S., et al. (2016). An adaptable seismic data format. *Geophysical Journal International*, 207(2), 1003–1011. <https://doi.org/10.1093/gji/ggw319>
- Krüger, F., & Ohrnberger, M. (2005). Tracking the rupture of the $M_w = 9.3$ Sumatra earthquake over 1,150 km at teleseismic distance. *Nature*, 435(7044), 937–939. <https://doi.org/10.1038/nature03696>

- Kurrle, D., & Widmer-Schmidrig, R. (2008). The horizontal hum of the Earth: A global background of spheroidal and toroidal modes. *Geophysical Research Letters*, 35(6), L06304. <https://doi.org/10.1029/2007gl033125>
- Kustowski, B., Ekström, G., & Dziewoński, A. (2008). Anisotropic shear-wave velocity structure of the Earth's mantle: A global model. *Journal of Geophysical Research*, 113(B6), B06306. <https://doi.org/10.1029/2007JB005169>
- LaCoste, L. J. B. (1983). LaCoste and Romberg straight-line gravity meter. *Geophysics*, 48(5), 606–610. <https://doi.org/10.1190/1.1441490>
- Lacroix, P., Grasso, J. R., Roulle, J., Giraud, G., Goetz, D., Morin, S., & Helmstetter, A. (2012). Monitoring of snow avalanches using a seismic array: Location, speed estimation, and relationships to meteorological variables. *Journal of Geophysical Research*, 117(F1), F01034. <https://doi.org/10.1029/2011jfo02106>
- Lambotte, S., Rivera, L., & Hinderer, J. (2006). Vertical and horizontal seismometric observations of tides. *Journal of Geodynamics*, 41(1), 39–58. (Earth tides and geodynamics: Probing the Earth at sub-seismic frequencies). <https://doi.org/10.1016/j.jog.2005.08.021>
- Landès, M., Ceranna, L., Le Pichon, A., & Matoza, R. S. (2012). Localization of microbarom sources using the IMS infrasound network. *Journal of Geophysical Research*, 117(D6), D06102. <https://doi.org/10.1029/2011JD016684>
- Lands, M., Hubans, F., Shapiro, N. M., Paul, A., & Campillo, M. (2010). Origin of deep ocean microseisms by using teleseismic body waves. *Journal of Geophysical Research: Solid Earth*, 115(B5), B05302. <https://doi.org/10.1029/2009jb006918>
- Larmat, C., Montagner, J.-P., Fink, M., Capdeville, Y., Tourin, A., & Clévéde, E. (2006). Time-reversal imaging of seismic sources and application to the great Sumatra earthquake. *Geophysical Research Letters*, 33(19), L19312. <https://doi.org/10.1029/2006gl026336>
- Larose, E., Carrière, S., Voisin, C., Bottelin, P., Baillet, L., Gueguen, P., et al. (2015). Environmental seismology: What can we learn on Earth surface processes with ambient noise? *Journal of Applied Geophysics*, 116, 62–74. <https://doi.org/10.1016/j.jappgeo.2015.02.001>
- Larson, K. M. (2009). GPS seismology. *Journal of Geodesy*, 83(3–4), 227–233. <https://doi.org/10.1007/s00190-008-0233-x>
- Larson, K. M., Bodin, P., & Gombert, J. (2003). Using 1-Hz GPS data to measure deformations caused by the Denali fault earthquake. *Science*, 300(5624), 1421–1424. <https://doi.org/10.1126/science.1084531>
- Laske, G. (1995). Global observation of off-great-circle propagation of long-period surface waves. *Geophysical Journal International*, 123(1), 245–259. <https://doi.org/10.1111/j.1365-246X.1995.tb06673.x>
- Laske, G., & Masters, G. (1999). Limits on differential rotation of the inner core from an analysis of the Earth's free oscillations. *Nature*, 402(6757), 66–69. <https://doi.org/10.1038/47011>
- Laske, G., & Masters, G. (2003). The Earth's free oscillations and the differential rotation of the inner core. In *Earth's core: Dynamics, structure, rotation* (pp. 5–21). American Geophysical Union (AGU). <https://doi.org/10.1029/GD031p0005>
- Lau, H. C. P., & Faul, U. H. (2019). Anelasticity from seismic to tidal timescales: Theory and observations. *Earth and Planetary Science Letters*, 508, 18–29. <https://doi.org/10.1016/j.epsl.2018.12.009>
- Lau, H. C. P., & Holtzman, B. K. (2019). “Measures of dissipation in viscoelastic media” extended: Toward continuous characterization across very broad geophysical time scales. *Geophysical Research Letters*, 46(16), 9544–9553. <https://doi.org/10.1029/2019GL083529>
- Lau, H. C. P., Mitrovica, J. X., Davis, J. L., Tromp, J., Yang, H.-Y., & Al-Antar, D. (2017). Tidal tomography constrains Earth's deep-mantle buoyancy. *Nature*, 551(7680), 321–326. <https://doi.org/10.1038/nature24452>
- Lau, H. C. P., & Romanowicz, B. A. (2021). Constraining jumps in density and elastic properties at the 660 km discontinuity using normal mode data via the Backus Gilbert Method. *Geophysical Research Letters*, 48(9), e92217. <https://doi.org/10.1029/2020GL092217>
- Lavallée, D., & Archuleta, R. J. (2005). Coupling of the random properties of the source and the ground motion for the 1999 Chi Chi earthquake. *Geophysical Research Letters*, 32(8), L08311. <https://doi.org/10.1029/2004gl022202>
- Lavallée, D., Liu, P., & Archuleta, R. J. (2006). Stochastic model of heterogeneity in earthquake slip spatial distributions. *Geophysical Journal International*, 165(2), 622–640. <https://doi.org/10.1111/j.1365-246X.2006.02943.x>
- Lay, T. (2015). The surge of great earthquakes from 2004 to 2014. *Earth and Planetary Science Letters*, 409, 133–146. <https://doi.org/10.1016/j.epsl.2014.10.047>
- Lay, T., Ammon, C. J., Kanamori, H., Rivera, L., Koper, K. D., & Hutko, A. R. (2010). The 2009 Samoa–Tonga great earthquake triggered doublet. *Nature*, 466(7309), 964–968. <https://doi.org/10.1038/nature09214>
- Lay, T., Aster, R., Forsyth, D., Romanowicz, B. A., Allen, R., Cormier, V., et al. (2009). Seismological grand challenges in understanding Earth's dynamic systems. *A report to the National Science Foundation, IRIS Consortium* (pp. 76).
- Lay, T., Berger, J., Buland, R., Butler, R., Ekstrom, G., Hutt, B., & Romanowicz, B. (2002). Global seismic network design goals update 2002. In *IRIS Consortium*. Retrieved from http://www.iris.washington.edu/about/GSN/docs/GSN_Design_Goals.pdf
- Lay, T., Kanamori, H., Ammon, C. J., Hutko, A. R., Furlong, K., & Rivera, L. (2009). The 2006–2007 Kuril Islands great earthquake sequence. *Journal of Geophysical Research*, 114(B11), B11308. <https://doi.org/10.1029/2008jb006280>
- Lay, T., Kanamori, H., Ammon, C. J., Koper, K. D., Hutko, A. R., Ye, L., et al. (2012). Depth-varying rupture properties of subduction zone megathrust faults. *Journal of Geophysical Research*, 117(B4), B04311. <https://doi.org/10.1029/2011jb009133>
- Lay, T., Kanamori, H., Ammon, C. J., Nettles, M., Ward, S. N., Aster, R. C., et al. (2005). The great Sumatra–Andaman earthquake of 26 December 2004. *Science*, 308(5725), 1127–1133. <https://doi.org/10.1126/Science.1112250>
- Lecoq, T., Arduin, F., Collin, F., & Camelbeek, T. (2020). On the extraction of microseismic ground motion from analog seismograms for the validation of ocean-climate models. *Seismological Research Letters*, 91(3), 1518–1530. <https://doi.org/10.1785/0220190276>
- Lecoq, T., Hicks, S. P., Van Noten, K., Van Wijk, K., Koelemeijer, P., De Plaen, R. S., et al. (2020). Global quieting of high-frequency seismic noise due to COVID-19 pandemic lockdown measures. *Science*, 369(6509), 1338–1343. <https://doi.org/10.1126/science.abd2438>
- Lecoq, T., Longuevergne, L., Pedersen, H. A., Brenguier, F., & Stammer, K. (2017). Monitoring ground water storage at mesoscale using seismic noise: 30 years of continuous observation and thermo-elastic and hydrological modeling. *Scientific Reports*, 7(1), 14241. <https://doi.org/10.1038/s41598-017-14468-9>
- Lee, W. H. K., Igel, H., & Trifunac, M. D. (2009). Recent advances in rotational seismology. *Seismological Research Letters*, 80(3), 479–490. <https://doi.org/10.1785/gssrl.80.3.479>
- Lei, W., Ruan, Y., Bozdağ, E., Peter, D., Lefebvre, M., Komatitsch, D., et al. (2020). Global adjoint tomography—Model GLAD-M25. *Geophysical Journal International*, 223(1), 1–21. <https://doi.org/10.1093/gji/egaa253>
- Leith, W. (2008). Challenges ahead for the global seismographic network. *Seismological Research Letters*, 79(2), 155–157. <https://doi.org/10.1785/gssrl.79.2.155>
- Lekic, V., Cottaar, S., Dziewoński, A., & Romanowicz, B. A. (2012). Cluster analysis of global lower mantle tomography: A new class of structure and implications for chemical heterogeneity. *Earth and Planetary Science Letters*, 357–358, 68–77. <https://doi.org/10.1016/j.epsl.2012.09.014>
- Lekić, V., Matas, J., Panning, M., & Romanowicz, B. A. (2009). Measurement and implications of frequency dependence of attenuation. *Earth and Planetary Science Letters*, 282(1–4), 285–293. <https://doi.org/10.1016/j.epsl.2009.03.030>
- Lekić, V., & Romanowicz, B. A. (2011). Inferring upper-mantle structure by full waveform tomography with the spectral element method. *Geophysical Journal International*, 185(2), 799–831. <https://doi.org/10.1111/j.1365-246x.2011.04969.x>

- Le Pape, F., Craig, D., & Bean, C. J. (2021). How deep ocean-land coupling controls the generation of secondary microseism Love waves. *Nature Communications*, *12*(1), 2332. <https://doi.org/10.1038/s41467-021-22591-5>
- Le Pichon, A., Mialle, P., Guilbert, J., & Vergoz, J. (2006). Multistation infrasonic observations of the Chilean earthquake of 2005 June 13. *Geophysical Journal International*, *167*(2), 838–844. <https://doi.org/10.1111/j.1365-246X.2006.03190.x>
- Levin, V., & Park, J. (1997). Crustal anisotropy in the Ural Mountains foredeep from teleseismic receiver functions. *Geophysical Research Letters*, *24*(11), 1283–1286. <https://doi.org/10.1029/97gl51321>
- Levin, V., & Park, J. (1998). Quasi-love phases between Tonga and Hawaii: Observations, simulations, and explanations. *Journal of Geophysical Research*, *103*(B10), 24321–24331. <https://doi.org/10.1029/98jb02342>
- Lhermitte, S., Sun, S., Shuman, C., Wouters, B., Pattyn, F., Wuite, J., et al. (2020). Damage accelerates ice shelf instability and mass loss in Amundsen Sea Embayment. *Proceedings from the National Academy of Science U.S.A.*, *117*(40), 24735–24741. <https://doi.org/10.1073/pnas.1912890117>
- Li, A., & Richards, P. G. (2003). Using earthquake doublets to study inner core rotation and seismicity catalog precision. *Geochemistry, Geophysics, Geosystems*, *4*(9), 1072. <https://doi.org/10.1029/2002GC000379>
- Li, C., Peng, Z., Chaput, J. A., Walter, J. I., & Aster, R. C. (2021). Remote triggering of icequakes at Mt. Erebus, Antarctica by large teleseismic earthquakes. *Seismological Research Letters*, *92*(5), 2866–2875. <https://doi.org/10.1785/0220210027>
- Li, L., Boué, P., Retailleau, L., & Campillo, M. (2020). Spatiotemporal correlation analysis of noise-derived seismic body waves with ocean wave climate and microseism sources. *Geochemistry, Geophysics, Geosystems*, *21*(9), e2020GC009112. <https://doi.org/10.1029/2020gc009112>
- Li, X.-D., Giardini, D., & Woodhouse, J. H. (1991). The relative amplitudes of mantle heterogeneity in P velocity, S velocity and density from free-oscillation data. *Geophysical Journal International*, *105*(3), 649–657. <https://doi.org/10.1111/j.1365-246X.1991.tb00802.x>
- Lin, F.-C., Schmandt, B., & Tsai, V. C. (2012). Joint inversion of Rayleigh wave phase velocity and ellipticity using USArray: Constraining velocity and density structure in the upper crust. *Geophysical Research Letters*, *39*(12), L12303. <https://doi.org/10.1029/2012gl052196>
- Lin, F.-C., Tsai, V. C., Schmandt, B., Duputel, Z., & Zhan, Z. (2013). Extracting seismic core phases with array interferometry. *Geophysical Research Letters*, *40*(6), 1049–1053. <https://doi.org/10.1002/grl.50237>
- Lindner, D., Song, X., Ma, P., & Christensen, D. H. (2010). Inner core rotation and its variability from nonparametric modeling. *Journal of Geophysical Research*, *115*(B4), B04307. <https://doi.org/10.1029/2009JB006294>
- Lindsey, N. J., Rademacher, H., & Ajo-Franklin, J. B. (2020). On the broadband instrument response of fiber-optic DAS arrays. *Journal of Geophysical Research: Solid Earth*, *125*(2), e2019JB018145. <https://doi.org/10.1029/2019jb018145>
- Lloyd, A. J., Wiens, D. A., Zhu, H., Tromp, J., Nyblade, A. A., Aster, R. C., et al. (2019). Seismic structure of the Antarctic upper mantle based on adjoint tomography. *Journal of Geophysical Research: Solid Earth*, *125*(3). <https://doi.org/10.1029/2019jb017823>
- Lognonné, P., Banerdt, W., Pike, W., Giardini, D., Christensen, U., Garcia, R. F., et al. (2020). Constraints on the shallow elastic and anelastic structure of Mars from insight seismic data. *Nature Geoscience*, *13*(3), 213–220. <https://doi.org/10.1038/s41561-020-0536-y>
- Lognonné, P., Banerdt, W. B., Giardini, D., Pike, W. T., Christensen, U., Laudet, P., et al. (2019). SEIS: Insight's seismic experiment for internal structure of Mars. *Space Science Reviews*, *215*(1), 1–170.
- Lognonné, P., Clevede, E., & Kanamori, H. (1998). Computation of seismograms and atmospheric oscillations by normal-mode summation for a spherical Earth model with realistic atmosphere. *Geophysical Journal International*, *135*(2), 388–406. <https://doi.org/10.1046/j.1365-246x.1998.00665.x>
- Lomax, A., & Michelini, A. (2009). M_{wpd} : A duration–amplitude procedure for rapid determination of earthquake magnitude and tsunamigenic potential from P waveforms. *Geophysical Journal International*, *176*(1), 200–214. <https://doi.org/10.1111/j.1365-246X.2008.03974.x>
- Lomax, A., Michelini, A., & Piatanesi, A. (2007). An energy-duration procedure for rapid determination of earthquake magnitude and tsunamigenic potential. *Geophysical Journal International*, *170*(3), 1195–1209. <https://doi.org/10.1111/j.1365-246X.2007.03469.x>
- Long, M. D., & Silver, P. G. (2009). Shear wave splitting and mantle anisotropy: Measurements, interpretations, and new directions. *Surveys in Geophysics*, *30*(4), 407–461. <https://doi.org/10.1007/s10712-009-9075-1>
- Longuet-Higgins, M. (1950). A theory of the origin of microseisms. *Philosophical Transactions of the Royal Society of London – Series A: Mathematical and Physical Sciences*, *243*(857), 1–35. <https://doi.org/10.1098/rsta.1950.0012>
- Lorenz, R., Panning, M., Stähler, S., Shiraiishi, H., Yamada, R., Turtle, E., et al. (2019). Titan seismology with dragonfly: Probing the internal structure of the most accessible ocean world. In *Lunar and Planetary Science Conference* (Vol. 50, pp. 2173).
- Lorito, S., Romano, F., Atzori, S., Tong, X., Avallone, A., McCloskey, J., et al. (2011). Limited overlap between the seismic gap and coseismic slip of the great 2010 Chile earthquake. *Nature Geoscience*, *4*(3), 173–177. <https://doi.org/10.1038/ngeo1073>
- Love, J. J., & Chulliat, A. (2013). An international network of magnetic observatories. *EOS, Transactions – American Geophysical Union*, *94*(42), 373–374. <https://doi.org/10.1002/2013EO420001>
- Lu, C., & Grand, S. P. (2016). The effect of subducting slabs in global shear wave tomography. *Geophysical Journal International*, *205*(2), 1074–1085. <https://doi.org/10.1093/gji/ggw072>
- Lythgoe, K. H., Ingrid, M. I., & Yao, J. (2020). On waveform correlation measurement uncertainty with implications for temporal changes in inner core seismic waves. *Physics of the Earth and Planetary Interiors*, *309*, 106606. <https://doi.org/10.1016/j.pepi.2020.106606>
- Ma, Z., Masters, G., & Mancinelli, N. (2016). Two-dimensional global Rayleigh wave attenuation model by accounting for finite-frequency focusing and defocusing effect. *Geophysical Journal International*, *204*(1), 631–649. <https://doi.org/10.1093/gji/ggv480>
- MacAyeal, D. R. (2018). Seismology gets under the skin of the Antarctic ice sheet. *Geophysical Research Letters*, *45*(20), 11173–11176. <https://doi.org/10.1029/2018GL080366>
- MacAyeal, D. R., Banwell, A., Okal, E., Lin, J., Willis, I., Boodsell, B., & Macdonald, G. (2018). Diurnal seismicity cycle linked to subsurface melting on an ice shelf. *Annals of Glaciology*, *60*(79), 137–157. <https://doi.org/10.1017/aog.2018.29>
- MacAyeal, D. R., Okal, E. A., Aster, R., & Bassis, J. N. (2008). Seismic and hydroacoustic tremor generated by colliding icebergs. *Journal of Geophysical Research*, *113*(F3), F03011. <https://doi.org/10.1029/2008jf001005>
- MacAyeal, D. R., Okal, M. H., Thom, J. E., Brunt, K. M., Kim, Y.-J., & Bliss, A. K. (2008). Tabular iceberg collisions within the coastal regime. *Journal of Glaciology*, *54*(185), 371–386. <https://doi.org/10.3189/002214308784886180>
- Magrini, F., Diaferia, G., Boschi, L., & Cammarano, F. (2020). Arrival-angle effects on two-receiver measurements of phase velocity. *Geophysical Journal International*, *220*(3), 1838–1844. <https://doi.org/10.1093/gji/ggz560>
- Mai, P. M., & Beroza, G. C. (2002). A spatial random field model to characterize complexity in earthquake slip. *Journal of Geophysical Research*, *107*(B11), ESE10-1–ESE10-21. <https://doi.org/10.1029/2001jb000588>
- Mai, P. M., Schorlemmer, D., Page, M., Ampuero, J., Asano, K., Causse, M., et al. (2016). The earthquake-source inversion validation (SIV) project. *Seismological Research Letters*, *87*(3), 690–708. <https://doi.org/10.1785/0220150231>
- Mai, P. M., & Thingbaijam, K. K. S. (2014). SRCMOD: An online database of finite-fault rupture models. *Seismological Research Letters*, *85*(6), 1348–1357. <https://doi.org/10.1785/0220140077>

- Majstorović, J., Rosat, S., Lambotte, S., & Rogister, Y. (2018). Testing performances of the optimal sequence estimation and autoregressive method in the frequency domain for estimating eigenfrequencies and zonal structure coefficients of low-frequency normal modes. *Geophysical Journal International*, 216(2), 1157–1176. <https://doi.org/10.1093/gji/ggy483>
- Mäkinen, A. M., & Deuss, A. (2013). Normal mode splitting function measurements of anelasticity and attenuation in the Earth's inner core. *Geophysical Journal International*, 194(1), 401–416. <https://doi.org/10.1093/gji/ggt092>
- Marchetti, E., van Herwijnen, A., Christen, M., Silengo, M. C., & Barfucci, G. (2020). Seismo-acoustic energy partitioning of a powder snow avalanche. *Earth Surface Dynamics*, 8(2), 399–411. <https://doi.org/10.5194/esurf-8-399-2020>
- Marchitelli, V., Harabaglia, P., Troise, C., & De Natale, G. (2020). On the correlation between solar activity and large earthquakes worldwide. *Scientific Reports*, 10(1), 11495. <https://doi.org/10.1038/s41598-020-67860-3>
- Martin, S., Drucker, R., Aster, R., Davey, F., Okal, E., Scambos, T., & MacAyeal, D. R. (2010). Kinematic and seismic analysis of giant tabular iceberg breakup at Cape Adare, Antarctica. *Journal of Geophysical Research*, 115(B6), B06311. <https://doi.org/10.1029/2009JB006700>
- Marusiak, A. G., Schmerr, N. C., Banks, M. E., & Daubar, I. J. (2020). Terrestrial single-station analog for constraining the Martian core and deep interior: Implications for insight. *Icarus*, 335, 113396. <https://doi.org/10.1016/j.icarus.2019.113396>
- Massonnet, D., Rossi, M., Carmona, C., Adragna, F., Peltzer, G., Feigl, K., & Rabaute, T. (1993). The displacement field of the Landers earthquake mapped by radar interferometry. *Nature*, 364(6433), 138–142. <https://doi.org/10.1038/364138a0>
- Masters, G., Barmine, M., & Kientz, S. (2014). Mineos user manual version 1.0.2. *Computational Infrastructure for Geodynamics*. Retrieved from <http://geoweb.cse.ucdavis.edu/cig/software/mineos/mineos-manual.pdf>
- Masters, G., & Gilbert, F. (1981). Structure of the inner core inferred from observations of its spheroidal shear modes. *Geophysical Research Letters*, 8(6), 569–571. <https://doi.org/10.1029/GL008i006p00569>
- Masters, G., & Gubbins, D. (2003). On the resolution of density within the Earth. *Physics of the Earth and Planetary Interiors*, 140(1–3), 159–167. <https://doi.org/10.1016/j.pepi.2003.07.008>
- Masters, G., Jordan, T., Silver, P., & Gilbert, F. (1982). Aspherical Earth structure from fundamental spheroidal-mode data. *Nature*, 298(5875), 609–613. <https://doi.org/10.1038/298609a0>
- Masters, G., Laske, G., Bolton, H., & Dziewonski, A. (2000). The relative behavior of shear velocity, bulk sound speed, and compressional velocity in the mantle: Implications for chemical and thermal structure. In *Earth's deep interior: Mineral physics and tomography from the atomic to the global scale* (pp. 63–87). American Geophysical Union (AGU). <https://doi.org/10.1029/GM117p0063>
- Masters, G., Laske, G., & Gilbert, F. (2000). Matrix autoregressive analysis of free-oscillation coupling and splitting. *Geophysical Journal International*, 143(2), 478–489. <https://doi.org/10.1046/j.1365-246x.2000.01261.x>
- Masters, T., & Widmer, R. (1995). Free oscillations: Frequencies and attenuations. *Global Earth Physics: A Handbook of Physical Constants*, 1, 104.
- Matoza, R. S., Fee, D., Assink, J. D., Iezzi, A. M., Green, D. N., Kim, K., et al. (2022). Atmospheric waves and global seismoacoustic observations of the January 2022 Hunga eruption, Tonga. *Science*, 377(6601), 95–100. <https://doi.org/10.1126/science.abo7063>
- Matoza, R. S., Green, D. N., Le Pichon, A., Shearer, P. M., Fee, D., Mialle, P., & Ceranna, L. (2017). Automated detection and cataloging of global explosive volcanism using the International Monitoring System infrasound network. *Journal of Geophysical Research: Solid Earth*, 122(4), 2946–2971. <https://doi.org/10.1002/2016JB013356>
- Matsumoto, H., Bohnenstiehl, D. R., Touradre, J., Dziak, R., Haxel, J., Lau, T.-K., et al. (2014). Antarctic icebergs: A significant natural ocean sound source in the southern hemisphere. *Geochemistry, Geophysics, Geosystems*, 15(8), 3448–3458. <https://doi.org/10.1002/2014GC005454>
- Maupin, V. (2017). 3-D sensitivity kernels of the Rayleigh wave ellipticity. *Geophysical Journal International*, 211(1), 107–119. <https://doi.org/10.1093/gji/ggx294>
- Mazza, S., Olivieri, M., Mandiello, A., & Casale, P. (2008). The mediterranean broad band seismographic network Anno 2005/06. In E. S. Husebye (Ed.), *Earthquake monitoring and seismic hazard mitigation in Balkan countries* (pp. 133–149). Springer Netherlands.
- McCaffrey, R. (2008). Global frequency of magnitude 9 earthquakes. *Geology*, 36(3), 263. <https://doi.org/10.1130/g24402a.1>
- MedNet Project Partner Institutions. (1988). *Mediterranean very broadband seismographic network (MedNet)*. Istituto Nazionale di Geofisica e Vulcanologia (INGV). <https://doi.org/10.13127/SD/FBBTDTD6Q>
- Mégnin, C., & Romanowicz, B. (2000). The three-dimensional shear velocity structure of the mantle from the inversion of body, surface and higher-mode waveforms. *Geophysical Journal International*, 143(3), 709–728. <https://doi.org/10.1046/j.1365-246x.2000.00298.x>
- Meinig, C., Stalin, S. E., Nakamura, A. I., & Milburn, H. B. (2005). Real-time deep-ocean tsunami measuring, monitoring, and reporting system: The NOAA DART II description and disclosure. *NOAA, Pacific Marine Environmental Laboratory (PMEL)*, 1–15.
- Melbourne, T. I., Szeliga, W. M., Marcelo Santillan, V., & Scrivner, C. W. (2021). Global navigational satellite system seismic monitoring. *Bulletin of the Seismological Society of America*, 111(3), 1248–1262. <https://doi.org/10.1785/0120200356>
- Melgar, D., Crowell, B. W., Bock, Y., & Haase, J. S. (2013). Rapid modeling of the 2011 M_w 9.0 Tohoku-Oki earthquake with seismogeodesy. *Geophysical Research Letters*, 40(12), 2963–2968. <https://doi.org/10.1002/grl.50590>
- Melton, B. S. (1979). The sensitivity and dynamic range of inertial seismographs. *Physics of the Earth and Planetary Interiors*, 18(2), 64–70. [https://doi.org/10.1016/0031-9201\(79\)90133-X](https://doi.org/10.1016/0031-9201(79)90133-X)
- Meng, L., Ampuero, J.-P., Stock, J., Duputel, Z., Luo, Y., & Tsai, V. (2012). Earthquake in a maze: Compressional rupture branching during the 2012 M_w 8.6 Sumatra earthquake. *Science*, 337(6095), 724–726. <https://doi.org/10.1126/science.1224030>
- Miller, W. F. (1963). The Caltech digital seismograph. *Journal of Geophysical Research*, 68(3), 841–847. <https://doi.org/10.1029/JZ068i003p00841>
- Milne, J. (1900). *Fifth Report of the Committee on Seismological Investigations Plate II*. British Association for the Advancement of Science.
- Mitsui, Y., & Heki, K. (2012). Observation of Earth's free oscillation by dense GPS array: After the 2011 Tohoku megathrust earthquake. *Scientific Reports*, 2(1), 931. <https://doi.org/10.1038/srep00931>
- Montagner, J.-P., Juhel, K., Barsuglia, M., Ampuero, J. P., Chassande-Mottin, E., Harms, J., et al. (2016). Prompt gravity signal induced by the 2011 Tohoku-Oki earthquake. *Nature Communications*, 7(1), 1–7. <https://doi.org/10.1038/ncomms13349>
- Montagner, J.-P., & Kennett, B. L. N. (1996). How to reconcile body-wave and normal-mode reference Earth models. *Geophysical Journal International*, 125(1), 229–248. <https://doi.org/10.1111/j.1365-246x.1996.tb06548.x>
- Montagner, J.-P., Lognonné, P., Beaujuin, R., Roullet, G., Karczewski, J.-F., & Stutzmann, E. (1998). Towards multiscalar and multiparameter networks for the next century: The French efforts. *Physics of the Earth and Planetary Interiors*, 108(2), 155–174. [https://doi.org/10.1016/s0031-9201\(98\)00093-4](https://doi.org/10.1016/s0031-9201(98)00093-4)
- Montagner, J.-P., & Tanimoto, T. (1991). Global upper mantle tomography of seismic velocities and anisotropies. *Journal of Geophysical Research*, 96(B12), 20337–20351. <https://doi.org/10.1029/91jb01890>
- Montelli, R., Nolet, G., Dahlen, F., & Masters, G. (2006). A catalogue of deep mantle plumes: New results from finite-frequency tomography. *Geochemistry, Geophysics, Geosystems*, 7(11). <https://doi.org/10.1029/2006GC001248>

- Moore, J. R., Geimer, P. R., Finnegan, R., & Thorne, M. S. (2018). Use of seismic resonance measurements to determine the elastic modulus of freestanding rock masses. *Rock Mechanics and Rock Engineering*, 51(12), 3937–3944. <https://doi.org/10.1007/s00603-018-1554-6>
- Mordret, A., Mikesell, T., Harig, C., Lipovsky, B., & Prieto, G. A. (2016). Monitoring southwest Greenland's ice sheet melt with ambient seismic noise. *Science Advances*, 2(5), e1501538. <https://doi.org/10.1126/sciadv.a1501538>
- Morra, G., Geller, R. J., Grilli, S. T., Karato, S.-i., King, S., Lee, S.-M., et al. (2013). Growing understanding of subduction dynamics indicates need to rethink seismic hazards. *Eos, Transactions American Geophysical Union*, 94(13), 125–126. <https://doi.org/10.1002/2013eo130008>
- Mosca, I., Cobden, L., Deuss, A., Ritsema, J., & Trampert, J. (2012). Seismic and mineralogical structures of the lower mantle from probabilistic tomography. *Journal of Geophysical Research*, 117(B6), B06304. <https://doi.org/10.1029/2011jb008851>
- Moschella, S., Cannata, A., Cannavò, F., Di Grazia, G., Nardone, G., Orasi, A., et al. (2020). Insights into microseism sources by array and machine learning techniques: Ionian and Tyrrhenian Sea case of study. *Frontiers of Earth Science*, 8, 114. <https://doi.org/10.3389/feart.2020.00114>
- Moulik, P., & Ekström, G. (2014). An anisotropic shear velocity model of the Earth's mantle using normal modes, body waves, surface waves and long-period waveforms. *Geophysical Journal International*, 199(3), 1713–1738. <https://doi.org/10.1093/gji/ggu356>
- Moulik, P., & Ekström, G. (2016). The relationships between large-scale variations in shear velocity, density, and compressional velocity in the Earth's mantle. *Journal of Geophysical Research: Solid Earth*, 121(4), 2737–2771. <https://doi.org/10.1002/2015JB012679>
- Moulik, P., Lekic, V., Romanowicz, B. A., Ma, Z., Schaeffer, A., Ho, T., et al. (2022). Global reference seismological data sets: Multimode surface wave dispersion. *Geophysical Journal International*, 228(3), 1808–1849. <https://doi.org/10.1093/gji/ggab418>
- Mousavi, S. M., & Beroza, G. C. (2020). Bayesian-deep-learning estimation of earthquake location from single-station observations. *IEEE Transactions on Geoscience and Remote Sensing*, 58(11), 8211–8224. <https://doi.org/10.1109/TGRS.2020.2988770>
- Mousavi, S. M., Ellsworth, W. L., Zhu, W., Chuang, L. Y., & Beroza, G. C. (2020). Earthquake transformer—An attentive deep-learning model for simultaneous earthquake detection and phase picking. *Nature Communications*, 11(1), 1–12. <https://doi.org/10.1038/s41467-020-17591-w>
- Müller, C., Schlindwein, V., Eckstaller, A., & Miller, H. (2005). Singing icebergs. *Science*, 310(5752), 1299. <https://doi.org/10.1126/science.1117145>
- Murphy, J. R., Rodi, W., Johnson, M., Sultanov, D. D., Bennett, T. J., Toksöz, M. N., et al. (2005). Calibration of International Monitoring System (IMS) stations in central and eastern Asia for improved seismic event location. *Bulletin of the Seismological Society of America*, 95(4), 1535–1560. <https://doi.org/10.1785/0120040087>
- Murray, T., Nettles, M., Selmes, N., Cathles, L. M., Burton, J., James, T., et al. (2015). Reverse glacier motion during iceberg calving and the cause of glacial earthquakes. *Science*, 349(6245), 305–308. <https://doi.org/10.1126/science.aab0460>
- Myers, S. C., Begnaud, M. L., Ballard, S., Pasyanos, M. E., Scott Phillips, W., Ramirez, A. L., et al. (2010). A crust and upper-mantle model of Eurasia and North Africa for P_n travel-time calculation. *Bulletin of the Seismological Society of America*, 100(2), 640–656. <https://doi.org/10.1785/0120090198>
- Nader, M., Igel, H., Ferreira, A., Kurrle, D., Wassermann, J., & Schreiber, K. (2012). Toroidal free oscillations of the Earth observed by a ring laser system: A comparative study. *Journal of Seismology*, 16(4), 745–755. <https://doi.org/10.1007/s10950-012-9304-9>
- Nakamura, Y., Latham, G. V., & Dorman, H. J. (1982). Apollo lunar seismic experiment—Final summary. *Journal of Geophysical Research*, 87(S01), A117–A123. <https://doi.org/10.1029/JB087iS01p0A117>
- Nakata, N., Gualtieri, L., & Fichtner, A. (2019). *Seismic ambient noise*. Cambridge University Press. <https://doi.org/10.1017/9781108264808>
- Natawidjaja, D. H., Sieh, K., Chlieh, M., Galetzka, J., Suwargadi, B. W., Cheng, H., et al. (2006). Source parameters of the great Sumatran megathrust earthquakes of 1797 and 1833 inferred from coral microatolls. *Journal of Geophysical Research*, 111(B6), B06403. <https://doi.org/10.1029/2005jb004025>
- National Academy of Sciences. (2002). Technical issues related to the comprehensive nuclear test ban treaty. <https://doi.org/10.17226/10471>
- National Research Council. (1977). *Global earthquake monitoring: Its uses, potential, and support requirements* (pp. 87). The National Academies Press. <https://doi.org/10.17226/18566>
- National Research Council. (2012). The comprehensive nuclear test ban treaty: Technical issues for the United States. <https://doi.org/10.17226/12849>
- Nettles, M., & Ekstrom, G. (2010). Glacial earthquakes in Greenland and Antarctica. *Annual Review of Earth and Planetary Sciences*, 38(1), 467–491. <https://doi.org/10.1146/annurev-earth-040809-152414>
- Nettles, M., Ekström, G., & Koss, H. C. (2011). Centroid-moment-tensor analysis of the 2011 off the Pacific coast of Tohoku Earthquake and its larger foreshocks and aftershocks. *Earth Planets and Space*, 63(7), 2–523. <https://doi.org/10.5047/eps.2011.06.009>
- Newman, A. V., Hayes, G., Wei, Y., & Convers, J. (2011). The 25 October 2010 Mentawai tsunami earthquake, from real-time discriminants, finite-fault rupture, and tsunami excitation. *Geophysical Research Letters*, 38(5), L05302. <https://doi.org/10.1029/2010gl0146498>
- Newman, A. V., & Okal, E. A. (1998). Teleseismic estimates of radiated seismic energy: The E/M_0 discriminant for tsunami earthquakes. *Journal of Geophysical Research*, 103(B11), 26885–26898. <https://doi.org/10.1029/98jb02236>
- Ni, S., Kanamori, H., & Helmberger, D. (2005). Energy radiation from the Sumatra earthquake. *Nature*, 434(7033), 582. <https://doi.org/10.1038/434582a>
- Nie, Z., Zhang, R., Liu, G., Jia, Z., Wang, D., Zhou, Y., & Lin, M. (2016). GNSS seismometer: Seismic phase recognition of real-time high-rate GNSS deformation waves. *Journal of Applied Geophysics*, 135, 328–337. <https://doi.org/10.1016/j.jappgeo.2016.10.026>
- Nishida, K. (2013). Global propagation of body waves revealed by cross-correlation analysis of seismic hum. *Geophysical Research Letters*, 40(9), 1691–1696. <https://doi.org/10.1002/grl.50269>
- Nishida, K. (2014). Source spectra of seismic hum. *Geophysical Journal International*, 199(1), 416–429. <https://doi.org/10.1093/gji/ggu272>
- Nishida, K., & Kobayashi, N. (1999). Statistical features of Earth's continuous free oscillations. *Journal of Geophysical Research*, 104(B12), 28741–28750. <https://doi.org/10.1029/1999jb900286>
- Nishida, K., Montagner, J. P., & Kawakatsu, H. (2009). Global surface wave tomography using seismic hum. *Science*, 326(5949), 112. <https://doi.org/10.1126/science.1176389>
- Nishida, K., & Takagi, R. (2022). A global centroid single force catalog of P-wave microseisms. *Journal of Geophysical Research: Solid Earth*, 127(4), e2021JB023484. <https://doi.org/10.1029/2021jb023484>
- Nissen, E., Ghods, A., Karasözen, E., Elliott, J. R., Barnhart, W. D., Bergman, E. A., et al. (2019). The 12 November 2017 M_w 7.3 Ezgeleh-Sarpolzahab (Iran) earthquake and active tectonics of the Lurestan arc. *Journal of Geophysical Research: Solid Earth*, 124(2), 2124–2152. <https://doi.org/10.1029/2018JB016221>
- Nissen-Meyer, T., van Driel, M., Stähler, S. C., Hosseini, K., Hempel, S., Auer, L., et al. (2014). Axisem: Broadband 3-D seismic wavefields in axisymmetric media. *Solid Earth*, 5(1), 425–445. <https://doi.org/10.5194/se-5-425-2014>
- Noquet, J.-M., Jarrin, P., Vallée, M., Mothes, P. A., Grandin, R., Rolandone, F., et al. (2017). Supercycle at the Ecuadorian subduction zone revealed after the 2016 pedernales earthquake. *Nature Geoscience*, 10(2), 145–149. <https://doi.org/10.1038/ngeo2864>

- Nolet, G., Hello, Y., Lee, S. V., Bonnieux, S., Ruiz, M. C., Pazmino, N. A., et al. (2019). Imaging the Galapagos mantle plume with an unconventional application of floating seismometers. *Scientific Reports*, 9(1), 1326. <https://doi.org/10.1038/s41598-018-36835-w>
- Nolet, G., & Vlaar, N. J. (1981). The NARS project: Probing the Earth's interior with a large seismic antenna. *Terra Cognita*, 2, 17–25.
- Norris, R. (1994). Seismicity of rockfalls and avalanches at three Cascade Range volcanoes: Implications for seismic detection of hazardous mass movements. *Bulletin of the Seismological Society of America*, 84(6), 1925–1939. <https://doi.org/10.1785/BSSA0840061925>
- Nyblade, A., Dirks, P., Durrheim, R., Webb, S., Jones, M., Cooper, G., & Graham, G. (2008). AfricaArray: Developing a geosciences workforce for Africa's natural resource sector. *The Leading Edge*, 27(10), 1358–1361. <https://doi.org/10.1190/1.2996547>
- Okal, E., & Cansi, Y. (1998). Detection of PKJKP at intermediate periods by progressive multi-channel correlation. *Earth and Planetary Science Letters*, 164(1–2), 23–30. [https://doi.org/10.1016/S0012-821X\(98\)00210-6](https://doi.org/10.1016/S0012-821X(98)00210-6)
- Oldham, R. D. (1906). The constitution of the interior of the Earth, as revealed by earthquakes. *Quarterly Journal of the Geological Society*, 62(1–4), 456–475. <https://doi.org/10.1144/gsl.jgs.1906.062.01-04.21>
- Olinger, S., Lipovsky Bradley, P., Wiens, D., Aster, R., Bromirski, P., Chen, Z., et al. (2019). Tidal and thermal stresses drive seismicity along a major Ross Ice Shelf rift. *Geophysical Research Letters*, 46(12), 6644–6652. <https://doi.org/10.1029/2019GL082842>
- Oliver, J. (1962). A worldwide storm of microseisms with periods of about 27 seconds. *Bulletin of the Seismological Society of America*, 52(3), 507–517. <https://doi.org/10.1785/bssa0520030507>
- Oliver, J., & Murphy, L. (1971). WWNSS: Seismology's global network of observing stations. *Science*, 174(4006), 254–261. <https://doi.org/10.1126/science.174.4006.254>
- Olsen, K. B., Begnaud, M., Phillips, S., & Jacobsen, B. H. (2018). Constraints of crustal heterogeneity and $Q(f)$ from regional (<4 Hz) wave propagation for the 2009 North Korea nuclear test. *Bulletin of the Seismological Society of America*, 108(3A), 1369–1383. <https://doi.org/10.1785/0120170195>
- Olsen, K. G., Hurford, T. A., Schmerr, N. C., Huang, M. H., Brunt, K. M., Zipparo, S., et al. (2021). Projected seismic activity at the Tiger Stripe fractures on Enceladus, Saturn from an analog study of tidally modulated icequakes within the Ross Ice Shelf, Antarctica. *Journal of Geophysical Research: Planets*, 126(6), e2021JE006862. <https://doi.org/10.1029/2021je006862>
- Olsen, K. G., & Nettles, M. (2017). Patterns in glacial-earthquake activity around Greenland, 2011–13. *Journal of Glaciology*, 63(242), 1077–1089. <https://doi.org/10.1017/jog.2017.78>
- Olson, A. H., & Apsel, R. J. (1982). Finite faults and inverse theory with applications to the 1979 Imperial Valley earthquake. *Bulletin of the Seismological Society of America*, 72(6A), 1969–2001. <https://doi.org/10.1785/bssa07206a1969>
- Olugboji, T. M., & Park, J. (2016). Crustal anisotropy beneath Pacific ocean-islands from harmonic decomposition of receiver functions. *Geochemistry, Geophysics, Geosystems*, 17(3), 810–832. <https://doi.org/10.1002/2015GC006166>
- Pan, C.-Z., Jin, P., & Wang, H.-C. (2007). Applicability of P/S amplitude ratios for the discrimination of low magnitude seismic events. *Acta Seismologica Sinica*, 20(5), 553–561. <https://doi.org/10.1007/s11589-007-0553-6>
- Panning, M. P., Beucler, É., Drilleau, M., Mocquet, A., Lognonné, P., & Banerdt, W. B. (2015). Verifying single-station seismic approaches using Earth-based data: Preparation for data return from the insight mission to Mars. *Icarus*, 248, 230–242. <https://doi.org/10.1016/j.icarus.2014.10.035>
- Panning, M. P., Kedar, S., Bowles, N., Bugby, D., Calcutt, S., Cutler, J., et al. (2022). Farside seismic suite (FSS): Surviving the lunar night and delivering the first seismic data from the farside of the moon. *LPI Contribution*, 2678, 1576.
- Paolo, F., Fricker, H. A., & Padman, L. (2015). Volume loss from Antarctic ice shelves is accelerating. *Science*, 348(6232), 327–331. <https://doi.org/10.1126/science.aaa0940>
- Parizek, B. R., Christianson, K., Alley, R. B., Voytenko, D., Vaňková, I., Dixon, T. H., et al. (2019). Ice-cliff failure via retrogressive slumping. *Geology*, 47(5), 449–452. <https://doi.org/10.1130/g45880.1>
- Park, J., Amoruso, A., Crescentini, L., & Boschi, E. (2008). Long-period toroidal Earth free oscillations from the great Sumatra–Andaman earthquake observed by paired laser extensometers in Gran Sasso, Italy. *Geophysical Journal International*, 173(3), 887–905. <https://doi.org/10.1111/j.1365-246X.2008.03769.x>
- Park, J., Butler, R., Anderson, K., Berger, J., Davis, P., Benz, H., et al. (2005). Performance review of the global seismographic network for the Sumatra–Andaman megathrust earthquake. *Seismological Research Letters*, 76(3), 331–343. <https://doi.org/10.1785/gssrl.76.3.331>
- Park, J., & Levin, V. (2002). Seismic anisotropy: Tracing plate dynamics in the mantle. *Science*, 296(5567), 485–489. <https://doi.org/10.1126/science.1067319>
- Park, J., & Yu, Y. (1993). Seismic determination of elastic anisotropy and mantle flow. *Science*, 261(5125), 1159–1162. <https://doi.org/10.1126/science.261.5125.1159>
- Pedersen, H. A., Leroy, N., Zigone, D., Vallée, M., Ringler, A. T., & Wilson, D. C. (2019). Using component ratios to detect metadata and instrument problems of seismic stations: Examples from 18 yr. of GEOSCOPE data. *Seismological Research Letters*, 91(1), 272–286. <https://doi.org/10.1785/0220190180>
- Pejić, T., Tkalčić, H., Sambridge, M., Cormier, V. F., & Benavente, R. (2017). Attenuation tomography of the upper inner core. *Journal of Geophysical Research: Solid Earth*, 122(4), 3008–3032. <https://doi.org/10.1002/2016JB013692>
- Pekeris, C. L., Alterman, Z., & Jarosch, H. (1961). Rotational multiplets in the spectrum of the Earth. *Physics Reviews*, 122(6), 1692–1700. <https://doi.org/10.1103/PhysRev.122.1692>
- Peng, Z., Walter, J., Aster, R., Nyblade, A., Wiens, D., & Anandkrishnan, S. (2014). Antarctic icequakes triggered by the 2010 Maule earthquake in Chile. *Nature Geoscience*, 7(9), 677–681. <https://doi.org/10.1038/ngeo2212>
- Perol, T., Gharbi, M., & Denolle, M. (2018). Convolutional neural network for earthquake detection and location. *Science Advances*, 4(2), e1700578. <https://doi.org/10.1126/sciadv.1700578>
- Peterson, J. (1993). *Observations and modeling of seismic background noise* (Open-File Report, 93-322, pp. 94). U.S. Geological Survey. <https://doi.org/10.3133/ofr93322>
- Peterson, J., & Hutt, C. R. (1989). *IRIS/USGS plans for upgrading the global seismograph network* (Open-File Report, 89-471, pp. 43). U.S. Geological Survey. <https://doi.org/10.3133/ofr89471>
- Peterson, J., & Hutt, C. R. (2014). *World-Wide Standardized Seismograph Network: A data users guide* (Open-File Report, 2014-1218, pp. 74). U.S. Geological Survey. <https://doi.org/10.3133/ofr20141218>
- Phạm, T.-S., Tkalčić, H., Sambridge, M., & Kennett, B. L. N. (2018). Earth's correlation wavefield: Late coda correlation. *Geophysical Research Letters*, 45(7), 3035–3042. <https://doi.org/10.1002/2018GL077244>
- Pirli, M., & Voss, P. H. (2021). Preface to the focus section on Arctic and Antarctic seismology. *Seismological Research Letters*, 92(5), 2691–2694. <https://doi.org/10.1785/0220210163>
- Podolskiy, E. A., Murai, Y., Kanna, N., & Sugiyama, S. (2021). Ocean-bottom seismology of glacial earthquakes: The concept, lessons learned, and mind the sediments. *Seismological Research Letters*, 92(5), 2850–2865. <https://doi.org/10.1785/0220200465>

- Podolskiy, E. A., & Walter, F. (2016). Cryoseismology. *Reviews of Geophysics*, 54(4), 708–758. <https://doi.org/10.1002/2016RG000526>
- Poli, P., Campillo, M., & de Hoop, M. (2017). Analysis of intermediate period correlations of coda from deep earthquakes. *Earth and Planetary Science Letters*, 477, 147–155. <https://doi.org/10.1016/j.epsl.2017.08.026>
- Porritt, R., & Conley, A. (2021). *Challenges and potential of waveform modeling for crustal scale predictions* (osti.gov, Technical Report). U.S. Department of Energy. <https://doi.org/10.2172/1827491>
- Poupinet, G., Souriau, A., & Coutant, O. (2000). The existence of an inner core super-rotation questioned by teleseismic doublets. *Physics of the Earth and Planetary Interiors*, 118(1), 77–88. [https://doi.org/10.1016/S0031-9201\(99\)00129-6](https://doi.org/10.1016/S0031-9201(99)00129-6)
- Powell, T. W., & Neuberg, J. (2003). Time dependent features in tremor spectra. *Journal of Volcanology and Geothermal Research*, 128(1–3), 177–185. [https://doi.org/10.1016/s0377-0273\(03\)00253-1](https://doi.org/10.1016/s0377-0273(03)00253-1)
- Purdy, G., Dziewonski, A., Montagner, J., & Lancelot, Y. (1995). Towards a permanent network of ocean floor seismological observatories. In *Proceedings, ION/ODP Workshop on Multidisciplinary Observatories on the Deep Sea Floor* (pp. 165–167).
- Rao, H., Luo, Y., Zhao, K., & Yang, Y. (2021). Extracting surface wave dispersion curves from asynchronous seismic stations: Method and application. *Geophysical Journal International*, 226(2), 1148–1158. <https://doi.org/10.1093/gji/ggab153>
- Razafindrakoto, H. N. T., Mai, P. M., Genton, M. G., Zhang, L., & Thingbaijam, K. K. S. (2015). Quantifying variability in earthquake rupture models using multidimensional scaling: Application to the 2011 Tohoku earthquake. *Geophysical Journal International*, 202(1), 17–40. <https://doi.org/10.1093/gji/ggv088>
- Resovsky, J. S., & Ritzwoller, M. H. (1998). New and refined constraints on three-dimensional Earth structure from normal modes below 3 mHz. *Journal of Geophysical Research*, 103(B1), 783–810. <https://doi.org/10.1029/97jb02482>
- Resovsky, J. S., & Ritzwoller, M. H. (1999a). A degree 8 mantle shear velocity model from normal mode observations below 3 mHz. *Journal of Geophysical Research*, 104(B1), 993–1014. <https://doi.org/10.1029/1998jb900025>
- Resovsky, J. S., & Ritzwoller, M. H. (1999b). Regularization uncertainty in density models estimated from normal mode data. *Geophysical Research Letters*, 26(15), 2319–2322. <https://doi.org/10.1029/1999GL900540>
- Retailleau, L., & Gualtieri, L. (2019). Toward high-resolution period-dependent seismic monitoring of tropical cyclones. *Geophysical Research Letters*, 46(3), 1329–1337. <https://doi.org/10.1029/2018gl080785>
- Richards, P. G., Heck, S., Schaff, D. P., Slinkard, S. M., & Young, C. (2015). Preliminary results for a data-intensive study of China seismicity to detect small events and improve location estimates for event clusters. *Research and Technology Review, Kazakhstan*, 64(4), 127–131.
- Richards, P. G., & Kim, W.-Y. (1997). Testing the nuclear test-ban treaty. *Nature*, 389(6653), 781–782. <https://doi.org/10.1038/39720>
- Richards, P. G., Wu, Z., Kim, W.-Y., & Schaff, D. P. (2021). Seismic monitoring of nuclear explosions. In H. K. Gupta (Ed.), *Encyclopedia of Solid Earth Geophysics* (pp. 1429–1442). Springer International Publishing. https://doi.org/10.1007/978-3-030-58631-7_8
- Richards, P. G., & Zavales, J. (1996). Seismological methods for monitoring a CTBT: The technical issues arising in early negotiations. In E. S. Husebye & A. M. Dainty (Eds.), *Monitoring a Comprehensive Test Ban Treaty* (pp. 53–81). Springer Netherlands. https://doi.org/10.1007/978-94-011-0419-7_5
- Ringler, A. T., Evans, J. R., & Hutt, C. R. (2015). Self-noise models of five commercial strong-motion accelerometers. *Seismological Research Letters*, 86(4), 1143–1147. <https://doi.org/10.1785/0220150027>
- Ringler, A. T., Anthony, R. E., Dalton, C. A., & Wilson, D. C. (2021). Rayleigh-wave amplitude uncertainty across the Global Seismographic Network and potential implications for global tomography. *Bulletin of the Seismological Society of America*, 111(3), 1273–1292. <https://doi.org/10.1785/0120200255>
- Ringler, A. T., Anthony, R. E., Davis, P., Ebeling, C., Hafner, K., Mellors, R., et al. (2022). Improved resolution across the global seismographic network: A new ear in low-frequency seismology. *The Seismic Record*, 2, 78–87. <https://doi.org/10.1785/0320220008>
- Ringler, A. T., Anthony, R. E., Wilson, D. C., Auerbach, D., Bargabus, S., Davis, P., et al. (2021). A review of timing accuracy across the Global Seismographic Network. *Seismological Research Letters*, 92(4), 2270–2281. <https://doi.org/10.1785/0220200394>
- Ringler, A. T., Anthony, R. E., Wilson, D. C., Claycomb, A. C., & Spritzer, J. (2020). Magnetic field variations in Alaska: Recording space weather events on seismic stations in Alaska. *Bulletin of the Seismological Society of America*, 110(5), 2530–2540. <https://doi.org/10.1785/0120200019>
- Ringler, A. T., Anthony, R. E., Aster, R. C., Taka'aki, T., Shiro, B., Wilson, D., et al. (2022). The Global Seismographic Network reveals atmospherically coupled normal modes excited by the 2022 Hunga Tonga eruption. *Geophysical Journal International*. In review. <https://doi.org/10.1093/gji/ggac284/6650357>
- Ringler, A. T., Gee, L. S., Hutt, C. R., & McNamara, D. E. (2010). Temporal variations in global seismic station ambient noise power levels. *Seismological Research Letters*, 81(4), 605–613. <https://doi.org/10.1785/gssrl.81.4.605>
- Ringler, A. T., Hagerty, M. T., Holland, J., Gonzales, A., Gee, L. S., Edwards, J. D., et al. (2015). The data quality analyzer: A quality control program for seismic data. *Computers & Geosciences*, 76, 96–111. <https://doi.org/10.1016/j.cageo.2014.12.006>
- Ringler, A. T., & Hutt, C. R. (2010). Self-noise models of seismic instruments. *Seismological Research Letters*, 81(6), 972–983. <https://doi.org/10.1785/gssrl.81.6.972>
- Ringler, A. T., Hutt, C. R., Aster, R., Bolton, H., Gee, L. S., & Storm, T. (2012). Estimating pole-zero errors in GSN-IRIS/USGS network calibration metadata. *Bulletin of the Seismological Society of America*, 102(2), 836–841. <https://doi.org/10.1785/0120110195>
- Ringler, A. T., Sleeman, R., Hutt, C. R., & Gee, L. S. (2014). Seismometer self-noise and measuring methods. In M. Beer, I. A. Kogioumtzoglou, E. Patelli, & I. S.-K. Au (Eds.), *Encyclopedia of earthquake engineering* (pp. 1–13). Springer Berlin Heidelberg. https://doi.org/10.1007/978-3-642-36197-5_175-1
- Ringler, A. T., Steim, J., Wilson, D. C., Widmer-Schmidrig, R., & Anthony, R. E. (2019). Improvements in seismic resolution and current limitations in the Global Seismographic Network. *Geophysical Journal International*, 220(1), 508–521. <https://doi.org/10.1093/gji/ggz473>
- Ringler, A. T., Storm, T., Gee, L. S., Hutt, C. R., & Wilson, D. (2015). Uncertainty estimates in broadband seismometer sensitivities using micro-seisms. *Journal of Seismology*, 19(2), 317–327. <https://doi.org/10.1007/s10950-014-9467-7>
- Ringler, A. T., Wilson, D. C., Zürn, W., & Anthony, R. E. (2018). Rayleigh wave ellipticity measurement uncertainty across the IRIS/USGS and New China Digital Seismograph Networks. *Geophysical Journal International*, 217(1), 219–237. <https://doi.org/10.1093/gji/ggy527>
- Riquelme, S., Bravo, F., Melgar, D., Benavente, R., Geng, J., Barrientos, S., & Campos, J. (2016). W phase source inversion using high-rate regional GPS data for large earthquakes. *Geophysical Research Letters*, 43(7), 3178–3185. <https://doi.org/10.1002/2016GL068302>
- Riser, S. C., Freeland, H. J., Roemmich, D., Wijffels, S., Troisi, A., Belbéoch, M., et al. (2016). Fifteen years of ocean observations with the global Argo array. *Nature Climate Change*, 6(2), 145–153. <https://doi.org/10.1038/nclimate2872>
- Ritsema, J., Deuss, A., van Heijst, H. J., & Woodhouse, J. H. (2011). S40RTS: A degree-40 shear-velocity model for the mantle from new Rayleigh wave dispersion, teleseismic traveltime and normal-mode splitting function measurements. *Geophysical Journal International*, 184(3), 1223–1236. <https://doi.org/10.1111/j.1365-246X.2010.04884.x>
- Ritsema, J., & Lekić, V. (2020). Heterogeneity of seismic wave velocity in Earth's mantle. *Annual Review of Earth and Planetary Sciences*, 48(1), 377–401. <https://doi.org/10.1146/annurev-earth-082119-065909>

- Ritsema, J., van Heijst, H.-J., & Woodhouse, J. (1999). Complex shear wave velocity structure imaged beneath Africa and Iceland. *Science*, 286(5446), 1925–1928. <https://doi.org/10.1126/science.286.5446.1925>
- Ritsema, J., Van Heijst, H. J., & Woodhouse, J. H. (2004). Global transition zone tomography. *Journal of Geophysical Research*, 109(B2), B02302. <https://doi.org/10.1029/2003JB002610>
- Ritzwoller, M., Masters, G., & Gilbert, F. (1986). Observations of anomalous splitting and their interpretation in terms of aspherical structure. *Journal of Geophysical Research*, 91(B10), 10203–10228. <https://doi.org/10.1029/JB091iB10p10203>
- Robson, A., Lau, H., Koelemeijer, P., & Romanowicz, B. (2022). An analysis of core-mantle boundary Stoneley mode sensitivity and sources of uncertainty. *Geophysical Journal International*, 228(3), 1962–1974. <https://doi.org/10.1093/gji/ggab448>
- Robson, A. J. S., & Romanowicz, B. A. (2019). New normal mode constraints on bulk inner core velocities and density. *Physics of the Earth and Planetary Interiors*, 295, 106310. <https://doi.org/10.1016/j.pepi.2019.106310>
- Romanowicz, B. (1990). The upper mantle degree 2: Constraints and inferences from global mantle wave attenuation measurements. *Journal of Geophysical Research*, 95(B7), 11051–11071. <https://doi.org/10.1029/JB095iB07p11051>
- Romanowicz, B. (2001). Can we resolve 3D density heterogeneity in the lower mantle? *Geophysical Research Letters*, 28(6), 1107–1110. <https://doi.org/10.1029/2000GL012278>
- Romanowicz, B. (2002). Inversion of surface waves: A review. *International Geophysics Series*, 81(A), 149–174.
- Romanowicz, B. A. (2021). Seismic tomography of the Earth's mantle. In D. Alderton & S. A. Elias (Eds.), *Encyclopedia of geology* (2nd ed., pp. 587–609). Academic Press. <https://doi.org/10.1016/B978-0-08-102908-4.00169-7>
- Romanowicz, B. A., Cara, M., Fel, J. F., & Rouland, D. (1984). Geoscope: A French initiative in long-period three-component global seismic networks. *Eos, Transactions American Geophysical Union*, 65(42), 753. <https://doi.org/10.1029/EO065i042p00753-01>
- Romanowicz, B. A., & Dziewonski, A. M. (1987). Global digital seismographic network: Research opportunities and recent initiatives. In *Composition, structure and dynamics of the lithosphere-asthenosphere system* (pp. 99–110). American Geophysical Union (AGU). <https://doi.org/10.1029/GD016p0099>
- Ross, Z. E., Meier, M., Hauksson, E., & Heaton, T. H. (2018). Generalized seismic phase detection with deep learning. *Bulletin of the Seismological Society of America*, 108(5A), 2894–2901. <https://doi.org/10.1785/0120180080>
- Ross, Z. E., Meier, M.-A., & Hauksson, E. (2018). P wave arrival picking and first-motion polarity determination with deep learning. *Journal of Geophysical Research: Solid Earth*, 123(6), 5120–5129. <https://doi.org/10.1029/2017jb015251>
- Ross, Z. E., Yue, Y., Meier, M.-A., Hauksson, E., & Heaton, T. H. (2019). Phaselink: A deep learning approach to seismic phase association. *Journal of Geophysical Research: Solid Earth*, 124(1), 856–869. <https://doi.org/10.1029/2018jb016674>
- Rost, S., & Thomas, C. (2002). Array seismology: Methods and applications. *Reviews of Geophysics*, 40(3), 2-1–2-27. <https://doi.org/10.1029/2000rg000100>
- Roth, D., Brodsky, E. E., Finnegan, N., Rickenmann, D., Turowski, J., & Badoux, A. (2016). Bed load sediment transport inferred from seismic signals near a river. *Journal of Geophysical Research: Earth Surface*, 121(4), 725–747. <https://doi.org/10.1002/2015JF003782>
- Roth, D., Finnegan, N., Brodsky, E. E., Cook, K., & Wang, H. (2014). Migration of a coarse fluvial sediment pulse detected by hysteresis in bedload generated seismic waves. *Earth and Planetary Science Letters*, 404, 144–153. <https://doi.org/10.1016/j.epsl.2014.07.019>
- Roult, G., Montagner, J.-P., Romanowicz, B. A., Cara, M., Rouland, D., Pilet, R., et al. (2010). The GEOSCOPE Program: Progress and challenges during the past 30 years. *Seismological Research Letters*, 81(3), 427–452. <https://doi.org/10.1785/02201020193>
- Roult, G., Rosat, S., Clévéché, E., Millot-Langet, R., & Hinderer, J. (2006). New determinations of Q quality factors and eigenfrequencies for the whole set of singlets of the Earth's normal modes ${}_0S_0$, ${}_0S_2$, ${}_0S_3$ and ${}_2S_1$ using superconducting gravimeter data from the GGP network. *Journal of Geodynamics*, 41(1–3), 345–357. <https://doi.org/10.1016/j.jog.2005.08.020>
- Rubinstein, J. L., & Beroza, G. C. (2004). Evidence for widespread nonlinear strong ground motion in the M_w 6.9 Loma Prieta Earthquake. *Bulletin of the Seismological Society of America*, 94(5), 1595–1608. <https://doi.org/10.1785/0120040009>
- Rudolph, M., Moulik, P., & Lekić, V. (2020). Bayesian inference of mantle viscosity from whole-mantle density models. *Geochemistry, Geophysics, Geosystems*, 21(11), e2020GC009335. <https://doi.org/10.1029/2020GC009335>
- Ruff, L., & Kanamori, H. (1980). Seismicity and the subduction process. *Physics of the Earth and Planetary Interiors*, 23(3), 240–252. [https://doi.org/10.1016/0031-9201\(80\)90117-x](https://doi.org/10.1016/0031-9201(80)90117-x)
- Ruff, L. J. (1989). Multi-trace deconvolution with unknown trace scale factors: Omnilinear inversion of P and S waves for source time functions. *Geophysical Research Letters*, 16(9), 1043–1046. <https://doi.org/10.1029/gl016i009p01043>
- Ruzhich, V. V., Psakhie, S. G., Chernykh, E. N., Bornyakov, S. A., & Granin, N. G. (2009). Deformation and seismic effects in the ice cover of Lake Baikal. *Russian Geology and Geophysics*, 50(3), 214–221. <https://doi.org/10.1016/j.rgg.2008.08.005>
- Sato, M., Ishikawa, T., Ujihara, N., Yoshida, S., Fujita, M., Mochizuki, M., & Asada, A. (2011). Displacement above the hypocenter of the 2011 Tohoku-Oki earthquake. *Science*, 332(6036), 1395. <https://doi.org/10.1126/science.1207401>
- Satriano, C., Kiraly, E., Bernard, P., & Vilotte, J.-P. (2012). The 2012 M_w 8.6 Sumatra earthquake: Evidence of westward sequential seismic ruptures associated to the reactivation of a N-S ocean fabric. *Geophysical Research Letters*, 39(15), L15302. <https://doi.org/10.1029/2012gl052387>
- Savage, M. K. (1998). Lower crustal anisotropy or dipping boundaries? Effects on receiver functions and a case study in New Zealand. *Journal of Geophysical Research*, 103(B7), 15069–15087. <https://doi.org/10.1029/98jb00795>
- Schaff, D. P., Kim, W., Richards, P. G., Jo, E., & Ryoo, Y. (2018). Using waveform cross correlation for detection, location, and identification of aftershocks of the 2017 nuclear explosion at the North Korea test site. *Seismological Research Letters*, 89(6), 2113–2119. <https://doi.org/10.1785/0220180132>
- Schaff, D. P., Kim, W.-Y., & Richards, P. G. (2012). Seismological constraints on proposed low-yield nuclear testing in particular regions and time periods in the past, with comments on “Radionuclide evidence for low-yield nuclear testing in North Korea in April/May 2010” by Lars-Erik De Geer. *Science and Global Security*, 20(2–3), 155–171. <https://doi.org/10.1080/08929882.2012.711183>
- Schaff, D. P., & Richards, P. G. (2004a). Lg-wave cross correlation and double-difference location: Application to the 1999 Xiuyan, China, sequence. *Bulletin of the Seismological Society of America*, 94(3), 867–879. <https://doi.org/10.1785/0120030136>
- Schaff, D. P., & Richards, P. G. (2004b). Repeating seismic events in China. *Science*, 303(5661), 1176–1178. <https://doi.org/10.1126/science.1093422>
- Schaff, D. P., & Richards, P. G. (2011). On finding and using repeating seismic events in and near China. *Journal of Geophysical Research*, 116(B3), B03309. <https://doi.org/10.1029/2010JB007895>
- Schaff, D. P., Richards, P. G., Slinkard, M., Heck, S., & Young, C. (2018). Lg-wave cross correlation and epicentral double-difference location in and near China. *Bulletin of the Seismological Society of America*, 108(3A), 1326–1345. <https://doi.org/10.1785/0120170137>
- Schmandt, B., Aster, R., Scherler, D., Tsai, V. C., & Karlstrom, K. (2013). Multiple fluvial processes detected by riverside seismic and infrasound monitoring of a controlled flood in the Grand Canyon. *Geophysical Research Letters*, 40(18), 4858–4863. <https://doi.org/10.1002/grl.5095>

- Schmandt, B., & Lin, F.-C. (2014). P and S wave tomography of the mantle beneath the United States. *Geophysical Research Letters*, *41*(18), 6342–6349. <https://doi.org/10.1002/2014gl061231>
- Schmelzbach, C., Donner, S., Igel, H., Sollberger, D., Taufiqurrahman, T., Bernauer, F., et al. (2018). Advances in 6C seismology: Applications of combined translational and rotational motion measurements in global and exploration seismology. *Geophysics*, *83*(3), WC53–WC69. <https://doi.org/10.1190/geo2017-0492.1>
- Schneider, S., & Deuss, A. (2020). A new catalogue of toroidal-mode overtone splitting function measurements. *Geophysical Journal International*, *225*(1), 329–341. <https://doi.org/10.1093/gji/ggaa567>
- Schuster, G. T. (2009). *Seismic interferometry*. Cambridge University Press. <https://doi.org/10.1017/CBO9780511581557>
- Schuster, G. T., Yu, J., Sheng, J., & Rickett, J. (2004). Interferometric/daylight seismic imaging. *Geophysical Journal International*, *157*(2), 838–852. <https://doi.org/10.1111/j.1365-246X.2004.02251.x>
- Schweitzer, J., Fyen, J., Mykkeltveit, S., Gibbons, S. J., Pirl, M., Kühn, D., & Kväerna, T. (2012). Seismic arrays. In *New Manual of Seismological Observatory Practice 2 (NMSOP-2)* (pp. 1–80). Deutsches GeoForschungsZentrum GFZ.
- Scripps Institution of Oceanography. (1975). *Project IDA VLP seismometer network – UCSD/SIO/GPP*. International Federation of Digital Seismograph Networks. <https://doi.org/10.7914/SN/ID>
- Scripps Institution of Oceanography. (1986). *Global seismograph network – IRIS/IDA*. International Federation of Digital Seismograph Networks. <https://doi.org/10.7914/SN/II>
- Sergeant, A., Manganay, A., Stutzmann, E., Montagner, J. P., Walter, F., Moretti, L., & Castelnaud, O. (2016). Complex force history of a calving-generated glacial earthquake derived from broadband seismic inversion. *Geophysical Research Letters*, *43*(3), 1055–1065. <https://doi.org/10.1002/2015GL066785>
- Seydoux, L., Balestrieri, R., Poli, P., Hoop, M. D., Campillo, M., & Baraniuk, R. (2020). Clustering earthquake signals and background noises in continuous seismic data with unsupervised deep learning. *Nature Communications*, *11*(1), 1–12. <https://doi.org/10.1038/s41467-020-17841-x>
- Shani-Kadmiel, S., Averbuch, G., Smets, P., Assink, J., & Evers, L. (2021). The 2010 Haiti earthquake revisited: An acoustic intensity map from remote atmospheric infrasound observations. *Earth and Planetary Science Letters*, *560*, 116795. <https://doi.org/10.1016/j.epsl.2021.116795>
- Shapiro, N. M., & Campillo, M. (2004). Emergence of broadband Rayleigh waves from correlations of the ambient seismic noise. *Geophysical Research Letters*, *31*(7), L07614. <https://doi.org/10.1029/2004GL019491>
- Shapiro, N. M., Campillo, M., Stehly, L., & Ritzwoller, M. H. (2005). High-resolution surface-wave tomography from ambient seismic noise. *Science*, *307*(5715), 1615–1618. <https://doi.org/10.1126/science.1108339>
- Sharrock, D. S., & Woodhouse, J. H. (1998). Investigation of time dependent inner core structure by the analysis of free oscillation spectra. *Earth Planets and Space*, *50*(11), 1013–1018. <https://doi.org/10.1186/BF03352195>
- Shearer, P., & Bürgmann, R. (2010). Lessons learned from the 2004 Sumatra-Andaman megathrust rupture. *Annual Review of Earth and Planetary Sciences*, *38*(1), 103–131. <https://doi.org/10.1146/annurev-earth-040809-152537>
- Shearer, P. M., Rychert, C. A., & Liu, Q. (2011). On the visibility of the inner-core shear wave phase PKJKP at long periods. *Geophysical Journal International*, *185*(3), 1379–1383. <https://doi.org/10.1111/j.1365-246X.2011.05011.x>
- Shearer, P. M., & Stark, P. B. (2012). Global risk of big earthquakes has not recently increased. *Proceedings of the National Academy of Sciences of the United States of America*, *109*(3), 717–721. <https://doi.org/10.1073/pnas.1118525109>
- Shen, W., Wiens, D. A., Lloyd, A. J., & Nyblade, A. A. (2020). A geothermal heat flux map of Antarctica empirically constrained by seismic structure. *Geophysical Research Letters*, *47*(14), e2020GL086955. <https://doi.org/10.1029/2020gl086955>
- Sieh, K., Natawidjaja, D. H., Meltzner, A. J., Shen, C.-C., Cheng, H., Li, K.-S., et al. (2008). Earthquake supercycles inferred from sea-level changes recorded in the corals of west Sumatra. *Science*, *322*(5908), 1674–1678. <https://doi.org/10.1126/science.1163589>
- Silber, E., & Brown, P. (2019). Infrasound monitoring as a tool to characterize impacting near-Earth objects (NEOs). In *Infrasound monitoring for atmospheric studies* (pp. 939–986). Springer.
- Silver, P. G., & Chan, W. W. (1991). Shear wave splitting and subcontinental mantle deformation. *Journal of Geophysical Research*, *96*(B10), 16429–16454. <https://doi.org/10.1029/91jb00899>
- Simmons, N. A., Forte, A. M., Boschi, L., & Grand, S. P. (2010). GyPSuM: A joint tomographic model of mantle density and seismic wave speeds. *Journal of Geophysical Research*, *115*(B12), B12310. <https://doi.org/10.1029/2010JB007631>
- Simon, J. D., Simons, F. J., & Irving, J. C. E. (2021a). A MERMAID miscellany: Seismoacoustic signals beyond the P wave. *Seismological Research Letters*, *92*(6), 3657–3667. <https://doi.org/10.1785/0220210052>
- Simon, J. D., Simons, F. J., & Irving, J. C. (2021b). Recording earthquakes for tomographic imaging of the mantle beneath the South Pacific by autonomous MERMAID floats. *Geophysical Journal International*, *228*(1), 147–170. <https://doi.org/10.1093/gji/ggab271>
- Simons, F. J., Nolet, G., Georgief, P., Babcock, J. M., Regier, L. A., & Davis, R. E. (2009). On the potential of recording earthquakes for global seismic tomography by low-cost autonomous instruments in the oceans. *Journal of Geophysical Research*, *114*(B5), B05307. <https://doi.org/10.1029/2008jb006088>
- Simons, M., Minson, S. E., Sladen, A., Ortega, F., Jiang, J., Owen, S. E., et al. (2011). The 2011 Magnitude 9.0 Tohoku-Oki earthquake: Mosaicking the megathrust from seconds to centuries. *Science*, *332*(6036), 1421–1425. <https://doi.org/10.1126/science.1206731>
- Sladen, A., Rivet, D., Ampuero, J. P., De Barros, L., Hello, Y., Calbris, G., & Lamare, P. (2019). Distributed sensing of earthquakes and ocean-solid Earth interactions on seafloor telecom cables. *Nature Communications*, *10*(1), 5777. <https://doi.org/10.1038/s41467-019-13793-z>
- Slinkard, M., Heck, S., Schaff, D., Bonal, N., Daily, D., Young, C., & Richards, P. (2016). Detection of the Wenchuan aftershock sequence using waveform correlation with a composite regional network. *Bulletin of the Seismological Society of America*, *106*(4), 1371–1379. <https://doi.org/10.1785/0120150333>
- Slinkard, M., Schaff, D., Mikhailova, N., Heck, S., Young, C., & Richards, P. G. (2014). Multistation validation of waveform correlation techniques as applied to broad regional monitoring. *Bulletin of the Seismological Society of America*, *104*(6), 2768–2781. <https://doi.org/10.1785/0120140140>
- Slunga, R., Rögnvaldsson, S. T., & Bödvarsson, R. (1995). 11 Absolute and relative locations of similar events with application to microearthquakes in southern Iceland. *Geophysical Journal International*, *123*(2), 409–419. <https://doi.org/10.1111/j.1365-246X.1995.tb06862.x>
- Smith, S. (1986). IRIS: A program for the next decade. *EOS, Transactions of the American Geophysical Union*, *67*(16), 213. <https://doi.org/10.1029/eo067i016p00213>
- Sollberger, D., Igel, H., Schmelzbach, C., Edme, P., van Manen, D. J., Bernauer, F., et al. (2020). Seismological processing of six degree-of-freedom ground-motion data. *Sensors*, *20*(23), 6904. <https://doi.org/10.3390/s20236904>
- Song, X. (2000). Joint inversion for inner core rotation, inner core anisotropy, and mantle heterogeneity. *Journal of Geophysical Research*, *105*(B4), 7931–7943. <https://doi.org/10.1029/1999JB900436>
- Song, X., & Dai, W. (2008). Topography of Earth's inner core boundary from high-quality waveform doublets. *Geophysical Journal International*, *175*(1), 386–399. <https://doi.org/10.1111/j.1365-246X.2008.03909.x>

- Song, X., & Li, A. (2000). Support for differential inner core superrotation from earthquakes in Alaska recorded at South Pole station. *Journal of Geophysical Research*, 105(B1), 623–630. <https://doi.org/10.1029/1999JB900341>
- Song, X., & Poupinet, G. (2007). Inner core rotation from event-pair analysis. *Earth and Planetary Science Letters*, 261(1), 259–266. <https://doi.org/10.1016/j.epsl.2007.06.034>
- Song, X., & Richards, P. G. (1996). Seismological evidence for differential rotation of the Earth's inner core. *Nature*, 382(6588), 221–224. <https://doi.org/10.1038/382221a0>
- Sorrells, G. G. (1971). A preliminary investigation into the relationship between long-period seismic noise and local fluctuations in the atmospheric pressure field. *Geophysical Journal International*, 26(1–4), 71–82. <https://doi.org/10.1111/j.1365-246x.1971.tb03383.x>
- Souriau, A. (1998a). Is the rotation real? *Science*, 281(5373), 55–56. <https://doi.org/10.1126/science.281.5373.55>
- Souriau, A. (1998b). New seismological constraints on differential rotation of the inner core from Novaya Zemlya events recorded at DRV, Antarctica. *Geophysical Journal International*, 134(2), F1–F5. <https://doi.org/10.1046/j.1365-246x.1998.00637.x>
- Souriau, A., & Poupinet, G. (2000). Inner core rotation: A test at the worldwide scale. *Physics of the Earth and Planetary Interiors*, 118(1), 13–27. [https://doi.org/10.1016/S0031-9201\(99\)00131-4](https://doi.org/10.1016/S0031-9201(99)00131-4)
- Stähler, S. C., Khan, A., Banerdt, W. B., Lognonné, P., Giardini, D., Ceylan, S., et al. (2021). Seismic detection of the Martian core. *Science*, 373(6553), 443–448. <https://doi.org/10.1126/science.abi7730>
- Steblov, G. M., Kogan, M. G., Levin, B. V., Vasilenko, N. F., Prytkov, A. S., & Frolov, D. I. (2008). Spatially linked asperities of the 2006–2007 great Kuril earthquakes revealed by GPS. *Geophysical Research Letters*, 35(22), L22306. <https://doi.org/10.1029/2008gl035572>
- Stehly, L., Campillo, M., & Shapiro, N. M. (2006). A study of the seismic noise from its long-range correlation properties. *Journal of Geophysical Research*, 111(B10), 1–12. <https://doi.org/10.1029/2005JB004237>
- Stein, J. M. (1987). Dial-a-broadband seismogram. *EOS, Transactions of the American Geophysical Union*, 68(27), 628.
- Stein, J. M. (2015). 1.02 – Theory and observations – Instrumentation for global and regional seismology. In G. Schubert (Ed.), *Treatise on geophysics* (pp. 29–78). Elsevier. <https://doi.org/10.1016/B978-0-444-53802-4.00023-3>
- Stein, S., Geller, R. J., & Liu, M. (2012). Why earthquake hazard maps often fail and what to do about it. *Tectonophysics*, 562, 1–25. <https://doi.org/10.1016/j.tecto.2012.06.047>
- Stoneley, R. (1924). Elastic waves at the surface of separation of two solids. *Proceedings of the Royal Society of London, Series A*, 106(738), 416–428. <https://doi.org/10.1098/rspa.1924.0079>
- Storchak, D. A., Di Giacomo, D., Bondar, I., Engdahl, E. R., Harris, J., Lee, W. H. K., et al. (2013). Public release of the ISC-GEM global instrumental earthquake catalogue (1900–2009). *Seismological Research Letters*, 84(5), 810–815. <https://doi.org/10.1785/0220130034>
- Storchak, D. A., Di Giacomo, D., Engdahl, E. R., Harris, J., Bondar, I., Lee, W. H. K., et al. (2015). The ISC-GEM global instrumental earthquake catalogue (1900–2009): Introduction. *Physics of the Earth and Planetary Interiors*, 239, 48–63. <https://doi.org/10.1016/j.pepi.2014.06.009>
- Stutzmann, E., Roullet, G., & Astiz, L. (2000). Geoscope station noise levels. *Bulletin of the Seismological Society of America*, 90(3), 690–701. <https://doi.org/10.1785/0119990025>
- Su, W., Dziewonski, A. M., & Jeanloz, R. (1996). Planet within a planet: Rotation of the inner core of Earth. *Science*, 274(5294), 1883–1887. <https://doi.org/10.1126/science.274.5294.1883>
- Suarez, G., van Eck, T., Giardini, D., Aherm, T., Butler, R., & Tsuboi, S. (2008). The international Federation of Digital Seismograph Networks (FDSN): An integrated system of seismological observatories. *IEEE Systems Journal*, 2(3), 431–438. <https://doi.org/10.1109/JSYST.2008.2003294>
- Suda, N., Nawa, K., & Fukao, Y. (1998). Earth's background free oscillations. *Science*, 279(5359), 2089–2091. <https://doi.org/10.1126/science.279.5359.2089>
- Sukhovich, A., Bonnieux, S., Hello, Y., Irissou, J. O., Simons, F. J., & Nolet, G. (2015). Seismic monitoring in the oceans by autonomous floats. *Nature Communications*, 6(1), 8027. <https://doi.org/10.1038/ncomms9027>
- Suriñach, E., Furdada, G., Sabot, F., Biesca, B., & Vilaplana, J. M. (2001). On the characterization of seismic signals generated by snow avalanches for monitoring purposes. *Annals of Glaciology*, 32, 268–274. <https://doi.org/10.3189/172756401781819634>
- Survey, U. S. G., Peterson, J., & Orsini, N. A. (1982). Design concepts for a Global Telemetered Seismograph Network (Tech. Rep.). <https://doi.org/10.3133/ofr82703>
- Suyehiro, K., Montagner, J., Stephen, R. A., Araki, E., Kanazawa, T., Orcutt, J., et al. (2006). Ocean seismic observatories. *Oceanography-Washington DC-Oceanography Society*, 19(4), 144–149. <https://doi.org/10.5670/oceanog.2006.12>
- Talandier, J., Hyvernaud, O., Okal, E. A., & Piserchia, P. F. (2002). Long-range detection of hydroacoustic signals from large icebergs in the Ross Sea, Antarctica. *Earth and Planetary Science Letters*, 203(1), 519–534. [https://doi.org/10.1016/S0012-821X\(02\)00867-1](https://doi.org/10.1016/S0012-821X(02)00867-1)
- Talandier, J., Hyvernaud, O., Raymond, D., & Okal, E. A. (2006). Hydroacoustic signals generated by parked and drifting icebergs in the Southern Indian and Pacific Oceans. *Geophysical Journal International*, 165(3), 817–834. <https://doi.org/10.1111/j.1365-246X.2006.02911.x>
- Talandier, J., & Okal, E. A. (1998). On the mechanism of conversion of seismic waves to and from T waves in the vicinity of island shores. *Bulletin of the Seismological Society of America*, 88(2), 621–632. <https://doi.org/10.1785/BSSA0880020621>
- Talavera-Soza, S., & Deuss, A. (2020). New measurements of long-period radial modes using large earthquakes. *Geophysical Journal International*, 224(2), 1211–1224. <https://doi.org/10.1093/gji/ggaa499>
- Tanaka, Y., Hiramatsu, Y., Ishihara, Y., & Kanao, M. (2019). Characteristics of non-tectonic tremors around the Lützow-Holm Bay, East Antarctica, during 2013–2015. *Polar Science*, 19, 77–85. <https://doi.org/10.1016/j.polar.2018.11.010>
- Tanimoto, T. (2007). Excitation of normal modes by non-linear interaction of ocean waves. *Geophysical Journal International*, 168(2), 571–582. <https://doi.org/10.1111/j.1365-246X.2006.03240.x>
- Tanimoto, T., & Anderson, D. L. (1985). Lateral heterogeneity and azimuthal anisotropy of the upper mantle: Love and Rayleigh waves 100–250 s. *Journal of Geophysical Research*, 90(B2), 1842–1858. <https://doi.org/10.1029/jb090ib02p01842>
- Tanimoto, T., Hadziioannou, C., Igel, H., Wasserman, J., Schreiber, U., & Gebauer, A. (2015). Estimate of Rayleigh-to-Love wave ratio in the secondary microseism by colocated ring laser and seismograph. *Geophysical Research Letters*, 42(8), 2650–2655. <https://doi.org/10.1002/2015GL063637>
- Tanimoto, T., & Rivera, L. (2008). The ZH ratio method for long-period seismic data: Sensitivity kernels and observational techniques. *Geophysical Journal International*, 172(1), 187–198. <https://doi.org/10.1111/j.1365-246X.2007.03609.x>
- Tanimoto, T., & Wang, J. (2020). Shallow elasticity structure from colocated pressure and seismic stations in the Piñon Flat Observatory and estimation of Vs30. *Geophysical Journal International*, 222(1), 678–696. <https://doi.org/10.1093/gji/ggaa195>
- Tanioka, Y., & Ruff, L. J. (1997). Source time functions. *Seismological Research Letters*, 68(3), 386–400. <https://doi.org/10.1785/gssrl.68.3.386>
- Tao, K., Grand, S. P., & Niu, F. (2018). Seismic structure of the upper mantle beneath eastern Asia from full waveform seismic tomography. *Journal of Geophysical Research: Solid Earth*, 19(8), 2732–2763. <https://doi.org/10.1029/2018GC007460>

- Tape, C., Liu, Q., Maggi, A., & Tromp, J. (2009). Adjoint tomography of the southern California crust. *Science*, 325(5943), 988–992. <https://doi.org/10.1126/science.1175298>
- Tape, C., Ringler, A. T., & Hampton, D. L. (2020). Recording the aurora at seismometers across Alaska. *Seismological Research Letters*, 91(6), 3039–3053. <https://doi.org/10.1785/0220200161>
- Tauzin, B., Debayle, E., Quantin, C., & Coltice, N. (2013). Seismoacoustic coupling induced by the breakup of the 15 February 2013 Chelyabinsk meteor. *Geophysical Research Letters*, 40(14), 3522–3526. <https://doi.org/10.1002/grl.50683>
- Tesoniero, A., Auer, L., Boschi, L., & Cammarano, F. (2015). Hydration of marginal basins and compositional variations within the continental lithospheric mantle inferred from a new global model of shear and compressional velocity. *Journal of Geophysical Research*, 120(11), 7789–7813. <https://doi.org/10.1002/2015JB012026>
- Tkalčić, H., & Pham, T.-S. (2018). Shear properties of Earth's inner core constrained by a detection of J waves in global correlation wavefield. *Science*, 362(6412), 329–332. <https://doi.org/10.1126/science.aau7649>
- Tkalčić, H., Young, M., Bodin, T., Ngo, S., & Sambridge, M. (2013). The shuffling rotation of the Earth's inner core revealed by earthquake doublets. *Nature Geoscience*, 6(6), 497–502. <https://doi.org/10.1038/ngeo1813>
- Tkalčić, H., Pham, T.-S., & Wang, S. (2020). The Earth's coda correlation wavefield: Rise of the new paradigm and recent advances. *Earth-Science Reviews*, 208, 103285. <https://doi.org/10.1016/j.earscirev.2020.103285>
- Tomiyama, K., & Oda, H. (2008). Estimation of inner-core rotation rate by using the Earth's free oscillation. *Acta Geophysica*, 56(4), 939–956. <https://doi.org/10.2478/s11600-008-0053-7>
- Toyokuni, G., Matsuno, T., & Zhao, D. (2020). P wave tomography beneath Greenland and surrounding regions: 2. Lower mantle. *Journal of Geophysical Research: Solid Earth*, 125(12), e2020JB019837. <https://doi.org/10.1029/2020jb019837>
- Trabant, C., Hutko, A. R., Manochehr, B., Karstens, R., Ahern, T., & Aster, R. (2012). Data products of the IRIS DMC: Stepping stones for research and other applications. *Seismological Research Letters*, 83(5), 846–854. <https://doi.org/10.1785/0220120032>
- Traer, J., Gerstoft, P., Bromirski, P. D., & Shearer, P. (2012). Microseisms and hum from ocean surface gravity waves. *Journal of Geophysical Research*, 117, B11307. <https://doi.org/10.1029/2012JB009550>
- Trampert, J., Deschamps, F., Resovsky, J., & Yuen, D. (2004). Probabilistic tomography maps chemical heterogeneities throughout the lower mantle. *Science*, 306(5697), 853–856. <https://doi.org/10.1126/science.1101996>
- Tromp, J. (1995). Normal-mode splitting due to inner-core anisotropy. *Geophysical Journal International*, 121(3), 963–968. <https://doi.org/10.1111/j.1365-246X.1995.tb06451.x>
- Tromp, J., Komatitsch, D., Hjörleifsdóttir, V., Liu, Q., Zhu, H., Peter, D., et al. (2010). Near real-time simulations of global CMT earthquakes. *Geophysical Journal International*, 183(1), 381–389. <https://doi.org/10.1111/j.1365-246X.2010.04734.x>
- Tromp, J., Tape, C., & Liu, Q. (2005). Seismic tomography, adjoint methods, time reversal, and banana-doughnut kernels. *Geophysical Journal International*, 160(1), 195–216. <https://doi.org/10.1111/j.1365-246X.2004.02453.x>
- Tsai, V. C., & McNamara, D. (2011). Quantifying the influence of sea ice on ocean microseism using observations from the Bering Sea, Alaska. *Geophysical Research Letters*, 38(22), L22502. <https://doi.org/10.1029/2011GL049791>
- Tsai, V. C., Minchew, B., Lamb, M., & Ampuero, J.-P. (2012). A physical model for seismic noise generation from sediment transport in rivers. *Geophysical Research Letters*, 39(2), L02404. <https://doi.org/10.1029/2011GL050255>
- Tsai, V. C., Nettles, M., Ekström, G., & Dziewonski, A. M. (2005). Multiple CMT source analysis of the 2004 Sumatra earthquake. *Geophysical Research Letters*, 32(17), L17304. <https://doi.org/10.1029/2005GL023813>
- Tsai, V. C., Rice, J. R., & Fahnestock, M. (2008). Possible mechanisms for glacial earthquakes. *Journal of Geophysical Research*, 113(F3), F03014. <https://doi.org/10.1029/2007jf000944>
- Tyttell, J., Vernon, F., Hedlin, M., de Groot Hedlin, C., Reyes, J., Busby, B., et al. (2016). The USArray Transportable Array as a platform for weather observation and research. *Bulletin of the American Meteorological Society*, 97(4), 603–619. <https://doi.org/10.1175/BAMS-D-14-00204.1>
- Uchida, N., & Bürgmann, R. (2019). Repeating earthquakes. *Annual Review of Earth and Planetary Sciences*, 47(1), 305–332. <https://doi.org/10.1146/annurev-earth-053018-060119>
- Udias, A., & Stauder, W. (1996). The Jesuit contribution to seismology. *Seismological Research Letters*, 67(3), 10–19. <https://doi.org/10.1785/gssrl.67.3.10>
- UK Meteorological Office. (2010). *Cartopy: A cartographic python library with a Matplotlib interface* (Computer software manual). Exeter.
- Valentine, A. P., & Trampert, J. (2012). Data space reduction, quality assessment and searching of seismograms: Autoencoder networks for waveform data. *Geophysical Journal International*, 189(2), 1183–1202. <https://doi.org/10.1111/j.1365-246X.2012.05429.x>
- Vallée, M. (2013). Source time function properties indicate a strain drop independent of earthquake depth and magnitude. *Nature Communications*, 4(1), 1–6. <https://doi.org/10.1038/ncomms3606>
- Vallée, M., Ampuero, J. P., Juhel, K., Bernard, P., Montagner, J.-P., & Barsuglia, M. (2017). Observations and modeling of the elastogravity signals preceding direct seismic waves. *Science*, 358(6367), 1164–1168. <https://doi.org/10.1126/science.aao0746>
- Vallée, M., & Douet, V. (2016). A new database of source time functions (STFs) extracted from the SCARDEC method. *Physics of the Earth and Planetary Interiors*, 257, 149–157. <https://doi.org/10.1016/j.pepi.2016.05.012>
- Vallée, M., & Juhel, K. (2019). Multiple observations of the prompt elastogravity signals heralding direct seismic waves. *Journal of Geophysical Research: Solid Earth*, 124(3), 2970–2989. <https://doi.org/10.1029/2018JB017130>
- Valovcin, A., & Tanimoto, T. (2017). Modeling the excitation of seismic waves by the Joplin tornado. *Geophysical Research Letters*, 44(20), 10256–10261. <https://doi.org/10.1002/2017gl074185>
- Van Camp, M., Meurers, B., de Viron, O., & Forbriger, T. (2016). Optimized strategy for the calibration of superconducting gravimeters at the one per mille level. *Journal of Geodesy*, 90(1), 91–99. <https://doi.org/10.1007/s00190-015-0856-7>
- Vance, S. D., Kedar, S., Panning, M. P., Stähler, S. C., Bills, B. G., Lorenz, R. D., et al. (2018). Vital signs: Seismology of icy ocean worlds. *Astrobio*, 18(1), 37–53. <http://doi.org/10.1089/ast.2016.1612>
- van Driel, M., Krischer, L., Stähler, S. C., Hosseini, K., & Nissen-Meyer, T. (2015). Instaseis: Instant global seismograms based on a broadband waveform database. *Solid Earth*, 6(2), 701–717. <https://doi.org/10.5194/se-6-701-2015>
- Van Fossen, M., Trabant, C., Ahern, T. K., & Weekly, R. T. (2015). The IRIS federator: Accessing seismological data across data centers. In *Presented at AGU Fall Meeting, 14–18 December* (pp. IN31B-1767).
- van Heijst, H. J., & Woodhouse, J. (1997). Measuring surface-wave overtone phase velocities using a mode-branch stripping technique. *Geophysical Journal International*, 131(2), 209–230. <https://doi.org/10.1111/j.1365-246X.1997.tb01217.x>
- van Herwaarden, D. P., Afanasiev, M., Thrastarson, S., & Fichtner, A. (2021). Evolutionary full-waveform inversion. *Geophysical Journal International*, 224(1), 306–311. <https://doi.org/10.1093/gji/ggaa459>
- van Herwijnen, A., & Schweizer, J. (2011). Monitoring avalanche activity using a seismic sensor. *Cold Regions Science and Technology*, 69(2–3), 165–176. <https://doi.org/10.1016/j.coldregions.2011.06.008>

- Veitch, S., & Nettles, M. (2012). Spatial and temporal variations in Greenland glacial-earthquake activity, 1993–2010. *Journal of Geophysical Research*, 117(F4), F04007. <https://doi.org/10.1029/2012JF002412>
- Veitch, S., & Nettles, M. (2017). Assessment of glacial-earthquake source parameters. *Journal of Glaciology*, 63(241), 867–876. <https://doi.org/10.1017/jog.2017.52>
- Ventosa, S., Schimmel, M., & Stutzmann, E. (2017). Extracting surface waves, hum and normal modes: Time-scale phase-weighted stack and beyond. *Geophysical Journal International*, 211(1), 30–44. <https://doi.org/10.1093/gji/ggx284>
- Vidale, J. E., Dodge, D. A., & Earle, P. S. (2000). Slow differential rotation of the Earth's inner core indicated by temporal changes in scattering. *Nature*, 405(6785), 445–448. <https://doi.org/10.1038/35013039>
- Vidale, J. E., & Earle, P. S. (2005). Evidence for inner-core rotation from possible changes with time in PKP coda. *Geophysical Research Letters*, 32(1), L01309. <https://doi.org/10.1029/2004GL021240>
- Vinnik, L. P., Farra, V., & Romanowicz, B. (1989). Azimuthal anisotropy in the Earth from observations of SKS at GEOSCOPE and NARS broadband stations. *Bulletin of the Seismological Society of America*, 79(5), 1542–1558. <https://doi.org/10.1785/BSSA0790051542>
- Vinnikand, L., & Montagner, J. P. (1996). Shear wave splitting in the mantle Ps phases. *Geophysical Research Letters*, 23(18), 2449–2452. <https://doi.org/10.1029/96GL02263>
- Visser, K., Lebedev, S., Trampert, J., & Kennett, B. (2007). Global Love wave overtone measurements. *Geophysical Research Letters*, 34(3), L03302. <https://doi.org/10.1029/2006GL028671>
- Voisin, C., Guzmán, M. A. R., Réfloch, A., Taruselli, M., & Garambois, S. (2017). Groundwater monitoring with passive seismic interferometry. *Journal of Water Resource and Protection*, 09(12), 1414–1427. <https://doi.org/10.4236/jwarp.2017.912091>
- Von Rebeur-Paschwitz, E. (1889). The earthquake of Tokio, April 18, 1889. *Nature*, 40(1030), 294–295. <https://doi.org/10.1038/040294e0>
- Voosen, P. (2022). The planet inside. *Science*, 376(6588), 18–22. <https://doi.org/10.1126/science.abq2618>
- Wald, D. J., Heaton, T. H., & Hudnut, K. W. (1996). The slip history of the 1994 Northridge, California, earthquake determined from strong-motion, teleseismic, GPS, and leveling data. *Bulletin of the Seismological Society of America*, 86(1B), S49–S70. <https://doi.org/10.1785/bssa08601b0s49>
- Wald, D. J., Jaiswal, K. S., Marano, K. D., Bausch, D. B., & Hearne, M. G. (2010). *PAGER-rapid assessment of an earthquake's impact* (Fact Sheet, 2010-3036, pp. 4). U.S. Geological Survey.
- Waldhauser, F., & Ellsworth, W. L. (2000). A double-difference earthquake location algorithm: Method and application to the northern Hayward Fault, California. *Bulletin of the Seismological Society of America*, 90(6), 1353–1368. <https://doi.org/10.1785/0120000006>
- Walker, K. T., Ishii, M., & Shearer, P. M. (2005). Rupture details of the 28 March 2005 Sumatra M_w 8.6 earthquake imaged with teleseismic P waves. *Geophysical Research Letters*, 32(24), L24303. <https://doi.org/10.1029/2005gl024395>
- Walker, K. T., & Shearer, P. M. (2009). Illuminating the near-sonic rupture velocities of the intracontinental Kokoxili M_w 7.8 and Denali fault M_w 7.9 strike-slip earthquakes with global P wave back projection imaging. *Journal of Geophysical Research*, 114(B2), B02304. <https://doi.org/10.1029/2008jb005738>
- Walter, J. I., Brodsky, E. E., Tulaczyk, S., Schwartz, S. Y., & Pettersson, R. (2011). Transient slip events from near-field seismic and geodetic data on a glacier fault, Whillans Ice Plain, West Antarctica. *Journal of Geophysical Research*, 116(F1), F01021. <https://doi.org/10.1029/2010jf001754>
- Wang, M., Gao, G., Feng, J., Jiang, Q., & Pan, Z. (2014). A new curve tracing algorithm based on local feature in the vectorization of paper seismograms. *Sensors & Transducers*, 165(2), 108–111.
- Wang, Q., Campillo, M., Brenguier, F., Lecoindre, A., Takeda, T., & Hashima, A. (2019). Evidence of changes of seismic properties in the entire crust beneath Japan after the M_w 9.0, 2011 Tohoku-Oki earthquake. *Journal of Geophysical Research: Solid Earth*, 124(8), 8924–8941. <https://doi.org/10.1029/2019jb017803>
- Wang, S., & Tkalčić, H. (2020). Seismic event coda-correlation's formation: Implications for global seismology. *Geophysical Journal International*, 222(2), 1283–1294. <https://doi.org/10.1093/gji/ggaa259>
- Wang, Z., Niu, F., Huang, J., Li, Z., & Chen, H. (2021). Distribution of Rayleigh wave microseisms constrained by multiple seismic arrays. *Journal of Geophysical Research: Solid Earth*, 126(9), e2021JB022084. <https://doi.org/10.1029/2021JB022084>
- Waszek, L., Irving, J., & Deuss, A. (2011). Reconciling the hemispherical structure of Earth's inner core with its super-rotation. *Nature Geoscience*, 4(4), 264–267. <https://doi.org/10.1038/ngeo1083>
- Weaver, R. L., & Lobkis, O. I. (2001). Ultrasonics without a source: Thermal fluctuation correlations at MHz frequencies. *Physical Review Letters*, 87(13), 134301. <https://doi.org/10.1103/PhysRevLett.87.134301>
- Webb, S. C. (2008). The Earth's hum: The excitation of Earth normal modes by ocean waves. *Geophysical Journal International*, 174(2), 542–566. <https://doi.org/10.1111/j.1365-246x.2008.03801.x>
- Weber, S., Beutel, J., Häusler, M., Geimer, P. R., Fäh, D., & Moore, J. R. (2022). Spectral amplification of ground motion linked to resonance of large-scale mountain landforms. *Earth and Planetary Science Letters*, 578, 117295. <https://doi.org/10.1016/j.epsl.2021.117295>
- Wegler, U., & Sens-Schönfelder, C. (2007). Fault zone monitoring with passive image interferometry. *Geophysical Journal International*, 168(3), 1029–1033. <https://doi.org/10.1111/j.1365-246x.2006.03284.x>
- Wessel, P., Luis, J. F., Uieda, L., Scharroo, R., Wobbe, F., Smith, W. H. F., & Tian, D. (2019). The generic mapping tools version 6. *Geochemistry, Geophysics, Geosystems*, 20(11), 5556–5564. <https://doi.org/10.1029/2019GC008515>
- Westerhausl, M., & Zürn, W. (2001). On the use of Earth tides in geodynamic research. *Journal of the Geodetic Society of Japan*, 47(1), 1–9. <https://doi.org/10.11366/sokuchi1954.47.1>
- Widmer, R., Masters, G., & Gilbert, F. (1991). Spherically symmetric attenuation within the Earth from natural mode data. *Geophysical Journal International*, 104(3), 541–553. <https://doi.org/10.1111/j.1365-246X.1991.tb05700.x>
- Widmer-Schmidrig, R. (2003). What can superconducting gravimeters contribute to normal-mode seismology? *Bulletin of the Seismological Society of America*, 93(3), 1370–1380. <https://doi.org/10.1785/0120020149>
- Wielandt, E. (2012). Seismic sensors and their calibration. In *New manual of seismological observatory practice 2 (NMSOP-2)* (pp. 1–51). Deutsches GeoForschungsZentrum GFZ.
- Wielandt, E., & Steim, J. (1986). A digital very-broad-band seismograph. *Annales Geophysicae*, 4(B3), 227–232.
- Wielandt, E., & Streckeisen, G. (1982). The leaf-spring seismometer: Design and performance. *Bulletin of the Seismological Society of America*, 72(6A), 2349–2367. <https://doi.org/10.1785/BSSA07206A2349>
- Wiens, D. A., Anandkrishnan, S., Winberry, J. P., & King, M. A. (2008). Simultaneous teleseismic and geodetic observations of the stick-slip motion of an Antarctic ice stream. *Nature*, 453(7196), 770–773. <https://doi.org/10.1038/nature06990>
- Williams, P. D., Alexander, M. J., Barnes, E. A., Butler, A. H., Davies, H. C., Garfinkel, C. I., et al. (2017). A census of atmospheric variability from seconds to decades. *Geophysical Research Letters*, 44(21), 11–201. <https://doi.org/10.1002/2017GL075483>
- Wilson, D. C., Davis, P., Ebeling, C., Hutt, C. R., & Hafner, K. (2018). Seismic sensors record a hurricane's roar. *EOS, Transactions of the American Geophysical Union*, 99. <https://doi.org/10.1029/2018EO102963>

- Winberry, J. P., Anandakrishnan, S., Alley, R. B., Wiens, D. A., & Pratt, M. J. (2017). Tidal pacing, skipped slips and the slowdown of Whillans Ice Stream, Antarctica. *Journal of Glaciology*, 60(222), 795–807. <https://doi.org/10.3189/2014JG14J038>
- Winberry, J. P., Huerta, A. D., Anandakrishnan, S., Aster, R., Nyblade, A., & Wiens, D. A. (2020). Glacial earthquakes and precursory seismicity associated with Thwaites Glacier calving. *Geophysical Research Letters*, 47(3), e2019GL086178. <https://doi.org/10.1029/2019gl086178>
- Withers, M. M., Aster, R. C., Young, C., Beiriger, J., Harris, M., Moore, S., & Trujillo, J. (1998). A comparison of select trigger algorithms for automated global seismic phase and event detection. *Bulletin of the Seismological Society of America*, 88(1), 95–106. <https://doi.org/10.1785/bssa0880010095>
- Withers, M. M., Aster, R. C., Young, C. J., & Chael, E. P. (1996). High-frequency analysis of seismic background noise as a function of wind speed and shallow depth. *Bulletin of the Seismological Society of America*, 86(5), 1507–1515. <https://doi.org/10.1785/bssa0860051507>
- Witze, A. (2022). Why the Tongan eruption will go down in the history of volcanology. *Nature*, 602(7897), 376–378. <https://doi.org/10.1038/d41586-022-00394-y>
- Woodhouse, J. H., & Dahlen, F. A. (1978). The effect of a general aspherical perturbation on the free oscillations of the Earth. *Geophysical Journal International*, 53(2), 335–354. <https://doi.org/10.1111/j.1365-246X.1978.tb03746.x>
- Woodhouse, J. H., & Deuss, A. (2015). Theory and observations—Earth’s free oscillations. *Treatise on Geophysics*, 79–115. <https://doi.org/10.1016/B978-0-444-52748-6.00002-X>
- Woodhouse, J. H., & Dziewonski, A. M. (1984). Mapping the upper mantle: Three-dimensional modeling of Earth structure by inversion of seismic waveforms. *Journal of Geophysical Research*, 89(B7), 5953–5986. <https://doi.org/10.1029/jb089i07p05953>
- Woodhouse, J. H., & Giardini, D. (1985). Inversion for the splitting function of isolated low order normal mode multiplets. *Eos, Transactions American Geophysical Union*, 66, 300.
- Woodhouse, J. H., Giardini, D., & Li, X.-D. (1986). Evidence for inner core anisotropy from free oscillations. *Geophysical Research Letters*, 13(13), 1549–1552. <https://doi.org/10.1029/GL013i013p01549>
- Woodhouse, J. H., & Wong, Y. (1986). Amplitude, phase and path anomalies of mantle waves. *Geophysical Journal International*, 87(3), 753–773. <https://doi.org/10.1111/j.1365-246X.1986.tb01970.x>
- Woodward, R. L., & Masters, G. (1989). Calibration and data quality of the long-period SRO/ASRO networks, 1977 to 1980. *Bulletin of the Seismological Society of America*, 79(6), 1972–1983. <https://doi.org/10.1785/BSSA0790061972>
- Wu, W., Zhan, Z., Peng, S., Ni, S., & Callies, J. (2020). Seismic ocean thermometry. *Science*, 369(6510), 1510–1515. <https://doi.org/10.1126/science.abb9519>
- Wunsch, C. (2020). Advance in global ocean acoustics. *Science*, 369(6510), 1433–1434. <https://doi.org/10.1126/science.abe0960>
- Xiao, H., Tanimoto, T., & Xue, M. (2021). Study of S-wave microseisms generated by storms in Southeast Australia and the north Atlantic. *Geophysical Research Letters*, 48(15), e2021GL093728. <https://doi.org/10.1029/2021GL093728>
- Xu, C., Gong, Z., & Niu, J. (2016). Recent developments in seismological geodesy. *Geodesy and Geodynamics*, 7(3), 157–164. (Special Issue: Geodetic and Geophysical Observations and Applications and Implications). <https://doi.org/10.1016/j.geog.2016.04.009>
- Xu, W., Davis, P., Auerbach, D., & Klimczak, E. (2018). Revision of metadata sensitivities at IRIS/IDA stations. *Seismological Research Letters*, 89(3), 1084–1092. <https://doi.org/10.1785/0220170280>
- Xu, X., & Song, X. (2003). Evidence for inner core super-rotation from time-dependent differential PKP traveltimes observed at Beijing Seismic Network. *Geophysical Journal International*, 152(3), 509–514. <https://doi.org/10.1046/j.1365-246X.2003.01852.x>
- Xu, Y., Koper, K. D., Sufri, O., Zhu, L., & Hutko, A. R. (2009). Rupture imaging of the M_w 7.9 12 May 2008 Wenchuan earthquake from back projection of teleseismic P waves. *Geochemistry, Geophysics, Geosystems*, 10(4), Q04006. <https://doi.org/10.1029/2008gc002335>
- Yang, H.-Y., & Tromp, J. (2015). Synthetic free-oscillation spectra: An appraisal of various mode-coupling methods. *Geophysical Journal International*, 203(2), 1179–1192. <https://doi.org/10.1093/gji/ggv349>
- Yang, Y., Atterholt, J. W., Shen, Z., Muir, J. B., Williams, E. F., & Zhan, Z. (2021). Sub-kilometer correlation between near-surface structure and ground motion measured with distributed acoustic sensing. *Geophysical Research Letters*, 49(1), e2021GL096503. <https://doi.org/10.1029/2021gl096503>
- Yang, Y., & Song, X. (2020). Origin of temporal changes of inner-core seismic waves. *Earth and Planetary Science Letters*, 541, 116267. <https://doi.org/10.1016/j.epsl.2020.116267>
- Yang, Y., & Song, X. (2021). Reply to Yao et al.’s comment on “Origin of temporal changes of inner-core seismic waves”. *Earth and Planetary Science Letters*, 553, 116639. <https://doi.org/10.1016/j.epsl.2020.116639>
- Yano, T., Tanimoto, T., & Rivera, L. (2009). The ZH ratio method for long-period seismic data: Inversion for S-wave velocity structure. *Geophysical Journal International*, 179(1), 413–424. <https://doi.org/10.1111/j.1365-246X.2009.04293.x>
- Yao, H., Shearer, P. M., & Gerstoft, P. (2013). Compressive sensing of frequency-dependent seismic radiation from subduction zone megathrust ruptures. *Proceedings of the National Academy of Sciences*, 110(12), 4512–4517. <https://doi.org/10.1073/pnas.1212790110>
- Yao, J., Tian, D., Sun, L., & Wen, L. (2021). Comment on “Origin of temporal changes of inner-core seismic waves” by Yang and Song (2020). *Earth and Planetary Science Letters*, 553, 116640. <https://doi.org/10.1016/j.epsl.2020.116640>
- Ye, L., Lay, T., Kanamori, H., & Rivera, L. (2016). Rupture characteristics of major and great ($M_w \geq 7.0$) megathrust earthquakes from 1990 to 2015: 1. Source parameter scaling relationships. *Journal of Geophysical Research: Solid Earth*, 121(2), 826–844. <https://doi.org/10.1002/2015jb012426>
- Yeck, W. L., Patton, J. M., Johnson, C. E., Kragness, D., Benz, H. M., Earle, P. S., et al. (2019). GLASS3: A standalone multiscale seismic detection associator. *Bulletin of the Seismological Society of America*, 109(4), 1469–1478. <https://doi.org/10.1785/0120180308>
- Yeck, W. L., Patton, J. M., Ross, Z. E., Hayes, G. P., Guy, M. R., Ambruz, N. B., et al. (2020). Leveraging deep learning in global 24/7 real-time earthquake monitoring at the National Earthquake Information Center. *Seismological Research Letters*, 92(1), 469–480. <https://doi.org/10.1785/0220200178>
- Yi, L., Xu, C., Zhang, X., Wen, Y., Jiang, G., Li, M., & Wang, Y. (2017). Joint inversion of GPS, InSAR and teleseismic data sets for the rupture process of the 2015 Gorkha, Nepal, earthquake using a generalized ABIC method. *Journal of Asian Earth Sciences*, 148, 121–130. <https://doi.org/10.1016/j.jseaes.2017.08.029>
- Yoon, C. E., O’Reilly, O., Bergen, K. J., & Beroza, G. C. (2015). Earthquake detection through computationally efficient similarity search. *Science Advances*, 1(11), e1501057. <https://doi.org/10.1126/sciadv.1501057>
- Yoshizawa, K., Yomogida, K., & Tsuboi, S. (1999). Resolving power of surface wave polarization data for higher-order heterogeneities. *Geophysical Journal International*, 138(1), 205–220. <https://doi.org/10.1046/j.1365-246x.1999.00861.x>
- Young, C. J., Chael, E. P., Withers, M. M., & Aster, R. C. (1996). A comparison of the high-frequency (>1 Hz) surface and subsurface noise environment at three sites in the United States. *Bulletin of the Seismological Society of America*, 86(5), 1516–1528. <https://doi.org/10.1785/bssa0860051516>

- Yuan, S., Simonelli, A., Lin, C., Bernauer, F., Donner, S., Braun, T., et al. (2020). Six degree-of-freedom broadband ground-motion observations with portable sensors: Validation, local earthquakes, and signal processing. *Bulletin of the Seismological Society of America*, *110*(3), 953–969. <https://doi.org/10.1785/0120190277>
- Zanna, L., Khaliwala, S., Gregory, J. M., Ison, J., & Heimbach, P. (2019). Global reconstruction of historical ocean heat storage and transport. *Proceedings of the National Academy of Sciences of the United States of America*, *116*(4), 1126–1131. <https://doi.org/10.1073/pnas.1808838115>
- Zhan, Z. (2019). Seismic noise interferometry reveals transverse drainage configuration beneath the surging Bering Glacier. *Geophysical Research Letters*, *46*(9), 4747–4756. <https://doi.org/10.1029/2019gl082411>
- Zhan, Z., Cantono, M., Kamalov, V., Mecozzi, A., Muller, R., Yin, S., & Castellanos, J. (2021). Optical polarization-based seismic and water wave sensing on transoceanic cables. *Science*, *371*(6532), 931–936. <https://doi.org/10.1126/science.abe6648>
- Zhan, Z., Helmberger, D. V., Kanamori, H., & Shearer, P. M. (2014). Supershear rupture in a M_w 6.7 aftershock of the 2013 sea of Okhotsk earthquake. *Science*, *345*(6193), 204–207. <https://doi.org/10.1126/science.1252717>
- Zhang, J., Richards, P. G., & Schaff, D. P. (2008). Wide-scale detection of earthquake waveform doublets and further evidence for inner core super-rotation. *Geophysical Journal International*, *174*(3), 993–1006. <https://doi.org/10.1111/j.1365-246X.2008.03856.x>
- Zhang, J., Song, X., Li, Y., Richards, P. G., Sun, X., & Waldhauser, F. (2005). Inner core differential motion confirmed by earthquake waveform doublets. *Science*, *309*(5739), 1357–1360. <https://doi.org/10.1126/science.1113193>
- Zhang, M., & Wen, L. (2015). Seismological evidence for a low-yield nuclear test on 12 May 2010 in North Korea. *Seismological Research Letters*, *86*(1), 138–145. <https://doi.org/10.1785/02201401170>
- Zhang, S., Wang, R., Dahm, T., Zhou, S., & Heimann, S. (2020). Prompt elasto-gravity signals (PEGS) and their potential use in modern seismology. *Earth and Planetary Science Letters*, *536*, 116150. <https://doi.org/10.1016/j.epsl.2020.116150>
- Zhu, H., Bozdağ, E., Duffy, T. S., & Tromp, J. (2013). Seismic attenuation beneath Europe and the North Atlantic: Implications for water in the mantle. *Earth and Planetary Science Letters*, *381*, 1–11. <https://doi.org/10.1016/j.epsl.2013.08.030>
- Zhu, H., Bozdağ, E., Peter, D., & Tromp, J. (2012). Structure of the European upper mantle revealed by adjoint tomography. *Nature Geoscience*, *5*(7), 493–498. <https://doi.org/10.1038/ngeo1501>
- Zhu, W., & Beroza, G. C. (2018). PhaseNet: A deep-neural-network-based seismic arrival-time picking method. *Geophysical Journal International*, *216*(1), 261–273. <https://doi.org/10.1093/gji/ggy423>
- Zhu, W., Mousavi, S. M., & Beroza, G. C. (2019). Seismic signal denoising and decomposition using deep neural networks. *IEEE Transactions on Geoscience and Remote Sensing*, *57*(11), 9476–9488. <https://doi.org/10.1109/TGRS.2019.2926772>
- Zielhuis, A., & van der Hilst, R. D. (1996). Upper-mantle shear velocity beneath eastern Australia from inversion of waveforms from SKIPPY portable arrays. *Geophysical Journal International*, *127*(1), 1–16. <https://doi.org/10.1111/j.1365-246X.1996.tb01530.x>
- Zürn, W., ExB, J., Steffen, H., Kroner, C., Jahr, T., & Westerhaus, M. (2007). On reduction of long-period horizontal seismic noise using local barometric pressure. *Geophysical Journal International*, *171*(2), 780–796. <https://doi.org/10.1111/j.1365-246X.2007.03553.x>
- Zürn, W., Ferreira, A., Widmer-Schmidrig, R., Lentas, K., Rivera, L., & Clévéde, E. (2015). High-quality lowest-frequency normal mode strain observations at the Black Forest Observatory (SW-Germany) and comparison with horizontal broad-band seismometer data and synthetics. *Geophysical Journal International*, *203*(3), 1787–1803. <https://doi.org/10.1093/gji/ggv381>
- Zürn, W., & Widmer, R. (1995). On noise reduction in vertical seismic records below 2 mHz using local barometric pressure. *Geophysical Research Letters*, *22*(24), 3537–3540. <https://doi.org/10.1029/95GL03369>
- Zürn, W., & Wielandt, E. (2007). On the minimum of vertical seismic noise near 3 mHz. *Geophysical Journal International*, *168*(2), 647–658. <https://doi.org/10.1111/j.1365-246X.2006.03189.x>